The STK38 kinase regulates the subcellular distribution of downstream partners by phosphorylating the auto-inhibitory domain of XPO1

Alexandre Martin

PSL UNIVERSITÉ PARIS

THÈSE DE DOCTORAT
DE L'UNIVERSITÉ PSL

Préparée à Institut Curie

The STK38 kinase regulates the subcellular distribution of downstream partners by phosphorylating the auto-inhibitory domain of XPO1

Soutenue par
Alexandre MARTIN
Le 28 mars 2019

Ecole doctorale n° 582
Cancérologie : biologie, médecine, santé

Spécialité
Aspects Moléculaires et Cellulaires de la Biologie

institutCurie

Composition du jury :

Dr Alain, EYCHENE Directeur de Recherche Institut Curie - UMR3347	*Président*
Dr Sophie, PATTINGRE Chargé de Recherche Institut de Cancérologie de Montpellier - Inserm U1194	*Rapporteur*
Dr Etienne, MOREL Chargé de Recherche Institut Necker Enfants Malades - Inserm U1151	*Rapporteur*
Dr Carine, JOFFRE Chargé de Recherche Centre de Recherche en Cancérologie de Toulouse - UMR1037	*Examinateur*
Dr Patrice, CODOGNO Directeur de Recherche émérite Institut Necker Enfants Malades - Inserm U1151	*Examinateur*
Dr Jacques, CAMONIS Directeur de Recherche Institut Curie - Inserm U830	*Directeur de thèse*
Dr Alexander, Hergovich Group Leader, UCL - London	*Membre invité*

The Hippo pathway STK38 serine/threonine protein kinase is implicated in multifarious biological processes in both normal and cancer cells. Previous work performed by our team and collaborators have identified the central role of STK38 in cell cycle progression, centrosome duplication, apoptosis, and transcriptional activity. Importantly, STK38 has been characterized to act downstream of the Ral proteins (effectors of Ras proteins family) in two cellular processes required for proper cellular homeostasis and deregulated in cancer cells. On one hand, STK38 establish a bridge between the Ras-Ral and Hippo transduction pathways by positively regulating autophagy. On the other hand, STK38 is required for anoïkis resistance in Ras-driven cancer cells. All these observations reveal the implication of STK38 in unrelated cellular functions regulated by diverse transduction pathways.

In this work, we discovered that STK38 associates with more than 250 identified interactors, depending on the cellular context. In details, we found that STK38 increases its association with cytoplasmic proteins upon nutrient starvation-induced autophagy, while STK38 increases its interaction with nuclear proteins to the detriment of cytoplasmic ones upon ECM detachment. Furthermore, we discovered that STK38 shuttles between the nucleus and the cytoplasm depending on the context in a XPO1-dependent manner. We characterized STK38 as the first activator of XPO1 by phosphorylating XPO1's auto-inhibitory domain: this phosphorylation being required for the presentation of XPO1's cargo docking site. In addition of being its own gatekeeper, STK38 regulates the subcellular distribution of several effectors, such as Beclin1, YAP1, and Centrin, effectors that play a crucial role in STK38-related well characterized functions.

Taken together, these results presented in this work reveal that multifarious functions harboured by a single protein, a kinase in our case, STK38, can be explained by a unique molecular mechanism: regulating the subcellular distribution of key effectors by modulating XPO1 export activity through phosphorylation of its auto-inhibitory domain. STK38 is in charge of controlling the supply chain of components of these machineries assembled in the cytoplasm.

Les cellules normales sont caractérisées par un équilibre bien contrôlé entre prolifération, différenciation et apoptose. Cependant, certaines de ces cellules échappent au système de surveillance et commencent à devenir cancéreuses dès que cette homéostasie est rompue. Hanahan et Weinberg ont défini en 2000 et 2011 les attributs des cellules cancéreuses en établissant une liste définie (insensibilité aux signaux anti-croissance et autosuffisance en signaux de croissance, augmentation de l'angiogenèse, résistance à l'apoptose, etc.) de caractéristiques fonctionnelles dérégulées dans les cellules cancéreuses. Si nous devions simplifier ces informations, nous pourrions dire que les cellules cancéreuses se caractérisent principalement par leur capacité à maintenir une signalisation prolifératives soutenue.

Ras activé (chargé en GTP) se lie à plusieurs protéines et active des cascades de signalisation en aval afin d'affecter des mécanismes de régulation cellulaire tels que la prolifération cellulaire, la migration, la survie cellulaire et d'autres fonctions contribuant à la transformation cellulaire. Les trois effecteurs les mieux caractérisés sont ceux de la famille Ras/MEK, la phosphatidylinositol 3-kinase (Pi3K) et la famille Ral/RalGEF, où la voie de signalisation Raf/MEK/ERK étant l'effecteur le plus largement étudié.

En bref, l'activation de Raf par Ras provoque sa libération de la membrane plasmique et conduit à une cascade de phosphorylation et d'activation de MEK, capable de phosphoryler et d'activer les protéines kinases ERK1 et ERK2. Finalement, les protéines ERK phosphorylent et activent des facteurs de transcription (par exemple Elk1, Fos et c-Jun) qui déclenchent l'expression de gènes spécifiques.

Comme Ras, l'activation des protéines RalA et RalB repose sur leur liaison avec du GTP, qui peut être augmentée par des RalGEF. Le premier RalGEF, RalGDS (pour Ral guanine, un stimulateur de dissociation de nucléotide), a été identifié pour la première fois au début des années 1990 grâce à une recherche d'homologie de séquence avec RasGEF. Toutes les RalGEFs partagent un domaine d'homologie CDC25 responsable de l'activité catalytique mais peuvent être divisés en deux groupes distincts. L'un est composé de RalGEFs contenant un domaine de motif échangeur Ras N-terminal (REM) en plus d'un domaine d'association Ras C-terminal (RA) (RalGDS, RGL1 et RGL3 RGL3 chez l'homme). L'autre groupe est composé de deux protéines ne contenant aucun des sites cités précédemment mais possèdent à la place un domaine d'homologie pleckstrin (PH), suffisant pour diriger Ral à la membrane plasmique.

Les GTPases Ral possèdent une activité intrinsèque d'hydrolyse du GTP afin d'inhiber leur activité, mais comme Ras, des protéines peuvent accélérer cette hydrolyse du GTP par les GTPases et donc l'inactivation des protéines Ral. Bien que l'existence des RalGAP ait été signalée pour la première fois dans le cerveau au début des années 90, l'identification moléculaire des RalGAPs n'a été réalisée que récemment. Chaque RalGAP est composée de deux sous-unités: une sous-unité régulatrice

RalGAPβ de 170 kDa et une sous-unité catalytique RalGAPal (240 kDa) ou RalGAPal (220 kDa), formant ainsi un hétérodimère.

D'autres mécanismes peuvent affecter l'activité des GTPases Ral, telles que des modifications post-traductionnelles (avec par exemple la géranyl-géranylation). Les deux isoformes de Ral se terminent par un motif CAAX qui augmente leur hydrophobie et favorise ainsi leur ancrage à la membrane plasmique pour leur interaction appropriée avec des effecteurs tels que RalBP1 ou la calmoduline. Les protéines Ral sont également régulées par phosphorylation sur des résidus sérine dans leur région C-terminale, ce qui induit une relocalisation des protéines Ral de la membrane plasmique vers des membranes internes, telles que les vésicules, afin d'assurer un trafic adéquat de ces vésicules. Enfin, des travaux précédents effectués par notre équipe ont montré que les protéines RalA et RalB sont toutes deux ubiquitynilées.

La voie de signalisation Hippo est un régulateur essentiel de taille d'organe au cours de la croissance développementale, contrôlant de multiples processus cellulaires tels que la prolifération cellulaire, la mort cellulaire et la différenciation. Une voie Hippo dysfonctionnelle conduit à une prolifération tissulaire aberrante. Ici, nous allons brièvement présenter la voie suppresseur de tumeur Hippo avant de nous concentrer sur l'un de ses membres: la kinase STK38.

La voie Hippo peut être régulée par plusieurs mécanismes tels que la polarité cellulaire, l'adhésion cellulaire et la mécanotransduction. Certaines publications scientifiques ont rapporté que l'agiomotine (Amot), une protéine d'ancrage associée aux tight jonctions (TJ), est un régulateur essentiel de la voie Hippo en interagissant directement avec YAP/TAZ. De plus, un composant majeur des jonctions adhérentes (AJ) a également été lié à la voie Hippo: l'α-caténine fonctionne comme un suppresseur de tumeur en régulant négativement l'activité de YAP1 au cours de la prolifération des cellules souches de l'épiderme et de l'expansion des tissus. Des preuves ont également été trouvées concernant l'implication de la voie de signalisation Rho GTPases et la mécanotransduction sur la voie de signalisation Hippo.

La classe de protéines kinases AGC (pour la protéine kinase A (PKA)/PKG/PKC) est le troisième plus grand groupe de kinases représenté dans la cellule humaine, contenant 70 protéines classées dans 14 sous-groupes tels que la protéine kinase A (PKA), les isoformes de la protéine kinase B (PKB) et de la protéine kinase C (PKC). Tous les membres de cette classe de kinases nécessitent une phosphorylation sur un motif conservé pour leur activation. Sur la base de la séquence de leur domaine catalytique, les kinases STK38 et STK38L (respectivement NDR1 et NDR2 pour Nuclear Dbf2-related 1/2) définissent un sous-groupe de protéine kinases AGC. Pour simplifier la lecture, nous allons parler de la famille STK38 pour définir ces deux kinases.

Il semble que les kinases STK38/STK38L peuvent avoir des rôles opposés dans la tumorigenèse et pourraient fonctionner comme des protéines suppresseurs de tumeurs ou des oncogènes. En contrôlant positivement la duplication et la prolifération des centrosomes, STK38 pourrait fournir des propriétés oncogéniques. De plus, la surexpression de STK38 dans les cellules humaines conduit à une duplication aberrante des centrosomes, conduisant à une instabilité supplémentaire des centrosomes et à une instabilité chromosomique si les réseaux de régulation et de réparation sont dérégulés. En outre, STK38 pourrait agir comme un oncogène en contrôlant la progression du cycle cellulaire, où une surexpression de STK38 pourrait potentiellement conduire à une prolifération supplémentaire. Dans ce même domaine, il a été montré qu'une surexpression de STK38 conduisait à une surexpression du proto-oncogène c-myc. En outre, les niveaux d'ARNm de STK38 sont régulés positivement dans les cancers de l'adénocarcinome du poumon et du cancer de l'ovaire et le taux de protéine STK38 est augmenté dans certaines lignées cellulaires de mélanome.

D'autre part, STK38 peut également être qualifié de suppresseur de tumeur. Il a été rapporté que STK38 joue un rôle crucial dans l'induction de l'apoptose, ainsi que dans l'activation de l'inhibition de YAP1. De manière significative, l'expression des kinases STK38 est dérégulée dans de nombreux types de cancer. Dans la plupart des cas, les niveaux de STK38 sont diminués mais on peut constater une augmentation dans quelques cas. Ces résultats confirment que STK38 pourrait avoir des rôles opposés dans le cancer, en agissant soit comme protéine suppresseur de tumeur, soit comme proto-oncogène, comme cela a déjà été signalé pour des facteurs tels que Ras, TFBβ ou NOTCH1. Réciproquement, le rôle de STK38 dans le mécanisme de réparation de l'ADN pourrait aider à surmonter les lésions à l'ADN induites par les chimiothérapies. En outre, il existe une valeur prédictive du niveau d'ARNm de STK38 dans l'évolution des patients atteints de cancer du sein, de l'ovaire et du poumon, mais pas pour le cancer de l'estomac.

La kinase STK38, également connue sous le nom de NDR1, joue un rôle important dans de multiples fonctions biologiques mais néanmoins non liées, telles que la progression du cycle cellulaire, l'apoptose et la duplication centrosomale. En tant que membre de la voie de signalisation Hippo, STK38 phosphoryle directement l’effecteur terminal de cette voie, YAP1, sur S127, entraînant l’inactivation de YAP1 par séquestration cytoplasmique. De plus, STK38 agit sur la survie des cellules pro-cancéreuses dans la réponse au stress et l’adaptation cellulaire. STK38 répond au choc osmotique et à l'expression de RASSF1A, un régulateur de la voie Hippo. De plus, l'activité kinase de STK38 est nécessaire pour l'induction de l'autophagie en réponse à la carence en régulant Beclin1. Enfin, STK38 est également impliqué dans la résistance à l’anoïkis des cellules cancéreuses dépendantes à Ras sous détachement de la matrice extracellulaire.

Cet inventaire non exhaustif illustre la variété et la multiplicité des fonctions cellulaires pilotées par et/ou dépendantes de STK38. Comment une seule kinase peut-elle remplir ces fonctions cruciales mais clairement distinctes ? Aurait-elle des substrats spécifiques à une fonction ou un régulateur commun encore inconnu qui serait permissif pour toutes ces multiples fonctions ? Pour répondre à cette question, nous avons cartographié l'interactome de STK38 dans différents contextes cellulaires. Cela a révélé que STK38 interagissait principalement avec des protéines cytoplasmiques lors de l'autophagie induite par carence alimentaire, et avec des protéines nucléaires lors du détachement de la matrice extracellulaire, suggérant que la localisation subcellulaire de STK38 joue un rôle régulateur en réponse à ces divers stimuli. En outre, nous avons confirmé qu'un transport nucléo/cytoplasmique de STK38 dépendait de sa propre activité kinase et de l'export nucléaire médié par XPO1 (Exportin-1, aussi appelée CRM1). De plus, nous avons découvert que STK38 phosphorylait la sérine 1055 située dans le domaine auto-inhibiteur de XPO1, déclenchant ainsi l'export nucléaire de STK38 lui-même ainsi que d'autres cargos de XPO1 tels que Beclin1 et YAP1. Ces résultats suggèrent que STK38 régule la localisation subcellulaire, et donc la fonction des composants cellulaires centraux, en modulant leur exportation nucléaire via la phosphorylation de XPO1 sur son domaine auto-inhibiteur.

Pour identifier les protéines qui interagissent avec STK38 lors de l'autophagie induite par carence alimentaire, ou lorsque les cellules résistent à l'anoïkis après mise en suspension, nous avons adopté une approche protéomique en fonction du contexte en établissant des lignées cellulaires exprimant de manière stable APEX2 fusionné à STK38. Des cellules HeLa ont été utilisées pour l'autophagie induite par carence alimentaire et des cellules HEK-HT-HRasG12V (HekRasV12) pour la condition de résistance à l'anoïkis, pour correspondre respectivement aux études précédentes sur le rôle de STK38 dans l'autophagie et la survie après détachement de l'ECM. Pour faire la distinction entre les intéracteurs basaux de STK38 et ceux dépendant du contexte, nous avons appliqué une méthodologie protéomique quantitative par SILAC. En bref, une condition référentielle a été réalisée parallèlement aux conditions étudiées dans chaque contexte : incubation des cellules en milieu complet *versus* autophagie induite par carence alimentaire pour le premier contexte et culture de cellules attachée vs culture de cellules en suspension pour la seconde. La validation du flux d'autophagie et de l'efficacité de la biotinylation dans les deux contextes a été effectuée avant l'identification par spectrométrie de masse. Chaque réplica montre une bonne corrélation entre les expériences, indiquant une reproductibilité élevée entre les échantillons biologiques en triple exemplaire.

Un total de 97 partenaires de STK38 a été identifié dans le contexte autophagique et 221 partenaires dans le contexte de résistance à l'anoïkis. Plusieurs intéracteurs connus de STK38 ont été retrouvé, tels que MAP4K4, HIST2H2AC, EWSR1, NPM1, YWHAZ et MAGOH. Parmi les 97 intéracteurs identifiés pour l'autophagie, 32 augmentent leur interaction avec STK38 lors de la carence alimentaire stimulant le flux autophagique tandis qu'une seule protéine voit son interaction avec STK38 diminuer. Lors du détachement à la matrice extracellulaire, 44 protéines augmentent leur interaction avec STK38 tandis que 72 protéines diminuent leur interaction avec STK38. Fait intéressant, 50 partenaires sont communs aux deux conditions étudiées, mais affichent un statut d'association différentiel avec STK38, en fonction du contexte. La classification hiérarchique non supervisée de ces 50 partenaires communs a été entreprise, révélant que STK38 augmente son interaction avec des protéines cytoplasmiques lors de l'autophagie induite par carence alimentaire, alors que STK38 diminue son interaction avec ces mêmes partenaires cytoplasmiques lors de la résistance à l'anoïkis au profit d'une interaction avec des partenaires nucléaires.

Les observations faites précédemment impliquent un transport nucleo/cytoplasmique de STK38. L'exportine-1 (XPO1), également connue sous le nom de Chromosome Region Maintenance 1 (CRM1), est le principal facteur d'export nucléaire, transportant une grande diversité de protéines du noyau vers le cytoplasme, a été retrouvé dans notre screen comme un nouvel intéracteur de STK38. Pour déterminer si STK38 interagit biochimiquement avec XPO1, nous avons effectué une expérience de pull-down. STK38 fusionné à Myc a été co-exprimé avec Flag-XPO1 ou Flag-Sirt3 comme contrôle. Lors de la capture anti-Flag, STK38 a co-immunoprécipité avec XPO1 mais pas avec Flag-Sirt3, suggérant que STK38 interagit physiquement avec XPO1. De plus, l'inhibition de la protéine phosphatase de type 2A (PP2A) avec l'acide okadaïque (OA), augmentant l'activité kinase de STK38, n'a pas modifié l'interaction de STK38 avec XPO1, indiquant donc que l'activation de STK38 n'est pas nécessaire pour son association avec XPO1.

Nos précédentes expériences ont montré que STK38 interagissait principalement avec des protéines cytoplasmiques en cas de carence, ce qui suggère que, dans cet état, STK38 est localisé dans le cytoplasme. L'immunomarquage de STK38 dans des cellules en carence alimentaire a démontré que STK38 se localisait principalement dans le cytoplasme, tandis que dans un milieu riche en nutriments STK38 était principalement localisé dans le noyau. Les inhibiteurs spécifiques de XPO1, les KPT-185 et KPT-330, ont inhibé la sortie du STK38 du noyau, indiquant que STK38 est transporté depuis le noyau vers le cytoplasme en cas de carence alimentaire sous la dépendance de XPO1.

Nous avons ensuite étudié si l'export nucléaire de STK38, dépendant de XPO1, contribue à sa fonction en autophagie. Comme prévu, l'incubation en EBSS induit une baisse significative du niveau de p62, un marqueur d'autophagie, indiquant la présence d'un flux autophagique. Cependant, l'inhibition de XPO1, induisant la rétention nucléaire de STK38, empêche en parallèle la dégradation

de p62, indiquant un défaut du flux d'autophagie. En complément, nous avons généré une lignée cellulaire exprimant une sonde de flux autophagique (GFP-LC3-RFP-LC3ΔG). De manière significative, l'inhibition de XPO1 par les inhibiteurs spécifiques KPT-185 et KPT-330 altère significativement l'autophagie, telle que mesurée par les rapports GFP / RFP. Ces données indiquent que XPO1 exporte STK38 vers le cytoplasme sous carence alimentaire et que XPO1 doit être fonctionnel pour le processus d'autophagie résultant.

Afin de déterminer si l'activité kinase de STK38 est nécessaire à son export nucléaire et à l'autophagie sous carence alimentaire, l'expression de STK38 endogène a été inhibée à l'aide de siRNA en parallèle de l'expression transitoire d'une forme wild-type (wt), kinase-dead (K118R), ou constitutivement active (PIF) de STK38, toutes résistantes au siRNA. Les cellules transfectées ont ensuite été soumises à carence alimentaire et la localisation cellulaire des différentes formes de STK38 étudiée. Comme prévu, STK38 wt s'est accumulé dans le cytoplasme de cellules sous carence. Cependant, la forme kinase-dead de STK38 (K118R), exprimée à des niveaux similaires à ceux de la forme wt est restée nucléaire au moment de la carence, tandis que la version constitutivement active de STK38 (PIF) s'est accumulé dans le cytoplasme, quelles que soient les conditions de culture. Ces résultats indiquent que l'activité kinase de STK38 est requise et suffisante pour induire son export nucléaire vers le cytoplasme, indépendamment des conditions physiologiques.

Pour étudier plus en détail si l'activité kinase de STK38 est également impliquée dans l'autophagie résultante de la carence, nous avons mesuré le flux autophagique dans les mêmes conditions que celles citées précédemment. Comme prévu, l'inhibition de STK38 altère de manière significative l'autophagie sous carence, autophagie qui a été restaurée en réintroduisant la forme wild-type de STK38. En revanche, l'expression d'une forme kinase-dead de STK38 (K118R), n'a pas permis de restaurer l'autophagie sous carence, contrairement à la forme constitutivement active. De plus, nous avons révélé que l'expression de la forme constitutivement active de STK38 est suffisante pour induire une augmentation substantielle du flux autophagique, sans aucun besoin d'une mise en carence alimentaire des cellules. En conclusion, ces expériences confirment que l'activité kinase de STK38 est nécessaire à la fois pour sa localisation subcellulaire et l'autophagie, et que STK38 est instructive et permissive pour l'autophagie (une situation similaire à celle observée chez la drosophile).

La présence d'un motif de phosphorylation par STK38 (HxRxxS/T) dans la séquence protéique de XPO1 a permis d'envisager une potentielle relation kinase-substrat entre STK38 et XPO1. Ce motif est centré sur la sérine 1055, signalée comme étant phosphorylée dans les cellules humaines mais sans aucune pertinence fonctionnelle ni identification de la kinase. Nous avons généré un anticorps anti-S1055-P phospho-spécifique qui a été validé en utilisant une forme wt ou non phosphorylable de XPO1 (S1055A). L'anticorps anti-XPO1-S1055-P a montré une forte spécificité pour XPO1 sous incubation d'acide okadaic, un puissant inhibiteur de protéine phosphatase de type 2A (PP2A) qui stimule l'activité

de la plupart des kinases, y compris STK38, conduisant à la phosphorylation de la sérine 1055 de XPO1. Parallèlement, et comme prévu, le mutant XPO1 (S1055A) n'a pas été détecté avec cet anticorps dans les deux lysats de cellules entières et après purification des variants de XPO1.

En utilisant cet anticorps spécifique, nous avons examiné si STK38 pouvait phosphoryler la sérine 1055 de XPO1. Comme prévu, l'incubation des cellules avec de l'acide okadaic a induit à la fois la phosphorylation de STK38 sur sa T444, révélant ainsi son activation, et la phosphorylation de XPO1 sur S1055. D'autre part, l'inhibition de STK38 endogène par deux siRNA indépendants a considérablement réduit la phosphorylation de XPO1 sur S1055. Ces résultats démontrent que dans ces conditions, STK38 est nécessaire pour la phosphorylation de la sérine 1055 de XPO1, révélant ainsi une relation kinase-substrat entre STK38 et XPO1.

Nous avons ensuite émis l'hypothèse que la phosphorylation de XPO1 sur S1055 est importante pour sa fonction d'export nucléaire. Plus précisément, étant donné que la sérine 1055 se situe à l'extrémité de la région auto-inhibitrice de XPO1 et que l'activité kinase de STK38 est nécessaire pour son propre export nucléaire dépendant de XPO1, notre modèle de travail est que cette phosphorylation pourrait empêcher l'auto-inhibition de XPO1 et ainsi activer sa fonction d'export. Pour résoudre ce problème, nous avons analysé la localisation de STK38 dans des cellules transfectées de manière transitoire avec des mutants XPO1 insensibles à la phosphorylation (S1055A) ou mimant une phosphorylation constitutive (S1055D et S1055E). Afin d'éviter toute confusion liée à l'activité du XPO1 endogène, nous avons inhibé son activité avec l'inhibiteur KPT-185. Les mutants S1055 exogènes de XPO1 ont été mutés pour C528S, conférant une résistance de XPO1 exogène aux inhibiteurs KPT.

Comme prévu, STK38 localise dans le cytoplasme des cellules en carence mais resta nucléaire des cellules transfectées avec une version non phosphorylable de XPO1, suggérant que la phosphorylation de XPO1 sur S1055 est nécessaire pour l'export nucléaire de STK38. Inversement, l'expression de XPO1 portant des mutations phosphomimétiques (S1055D ou S1055E) entraine une accumulation cytoplasmique de STK38 même en milieu riche, confortant ainsi l'idée que la phosphorylation de XPO1 sur S1055 est importante et instructive pour l'export nucléaire de STK38. La localisation de la sérine 1055 dans le domaine auto-inhibiteur C-terminal de XPO1 nous a également incité à analyser l'effet d'un mutant XPO1 privé de ses 39 derniers acides aminés C-terminaux qui composent le domaine d'auto-inhibition. L'expression de ce mutant a en effet entraîné une accumulation cytoplasmique de STK38 quelles que soient les conditions de culture. Pris ensemble, ces résultats suggèrent un mécanisme par lequel la phosphorylation de la sérine 1055 libère XPO1 de son activité auto-inhibitrice pout découvrir le site de fixation au cargo et permettre à XPO1 de poursuivre sa fonction d'export nucléaire.

Pour sonder indépendamment ces résultats, nous avons créé des mutants XPO1 pour la sérine 1055 dans le locus génomique endogène de cellules HAP1 haploïdes à l'aide de Crispr/Cas9. Les cellules HAP1 portant un mutant XPO1/S1055A n'ont pas réussi à induire un flux autophagique sous carence, alors que des mutants phospho-mimétiques ont induit un flux autophagique sous carence mais également en milieu riche, indiquant que la phosphorylation de XPO1 sur S1055 est non seulement requise pour l'autophagie induite par carence, mais également suffisante pour induire l'autophagie.

En accord avec un précédent rapport, nous avons trouvé que Beclin1 s'accumulait dans le cytoplasme de cellules sous carence de façon XPO1 dépendante. Cet export nucléaire est médié par STK38, étant donné que Beclin1 est resté nucléaire lorsque l'expression de STK38 endogène était inhibée. Cette découverte a été confirmée par immunomarquage de Beclin1 dans nos lignées HAP1 modifiées pour XPO1 endogène. Tandis que Beclin1 accumulait dans le cytoplasme des lignées HAP1 wt sous carence, Beclin1 restait nucléaire dans les cellules contenant le mutant non phosphorylable de XPO1 (S1055A). Inversement, dans les cellules exprimant les mutants phospho-mimétiques S1055D ou S1055E, la sortie nucléaire de Beclin1 était favorisée même dans un milieu riche en nutriments. Ces résultats suggèrent que STK38, en plus de réguler son propre export nucléaire, contrôle également la distribution subcellulaire de Beclin1 au travers de la phosphorylation de XPO1, révélant ainsi comment STK38 peut réguler l'autophagie via Beclin1.

Nos observations et notre modèle peuvent-ils être généralisés à plusieurs cargos de XPO1, sinon à tous ? Nous avons testé cette hypothèse sur YAP1, qui est à la fois un cargo déjà connu de XPO1 mais également sur un substrat de STK38, où la phosphorylation de YAP1 sur S127 entraîne une exclusion nucléaire de YAP1. De plus, il a été rapporté que le transport nucléo/cytoplasmique de YAP1 dépendait de la densité cellulaire, tandis que son export nucléaire dépend de XPO1 tant dans les cellules humaines que chez la Drosophile.

Conformément à ce qui a été précédemment rapporté, nous avons constaté que YAP1 est exclu du noyau à densité cellulaire élevée, alors que le taux de protéine YAP1 totale reste inchangé. Nous avons remarqué que l'inhibition de XPO1 empêche l'exclusion nucléaire de YAP1 à densité cellulaire élevée. Il est intéressant de noter que l'inhibition de l'expression de STK38 phénocopie l'inhibition de XPO1 sur l'export nucléaire de YAP1 à haute densité cellulaire, indiquant que la sortie nucléaire de YAP1 est sous contrôle de STK38 et XPO1. En tant qu'approche indépendante, nous avons analysé la localisation de YAP1 dans nos cellules HAP1 modifiées. YAP1 est exclu du noyau dans les cellules HAP1 wt confluentes, tandis que le niveau de protéine YAP1 reste inchangé entre les conditions expérimentales. Cependant, les cellules exprimant une forme non phosphorylable de XPO1 (S1055A) n'ont pas réussi à induire l'exclusion nucléaire de YAP1 à haute densité cellulaire, alors que les cellules exprimant les mutants phospho-mimétiques S1055 (S1055D ou S1055E) induisent une exclusion nucléaire de YAP1, même à faible densité cellulaire. Ces résultats suggèrent que la localisation

subcellulaire de YAP1 peut être régulée par la phosphorylation de XPO1 par STK38 et soutient la généralisation de notre modèle à plusieurs cargos.

Nous avons récemment montré que la kinase STK38 était permissive pour l'autophagie induite par carence ainsi que pour la résistance des cellules transformées par Ras à l'anoïkis, ajoutant ces fonctions à une longue liste de fonctions dans lesquelles STK38 a précédemment été impliqué. La kinase STK38 est un composant essentiel de la voie Hippo, contrôlant des processus cellulaires tels que la réponse au stress, la progression du cycle cellulaire, la duplication centrosomale et l'activation de la voie NF-kB dans différents contextes.

Pour l'autophagie et ces dernières fonctions, les substrats faisant l'intermédiaire de l'action de STK38 restaient à découvrir ; nous avons cherché à identifier ces substrats en mettant l'accent sur deux contextes dans lesquels STK38 est impliqué et nécessaire : l'autophagie et la résistance à l'anoïkis. Un modèle sous-jacent postulerait que la diversité des fonctions de STK38 est supportée par une diversité de substrats : un nombre de substrats spécifiques à un nombre de fonctions spécifiques régulées par STK38. Nos résultats réfutent cette hypothèse, du moins pour l'autophagie, la régulation de la voie Hippo, la duplication centrosomale et l'activation de NF-KB: un substrat unique de STK38 finit par être le facteur limitant de ces événements, à savoir l'export nucléaire médié par XPO1.

Nous avons constaté que STK38 phosphoryle XPO1 sur son domaine auto-inhibiteur et que la phosphorylation de XPO1 sur S1055 est importante dans divers contextes cellulaires pour l'export nucléaire de transducteurs de signaux intracellulaires essentiels tels que Beclin1, YAP1 et, dans une moindre mesure, pour Centrin1. À cet égard, nous émettons l'hypothèse que la phosphorylation de XPO1 sur S1055 par STK38 induit un changement de conformation de XPO1 où son domaine C-terminal, qui entrave l'accès à la poche de liaison NES de XPO1 dans son état inactivé, déplace et libère l'accès du site de liaison du cargo, permettant la liaison du cargo à XPO1 pour son export nucléaire.

L'extrémité C-terminale de la séquence protéique de XPO1 est hautement conservée parmi tous les chordés, y compris le site S1055. Cependant, le motif de phosphorylation de STK38 approprié (HxRxxS/T) n'apparaît que chez les simiens mais pas chez tous les autres vertébrés (y compris les primates non simiens et tous les organismes habituellement utilisés en laboratoire tels que la souris, le xénope, le poisson zèbre, etc.) portant un motif HxLxxS/T. La question posée par cette observation est de savoir si, dans ces organismes, la réponse à ces contextes est régulée par une autre kinase du type STK38 ou une autre modification post-traductionnelle qui permettrait de réduire l'auto-inhibition qui verrouille XPO1 dans un état inactivé.

Les phénomènes révélés par ces travaux suggèrent également que l'auto-inhibition inhérente à la structure de XPO1 n'est pas anecdotique mais nécessaire à son bon fonctionnement et à sa réactivité aux indices physiologiques. Si XPO1 est activé de manière inappropriée, il déclenche alors un comportement incorrect et déconnecté de la physiologie cellulaire. En milieu riche, cela déclenche les

premiers événements de l'autophagie, censés avoir lieu uniquement en situation de carence. En revanche, dans les cellules capables de proliférer, XPO1 élimine YAP1 du noyau, tandis que YAP1 nucléaire est un important régulateur pro-prolifératif.

La phosphorylation de XPO1 sur S1055 par STK38 est importante pour l'export nucléaire de cargos de XPO1, du moins impliqués dans des fonctions liées à STK38. Cela permet des réponses cellulaires subtiles en fonction du contexte en modulant l'export nucléaire de régulateurs cruciaux. Bien que nous ayons démontré ici que Beclin1 et YAP1 sont d'importants cargos de XPO1 dont la localisation subcellulaire est régulée par STK38, il reste à déterminer combien de cargos sont réglementés par ce mécanisme, s'il est strictement circonscrit aux fonctions liées à STK38 ou si ce mécanisme de régulation peut être généralisé.

Je souhaite tout d'abord remercier l'ensemble des membres du jury qui ont accepté d'évaluer mon travail de thèse. Je tiens à remercier le Dr. Sophie Pattingre et le Dr. Etienne Morel pour avoir accepté d'être rapporteurs de thèse ainsi que pour leurs commentaires et suggestions. Je remercie également le Dr. Carine Joffre, le Dr. Patrice Codogno ainsi que le Dr. Alexander Hergovich d'avoir accepté d'être examinateurs de mon jury de thèse. Je remercie aussi le Dr. Alain Eychène d'avoir accepté d'être Président du jury.

Je remercie le Dr. Jacques Camonis pour m'avoir permis de faire ma thèse dans son équipe à l'institut Curie et pour m'avoir dirigé durant ces années. Merci de m'avoir enseigné tant de choses, de m'avoir fait confiance, soutenu et de m'avoir toujours prodigué les bons conseils. Un immense merci au Dr. Maria-Carla Parrini et au Pr Gérard Zalcman pour leur aide considérable, tant scientifiquement que personnellement. Merci pour votre soutien, votre motivation sans faille, vos avis critiques ainsi que vos coups de boost quand il en fallait. Merci à vous tous de m'avoir fait grandir scientifiquement et personnellement.

Je remercie le Dr. Olivier Delattre pour m'avoir accueilli au sein de son unité de recherche. Je remercie tout particulièrement le Dr. Patrice Codogno et le Dr. Alexander Hergovich pour leur aide tant à la fois globale que spécifique sur ce travail de recherche. Je tiens également à remercier le Dr. Fatima Mechta-Grigoriou et le Dr. Marc-Henry Stern pour leurs retours sur mon travail.

Je voudrais remercier tous les membres de l'équipe ART pour leur aide, leur motivation ainsi que leur bonne humeur : Paula, Giulia, Weijing, Manish, Irina, Fanny, Marie, Audrey. Un immense merci à Bibi pour son aide sur les manips et pour avoir supporté mes blagues (nulles pour la majorité…) pendant toutes ces années. Je remercie également tous les membres de l'U830 pour leur accueil chaleureux. Merci en particulier au Dr. Virginie Mieulet pour ses conseils sur mon travail.

Je remercie le Dr. Chiara Guerrera pour son expertise concernant la spectrométrie de masse ainsi que Sophie Grondin et Annick Viguier de la plateforme de cytométrie pour leur précieux conseils.

Un immense merci à toute ma famille et en particulier à mes parents et à ma sœur. Vous avez toujours cru en moi, et sans votre soutien indéfectible je ne serais pas là aujourd'hui.

Enfin, à Anne-Lise, ma petite fraicheur, tu es ma force, mon inspiration, mon souffle… Merci pour tout.

Ce mémoire de thèse est dédié à la mémoire du Dr. Pascal Verneyre

AIS	Auto-inhibitory sequence
Atg	Autophagy-related
ECM	Extracellular matrix
EMT	Epithelial-mesenchymal transition
ER	Endoplasmic reticulum
GAPs	GTPase-activating proteins
GDP	Guanosine diphosphate
GEFs	Guanine nucleotide-exchange factors
GTP	Guanosine triphosphate
HM	Hydrophobic motif
kd	Kinase-dead
kDa	Kilodalton
LMB	Leptomycin B
MAP4K4	Mitogen-activated protein kinase kinase kinase kinase 4
MEK	Mitogen-activated protein kinase kinases
MOB	Mps one binder
MS	Mass spectrometry
mTORC1	Mammalian Tor kinase complex 1
NDR1	Nuclear Dbf2-related 1
NES	Nuclear export signal
NF-κB	Nuclear factor-kappa B
NLS	Nuclear localization signal
NPC	Nuclear pore complex
NTR	N-terminal regulatory
PAS	Preautophagosomal structure
Pi3K	Phosphatidylinositol 3-kinase
PKA	Protein kinase A
PLD1	Phospholipase D1
PP2A	Protein phosphatase type 2A
Ral	Ras-like
RalBP1	Ral-binding protein 1
RalGDS	Ral guanine nucleotide dissociation stimulator
Ran	Ras-related nuclear protein
ROS	Reactive oxygen species
SINE	Selective inhibitors of nuclear export
siRNA	Small interfering RNA
STK38	Serine/Threonine kinase 38
TNFα	Tumor necrosis factor α
WRC	Wave regulatory complex
wt	Wild-type
XPO1	Exportin-1
Y2H	Yeast two hybrid
ZONAB	Zonula occludens 1-associated nucleic acid binding protein

Table of figures

FOREWORD

This thesis work that have been entrusted to me aims to characterize at the molecular level the role of the kinase STK38 in two of its related biological functions implicated in cancer cell survival: autophagy and anoïkis resistance. My three and half years of thesis focused on the development of this research project, becoming my main one, composing the core of this thesis. In addition, I also participated in two other projects (side projects) accomplished in our research team that are presented in appendices of this thesis, thanks to the skills I acquired during the course of my main project.

The global goal of our research team is to identify the molecular mechanisms underlying the functions, in both normal and cancer cells, of Ral GTPases. Previous work by our team characterized STK38 (aka NDR1), a kinase belonging to the Hippo pathway, as a downstream effector of Ral proteins in two biological processes, establishing a first bridge between these two signaling pathways. The main project of my thesis consisted first of the identification of STK38's interactors in two of its related contexts and the characterization of their dynamic of association, and, secondly, to unveil the molecular event(s) governing these above observations. A summary of this project, as well as the manuscript of the resulting scientific article entitled "**STK38 regulates the nuclear export of downstream partners by phosphorylating the auto-inhibitory domain of XPO1**" can be found in the result section of this thesis.

In the first appendix of this thesis, you will find a summary, my specific contribution and the manuscript of the resulting scientific article entitled "**Localization of the RGL2-RalB signaling axis at endomembrane compartments and its modulation by autophagy**" of the first side project in which I participated. This project, held by one of our team senior scientist and PI, focus on the implication of one of the Ral proteins and one of its activator, Rgl2, in endomembrane management upon autophagy.

The second appendix of this thesis displays my contribution to the second side project. A summary, a description of my specific contribution, and the manuscript of the resulting scientific article entitled "**RASSF1A role in pro-invasive bronchial cells properties and proper cytokinesis via NDR2 control**" can be found. This second side project focus on the implication of STK38L (aka NDR2), the isoform of STK38, in YAP-dependent epithelial-mesenchymal transition.

INTRODUCTION

1 – The Ras-Ral axis in cancer

Normal cells are characterized by a well controlled balance between proliferation, differentiation and apoptosis. However, some cells can escape from the surveillance system and start to become cancerous as soon as this homeostasis is shattered. Hanahan and Weinberg defined in 2000 and 2011 cancer cells though a list of functional characteristics that deregulate their well-established homeostasis (insensitivity to anti-growth signals and self-sufficiency in growth signals, enhanced angiogenesis, apoptosis resistance, etc) as shown in figure 1. If we have to simplify those informations we can say that cancer cells are mainly characterized by the ability to maintain proliferative signaling (Hanahan and Weinberg, 2000).

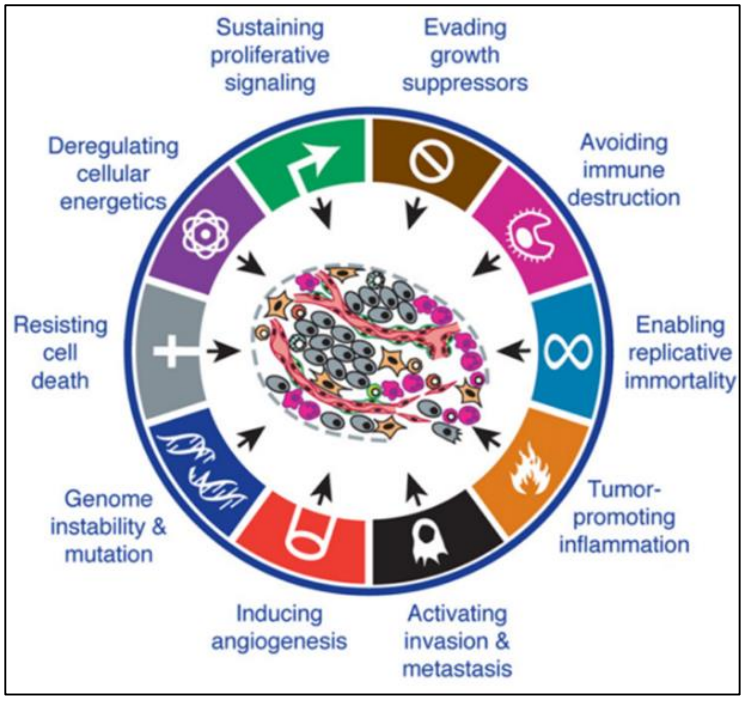

Figure 1 - The hallmarks of cancer.
Hanahan and Weinberg suggested that cancer cells have acquired the same set of functional capabilities during their development, although through various mechanistic strategies. Modified from Hanahan and Weinberg, 2011.

Some tumors are characterized by somatic mutations of genes implicated in the homeostasis regulation cited above allowing cells to decrease the number of events necessary to complete tumorigenesis. Those genes are qualified as oncogenes, tumor-suppressor genes and genes implicated in genome stability maintenance. In some tumors, somatic mutations result in constitutively activated circuits controlled by growth factors stimuli (Hanahan and Weinberg, 2011). In addition, negative-feedback loops regulating various type of proliferative signaling can be also deregulated in tumors resulting in enhanced proliferative signals. The most well-known example involves the Ras oncoprotein (Khan et al., 2018) where around 30% of human cancers harbour a Ras mutation (Lebleu et al., 2013).

1.1 – Ras GTPases

Historically, H-Ras oncogene was the first human oncogene identified and isolated from a human bladder carcinoma (Pulciani et al., 1982) and reported as homologue of Harvey sarcoma virus Ras gene where K-Ras and N-Ras were found from lung carcinomas, neuroblastomas and leukaemia cell lines (Shimizu et al., 1983). Ras protein family are members of a large super-family of guanosine-nucleotide-binding proteins of approximately 21 kDa. (kiloDalton) (Chardin and Tavitian, 1986) encoded by three genes (H-Ras, K-Ras and N-Ras) in mammalian cells (Rojas et al., 2012).

Ras proteins activation depends on whether they are bound to GTP (Guanosine triphosphate) or GDP (Guanosine diphosphate) defining a GTPase cycle. When loaded with GTP, Ras is active and can activate downstream effectors; however, Ras is inactive when loaded with GDP (Srivastava et al., 1989). As shown in figure 2, this activation/inactivation cycle is rigorously controlled by GTPase-activating proteins (GAPs) that accelerate the bounded GTP hydrolysis to GDP (in this case Ras is inactive and fails to interact with effectors) and by Guanine nucleotide exchange factors (GEFs) that exchange GDP for GTP (in which case, Ras is active and is able to engage downstream effectors) (Milburn et al., 1990).

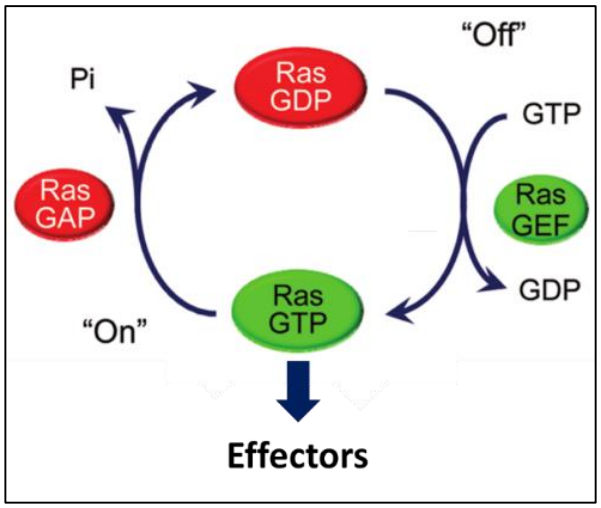

Figure 2 - The Ras GTPases cycle.
The Ras GTPase cycle is highly controlled by RasGEFs that stimulate the GDP exchange to GTP, making Ras active and by RasGAPs that accelerate the intrinsic GTP hydrolysis activity of Ras, making Ras inactive. Active Ras subsequently binds to effectors and activate them. Modified from Cox and Der, 2010.

1.2 – Ras effectors pathways

Activated Ras (loaded with GTP) will bind and activates several downstream proteins and signaling cascade in order to affect cellular regulatory mechanisms such as cell proliferation, migration, cell survival and other functions that contribute to cellular transformation (Wennerberg et al., 2005). As shown in figure 3, the three most well characterized Ras effectors are the Raf/MEK family, the

phosphatidylinositol 3-kinases (Pi3K) and the Ral/RalGEFs family. The Raf/MEK/ERK signaling cascade is the most widely studied Ras effector pathway, mainly because it was the first and the best characterized effector, in addition of being easily integrated in a comfortable model.

Briefly, activation of Raf by Ras cause relocation of Raf to the plasma membrane and lead to a cascade of phosphorylation and activation of the mitogen-activated protein kinase kinases (MEK) that are able to phosphorylate and activate mitogen-activated protein kinases ERK1 and ERK2 (for extracellular signal-regulated kinases 1 and 2). Finally, Erk proteins phosphorylate and activate downstream effectors such as transcription factors (e.g Elk1, Fos and c-Jun) that trigger gene expression (Leevers et al., 1994; Yordy and Muise-Helmericks, 2000).

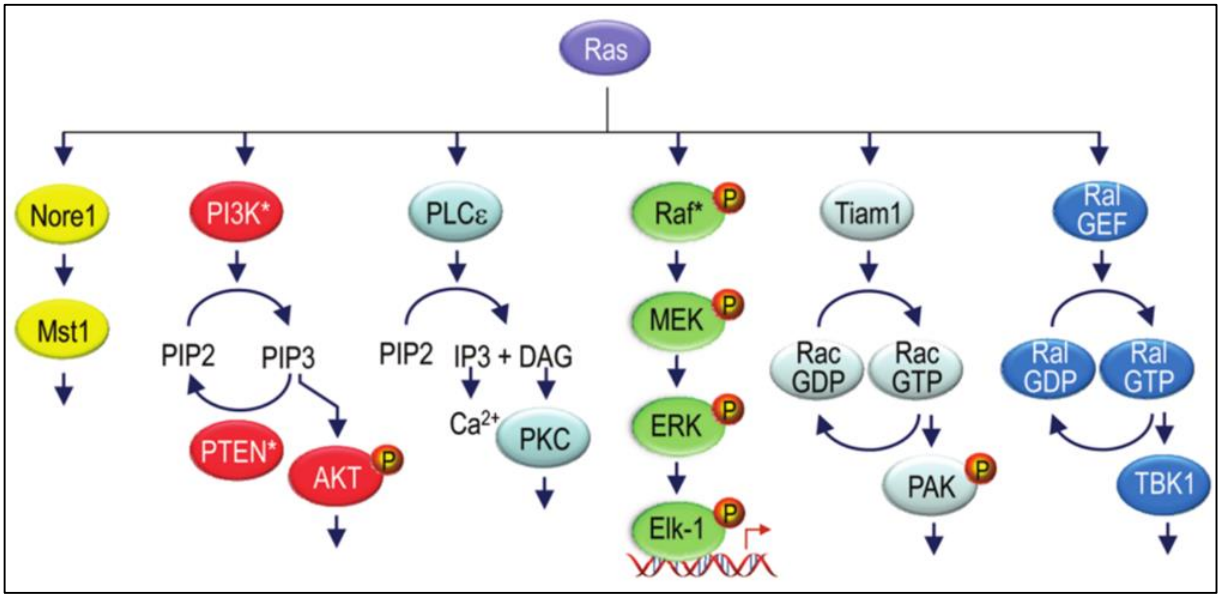

Figure 3 - Ras signaling network.
Ras proteins relay extracellular signals to cytoplasmic downstream effectors listed here. These pathways represent the ones implicate din Ras-mediated oncogenesis. From Cox and Der, 2010.

The second best characterized Ras effectors is the Pi3k signaling cascade. Activated Ras interacts directly with the catalytic subunit of Pi3k that becomes activated due to its translocation to the plasma membrane. Activated Pi3K phosphorylates then phosphatidylinositol-4,5-bisphosphate (PiP2) to produce phosphatidylinositol-3,4,5-trisphosphate (PiP3) that binds and control the activity of a large number of downstream effectors (Sheridan and Downward, 2013). The most important of these latters being AKT with its anti-apoptotic role, crucial for cancer cell survival.

1.3 – The Ral/RalGEFs signaling pathway

Ral (Ras Like) GTPases constitute the third main axis of Ras downstream effectors they were first identified in 1986 (Chardin and Tavitian, 1986). Like Ras, Ral proteins function according to a GTPase cycle but with specific GEFs and GAPs.

1.3.1 – Ral GTPases: RalA and RalB

1.3.1.1 – Ral GTPases structure

The two proteins isoforms, RalA and RalB, are encoded by two genes respectively located on chromosomes 7 and 2 at locus 7p15-p13 and 2q14.2 and are found in all vertebrate species (van Dam et al., 2011). As shown in figure 4, these 260 amino acid proteins share 82% of total sequence identity and contain a N-terminal extension domain, not found in Ras, followed by the G domain responsible for GTPase activity and a plasma membrane targeting C-terminal domain (Nicely et al., 2004). Both RalA and RalB G domain is included between amino acids 12-176 and share 88% of sequence identity (Gentry et al., 2014). This G domain contains four GTP binding motifs and two regions called "switch" (SI and SII) that share complete sequence identity between the two Ral proteins. Those "switch" regions have the ability to change conformation when Ral proteins are loaded with GTP allowing interaction with regulators and effectors as RalBP1, Sec5, and Exo84 for example (Fukai et al., 2003).

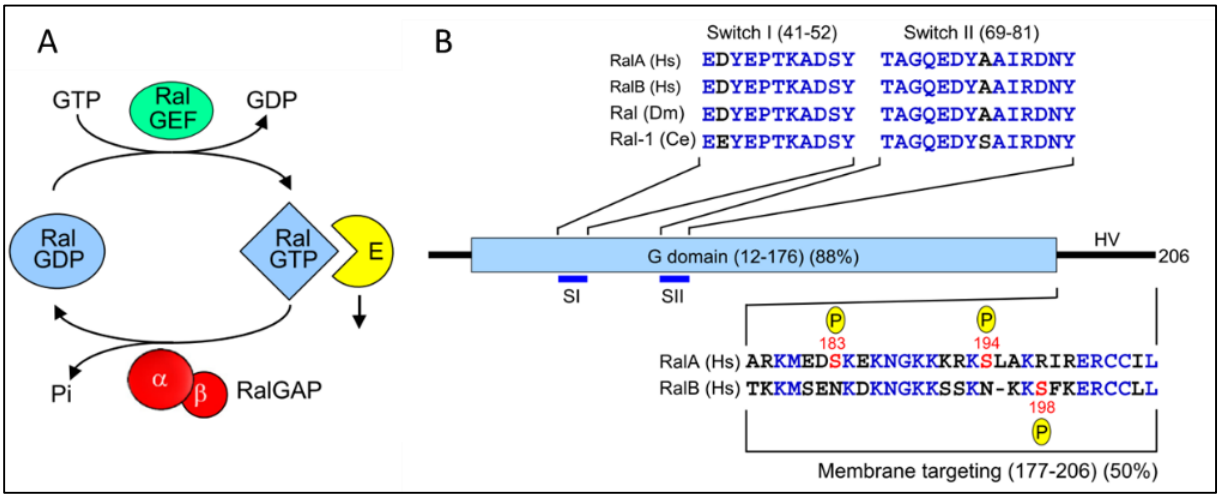

Figure 4 - The Ral GTPases cycle and Ral proteins.
A/ Regulation of Ral GDP-GTP cycling. Ral-selective GEFs and GAPs accelerate the low intrinsic exchange and GTP hydrolysis activities to pro- mote formation of active GTP-bound and inactive GDP-bound Ral. B/ Human RalA and RalB proteins. Human Ral proteins share 88% sequence identity in their G domain that contain the SI and SII domains that change conformation during GTP/GDP cycling. The hypervariable (HV) region contains phosphorylation sites that regulate Ral subcellular localization and effector interaction. Modified from Gentry et al., 2014.

The main sequence divergence between Ral isoforms occurs in the C-terminal hypervariable region where they share 50% of sequence homology (Fenwick et al., 2009). This hypervariable region contains two post-translational phosphorylation sites for RalA and one for RalB that regulate Ral subcellular localization and effector interaction (Gentry et al., 2014) and a CAXX (C= cysteine, A= aliphatic amino acid; X= terminal amino acid) tetrapeptide motif allowing geranyl-geranylation required for lipid membranes insertion such as plasma membrane or endosomes (van Dam and Robinson, 2006).

1.3.1.2 – Regulation of Ral GTPases

Like Ras, RalA and RalB activity rely on their binding with GTP that can be increased by RalGEFs (figure 4). The first RalGEF, RalGDS (for Ral guanine nucleotide dissociation stimulator), was first identified in the early 1990s by searching for homology with RasGEFs (Albright et al., 1993). All RalGEFs share CDC25 homology domain responsible for catalytic activity but can be divided in two distinct groups as shown in figure 5. One is composed of RalGEFs that contain a N-terminal Ras exchanger motif (REM) domain in addition to a C-terminal Ras-association (RA) domain (RalGDS, RGL1, RGL3 and RGL3 in human). The other group is composed of two RalGEFs that do not harbour neither a REM nor a RA but contain instead a C-terminal pleckstrin homology (PH) domain that uncouples them from direct association with Ras but is sufficient for targeting Ral proteins at the plasma membrane (Neel et al., 2011).

Ral GTPases possess intrinsic GTP hydrolysis activity attenuating their activity but like Ras, GTPase-activating proteins can accelerate this GTP hydrolysis. Despite the fact that RalGAPs existence was first reported in brain in the early 1990s (Emkey et al., 1991), the molecular identification of RalGAPs has been achieved only recently. Each RalGAP is composed of two subunits: a 170 kDa regulatory RalGAPβ subunit and a catalytic RalGAPα1 (240 kDa) or RalGAPα1 (220 kDa) subunit forming a heterodimer (Shirakawa et al., 2009).

Other mechanisms can affect Ral GTPases activity, such as post-translational modifications (i.e. geranyl-geranylation). Both Ral isoforms terminate by a CAAX motif that increase hydrophobicity and promote membrane anchoring for their proper interaction with effectors such as RalBP1 or calmodulin (Falsetti et al., 2007). Ral proteins are also regulated by phosphorylation on serine residues in their C-terminal region (as shown in figure 4) inducing a relocalization of Ral proteins from the plasma membrane to internal membranes such as endocytic vesicles for proper vesicle trafficking (Martin et al., 2012; Wang et al., 2010). Finally, previous work done by our team demonstrated that both RalA and RalB proteins are ubiquitylated (Neyraud et al., 2012).

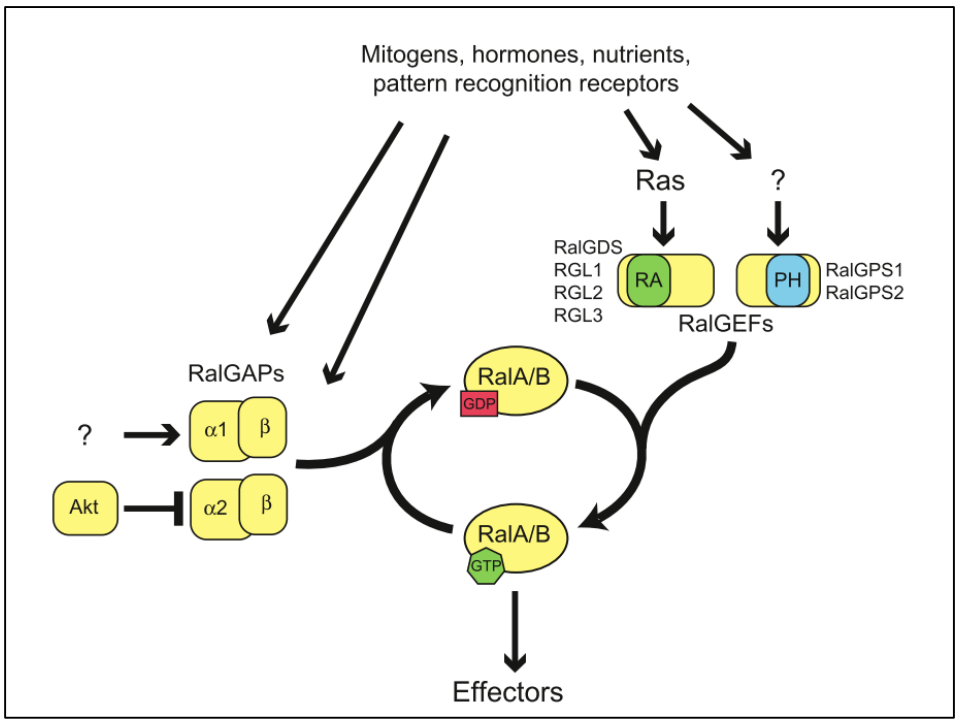

Figure 5 - Modulators of Ral GTPases.
The Ral guanine nucleotide exchange factors (RalGEFs) directly and specifically catalyze GDP/GTP exchange on Ral proteins, thus promoting an active signaling state in response to diverse stimuli. RalGEFs can be parsed into two main families based on the presence of a Ras-association (RA) domain (RalGDS, RGL1, RGL2/RLF, and RGL3) or the presence of a pleckstrin homology (PH) domain (RalGPS1A/B and RalGPS2). From Cooper et al., 2013.

1.3.2 – Effectors of Ral GTPases

Like other small GTPases, Ral proteins interact with a number of downstream effector when loaded with GTP in order to activate or modify key cellular mechanisms as shown in figure 6. *In vitro*, both RalA and RalB seems to interact with the same set of effectors, but the distinct biological functions of RalA and RalB are mediated by their subcellular localization and post-translational modifications, leading to distinct effector subset interaction.

1.3.2.1 – RalBP1/RLIP76

The first Ral effector to be described was RalBP1 (Ral-binding protein 1; also called RLIP76 or RIP1) in the 1990s (Jullien-Flores et al., 1995) who was identified as a Ral GTP-dependent interacting protein. RalBP1 highlighted a link between Ral proteins and the modulation of the actin cytoskeleton: RalBP1 harbour a RhoGAP catalytic domain activating CDC42 (that can stimulates filopodia) and Rac small GTPases (that stimulates lamellipodia formation) (Cantor et al., 1995). More, RalBP1 overexpression has been identified in a wide spectrum of cancers and suppression of RalBP1 can impair tumorigenic growth (Singhal et al., 2007).

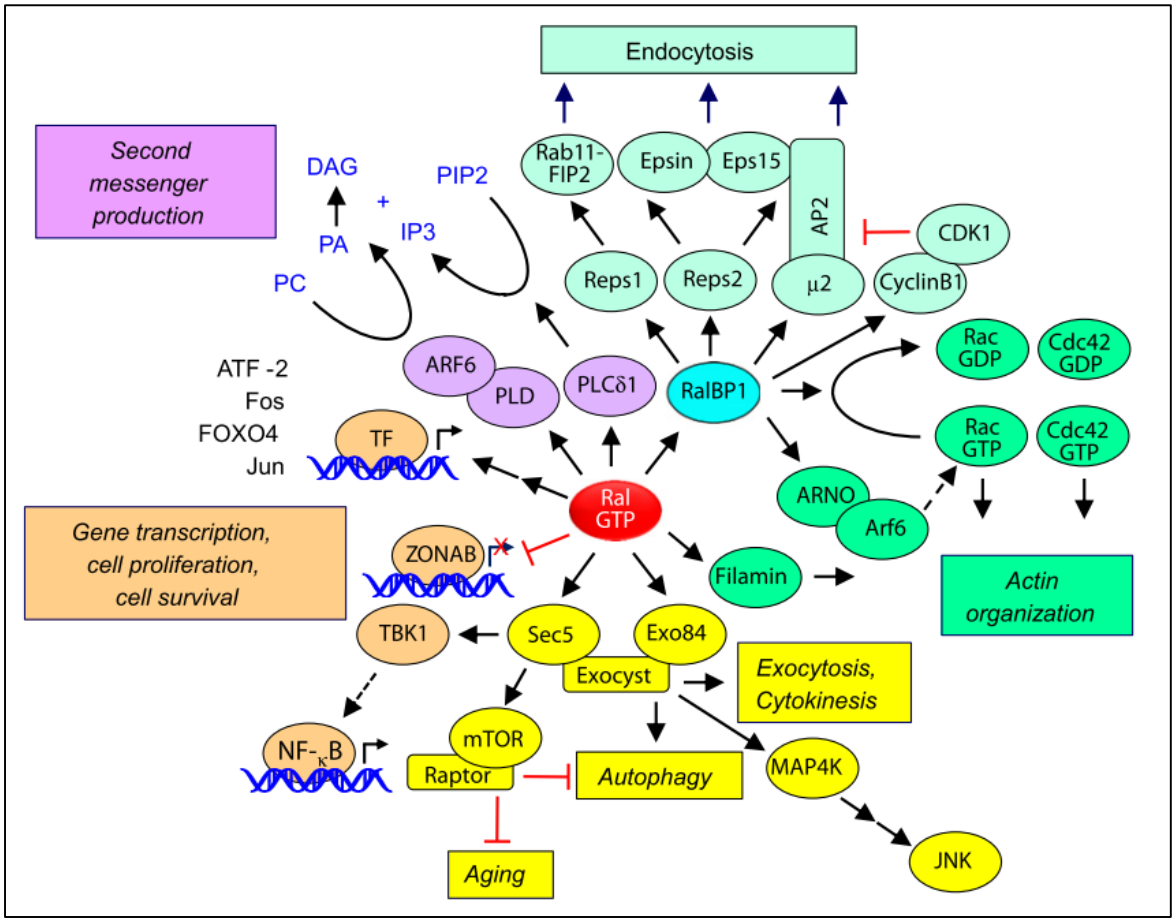

Figure 6 - Ral effectors and effector functions.
Active Ral can bind to a variety of downstream effectors and modulate numerous cellular activities. As example, RalBP1 acts as a RhoGAP as well as a scaffold for other proteins that regulate endocytosis and other cellular processes. More, Ral association with Sec5 or Exo84 can regulate Exocyst-dependent and -independent processes. Other effectors processes include regulation of cell cycle progression, actin organization and gene transcription. From Gentry et al., 2014.

1.3.2.2 – The Exocyst complex

The exocyst is an evolutionarily 734 kDa conserved eight-protein complex which comprises the Sec3, Sec5, Sec6, Sec8, Sec10, Sec15, Exo70 and Exo84 subunits (EauClaire and Guo, 2003) and was first identified in *Saccharomyces cerevisiae* in the late 1970s (Novick and Schekman, 1979). On the whole, the exocyst mediates the targeting and tethering of post-Golgi secretory vesicles to specific plasma membrane domains and more precisely, the exocyst complex is involved in various cellular functions such as epithelial cell polarity (Grindstaff et al., 1998), cell migration (Rossé et al., 2006) and autophagy (Bodemann et al., 2011) for example. Direct association of Ral proteins with the Sec5 and Exo84 subunits of the exocyst has been reported several time to be important for its subcellular localization. Inhibition of Ral GTPase activity lead to perturbed exocytosis disrupted delivery of membrane proteins in epithelial cells (Moskalenko et al., 2003). Moreover, expression of a constitutively activated Ral mutant is sufficient to promote delivery of secretory vesicles to basolateral membranes (Moskalenko et al., 2002).

1.3.2.3 – Other effectors

Another effector of Ral proteins is the phospholipase D1 (PLD1) but unlike other effectors, association with Ral is not GTP-dependent (Kim et al., 1998). For example, RalA – PLD1 interaction has been reported to promote proper p27 localization allowing proper TGF-β signaling (Tazat et al., 2013) as well as the mTORC1 signaling (Xu et al., 2011) and both RalA and RalB interaction with PLD1 has been shown to be critical for HeLa cell cytokinesis (Cascone et al., 2008). Filamin, an important component of the actin cytoskeleton involved in actin crosslinking, associates with RalA leading to lamellipodia formation in Swis-3T3 cells (where RalA fails to induces lamellipodia formation in human melanoma lacking in filamin expression) (Ohta et al., 1999). Finally, it has been reported that RalA is able to engage the transcription factor ZONAB (zonula occludens 1-associated nucleic acid binding protein) in a cell density manner: at high cell density, RalA engages ZONAB triggering the transcription of ZONAB target genes (Frankel et al., 2005).

1.4 – Functions of Ral GTPases and implication in tumorigenesis

Ral proteins have been shown to be potent players in regulating various mechanisms in the biology of cells such as cell cycle progression, trafficking of intracellular organelles, migration and motility, immune response, autophagy and anoïkis resistance (Gentry et al., 2014).

1.4.1 – Cytokinesis, vesicle trafficking, and cell polarity

Previous work by the team demonstrated that RalA and RalB play distinct roles in cytokinetic by mobilizing the Exocyst for two spatially and kinetically different steps. While RalA is required to tether the Exocyst to the cytokinetic furrow in the early steps of cytokinesis, RalB is required for Exocyst recruitment at this bridge, driving abscission and completion of cytokinesis (Cascone et al., 2008). Several publications have also highlighted the role of both RalA and RalB in both vesicle trafficking and cell polarity (Ngsee et al., 1991) and in cell polarity management (Hazelett et al., 2011). Finally, our team showed that Ral proteins are required the apical-basal polarity of post-mitotic epithelial cells maintenance during tissue remodeling where the lack of Ral activity resulted in subcellular localization defect of proteins implicated in apical-basal polarity (Belaiche et al., 2014).

1.4.2 – Cell migration

Our team reported in 2006, through loss-of-function analysis, that RalB, but not RalA, was permissive in cell migration. They highlighted, by wound-healing assay, that RalB depletion, but not RalA, reduced the re-population of the wound. They also reported that activated RalB associates with the Exocyst Sec5 subunit promoting both Exocyst assembly and its recruitment at the leading edge of

migrating cells (Rossé et al., 2006). Another publication from our team showed a more complex situation with the Ral-exocyst axis intervening at different legs: SH3BP1, a RhoGAP family protein, associates with the Exocyst complex in motile cells: they established a link between two motility-driving pathways, the Ral/Exocyst and the Rac signaling pathways (Parrini et al., 2011). Finally, another work from our team demonstrated a physical and functional connection between the Exocyst and the Wave regulatory complex (WRC) in cell motility. They reported that the Exocyst and the WRC complex associate independently of the Arp2/3 complex and that disruption of this interaction leads to impaired migration. Moreover, they also showed, using time-lapse microscopy coupled to image correlation analysis, that the Exocyst drive WRC recruitment at the leading edge in nascent protrusions resulting in cell edge movements (Biondini et al., 2016).

1.4.3 – Apoptosis/Survival and immune response

In 2003, a publication from collaborators of our team reported the distinct role of RalA and RalB in cancer cell survival (Chien and White, 2003). They revealed that RalA was dispensable for the proliferation of both normal and tumour-derived cell lines in adherent cultures but that RalA is required for anchorage-independent proliferation of transformed cells. On another hand, they showed that RalB is required to prevent transformed cells from initiating programmed cell death. More, they demonstrated that RalB activates TBK1 by promoting Sec5/TBK1 complex assembly, restricting initiation of apoptotic programs typically engaged In the context of oncogenic stress (Chien et al., 2006). Finally, our team demonstrated in *Drosophila melanogaster* that Ral acts as a negative regulator of a JNK-dependent apoptotic signaling through the exocyst complex (Balakireva et al., 2006). Taken together, these informations reveal the contribution of RalB to cancer cells survival and the implication of the RalB-Sec5 axis on TBK1-dependent innate immune signaling.

1.4.4 – Autophagy

Autophagy is a multi-step process that enable cells to survive to poor environmental growth conditions by recycling cell components. This recycling process is done by sequestration of cytoplasm portions in double-membrane cytosolic vesicles (called autophagosomes) that are degraded upon fusion with lysosome forming autophagolysosomes. Autophagy will be more extensively presented in section 3 of the introduction.

A publication from collaborators revealed that RalB, but not RalA, and the exocyst subunit Exo84 are required for autophagosome formation upon nutrient starvation (figure 7). In details, RalB is activated and localized to nascent autophagosomes on nutrient starvation and directly associates with Exo84. This direct interaction induces the assembly on the exocyst of catalytically active ULK1 and

Beclin1- VPS15-VPS34 -ATG14 complex that are required for proper membrane isolation and maturation during phagosome formation. In addition, expression of a constitutively active Ral (RalBG23V) in nutrient rich conditions was sufficient to induce autophagosome formation in human epithelial cells (Bodemann et al., 2011). It was reported that RalB ubiquitylation status is crucial for its functions in autophagy. In details, nutrient starvation induces RalB deubiquitylation by accumulation and relocalization of USP33 (a deubiquitylase) to RalB-positive vesicles (Simicek et al., 2013). This deubiquitylation promotes the assembly of the RalB-Exo84-Beclin1 complex cited above.

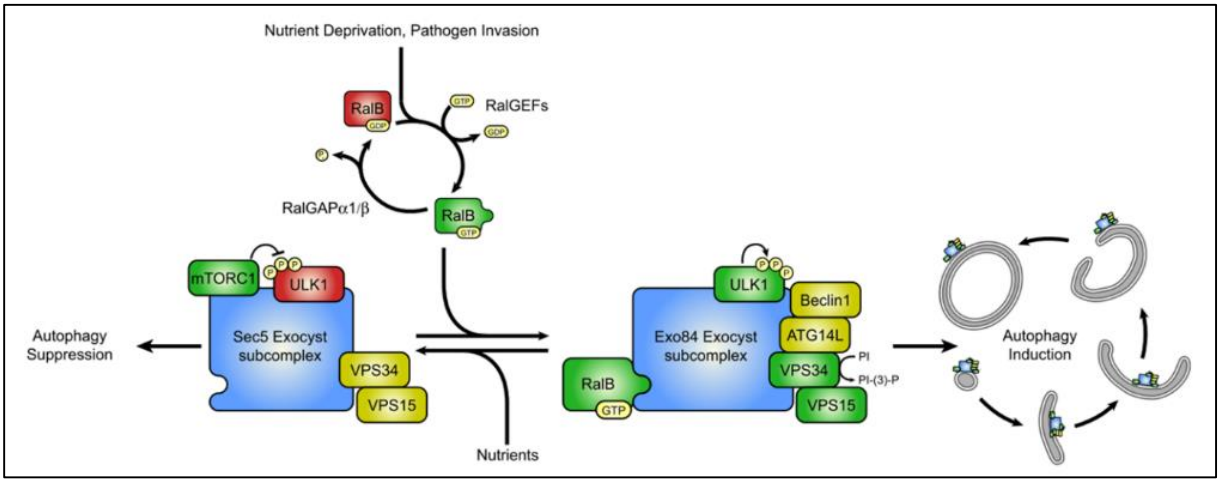

Figure 7 - Working model of RalB/exocyst dependent mobilization of autophagy.
Upon nutrient starvation, RalB is activated and associates with Exo84. This association mobilizes the assembly of Ulk1/Beclin1/ATG14/VPS15/VPS34 autophagy initiator complex. From Bodemann et al., 2011.

1.4.5 – Anoïkis resistance

Anoïkis means “homelessness” in Greek. When epithelial cells lose contact with their basement membrane, they undergo anoïkis-induced apoptosis, also known as suspension-induced apoptosis and implication of Ral proteins to this mechanism has been reported in the early 2000s (McFall et al., 2001). The authors started with epithelial cells characterized by oncogenic Ras supporting anoïkis resistance and found that Raf-1, Pi3K or RalGDS alone was not sufficient to promote Ras inhibition of anoïkis (they evaluated the implication of each Ras effector using specific Ras mutants that are able to select which effector to activate). They conclude that Pi3K and RalGEF likely cooperates with Raf to confer anoïkis resistance.

1.4.6 – RalA and RalB in Ras-oncogenesis

The oncogenic effects of Ral proteins were discovered only two decades ago, giving insights into the tumorigenic supportive role of Ral in a wide variety of cancer types. The chronic activation of both RalA and RalB was frequently reported in various tumor-derived cell lines vs non-tumorigenic

ones, supporting the functional significance of Ral proteins in cancer (Urano et al., 1996). A publication from 2003 highlighted the duality of function between Ral isoforms. They showed that RalA is required for anchorage-independent growth but not for the proliferation of adherent cells by using loss-of-functions experiments (Chien and White, 2003). Moreover, they reported that depletion of RalB leads to cancer cells apoptosis but has no impact on normal cell survival. Demonstrating that RalA, but not RalB is required for tumor initiation.

Finally, because Ras is one of the most mutated gene in human cancer it has been considered as a drug target since its discovery. Unfortunately, no drugs targeting Ras proteins directly or acting on Ras-driven effectors have been developed successfully (Gysin et al., 2011). Consequently, Ras downstream effectors have been studied as potential drug targets in Ras-driven cancers. Two of them, the RAS-MAPK pathway and the Pi3K-AKT pathway, have been intensively screened but have turned out as well to be quite disappointing in the clinic. RalGEF - Ral GTPases has not been yet explored as treatment target for patient harbouring Ras-driven cancer as much as the other Ras effectors. However, a team characterized small molecules targeting RalA and RalB which could be valuable as research tools and for cancer therapeutics few years ago (Yan et al., 2014) and it seems that focus start to concentrate on Ral GTPases as drug target since they start to be considered as therapeutic targets in cancer (Yan and Theodorescu, 2018).

One of the reason Ral was neglected is that is no easy to screen enzymatic activity activated by Ral and because the best target are protein-protein interaction? Not surprisingly, the best news on the front comes from academic research using stapled peptide approach (Thomas et al., 2016).

2 – The Hippo pathway, STK38, and cancer

The Hippo signal transduction pathway is an essential regulator of organ size during developmental growth by controlling multiple cellular processes such as cell proliferation, cell death, differentiation and stemness. Dysfunctional Hippo signaling pathway leads to dramatic tissue overgrowth (Yu and Guan, 2013). Here, we will briefly introduce the Hippo tumor suppressor pathway before focusing on one of its member: the STK38 kinase.

2.1 – The Hippo tumor suppressor pathway and its final contributor: YAP

The Hippo pathway was discovered more than a decade ago as a highly conserved signal transduction cascade that functions as a key co-ordinator of tissue growth control and homeostasis (Moon et al., 2018). From a classical point of view, the core cassette of the mammalian Hippo pathway comprises distinct signal transducers: the Ste20-like serine/threonine protein kinases MST1 and MST2 (also known respectively as STK4 and STK3), the AGC serine/threonine kinases LATS1 and LATS2, the SAV1 (aka WW45) and MOB1 scaffold proteins, and finally the transcriptional co-activators YAP and TAZ, functioning as major effectors of the Hippo pathway (Hong and Guan, 2012; Moroishi et al., 2015). As shown in figure 8, on its on-state, the Hippo pathway inhibits YAP/TAZ transcription activity through LATS1/2-mediated phosphorylation of YAP/TAZ on different serine residues, causing YAP/TAZ cytoplasmic retention and its latter degradation via the proteasome (Meng et al., 2016). When the Hippo pathway is turned off, the MST1/2 kinases does not activate LATS1/2, resulting in the nuclear accumulation of active YAP/TAZ and the transcription of target genes via association with TEAD1-4 transcription factors.

The Hippo pathway can be regulated by several mechanisms such as cell polarity, cell adhesion, and mechanotransduction. Some scientific publications reported that the tight junction (TJ)-associated scaffold protein agiomotin (Amot) is a critical regulator of the Hippo pathway by directly interacting with YAP/TAZ (Zhao et al., 2011). More, a major component of adherens junctions (AJs) has been also linked to the Hippo pathway: α-Catenin functions as a tumor suppressor by negatively regulating YAP1 activity during epidermal stem cell proliferation and tissue expansion (Schlegelmilch et al., 2011). Evidences have also been found about the implication of the Rho GTPases signaling pathway and mechanotransduction on the Hippo signaling pathway (Moon et al., 2018).

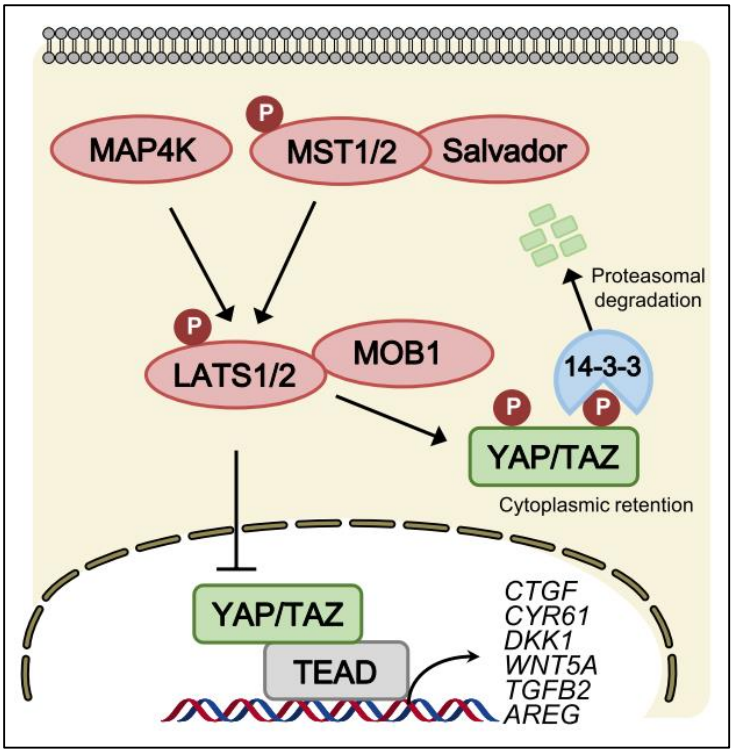

Figure 8 - Core Hippo pathway components in mammals.
The core Hippo pathway components are evolutionarily conserved. MST1/2 kinase phosphorylates LATS1/2 that in turn phosphorylates and inhibits YAP/TAZ by cytosolic sequestration and proteasomal degradation. From Moon et al., 2018.

Observations of overgrowth observed upon Hippo pathway dysregulation has led to the investigation of its role in cancer. It has been reported that hyperactivation of YAP/TAZ or TEAD, found in many human cancers, confers proliferative advantage, promotes cell migration, and enhances cell metastasis as well as drug resistance (Kim and Kim, 2017). Recent studies highlighted the role of the Hippo pathway in several aspects of altered metabolisms pathways in cancer cells. As example, YAP1 increases the glucose uptake in cancer cells by enhancing the transcription of the GLUT3 transporter (Wang et al., 2015). More, the mevalonate pathway of the cholesterol synthesis pathway activates YAP/TAZ via Rho GTPases, while inhibition of this pathway supresses YAP1 nuclear localization and YAP1-driven tumor growth (Wang et al., 2014). Finally, YAP1 activation by LATS1/2 deletion in cancer cells triggers an anti-tumor immune response via activation of the TLR–MYD88/TRIF pathway by secreting nucleic-acid-rich extracellular vesicles (Liu et al., 2016).

This linear signaling model served well for the initial studies of the Hippo pathway, but recent studies linked additional kinases as novel members of the Hippo signaling such as the AGC serine/threonine STK38 and STK38L (also known as NDR1 and NDR2, respectively) and members of the Ste20-like MAP4K family (see figure 9). In detail, members of the MAP4K kinase family are responsible of the phosphorylation of LATS1/2, resulting in YAP/TAZ transcription activity inhibition (Meng et al.,

2015a). Finally, a recent study, using a combination of biochemical, cell biological and genetic approaches, has established STK38/STK38L as additional YAP1 kinases (Zhang et al., 2015).

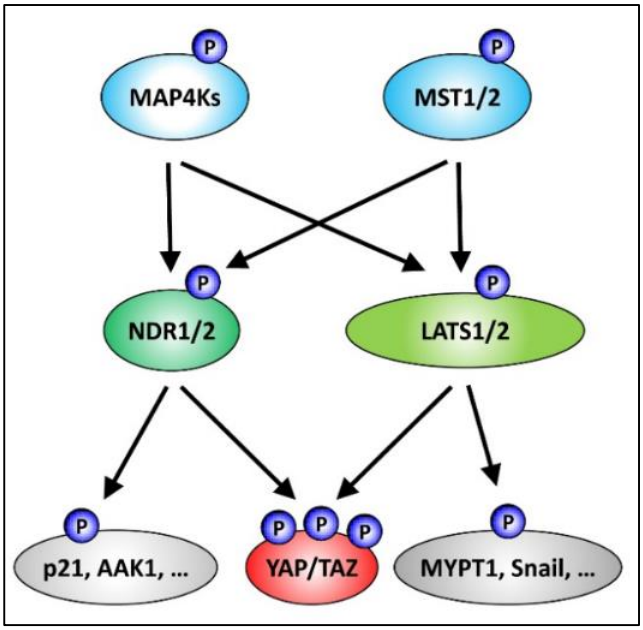

Figure 9 - New members in the Hippo signaling pathway: the STK38/STK38L kinases.
In addition to the previous members, the Hippo core cassette has been expended recently. ST1/2, members of the Ste20-like MAP4K. In addition to MST1/2, members of the kinase family can perform the activating phosphorylation of LATS1/2. Moreover, the AGC serine/threonine STK38/STK38L kinases can act as YAP kinases and can be activated by MAP4Ks and MST1/2. From Hergovich, 2016.

2.2 – The STK38 kinase family

The AGC (for protein kinase A (PKA)/PKG/PKC-like) class of protein kinases is the third largest represented group of kinases in the human cell by containing 70 proteins classed in 14 groups (Manning et al., 2002) such as the protein kinase A (PKA), the protein kinase B (PKB) and the protein kinase C (PKC) isoforms. All members of this class of protein kinases require phosphorylation on a conserved motif for their activation. Based on the sequence of their catalytic domain, the STK38 and STK38L (aka NDR1 and NDR2 respectively, for nuclear Dbf2-related 1/2) kinases define a subgroup of the AGC group of protein kinases. For reading simplicity, we will refer as the STK38 family to define these two kinases.

The STK38 family is evolutionarily conserved from yeast to human: members can be found in *Drosophila melanogaster* (Trc, tricornered), *Caenorhabditis elegans* (sensory axon guidance-1 (SAX-1)), Saccharomyces cerevisiae (Dbf2p and Dbf20p) *Schizosaccharomyces pombe* (Sid2p) and some other fundi and plants (Hergovich et al., 2006).

2.2.1 – Characteristics of STK38/STK38L

The primary structure of STK38 kinases family is well conserved from yeast to human as shown in figure 10. The activity segment that is located on subdomain VIII (yellow on the figure below) and the hydrophobic motif located at the C-terminus (brown in the figure below) are present in all STK38-family proteins and are essential for the catalytic activity of STK38 kinases, indicating a conserved activation mechanism (Millward et al., 1999). The STK38 family members contain typical features of AGC protein kinases: the activation segment and the hydrophobic motif above-cited, but also two specific features: an insertion in subdomains VII and VIII of 30-60 residues and a conserved N-terminal regulatory (NTR) domain (Hergovich et al., 2005). This NTR domain is also known as the S100B/hMOB1 association (SMA) domain because both S100B (a S100 family EF-hand calcium-binding protein) and hMOB1A can bind to this domain of human STK38 protein (Bichsel et al., 2004; Millward et al., 1998). This NTR domain contains a high number of basic hydrophobic amino acids that mediate the interaction of STK38 kinases with the MOB regulators (Hergovich et al., 2005).

Beside the NTR domain, the 30-60 residues insertion in subdomains VII and VIII above-cited contains a region rich in basic residues located at the C-terminal end of this insert. This positively charged domain is immediately followed by the activation segment and seems to negatively regulates STK38 activity: a significant increase of STK38 and STK38L kinase activity is reported when these positives residues are mutated to alanines (phospho-negatives) (Bichsel et al., 2004). This short motif is then referred as an auto-inhibitory sequence (AIS).

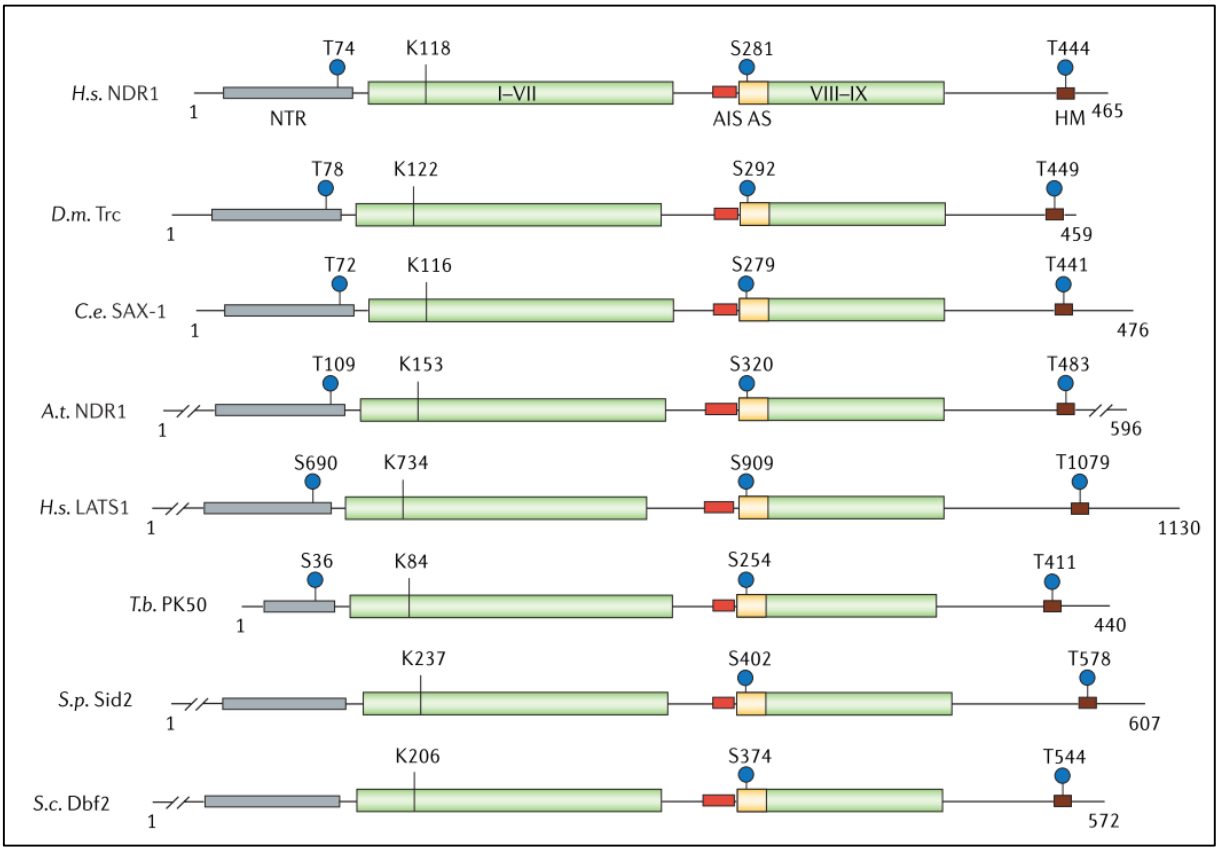

Figure 10 - Common characteristics of STK38 kinases.
Eight members of the STK38 kinase family are represented from unicellular and multicellular organisms (H.s. *Homo sapiens*, D.m. *Drosophila melanogaster*, C.e. *Caenorhabditis elegans*, A.t. *Arabidopsis thaliana*, T.b. *Trypanosoma brucei*). The NTR (grey), the kinase domain (green) with the activation segment (yellow) and the hydrophobic motif (brown) are indicated. In addition, the auto-inhibitory sequence (red) and conserved phosphorylation sites (blue dots) are highlighted. From Hergovich et al., 2006.

2.2.2 – Regulation of STK38

Extensive biochemical analysis have been carried out in mammalian cells in order to understand the molecular mechanisms regulating STK38 and STK38L kinases in the past years. In this section, we will resume how human STK38 (and STK38L) kinase is regulated by post-translational modifications such as phosphorylation or ISGylation (Takeuchi et al., 2006) and by their association with regulators.

2.2.2.1 – Regulation by phosphorylation

In a simple mindset, STK38 is activated by phosphorylation and inactivated by de-phosphorylation. STK38 contains two main regulatory phosphorylation sites required for its kinase activity: one in the activation segment at Ser281/Ser282 and one in the hydrophobic motif at Thr442/Thr444 (as shown in figure 11) that are well conserved in all STK38 kinase family identified. It was discovered that MST1, MST2 and MST3 can phosphorylate both STK38 and STK38L on Thr442/Thr444 in their hydrophobic motif, inducing activation of the kinase (Hergovich, 2013). It has

also been reported that, unlike other AGC protein kinases, STK38 activation is also regulated by autophosphorylation on this same activation segment (Stegert et al., 2004).

In addition, mutation of both activation segment and hydrophobic motif phospho-acceptor residues into Alanine, almost completely abolishes the kinase activity of STK38 and STK38L (Millward et al., 1999). More, purified PP2A (for protein phosphatase type 2A) is able to completely inactivate STK38, indicating that this multi-site phosphorylation/de-phosphorylation cycle is a general mechanism controlling STK38 activation.

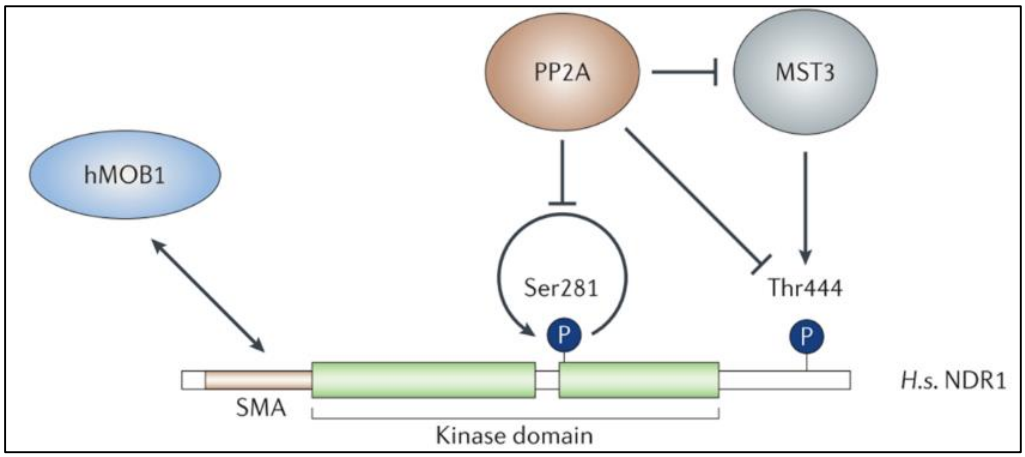

Figure 11 - Regulation of STK38 kinases at the molecular level.
Primary structure of human STK38 (aka NDR1). The hMOB1A/B association domain (SMA) and phosphorylation of Ser281 (activation segment) and Thr444 (hydrophobic motif) are shown. Binding of MOB1 to the N-terminus of STK38 (residues 15 to 80) stimulates the activity of STK38 which results in its auto-phosphorylation on Ser281. After phosphorylation on Thr444 by MST3, the STK38-MOB1 complex is fully active. PP2A removes the phosphate groups on Ser281 and Thr444, thus inactivating the kinase. From Hergovich et al., 2006.

2.2.2.2 – Ste20-like kinases

Ste20-like kinases interact with, and phosphorylate, members of the STK38 family, a role that have been first identified in fly and yeast. The yeast Ste20-like kinases (Kic1p, Nak1p, Sid1p, and Cdc15p) were shown to act upstream of the yeast STK38 kinases (Cbk1p, Orb6p, Sid2p, and Dbf2p), but only Cdc15p has been shown to activate its mammalian corresponding STK38 by direct phosphorylation (Mah et al., 2001). Moreover, the MST1/2 and the MST3 kinases, other closely-related Ste20-like kinases, can phosphorylate both STK38 and STK38L on their specific Thr444 residue located in the HM (Dan et al., 2001; Stegert et al., 2005a) depending on STK38 subcellular localization (Visintin and Amon, 2001). Additionally, MAP4K (mitogen-activated protein kinase kinase kinase kinase)-type kinases, which are also members of the Ste20-like kinases family, can regulate STK38/STK38L through phosphorylation on their HM (Meng et al., 2015b).

In this context, our team recently reported that RalA and MAP4K4 activate STK38 upon stress response and apoptotic signaling. In detail, we reported that the Ste20-like kinase MAP4K4, an effector of RalA via the exocyst complex, directly phosphorylates STK38 on its Thr444 under osmotic and oxidative stress (Selimoglu et al., 2014). Moreover, we found that TNF-α (for tumor necrosis factor α) triggered apoptosis induction signals through this RalA-MAP4K4-STK38 pathway.

2.2.2.3 – Activation by MOBs

Another layer of complexity can be added on the STK38 activation processes: the MOB family adaptor proteins (for Mps one binder). In the Hippo core signaling, MOB1 can acts as a central adaptor by directly interacting with MST1/2, LATS1/2 and STK38/STK38L kinases (Hergovich, 2011). These interactions were first identified in *S. cerevisiae*: Mob1p has been characterized as a regulator of Dbf2 (homologue of human mammalian STK38) subcellular localization and activity (Komarnitsky et al., 1998). The human genome encodes 6 MOB related proteins (hMOB1A/B, hMOB2 and hMOB3A/B/C) while only MOB1A/B and MOB2 have been reported to directly interact with STK38 kinases. MOB proteins bind to the conserved NTR of STK38 that precedes the catalytic domain, releasing STK38 from autoinhibition (Hergovich, 2013), interaction that is well conserved in all members of the STK38 kinase family.

Regarding STK38 activation by MOB proteins, current evidences suggest that MOB1 phosphorylation on Thr12 and Thr35 by MST1/2 can regulate MOB1 binding to the NTR of STK38 where some studies showed that MOB1 binding to STK38 can have multiple functions. First, this binding can stimulate STK38 auto-phosphorylation on the serine residue located in the T-loop (Hoa et al., 2016). More, it has been reported that MOB1 binding to STK38/LATS kinases is required for their HM phosphorylation by MST1/2 in human cells (Hergovich et al., 2009). It has also been reported that the MOB1/STK38 complex formation seems to be essential for STK38 activation by STK38 autophosphorylation on Ser281 and HM phosphorylation at Thr444 by MST1 (Cook et al., 2014). See figure 12 for a model of activation of STK38 kinases family by MST and MOB proteins.

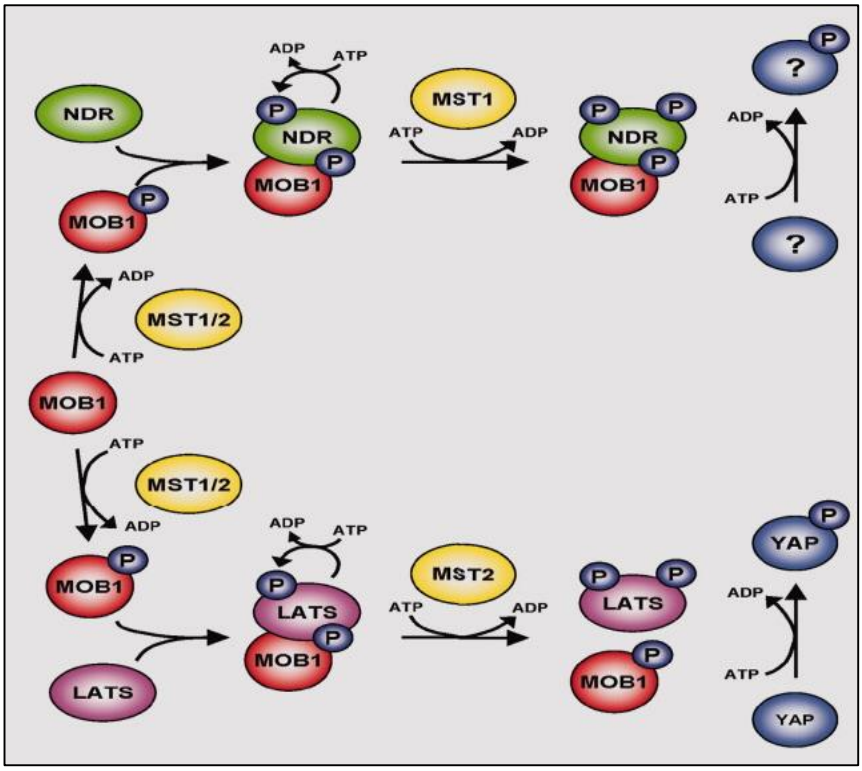

Figure 12 - Current model of STK38 family kinase activation by MST kinases and MOB1 proteins.
MST1/2 phosphorylate MOB1 which results in efficient complex formation with STK38 kinases. Binding of MOB1 to STK38 kinases facilitates auto-phosphorylation on the activation segment (Ser281 of STK38). Fully active STK38 kinases subsequently phosphorylate substrates such as YAP. It seems that for substrate phosphorylation, STK38/STK38L seem to stay in a complex with MOB1, whereas LATS1/2 do not seem to depend on MOB1 binding for persistent activity. From Hergovich and Hemmings, 2009.

2.2.2.4 – Scaffolding proteins and cellular localization

A group of scaffolding proteins have been identified in yeast, *C. elegans*, *D. melanogaster*, and human as the third main component in the regulation of STK38 kinase family (Gallegos and Bargmann, 2004). In detail, it has been shown in yeast that Tao3p and Mob2p interact genetically and biochemically with the Cbk1p and Orb6p kinases (homologues of human STK38), respectively, interaction important for kinases activation. In *C. elegans* and *D. melanogaster*, SAX-2 and Fry (for Furry) also exhibit a strong genetic interaction with SAX-1 and Trc, homologues of human STK38 (Hergovich et al., 2006), respectively. It has also been reported that STK38 kinase activity is required for chromosome alignment during cytokinesis, kinase activity being under the dependency of Fry and MST2 (Chiba et al., 2009). These results suggest that MST2, Fry, and MOB2 are crucial for STK38 activation. Finally, it has been shown that targeting MOB proteins to the plasma membrane was sufficient to activate both STK38 and STK38L (Stegert et al., 2005b).

It appears that STK38 kinases are regulated by a wide spectrum of mechanisms at various levels. Phosphorylation by Ste20-like kinases, dephosphorylation by PP2A, MOB binding to the N-terminus, association with scaffolding proteins, and cellular localization seems all to regulate STK38 activity and functions. These multiple regulations mechanisms reflect the requirement for stringent spatial and temporal activation systems.

2.2.3 – Biological functions of STK38

As a general model, it has been reported that mammalian STK38 is not essential for development because STK38 deficient mice are viable: loss of STK38 seems to be compensated by upregulation of STK38L protein level. Here, we will provide a general overview of the cellular functions of STK38 kinases as in cell cycle progression, centrosome biology, apoptosis, autophagy, DNA damage signalling, and other signaling pathways.

2.2.3.1 – Centrosome duplication

The first function in mammals attributed to both STK38 and STK38L are their role in centrosome duplication, a primary microtubule-organising center regulating many cell mechanisms. As a first insight, STK38 kinases have been detected on centrosomal structures throughout the entire cell cycle (Johnson et al., 1996). More, overexpression of STK38/STK38L resulted in centrosome overduplication in a kinase-dependent manner while expression of kinase-dead (kd) STK38/STK38L or depletion of STK38/STK38L by small interfering RNA (siRNA) negatively affected centrosome duplication (Hergovich et al., 2007). It has also been reported that STK38/STK38L kinase activity regulates centriole duplication directly on the centrosome in a Cdk2-dependent manner. As a final layer on STK38/STK38L impact on centrosome duplication, further work demonstrated that STK38/STK38L function on centrosome duplication rely on their interaction with MOB1A/B and the regulation of their HM phosphorylation by MST1 (Hergovich et al., 2006).

2.2.3.2 – Cell cycle progression

STK38 have also been linked to the regulation of G1/S cell cycle progression through the regulation of c-myc and p21/Cip1 protein level. In detail, it has been reported that STK38/STK38L control the G1/S transition downstream of the Hippo kinase MST3 (aka STK4) by stabilizing c-myc and preventing p21 accumulation (Cornils et al., 2011a). Interestingly, this research article identified p21 as the first direct *in vivo* substrate for mammalian STK38/STK38L kinases by phosphorylation on its Ser146. They reported that in the absence of STK38 kinases, unphosphorylated p21 accumulates in the cell, resulting in G1-arrest and impaired cell proliferation while overexpression of STK38/STK38L

resulted in p21 degradation. In addition, it has been shown that Cyclin D1 promotes cell cycle progression by enhancing STK38/STK38L kinase activity independently of Cdk4 (Du et al., 2013). In detail, it has been show that Cyclin D1 directly interact with STK38/STK38L, increasing their kinase activity required for the G1/S transition.

Additionally, it has been reported that both STK38 and STK38L directly bind to c-myc, independently of their kinase activity, and that this interaction requires the phosphorylation of their HM domain (Cornils et al., 2011b). C-myc is a transcription factor regulating cell proliferation, growth, apoptosis, and differentiation with protein levels tightly regulated by both transcriptional and post-transcriptional mechanisms, since defects in controlling c-myc levels result in tumor development (Adhikary and Eilers, 2005). C-myc directly interacts with the NTR (residues 1 to 82) of STK38 for its stabilization, interaction being modulated by STK38's HM phosphorylation status. It has been reported that STK38 overexpression increased the endogenous c-myc level, as well as stimulation of STK38's HM domain phosphorylation by MST3 overexpression. This relationship has been functionally tested in c-myc-addicted lymphoma: STK38 silencing resulted in c-myc protein level decrease and apoptosis of cancer cells (Bisikirska et al., 2013).

2.2.3.3 – DNA damage signaling

By competing with MOB1 for binding to STK38/STK38L, MOB2 can interfere with STK38/STK38L activation. Because MOB2 functions as a DNA damage response (DDR) factor, this binding competition could suggest a potential role of STK38/STK38L in the DDR (Gomez et al., 2015). As a first insight, it has been reported that STK38 interacts with XPA (Xeroderma pigmentosum A protein), a protein involved in DDR by triggering the nucleotide excision repair (NER) pathway (Park et al., 2015). In this publication, they showed that STK38 increases its nucleus localisation after UV irradiation of cells while STK38 silencing delayed the DNA repair after UV irradiation in both normal and cancer cells.

In addition, it has been reported that STK38 regulates also the DNA damage-induced G2/M checkpoint by directly phosphorylating CDC25A (for cell division cycle 25 homologue A) at Ser76, leading to CDC25A degradation (Fukasawa et al., 2015). This publication indicates that phosphorylation of CDC25A by STK38 and its subsequent degradation are required to promote DNA damage-induced G2/M checkpoint activation.

2.2.3.4 – Immune response

Studies performed with T-cell specific double knockout of STK38/STK38L in mice revealed that STK38/STK38L function downstream of MST1 in thymocytes and are required for thymocyte exit and migration (Tang et al., 2015). It has been also shown that STK38 plays an important role in the innate immune response by reducing cytokine secretion, limiting inflammation (Wen et al., 2015). Further evidences supporting the role of STK38/STK38L in immune system come from studies linking STK38/STK38L kinases to diseases associated with defective immunity system. As example, it has been reported that HIV-1 protease can target STK38/STK38L and that knockdown of STK38 reduced human influenza virus replication (Atkins et al., 2014; Devroe et al., 2005).

2.2.3.5 – Autophagy

A recent article from our team revealed the role of STK38 in autophagy regulation (see part 3 of the introduction). Using yeast two hybrid (Y2H) screens, we identified STK38 as a novel binding partner of Beclin1, a key regulator of autophagy (Joffre et al., 2015). We showed that STK38 promotes autophagosome formation in human cells and in *Drosophila* in a kinase-dependent manner. STK38-depleted cells displayed impaired LC3B-II conversion and reduced puncta formation of the autophagic markers ATG14L, ATG12, and WIPI-1 upon autophagy induction. More, we found that STK38 supports the interaction of the exocyst component Exo84 with Beclin1 and RalB (see part 1.3.2 of the introduction) and that STK38 activity is stimulated in a MOB1- and Exocyst-dependent manner.

In contrast, RalB depletion triggers hyperactivation of STK38, resulting in STK38-dependent apoptosis under prolonged autophagy conditions (Joffre et al., 2016). The figure 13 represents a current working model of STK38-dependent induction of autophagy. These results indicate that STK38 is a conserved regulator of autophagy in human cells and flies and that both STK38 and RalB assist the coordination between autophagic and apoptotic events upon autophagy induction.

2.2.3.6 – Mitochondrial quality control

Eukaryotes employ elaborated mitochondrial quality control (called mitophagy) in order to maintain the function of this power-generating organelle where Parkinson's disease-associated PINK1 and Parkin proteins are involved in. A publication from 2013 reported that, in flies, Pink1 induces STK38 (Trc) relocalization to the mitochondria, resulting in STK38 phosphorylation (Wu et al., 2013). They also reported in HeLa cells that knockdown of STK38, but not STK38L, led to altered mitochondrial distribution, compromised recruitment of Parkin by Pink1 to the mitochondria, and therefore delayed clearance of damaged mitochondria. Importantly, they showed that STK38 silencing significantly attenuated Parkin phosphorylation, consistent with Parkin acting downstream of STK38.

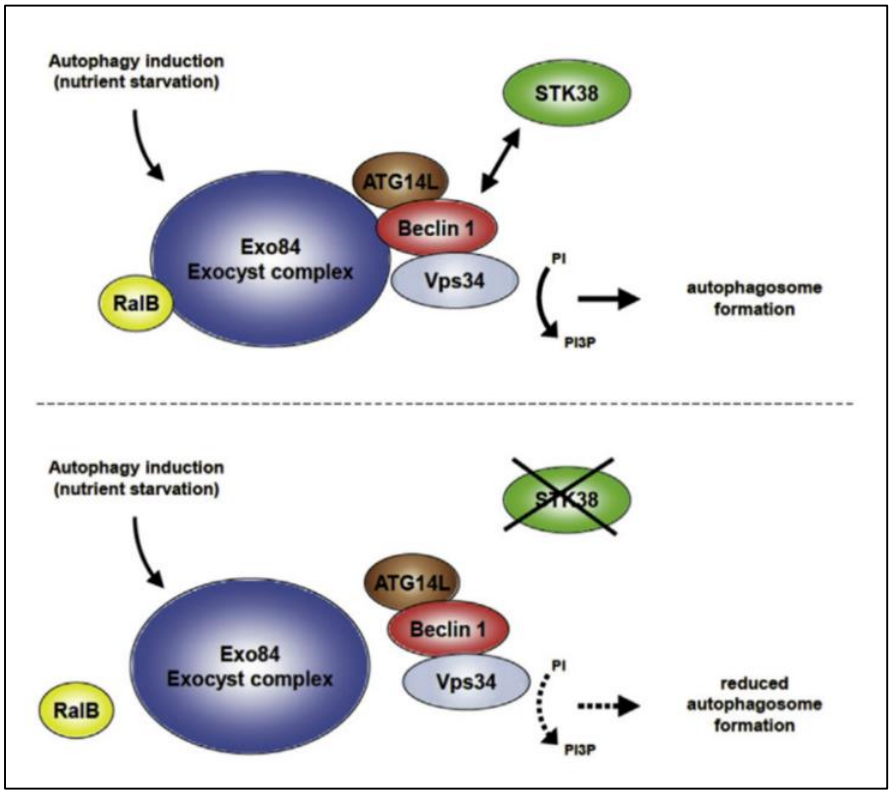

Figure 13 - Working model of STK38-dependent induction of autophagy.
STK38 loss of function interferes with Exo84/RalB and Exo84/Beclin1 interactions, which are required to efficiently initiate PI3P formation by the Beclin1-ATG14L-Vps34 complex. Therefore, upon STK38 depletion, PI3P levels are lower and ATG14L recruitment to autophagosomes is impaired, consequently resulting in reduced autophagosome formation. From Joffre et al., 2015.

2.2.3.7 – Anoïkis resistance

One of the last publication of our team provided its contribution to the role of STK38 to anoïkis survival in Ras-driven cancer cells (Bettoun et al., 2016). We reported that STK38 knockdown impaired anoïkis resistance, anchorage-independent soft agar growth, and *in vivo* xenograft growth of Ras-transformed human cells. We showed that STK38 supports Ras-driven transformation through promoting detachment-induced autophagy and that STK38 is required to sustain the removal of damaged mitochondria by mitophagy (see part 3.4.2.3 of this introduction for more detailed informations). Moreover, knockdown of Pink1 or Parkin, two positive regulators of mitophagy, also impaired anoïkis resistance and anchorage-independent growth of Ras transformed human cells. These results shed light on the supporting oncogenic role of STK38 in Ras-dependent cancer cells.

2.2.3.8 – STK38 and NF-κB

A link between STK38 and the NF-κB signaling pathway has emerged since few years. The first hint in this relationship started in 2012 when STK38 has been shown to potentiates NF-κB (for nuclear factor-kappa B) activation by its kinase activity (Shi et al., 2012). The authors showed that overexpression of STK38 potentiates NF-κB activation induced by TNFα whereas knockdown of STK38

inhibits NF-κB activation. They also revealed direct interaction of STK38 with multiple components of the NF-κB signaling pathway. More, siRNA against STK38 and its replacement with kd mutants resulted in defect of NF-κB activation by TRAF2 (a NF-κB activator).

Another publication reinforced the nascent role of STK38 on the NF-κB signaling pathway. The authors showed that SOCS2 (a pleiotropic E3 ligase) interacts with STK38 and promotes its degradation through K48-linked ubiquitination (Paul et al., 2017). In addition, overexpression of SOCS2 antagonizes STK38-induced TNFα-stimulated NF-κB activity. This study is the first report of an identified E3 ligase for STK38 and strengthen the role of STK38 on the NF-κB signaling pathway as shown in figure 14.

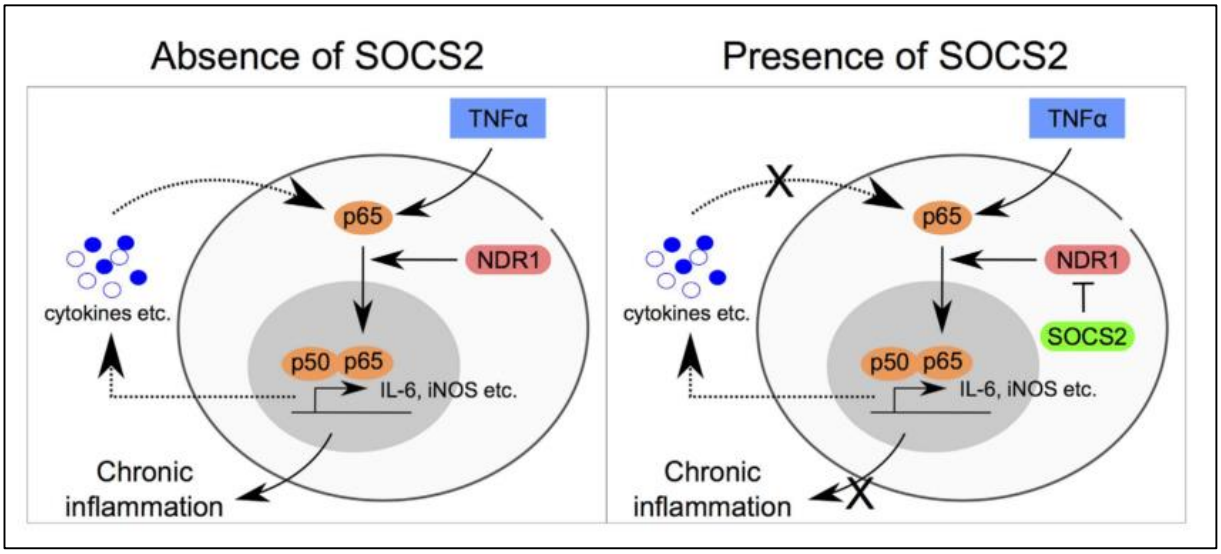

Figure 14 - Model of SOCS2-mediated regulation of TNFα/NF-κB signaling through STK38 ubiquitination and degradation. In the presence of SOCS2, STK38 (aka NDR1) is repressed and cannot induce NFκB targets genes expression and thus inflammation. From Paul et al., 2017.

2.2.4 – STK38 and cancer

It appears that mammalian STK38/STK38L kinases could have opposing roles in tumorigenesis and can function as tumor suppressor proteins or oncogenes. By positively controlling centrosome duplication and proliferation, STK38 could provide oncogenic properties. More, overexpression of STK38 in human cells leads to centrosome over-duplication, leading to extra centrosomes and chromosomal instability if regulation and repair networks are deregulated. In addition, STK38 could act as an oncogene by controlling the cell cycle progression where overexpression of STK38 could potentially leads to extra proliferation. In this same field, it has been shown that overexpression of STK38 leads to overexpression of the proto-oncogene c-myc. In addition, STK38 mRNA levels are found upregulated in both lung adenocarcinoma and ovarian cancer and STK38 protein level is found increased in some melanoma cell lines (Hergovich et al., 2008).

On another hand, STK38 can also be characterized as a tumor suppressor. It has been reported that STK38 plays a crucial role in apoptosis induction in response to death receptor activation, as well as in the inhibition YAP1 activation. Significantly, the expression of STK38 kinases is deregulated in numerous type of cancer. In most cases, levels of STK38 are decreased but can be found increased in few cases (Sharif and Hergovich, 2017). These results attest that STK38 might have opposing roles in cancer, by either functioning as tumour suppressor protein or oncogene, as already reported for factors such as Ras, TFBβ or NOTCH1 (Rowland and Peeper, 2006). Reciprocally, the role of STK38 supporting DNA repair mechanism could help to overcome chemotherapies-induced DNA injuries. Furthermore, there is a predictive value of the level of STK38 mRNA in the outcome of patients with breast, ovarian, and lung cancer but not for gastric cancer (figure 15).

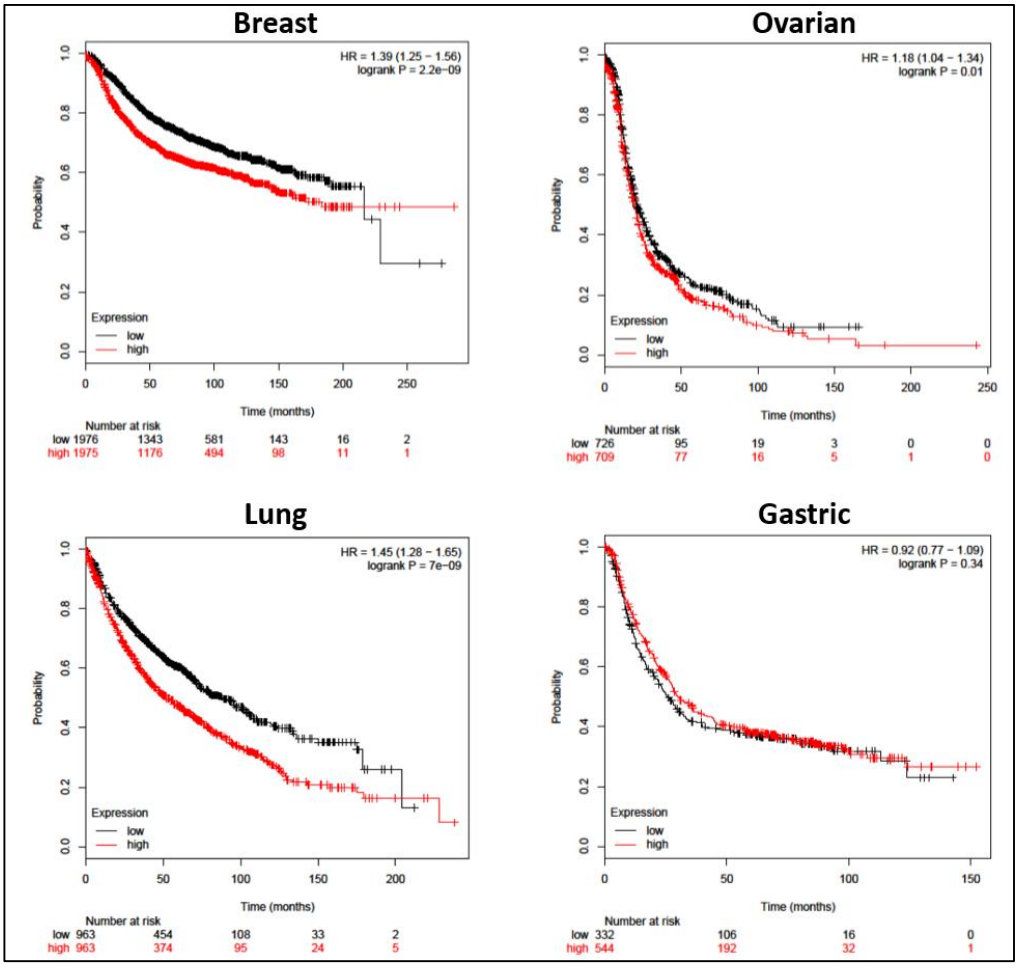

Figure 15 – STK38 mRNA impact on patients survival.
Overall survival information of patients with four different types of cancer according to the mRNA level of STK38. The *http://kmplot.com* online software was used to compute prognostic analysis in all types of patients from all available databases.

3 – Autophagy

Surprisingly, the term "autophagy" was already in use in the 1860s, almost a century before the discovery of the lysosome by Christian de Duve in 1955. At this time, this term referred to a concept that the human body possesses a self-nourishment mechanism, which permits to survive at times of nutrient deprivation by feeding off itself (Ktistakis, 2017). It was de Duve who used the term autophagy, in 1963, according to its current definition: the cellular process through which intracellular materials are delivered to the lysosome or vacuole for degradation (Klionsky, 2008). Here, we will define autophagy, describe its well-controlled steps, enumerates the mechanisms that can trigger autophagy and finally its contribution to tumorigenesis.

3.1 – Autophagy: definition

Autophagy is a cellular degradation of "self-eating" pathway highly conserved throughout all life kingdoms responsible for the degradation of proteins as well as excessive or damaged organelles whose disintegrated components are reused during biosynthesis of new macromolecules (Mizushima and Komatsu, 2011). This quality control mechanism plays an important role by maintaining cellular homeostasis and is constitutively active at basal level in most cell types, contributing to degradation of superabundant, abnormal, damaged or risk factors. However, autophagy can be additionally enhanced to meet the cellular demands during different stress conditions that will be detailed later in this introduction (Mizushima and Levine, 2010).

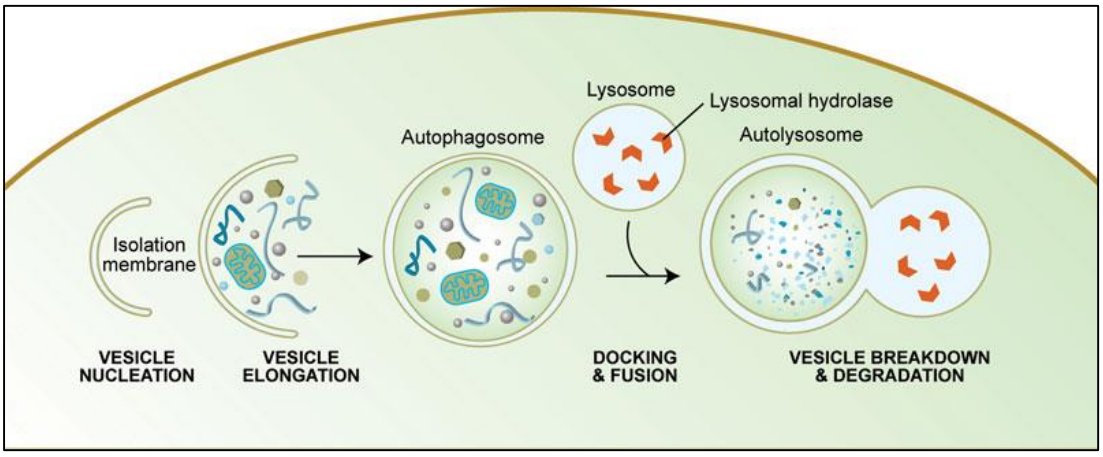

Figure 16 - Schematic diagram of the autophagy steps.
Autophagy begins with the formation of the phagophore and is followed by the expansion of the phagophore into an autophagosome (vesicle elongation). The autophagosome can engulf bulk cytoplasm non-specifically, including entire organelles, or target cargos specifically. When the outer membrane of the autophagosome fuses with an endosome, it forms an autophagolysosome. Finally, the sequestered material is degraded inside the autophagolysosomes and recycled. From Meléndez and Levine, 2009.

Three major subtypes of autophagy have been characterized according to the pathways that deliver cargo to the lysosomes: macroautophagy (that will be simply referred as autophagy hereafter), microautophagy, and chaperone-mediated autophagy. Macroautophagy is the best characterized form of autophagy and depends on specialized double-membrane vesicles, known as autophagosome, that progressively package autophagic cargoes and deliver them to the lysosomes by membrane fusion (figure 16). On another hand, microautophagy relies on the direct uptake of cytoplasmic material through lysosomal membrane invagination, a less complex mechanism. Finally, chaperone-mediated autophagy involves the lysosomal-associated membrane protein 2 (LAMP2)-dependent translocation of autophagic substrates bound to cytosolic chaperones of the heat shock protein family across the lysosomal membrane (Marinkovi et al., 2018) (figure 17).

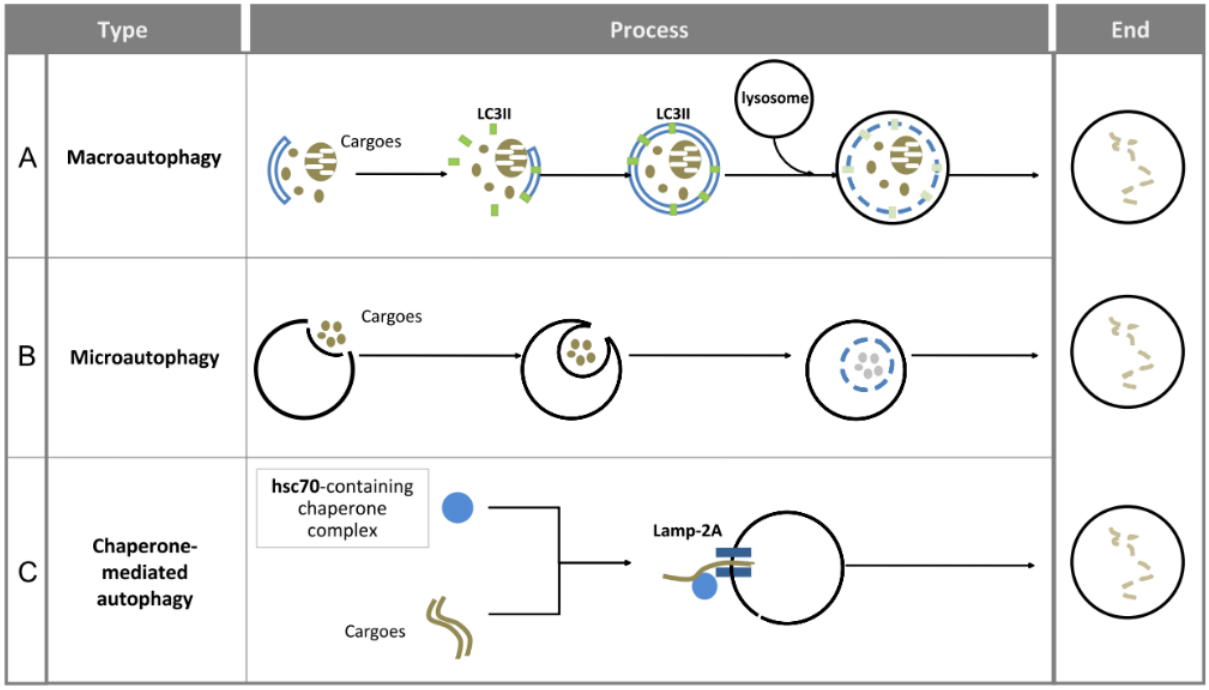

Figure 17 - Different forms of autophagy.
Macroautophagy, microautophagy and chaperone-mediated autophagy are three types of autophagy in mammals. Here, the main steps in these processes as well as the most important characteristic structures and the related mediators are presented. From Yang et al., 2013.

The process of classical autophagy mainly consists of five successive steps directly and rhythmically regulated by various autophagy-modulating genes and proteins: induction, vesicle nucleation, vesicle elongation, docking & fusion, and finally, degradation and recycling as shown in figure 17 (Ke et al., 2016). It have to be noticed that autophagy was thought to be an entirely non-selective process regarding the selection of cargoes to be degraded. However, current knowledge demonstrates that autophagy seems to be highly selective by regulation through specific cargo-receptor proteins (Xie and Klionsky, 2007).

The proper definition for microautophagy came in the early 1980s and is characterized by a lysosomal/vacuolar membrane randomly invaginated and differentiated into autophagic tubes enclosing portions of the cytosol (Li et al., 2012a). As macroautophagy, microautophagy was first described as non-selective but recent studies reported that some selective forms occur. The non-exclusive microautophagy (usually referred as microautophagy) engulfs soluble intracellular substrates by tubular invaginations while the selective microautophagy (*e.g.*, micropexophagy, piecemeal microautophagy of the nucleus, micromitophagy) sequesters specific organelles with arm-like protrusions.

The chaperone-mediated autophagy is one of the proteolytic mechanism that contributes to degradation of intracellular proteins in lysosomes. In details, the chaperone heat shock cognate protein of 70kDa (HSC70) recognizes soluble cytosolic target proteins containing KFERQ or KFERQ-like sequence motifs, and deliver them to the lysosomal lumen through specific interaction between the HSC70 protein complex and the lysosome-associated membrane glycoprotein type 2A (LAMP2A) (Cuervo and Wong, 2014).

3.2 – From initiation to degradation

As described above, autophagy can be divided into five distinct steps rigorously controlled by nearly 40 autophagy-related (Atg) proteins that can be grouped according to their functions at key stages (see figure 18). Here, we will see in detail the mechanisms and proteins involved in these five steps. Atg proteins are mostly clustered in the neighbourhood of the vacuole/lysosome and assembled into a structure named phagophore assembly site (or preautophagosomal structure, PAS) that also contains the forming vesicle (phagophore or isolation membrane) (Xie and Klionsky, 2007).

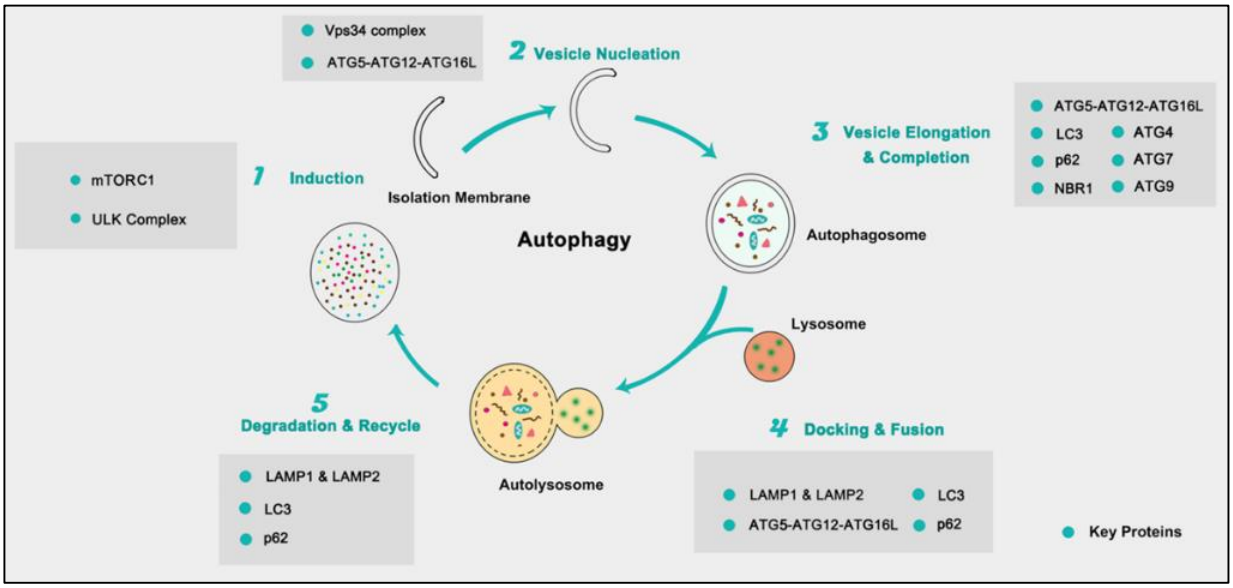

Figure 18 - Autophagy steps and key-regulators proteins.
The form of autophagy consists of several successive steps, including (1) induction, (2) vesicle nucleation, (3) vesicle elongation and completion, (4) docking and fusion, and (5) degradation and recycling. Each step can be positively or negatively regulated by key autophagy-related proteins. From Zhang et al., 2018.

3.2.1 – Initiation

Autophagy can be induced by a wide range of several stress signals, such as amino acid deprivation, DNA damage, low energy, and hypoxia that trigger activation of distinct pathways primarily converging to the nutrient sensor mTORC1 (for mammalian Tor kinase complex 1), as shown in figure 19. Under autophagic stimuli, mTORC1 activity is inhibited, leading to a rapid de-phosphorylation of Atg13. Consequently, this leads to the formation of the Atg1 (ULK1/2) complex (ULK1/2-Atg13-Atg101-FIP200) and its interaction with the Atg17 subcomplex (Atg17-Atg31-Atg29) at the PAS (Kamada et al., 2010).

It appears that Atg13 plays an essential role in recruiting the autophagic machinery at the PAS, Atg13 being considered as a key regulator and organizer during the early steps of autophagy. Atg1 (ULK1/2) is a serine/threonine protein kinase, regulated by both Atg13 binding and TORC1 phosphorylation, requiring its kinase activity for autophagy but not for its localization to the PAS (Chan et al., 2009; Kamada et al., 2010). The second complex, the Atg17 subcomplex (Atg17-Atg31-Atg29), is constitutively formed as a dimer, serving as a platform for the PAS assembly (Ragusa et al., 2012).

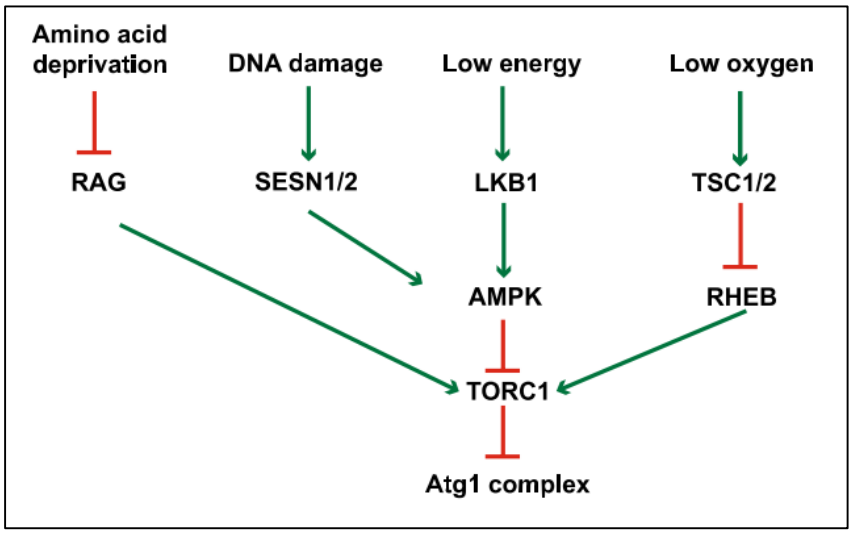

Figure 19 - Signaling pathways regulating TORC1-dependent autophagy.
TORC1-dependent autophagy can be regulated by a wide-range of metabolic and cellular changes such as nutrient starvation, DNA damage, both low energy and oxygen levels. All these mechanisms lead to inhibition of TORC1 activity promoting the formation of the Atg1 complex. From Zhi et al., 2017.

3.2.2 – Nucleation

After initiation, the nucleation (which means for phagophore biogenesis) requires the lipid kinase activity of the Vps34 complex in which Vps34 (a class III Pi3K) is the core enzyme. During autophagy, Vps34 is recruited to the local membrane of the PAS and a conformational switch happen in its structure. This change leads to phosphorylation by Vps34 of the membrane lipid phosphatidylinositol (PI), producing phosphatidylinositol 3-phosphate (PI3P) (Blommaart et al., 1997). As a result, the local membrane concentrations of PI3P increases, leading to increased membrane curvature.

The activity of Vps34 is mainly regulated by interactions with its partners, including both the regulatory subunit Vps15 and Beclin1 (aka Atg6, Vps30). Beclin1 functions as a protein platform recruiting additional factors, such as Atg14 and Vps38 (UVRAG), into the Vps34 complex to form the autophagy-specific complex and the endosome sorting complex (McKnight and Zhenyu, 2013).

3.2.3 – Elongation

The elongation process of the phagophore is mainly regulated by two key events: Atg9 shuttling and LC3 (Atg8) lipidation. Atg9 is recruited to the PAS during autophagy in an Atg17-dpendant manner, which is based on the Atg9-Atg17 interaction requiring the presence of ULK1/2. Atg9 mediates material exchange between the PAS and peripheral organelles by shuttling between them (Young et al., 2006).

LC3 is synthetized as a precursor form and is cleaved at its C-terminus by the protease Atg4B, resulting in its cytosolic isoform: LC3-I. LC3-I is then conjugated to phosphatidylethanolamine (PE) in a reaction involving Atg7 and Atg3, resulting in the LC3-II isoform (Tanida et al., 2004a). LC3-II is specifically targeted to the elongating autophagosome membrane and remains on completed autophagosomes until fusion with the lysosomes. LC3-II, localized on the cytoplasmic face of autolysosomes, is then delipidated by Atg4 and recycled (Tanida et al., 2004b). How cargoes are recruited to the expanding phagophores remains unclear but a number of cargo-specific receptors have been recently identified including Atg19, p62 and NBRA (neighbour of BRCA1 gene 1). Interestingly, the specific association of LC3-II with autophagosomes makes it an excellent marker for monitoring autophagy. At this step, the expanding phagophore becomes a mature double-membrane vesicle with both ends scaled.

3.2.4 – Fusion

Mature autophagosomes dissociate from the PAS and fuse with lysosomes to form autolysosomes where the outer membrane of the autophagosome quickly fuses with the lysosome membrane under the dependency of a number of factors such as LAMP-2 and the small GTPase Rab7. A SNARE complex controls this fusion step: syntaxin-17 (Stx17) recognizes and localizes at the outer membrane of mature autophagosomes and forms a complex with both SNAP29 and the lysosomal SNARE protein VAMP8, facilitating the membrane tethering and fusion (Itakura et al., 2012). It has been reported that Atg14 bind to Stx17 and SNAP29, promoting Stx17-mediated fusion events as shown in figure 20 (Diao et al., 2015).

3.2.5 – Degradation

After fusion of the autophagosome with the lysosome into an autolysosome, the inner membrane and encapsulated cargo are attacked by a series of lysosome-resident acidic hydrolases such as cathepsins, lipases, and glycosidases that break down the cargo into basic building blocks of proteins, lipids, and sugars (Bonten et al., 2014). Subsequently, the resultant monomeric units are transported back to the cytosol through lysosomal membrane transporters (permeases), and participate in the cellular maintenance of energy, metabolic, and organelle homeostasis (Mizushima and Klionsky, 2007).

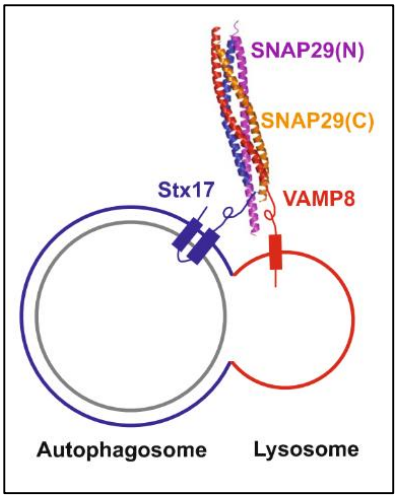

Figure 20 - Structural analysis of the autophagosome and lysosome fusion.
The factors involved in the autophagosomal fusion. Stx17, SNAP29, and VAMP8 form a SNARE complex that mediates the membrane tethering and fusion (4WY4). Positive regulators are: Atg14, HOPS, PLEKHM1, EPG5, TECPR1 and INPP5E. Negative regulators are: OGT, OR1L and PI(3,5)P2. From Zhi et al., 2017.

3.3 – Regulation of autophagy

As reported above, autophagy is constitutively active in all cell type at basal level but several mechanisms can upregulate this degradation process. Here, we will dress a short list of several cellular events that can trigger autophagy.

3.3.1 – Nutrient starvation

During nutrient deprivation, autophagosome formation is dramatically increased. Two well-characterized signaling cascades that sense nutrient status, activate both cell division and growth, and negatively regulate autophagy are the mTOR and Ras-cAMP-PKA pathways. Extracellular amino acids, that enter mammalian cells through transporters such as SLC1A5 (solute carrier family 1 member 5) and SLC7A5 , are directly sensed by mTORC1 that is phosphorylated in response to nutrient signals (Long et al., 2005a). Other observations reported that Rag proteins (Ras-related small GTPases) activate mTORC1 in response to amino acids through mediating translocation of mTORC1 to a specific subcellular compartment containing the mTORC1 activator Rheb (Ras homolog enriched in brain) (Sancak et al., 2008). Under high level of nutrient conditions, mTORC1 is active and phosphorylates both ULK1/2 and Atg13, blocking autophagy, while upon nutrient starvation, Atg13 and ULK1/2 are dephosphorylated, leading to autophagosome formation (Juhász et al., 2008).

The Ras/cAMP-dependent protein kinase A (PKA) signaling pathway plays an important role in glucose sensing. In nutrient-rich conditions, the small GTPases Ras1 and Ras2 are active and enhance cAMP generation by the adenylyl cyclase. This elevated level of cAMP binds the regulatory subunit of PKA and release it from its inhibitory effect. Constitutive activation of the Ras/PKA pathway suppresses

autophagy induced by TOR inhibition in yeast, indicating that the Ras-PKA pathway downregulates nutrient starvation-induced autophagy (Budovskaya et al., 2004).

3.3.2 – Stress response

Various intra and extracellular stresses could induce autophagy, which is crucial for organisms to adapt or to overcome unfavourable growth condition. Endoplasmic reticulum (ER) is the compartment that helps folding newly synthesized proteins and initiating pathway of vesicular movement of membrane and proteins to various organelles. In addition, the ER serve also as the major Ca^{2+} intracellular reservoir. A number of ER stress stimuli lead to the accumulation of unfolded proteins in the ER, exceeding its folding capacity. ER stress-induced autophagy is required for cell survival from the unfolded protein response (UPR) (Bernales et al., 2006).

Low levels of oxygen (below 1%, hypoxic stress) versus 2-9% (normoxia for most mammalian cell types) exist in many pathological conditions, such as solid tumors. Recent publications showed that hypoxia induces autophagy in mammalian cells but the underlined mechanistic still remain obscure. Enhanced mitochondrial autophagy (mitophagy) during hypoxia is suggested to be an alternative response by reducing the reactive oxygen species (ROS) levels and protecting cell integrity (Azad et al., 2008).

Another intracellular stress that leads to autophagy induction is the formation of ROS that are mainly produced in mitochondria. ROS-generating agents of chemical inhibition of the mitochondrial electron transport chain induce ROS production and autophagic cell death in transformed and cancer cell lines (Chen et al., 2008). The link between ROS and autophagy induction may be the cysteine protease Atg4: ROS targets Cys81 on Atg14 that inhibits its protease activity and promotes LC3 lipidation, an essential step for autophagy as detailed previously (Scherz-Shouval et al., 2007).

3.3.3 – Energy sensing

Activation of autophagy during periods of intracellular metabolic stress is essential for cell viability. In mammalian cells, a reduced cellular energy level (ATP) is sensed by the AMPK (5'-AMP-activated protein kinase), leading to its activation. Active AMPK leads to phosphorylation and activation of the TSC1/2 complex, which inhibits mTOR activity through Rheb (Inoki et al., 2003). In addition, it has been reported that AMPK phosphorylates p27, a cyclin-dependent kinase inhibitor, leading to cell cycle arrest (Liang et al., 2007). This mechanism is essential to prevent cells from undergoing apoptosis in addition to autophagy induction for survival under metabolic stress.

3.3.4 – Growth factor / Insulin pathways

When the extracellular environment is deprived in growth factors, autophagy is induced and is indispensable for maintaining cellular functions and energy production (Lum et al., 2005). The Ras effector Raf-1 is an amino acid sensor that positively regulates autophagy in HT-29 human colon cancer cells. Amino acids target and inhibit Raf-1 kinase activity which downregulates the downstream MEK1/2 and ERK1/2 kinases, leading to autophagy induction. Amino acid deprivation reverses this inhibition and induces ERK1/2 activation and autophagy (Pattingre et al., 2003).

In mammals, the pathways regulating autophagy through hormones are different from those of nutrients but converge also on mTOR. Upon insulin binding, autophosphorylation of the insulin receptor results in the recruitment and phosphorylation of IRS1 and IRS2 (insulin receptor substrate 1 and 2), which creates a docking scaffold that allows binding of adaptor proteins. A cascade of protein activation following this activation leads to mTORC1 activation and autophagy inhibition. When hormones are absent, mTORC1 is inactivated, releasing its inhibitory effect on autophagy (Long et al., 2005b).

3.4 – Autophagy dual role in tumorigenesis

In cancer cells, autophagy plays a dual role, having both tumor-promoting and tumor-suppressing properties (see figure 21 for an overview). Autophagy can inhibit tumorigenic transformation by preventing DNA damage and genomic instability, limiting ROS, and inducting senescence. In counterpart, autophagy can contribute to tumor progression by helping cells to survive to stressful conditions such as the metabolic reorganization that they encounter after oncogenic transformation.

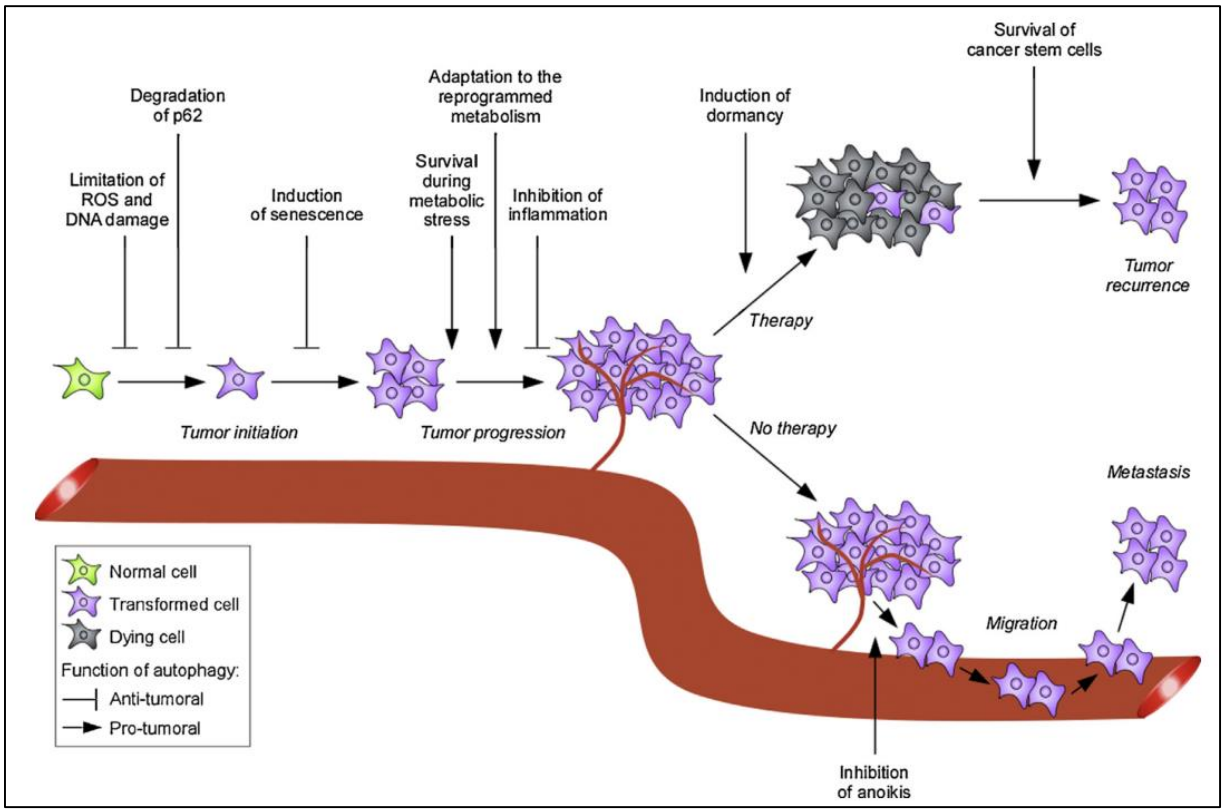

Figure 21 - Tumor-suppressing and tumor-promoting roles of autophagy.
Autophagy can either inhibit or promote tumorigenesis depending on the stage of the tumor and the stresses encountered. By limiting ROS production and p62 accumulation in normal cells, autophagy prevents tumoral transformation. On the other hand, autophagy also seems to be important for tumor progression, allowing tumor cells to survive metabolic stress or anoïkis, and sustaining their adaptation to the reprogrammed metabolism. From Lorin et al., 2013.

3.4.1 –Autophagy acts as a tumor suppressor

Because autophagy is an important mechanism required to maintain cellular homeostasis, any interference or deregulation of the autophagic machinery may disrupt cellular integrity and promote tumorigenesis.

3.4.1.1 – Atg's and Beclin1 are tumor-suppressor genes

It has been found that depletion of the autophagy gene Beclin1 is associated with several human cancers (Beclin1 is found homozygously deleted in 50% of both breast and pancreatic cancers and up to 75% of ovarian cancer) (Liang et al., 1999). In addition, monoallelic deletion of Belin1 in mice increases tumorigenesis and accelerates the development of hepatitis B virus-induced premalignant lesions (Qu et al., 2003), whereas restoration of its expression in breast cancer cells repress the tumor growth in mouse xenograft. Another gene regulating autophagy is found downregulated in human tumors. Bif-1, which works in concert with Beclin1 to promote autophagosome formation, show the

same properties than Beclin1 downregulation in both gastric and prostate cancers (Takahashi et al., 2007). More, mice lacking Bif-1 expression are more subject to develop tumors.

In addition, a high number of autophagy executor genes have also been linked to carcinogenesis. Mutations of Atg2B, Atg5, Atg9B, and Atg12 are found in both gastric and colorectal cancers (Kang et al., 2009). It was shown that frameshift mutation of these Atg genes, with mononucleotide repeats, are common in both gastric and colorectal carcinomas, suggesting that these mutations may contribute to cancer development by downregulating autophagy. Several tumor-suppressor genes such as PTEN (for phosphatase and tensin homolog), TSC1/2 (tuberous sclerosis 1 and 2), and $p19^{ARF}$ have been shown to stimulate autophagy by either inhibiting mTOR, activating the Ulk1 initiation complex or activating Beclin1 (He and Levine, 2010; Pimkina et al., 2009). Finally, it has been reported that mutant forms of p53 accumulate in the cytoplasm of cancer cells and subsequently suppress autophagy (Morselli et al., 2008).

3.4.1.2 – Oxidative stress

Autophagy has been shown to remove damaged organelles and proteins from the cytoplasm, which are the major sources of ROS, protecting cells against DNA damage and genomic instability. Autophagy defect is associated with an increased levels of ROS, an accumulation of damaged mitochondria, and an increased amount of DNA damage (Mathew et al., 2007a). Moreover, the gene encoding the mitophagy protein PARK2 is frequently mutated in various type of cancers, suggesting that ROS could lead to chromosomal instability, resulting in increased cancer initiation (Veeriah et al., 2010).

3.4.1.3 – p62 and tumorigenesis

Another autophagy-regulating gene that may contributes to cancer progression is p62, which binds both LC3 and ubiquitylated proteins, driving them to selective degradation. Mutations of this gene is frequently mutated in human cancers and is found overexpressed in Ral-transformed cells (Moscat and Diaz-Meco, 2009). It has been reported that p62 depletion reduced anchorage-independent growth (this mechanism will be detailed in part 4 of the introduction) in human hepatocellular carcinoma cells and abolished Ras-induced lung carcinomas development (Inami et al., 2011).

3.4.1.4 – Senescence induction

Additionally, autophagy can prevent tumorigenesis by restricting proliferation of transformed cells, activating oncogene-induced senescence. Senescence is a prolonged arrest of growth where diploid cells remains active but exit from the cell cycle, ceasing proliferation. This phenomenon helps to prevent proliferation and dissemination of mutated cells by promoting an irreversible cell cycle arrest (Gewirtz, 2009). It has been shown that both DNA damage and oncogenes expression promote autophagy and that depletion of autophagy genes allows cells to bypass senescence arrest (Young et al., 2009).

3.4.1.5 - Inflammation

Finally, autophagy can prevent necrosis and subsequent inflammation. It has been reported, in a tumor xenograft model, that apoptosis, combined with autophagy defect, leads to necrotic cell death, inflammation, and subsequent tumor growth (Degenhardt et al., 2006). Some studies have shown that autophagy prevented necrotic cell death of apoptotic-deficient tumor cells, limited local inflammation and prevented the subsequent tumor growth (Qu et al., 2007).

3.4.2 – Autophagy can support tumorigenesis

Beside the fact that autophagy can prevent tumor progression, it has also been reported by several publications that autophagy can support the development of tumors. One of the first report demonstrating that tumor cells are dependent on autophagy for their survival has been performed in pancreatic tumors. It has been shown that pancreatic cancer tumors display increased level of autophagy compared to normal cells, and that autophagy inhibition in these cells is associated with tumor regression in xenograft mouse models (Yang et al., 2011).

3.4.2.1 – Metabolic stress

Because autophagy is a crucial mechanism allowing cells to survive despite metabolic stress, the implication of autophagy on cancer cells survival and propagation has been extensively studied. First, it has been reported that several cancer cell lines can be resistant to long time nutrient deprivation, whereas normal cells don't survive more than one day in this situation (Izuishi et al., 2000). Another example is that because of dramatically increased cell proliferation, tumors are characterized by higher demand on nutrient and oxygen than normal cells. Because the blood supply in insufficient for tumors cells during the initial steps of tumor formation in the poorly vascularized regions of solid tumors, autophagy allows these cells to survive to this metabolic stress (Harris, 2002). More, in these

type of tumors, it has been reported that increased level of autophagy were localized in hypoxic regions, and that autophagy inhibition caused tumor cell death (Mathew et al., 2007b).

3.4.2.2 – Dormancy

Dormancy is a condition of cancer cells where they cease to divide in order to survive to poor environmental growth conditions (such as nutrient-deprivation) in a quiescent state, waiting for appropriate conditions to start proliferating again. It has been reported that autophagy can maintain cancer cell survival for several weeks by putting tumor cells in a dormant condition by suppressing both motility and proliferation in order to conserve energy (Jin et al., 2007; Lum et al., 2005). When growth environment improves again, the cancer cells can re-enter in proliferation state in less than 24 hours, allowing tumor growth (Degenhardt et al., 2006). In order to support this, it has been shown in mice that treatment with chloroquine, an autophagy inhibitor, delayed the tumor regrowth (Lu et al., 2008). Dormancy can be defined as a state where cancer cells enter after a metabolic stress such as chemotherapy and where other cells may die, due to the heterogeneity of the tumor. After this reduced-metabolic phase, these cells can resume proliferation, leading to tumor recurrence and propagation (Gewirtz, 2009).

3.4.2.3 – ECM detachment

The first informations on the role of autophagy on survival during extracellular matrix (ECM) detachment come from 2008. It has been reported that autophagy was active in the early stages following cellular detachment, and that autophagy supported cell survival by protecting them to anoïkis (cell death under anchorage-independence growth conditions). In detail, they reported that inhibition of several Atg's genes inhibited detachment-induced autophagy and increased cell death upon ECM detachment (Fung et al., 2008). It has also been reported that inhibition of autophagy reduced anchorage-independent growth of breast cancer cells. More, the same group revealed several years later that autophagy was induced following ECM detachment in both cell lines ectopically expressing oncogenic H-Ras and in human cancer cell lines harbouring endogenous K-Ras mutations (Lock et al., 2011). They also reported that Ras-mediated transformation and proliferation, in an adhesion-independent way, could be attenuated by depletion of some autophagic genes. In addition, this same team revealed the dual role of autophagy in detachment-induced growth. They showed, in breast epithelial cells transformed with an oncogenic version of Pi3K, that autophagy promoted resistance to anoïkis for acinar luminal formation, while proliferation in three dimensional morphogenesis required autophagy suppression (Chen et al., 2013).

Interestingly, it has been reported that detachment-induced autophagy was controlled by the activation of the RNA activated protein kinase like endoplasmic reticulum kinase (PERK), that phosphorylates and activates the eukaryotic translation initiation factor 2α, inducing the transcription and translation of Atg's genes (Avivar-Valderas et al., 2011). Finally, hints have been found on the potential role of autophagy in the formation and survival of metastasis: hyperactivation of autophagy have been reported in both melanoma and hepatocellular carcinoma early metastasis and have been correlated with poor prognosis for patients (Ding et al., 2008).

3.4.2.4 – Mitophagy and Ras-oncogenesis

Mitophagy dysregulation has been reported in cancer cells by many publications and Ras has been found to activate mitophagy by accelerating glycolysis to circumvent glucose deficiency (Kim et al., 2011a). Otto Warburg was the first to describe the phenomenon of aerobic glycolysis in cancer cells and attributed this effect to dysfunctional mitochondria, becoming a hallmark of cancer (Warburg, 1956). Moreover, Ras can reprogram gene expression of glucose transporters, such as SLC2A1/GLUT1, and promotes the switch of glucose metabolism from OXPHOAS into glycolysis (Liu et al., 2010). It has been reported that the maintenance of a high amount of mitochondrial mass is no longer essential for ATP production, once glycolysis is activated and transformed cells may maintain small numbers of mitochondria during rapid proliferation, minimizing the energy required for subcellular organelles maintenance. In this process, it has been shown that activated Ras promotes mitophagy by activating the MAPK/JNK signaling pathway (Kim et al., 2011a). Finally, it has been shown that pharmacological inhibition of autophagy in human breast epithelial cells completely blocked K-Ras^{V12}-induced anchorage independent growth on soft agar assay and that both protein and mRNA level of Atg5 and Atg7 were increased in cells transformed with K-Ras^{V12} (Kim et al., 2011b).

4 – Anoïkis

4.1 – Anoïkis: definition

The term Anoïkis means homelessness in Greek and is a sort of programmed cell death occurring in anchorage-independent cells when they detach from the surrounding extracellular matrix (Frisch and Screaton, 2001). Anoïkis can be induced by inadequate or inappropriate cell-matrix interactions and is involved in a wide diversity of tissue. Historically, anoïkis was first described in epithelial and endothelial cells in the 1990s (Frisch and Francis, 1994) and defined as a physiological process ensuring proper development and tissue homeostasis. In normal conditions, cells in tissue maintain contact between each other and between the ECM, regulating several cellular processes such as migration, proliferation, differentiation, and survival (Boudreau and Jones, 1999). It has been reported that endothelial cells underwent apoptotic death when cultivated in the absence of ECM contact through nuclear fragmentation, DNA degradation, cell shrinkage, and protein cross-linking (Frisch and Francis, 1994). This process acts as an important defense mechanism, preventing detached cells to re-adhere in incorrect locations. Deregulation of this mechanism could result in cell proliferation upon suspension condition and cell proliferation at ectopic sites where the ECM is totally different from the original one. This anoïkis deregulation is an emerging hallmark of cancer cells, contributing to both formation and survival of metastasis (Gilmore, 2005).

4.2 – Anoïkis in physiological conditions

Anoïkis can plays a crucial role in various physiological processes. The first example showing the importance of anoïkis in normal development was reported in breast development (Debnath et al., 2003). The authors reported that the lumen in breast acini is formed by a gradient of apoptotic luminal cells, due by anoïkis death following the primary detachment from the acinar basement membrane. They also showed that the suppression of anoïkis resulted in sustained luminal proliferation and filling, correlating with pathological formation of breast ductal carcinoma *in situ*. Another example is that endothelial cells rely on matrix attachment for their survival, attachment that seems to be disrupted by mechanical forces such as stress resulting to hypertension (Michel, 2003). It has also been reported that hypertension, through tensile forces, disrupted the vascular smooth muscle cellular attachment. With these informations, it appears that mechanical forces promote apoptosis of vascular cellular components, resulting in reduced vascular integrity and atherosclerosis (degenerative process) (Lee et al., 2008). Finally, this effect seems also to impact cardiac myocytes where their sensitivity to anoïkis could contribute to hypertrophy and heart failure (Michel, 2003).

4.3 – Molecular pathways of anoïkis

Anoïkis can be mediated by different signaling pathways, all converging into the activation of caspases and downstream molecular pathways, leading to activation of endonucleases, DNA fragmentation, and cell death. Induction of anoïkis depends on the interplay between two pro-apoptotic pathways: the perturbation of mitochondria (the intrinsic pathway) and the activation of cell surface death receptors (the extrinsic pathway) (Grossmann, 2002). As shown in figure 22, intrinsic and extrinsic pathways are triggered by different and specific stimuli.

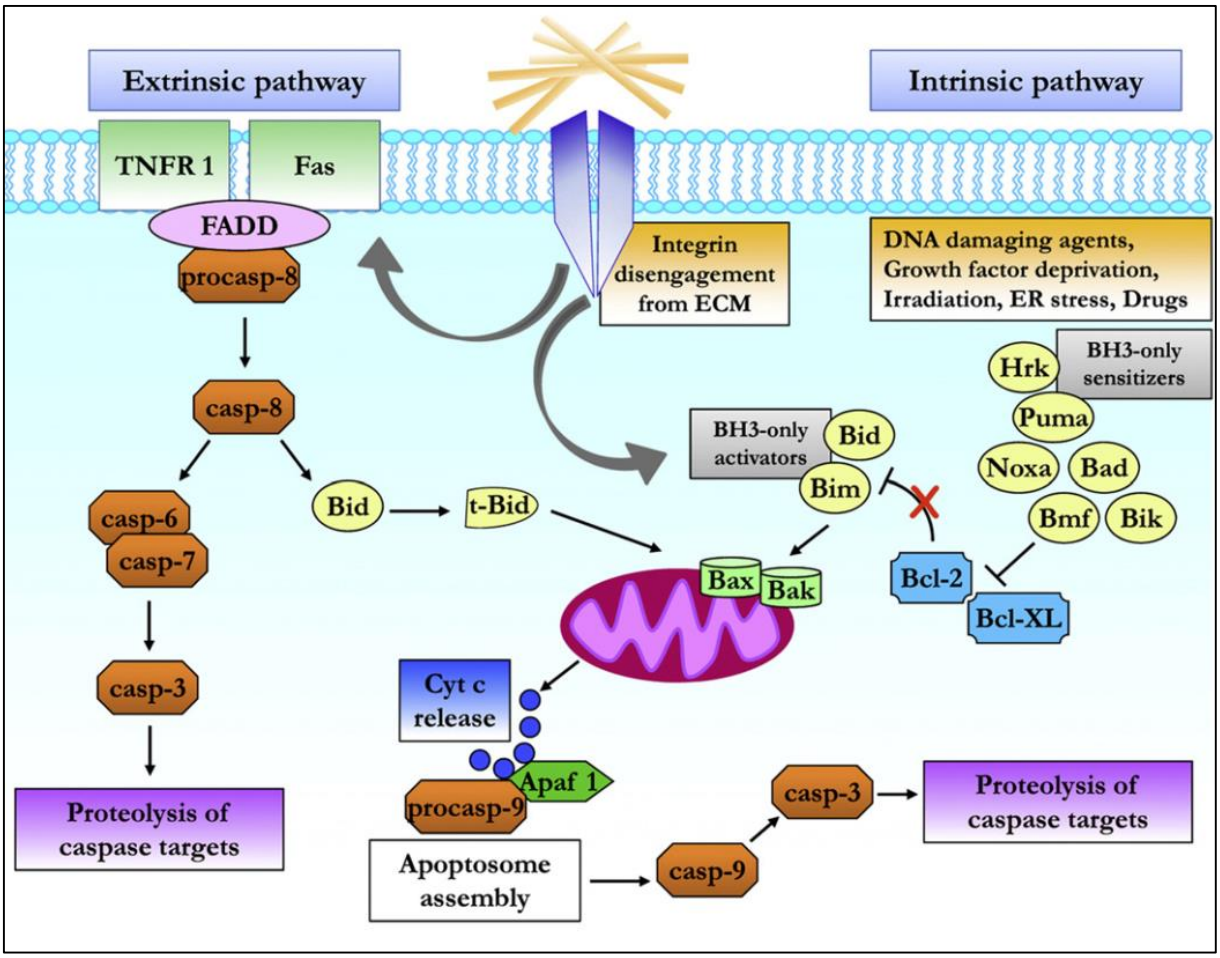

Figure 22 - Intrinsic and extrinsic apoptotic pathways.
The absence of ECM contact or the engagement with inappropriate ECM leads to the activation of anoïkis from death receptors (extrinsic pathway) and mitochondria (intrinsic pathway). In the extrinsic pathway of apoptosis, caspase-8 is activated upon engagement of death receptors leading to cleavage and activation of executioner caspases. In the intrinsic pathway, Bax/Bak activation is promoted by BH3-only proteins. Among them, Bid and Bim directly promote the assembly of Bax–Bak oligomers, while the BH3-sensitizers members, counteract the anti-apoptotic functions of Bcl-2. As a final outcome, cytochrome c is released to the cytoplasm, where it induces the formation of the apoptosome, leading to activation of executioner caspases. From Paoli et al., 2013.

4.3.1 – Intrinsic pathway

The intrinsic pathway (also called mitochondrial pathway of caspase activation) is a major cell death pathway contributing to anoïkis. The intrinsic pathway is activated in response to several intracellular signals such as DNA damage, growth factor deprivation, endoplasmic reticulum stress, and integrins disengagement (Kroemer et al., 2007). Upon apoptotic signals, the pro-apoptotic proteins Bax and Bak translocate from the cytosol to the outer mitochondrial membrane (OMM), under the activation of adaptor proteins, and create a channel in the OMM causing mitochondrial permeabilization and the release of cytochrome c, Smac/DIABLO, and Omi/Htra2. The release of cytochrome c from the mitochondria leads to the formation of the so-called apoptosome, composed of cytochrome c, pro-caspase 9, and the cofactor apoptosis protease activating factor 1 (Apaf 1), resulting into the cleavage of the pro-caspase 9 to its active form, the caspase 9. Activation of this caspase cascade initiator results in the activation of both caspases 3 and 7 and the execution of the apoptotic process (Thornberry, 1998; Zou et al., 1997).

The release of these death-promoting proteins from the mitochondria into the cytoplasm is modulated by pro- and anti-apoptotic proteins of the Bcl-2 family. Among these members, Bid and Bim are activated by the detachment of cells from the ECM and rapidly promote the assembly of the Bax/Bak oligomers within the OMM (Taylor et al., 2008a). Due to their activation role on anoïkis, members of this family are called “activators”. In detail, upon attached conditions, Bim is sequestered in a dynein cytoskeletal complex until cell detachment induces its release from these structures, causing its translocation to the mitochondria, in addition to its activation through Erk and Pi3K/Akt-mediated phosphorylation (Cheng et al., 2001).

Another group of this family is called “sensitizers” and comprises Bad, Bik, Bmf, Noxa, Puma, and Hrk. Contrarily to the “activators”, this group of proteins are unable to directly activate Bak and Bax oligomerization, but contribute to cell death by inactivating the anti-apoptotic functions of Bcl-2 (Vander Heiden et al., 1997; Kuwana et al., 2005). In details, Bcl-2 in considered as the master anti-apoptotic member of this family, inhibiting apoptosis by its interaction with the pro-apoptotic Bak/Bax, thus avoiding their clustering into pores of the OMM (Gazaryan and Brown, 2007). Finally, Mcl-1, another protein of this family, has been shown to maintain anoïkis sensitivity. In basal level, Mcl-1 inhibits Bim in the neighbourhood of the mitochondrial membrane, preventing induction of apoptosis. Under ECM detachment, Mcl-1 is degraded and Bim transcription is upregulated, leading to anoïkis proceed (Opferman et al., 2003).

4.3.2 – Extrinsic pathway

Beside the intrinsic pathway, the extrinsic pathway contributes also to anoïkis execution. Where the intrinsic pathway is activated by cellular and environmental growth conditions, the extrinsic pathway is only activated by binding of ligands to the cell receptors. In detail, the extrinsic pathway is initiated by ligand binding of the tumor necrosis factor (TNFR) superfamily members TNFR1, Fas receptor, and TNF-related apoptosis inducing ligand (TRAIL) receptor -1 and -2, resulting in the formation of the death-inducing signaling complex (DISC) (Taylor et al., 2008b). After this complex formation, DISC recruits caspase 8 proteins and activates them via interaction with adaptor proteins such as the Fas-associated death domain protein (FADD). Finally, active caspase 8 is released into the cytoplasm where it cleave and activates the caspases 3, 6 and 7, resulting in substrate proteolysis and cell death (Wajant, 2002).

In addition, caspase 8 activation can results in the cleavage and activation of Bid, promoting both mitochondrial cytochrome c release and assembly of the apoptosome, thus linking the intrinsic pathway to the extrinsic one (Valentijn and Gilmore, 2004). The activation of the death receptor pathway (extrinsic one) could be secondary to mitochondrial damage (intrinsic one), implementing a crosstalk between extrinsic death signals and the intrinsic pathway. Finally, it has been reported that detachment of ECM leads to the upregulation of Fas and Fas ligand, indicating the important role of the extrinsic pathway to anoïkis resistance (Aoudjit and Vuori, 2001).

4.4 – Anoïkis resistance in cancer cells

Cancer cells rapidly develop or modulate several mechanisms to resist anoïkis and exploit them both to survive and progress towards malignancy but also to spread metastases (Paoli et al., 2013). Anoïkis resistance is a hallmark of malignant tumors for anchorage independent growth and survival. The underlying purpose of evading anoïkis by cancer cells is to survive in an environment outside its own niche. Among the mechanisms allowing anoïkis resistance, it has been reported that cancer cells could resist to anoïkis by either remodelling their integrins pattern, activating anti-apoptotic pathways, undergoing EMT, deregulating their metabolism (mainly through Warburg metabolism or autophagy), or by activating the NF-κB signaling pathway.

4.4.1 – Integrin switch

Structurally, integrins are heterodimers that consist of an α subunit and a β subunit. In vertebrates, there are 18 α and 8 β subunits that combine to form 24 different heterodimers that interact with different components of the ECM. Normally, cells express a specific pattern of integrins (such as α1β1, α2β1, α3β1, α5β1, α6β1, α6β4, αvβ3), appropriate to the local matrix that transduce

ECM stimuli and therefore suppress anoïkis (Frisch and Screaton, 2001). In contrast, expression of unligated integrins by misplaced cells leads to cell death through integrin-mediated death (IMD) (Stupack et al., 2001). A strategy to avoid anoïkis is to modify the integrin expression pattern for both cells that are migrating to a new cell-matrix environment and cells that undergo oncogenic pressure, several examples of integrins switch have been reported in human cancer cells. It has been shown that downregulation of αvβ3 expression protects intestinal carcinoma cells in suspension from death, suggesting a contribution to anoïkis resistance (Morozevich et al., 2003). Moreover, αvβ3 integrin is found expressed in invasive melanoma cells but not in normal melanocytes, suggesting that αvβ3 expression is essential to cancer cells invasion and metastatization (Gehlsen et al., 1992). It has also been reported that squamous cell carcinoma displays an integrin switch by expressing αvβ6 integrins, activating the pro-survival PI3K-Akt pathway, rather than αvβ5 integrins, inducing the intrinsic apoptotic pathway when unligated (Janes and Watt, 2004).

Another example is that overexpression in oral squamous cell carcinoma of the β6 integrin stimulates migration and secretion of metalloproteinase-3 (MMP-3) that, in turn, stimulates cell invasion (Ramos et al., 2002).It has also been shown that overexpression of β4 integrin leads to constitutive activation of Pi3K, inducing anoïkis resistance and invasion of breast cancer cells, while β4 knockdown promotes apoptosis (Bon et al., 2006). Finally, it has been reported that expression of αvβ3 integrins in melanoma cells suppresses anoïkis by modifying the proportion of anti-apoptotic Bcl-2 and pro-apoptotic Bax proteins (Montgomery et al., 1994).

4.4.2 – Activation of anti-apoptotic pathways

Pi3K/Akt is one of the most important signaling pathway involved in anoïkis resistance in detached or migrating cancer cells that need to compensate their loss of integrins. Because Akt integrates most of the signals derived both from integrins and growth factors receptors, aberrant or constitutive Akt activation strongly contributes to sustain cancer growth (Altomare and Testa, 2005). Overexpression of several constitutive active receptor tyrosine kinase, activating Ras mutations, loss of the phosphatase and tensin homolog (PTEN), alteration of Pi3K activity, and amplification of Akt expression can lead to sustained pro-survival Akt activation. It has been shown that upregulation of N-cadherin expression leads to sustained Akt activation, where the switch from E-cadherin to N-cadherin is a common feature of cancer cells undergoing EMT (Gheldof and Berx, 2013). As reported above, PTEN is the most important negative regulator of the Pi3K/Akt signaling pathway: downregulation or inhibition of PTEN is commonly associated with achievement of anoïkis resistance whereas its overexpression triggers anoïkis (Davies et al., 1999).

Another element of anoïkis resistance in cancer cells is the Src kinase family. It has been reported that both elevated expression and activity of Src enhance EMT, and thus anoïkis resistance. In details, Src activation leads to Pi3K recruitment and activation through FAK phosphorylation on Tyr397. Akt activation results in, as described above, apoptosis inhibition in correlation with the Ras/MAPK pathway by the pro-apoptotic Bim protein degradation (Bouchard et al., 2007). It has also been reported that Src-mediated activation of FAK boosts Bad phosphorylation by Akt, inhibiting caspases 2, 3, 8, and 9 activation, and thus suppressing anoïkis. Another Akt substrate playing a role in both anoïkis resistance and cancer cell dissemination is the integrin-linked kinase (ILK). It has been shown that ILK overexpression and/or activation, caused by PTEN loss of function/downregulation, influence cell spreading and migration by stimulating cell contractility and motility (Hannigan et al., 2005).

Finally, another mechanism implicated in anoïkis resistance is related to deregulated expression of growth factor receptors. By autocrine signaling of growth factors, the receptors activation leads to the activation of cell survival pathways, promoting cell migration and invasion. As example, the neurotrophic tyrosine kinase receptor B (TrkB) is found overexpressed in tumors and has been described as one of the most efficient inductor of anoïkis resistance (Geiger and Peeper, 2007). TrkB is frequently overexpressed in aggressive tumors and is correlated to development of chemoresistance in gastric and prostate carcinomas (Tanaka et al., 2009). It is widely established that growth factor receptor overexpression, or sustained activation, is a typical mechanism adopted by cancer cells to escape from integrin control, by synergizing signals triggered by integrins in order to overcome anoïkis (Paoli et al., 2013).

4.4.3 – Epithelial to mesenchymal transition

EMT is a physiological process allowing epithelial cells to release linkage with neighbour cells, remodel cytoskeleton, and promote motility. It is well established that cancer cells undergo EMT, allowing them to overcome anoïkis, and move from their primary location, invading others tissues. As shown in figure 23, a wide range of mechanisms and signals can promote and support EMT. Upon EMT, cancer cells use epigenetic remodelling that leads to the downregulation of adhesion molecules such as E-cadherins, and, at the same time, to the expression of mesenchymal markers such as vimentin, fibronectin, α-smooth muscle actin (SMA), N-cadherins, and MMPs (Guadamillas et al., 2011). Anoïkis resistance during EMT is possible because most of the genes and proteins implicated in EMT activation modulate pro- and anti-apoptotic genes. In one hand, they can upregulate the expression of the Bcl2 anti-apoptotic family genes and activate pro-survival pathways such as Pi3K/Akt, while on the other

hand, they repress pro-apoptotic proteins such as p53-effector related pmp22 (PERP), p21, Bim, Bax, and Noxa (Wu and Zhou, 2010).

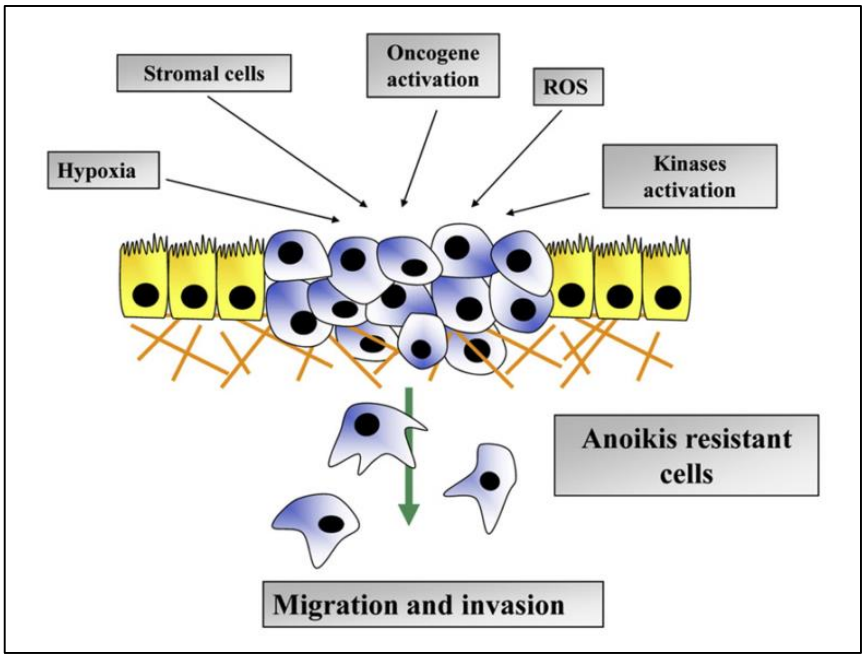

Figure 23 - EMT and anoïkis resistance.
Diverse stimuli such as hypoxia, oncogenic activation, reactive oxygen species, kinases and receptors activation have been shown to promote EMT, allowing cancer cells to avoid anoïkis. From Paoli et al., 2013.

Key regulators involved in EMT are transcription factors aberrantly expressed in cancer cells, such as Snail, ZEB1/2, Twist, NF-kB, and HIF1/2 that share the ability to decrease E-cadherin expression while increasing expression of mesenchymal markers (figure 24). In detail, Snail has been reported to directly represses E-cadherin transcription as well as Bid, caspase 6, or PTEN, genes involved in anoïkis (Barrallo-Gimeno and Nieto, 2005). ZEB1 transcription factor has been shown to contribute to EMT and malignancy by causing an increase of vimentin and a decrease of E-cadherin, leading to Akt pathway activation and anoïkis resistance (Takeyama et al., 2010). In addition, Twist activation strongly contributes to migration, invasion, and survival by upregulating the level of anti-apoptotic Bcl-2 protein (Blanco et al., 2002). Finally, downregulation of E-cadherin, by all mechanisms cited above, induces cytoplasmic accumulation of β-catenin, leading to upregulation of target genes involved in the regulation of cell motility and invasion such as c-Myc, cyclin D1, c-Jun, MMP-1 and -7 (Schmalhofer et al., 2009).

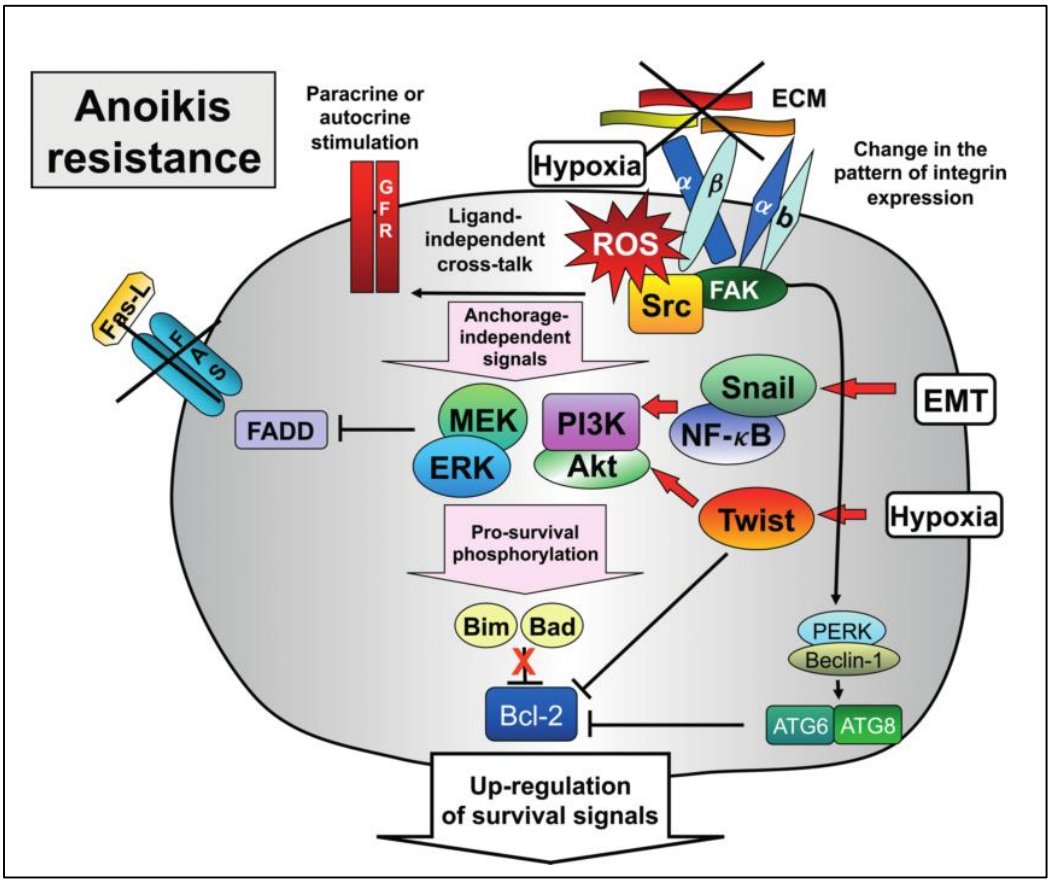

Figure 24 - Strategies for anoïkis resistance in cancer cells.
Integrin engagement by ECM triggers several pro-survival pathways through the activation of key players such as FAK, integrin-linked kinase (ILK), Src tyrosine kinase, PI3K, ERK and the adaptor protein Shc, finally leading to the transcription of Jun, Fos and NF-κB. In addition, pro-apoptotic proteins are inhibited, preventing both the extrinsic and intrinsic pathways of cell death. Growth factor receptors collaborate with integrin in promoting cell survival, largely converging on the same pathways. From Taddei et al., 2012.

4.4.4 – Oxidative stress and hypoxia

It is well established that cancer cells exhibit chronic ROS production that contributes to promote their survival, proliferation, and metastatic dissemination. Multiple mechanisms are at the source of these ROS, including activation of cellular receptors, EMT engagement, and p53 inactivation, but also some external factors such as exposition to radiation, chemicals or drugs (Giannoni et al., 2012). It has been reported that elevated ROS levels are important to overcome anoïkis in cancer cells. More, several studies showed that sustained ROS production leads to inactivation of pro-apoptotic enzymes such as PTEN, PTP-1B, SHP2, PP1a, and PP2a. On another hand, ROS triggers activation of Src kinase and several redox sensitive factors such as NF-κB, HIF-1α, and p53), leading to a sustained Pi3K/Akt signaling pathway (Parri and Chiarugi, 2013).

In addition, detached cancer cells are able to regulate the expression of several antioxidant enzyme through the transcription factor Nrf-2 in order to overcome anoïkis. When ROS increase, Keap-

1 oxidize and result in the release of Nrf-2 that migrates into the nucleus, leading to expression of antioxidant proteins (Li et al., 2012b), allowing cancer cells survival in pro-oxidant milieu, a common feature of tumor cells and their microenvironment. Importantly, several oncogenes, such as Ras, Raf, and Myc, contribute to activate the Nrf-2 pathway, protecting cancer cells from oncogene-addicted oxidative stress (Trachootham et al., 2008).

Hypoxia is a very common feature that rapid-growing tumors exhibit in intratumoral regions, leading compensatory mechanisms activation by tumour cells such as glycolytic metabolism increase, increased motility, and secretion of angiogenic growth factors. Importantly, it has been reported that hypoxia promotes EMT in melanoma, breast, prostate, and colon cancers (Lester et al., 2007). Cancer cells overcome hypoxia by activating pro-survival pathways that are linked to chemotherapy resistance in several cancer models (Cosse et al., 2007). Detached hypoxic cells exhibit both an anoïkis inhibition through HIF-1 dependent upregulation of both Snail and Twist and also the suppression of pro-apoptotic proteins such as Bim and Bmf (Whelan et al., 2010).

4.4.5 – Detachment-induced autophagy

As described previously, autophagy can support anoïkis resistance. Autophagy and anoïkis can function as important ways to adapt to outer stresses in normal epithelial cells by maintaining cellular homeostasis in addition to pro-metastatic functions (figure 25). It has been reported in 3D culture model of MCF-10A, that Atg5 and Atg7 knockdown induced luminal apoptosis, indicating that autophagy promotes epithelial cell survival during anoïkis (Fung et al., 2008). More, it has been reported that BNIP3 and BNIP3L, key regulators of autophagy and apoptosis, are found as a signature in tumor cell lines cultivated in spheroid (Chen et al., 2017). Elevated levels of both BNIP3 mRNA and protein expression are associated with poor survival in ovarian cancer patients. They also reported that induction of autophagy with rapamycin increased spheroid formation and survival while decreasing apoptosis.

As said previously, STK38 has been reported to support anoïkis resistance in Ras-transformed epithelial cells (Bettoun et al., 2016). The authors revealed that STK38 depletion displayed significantly decreased colony formation in soft agar assay of Ras-transformed cells, and that its kinase activity supported the anchorage-independent growth of these Ras-transformed cell lines. More, they reported that STK38 depletion in adherent cells reduced the autophagic activity, and that the detachment-induced autophagy is mediated, at least partly, by STK38. They also reported that both RalA and RalB are at least in part critical for detachment-induced STK38 activation, suggesting a Ral-Exocyst-STK38 pathway promoting anchorage-independent growth downstream of oncogenic Ras.

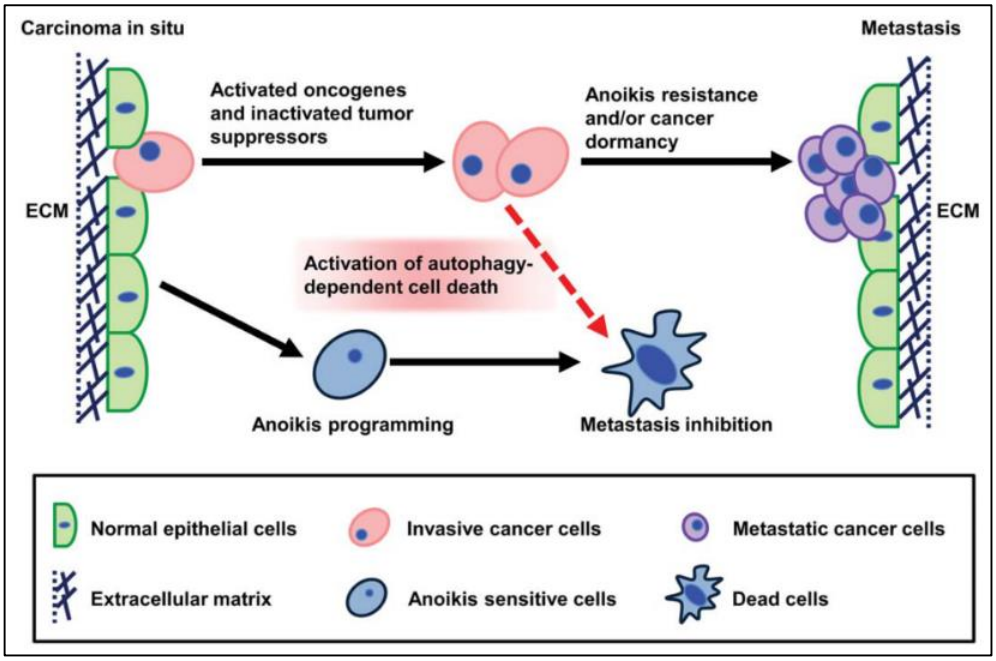

Figure 25 - Potential roles of autophagy and anoïkis during metastasis.
In normal epithelial cells, autophagy and anoïkis can function as important ways to adapt to outer stresses, such as ECM detachment by maintaining cellular homeostasis. However, in primary tumors, autophagy may serve as a pro-metastatic function and promote metastasis by allowing tumor cells to resist anoïkis and gain dormancy. Thus, manipulation of autophagy-dependent cell death pathways and activation of anoïkis pathways may promote metastasis inhibition with loss of anchorage dependence. From Yang et al., 2013.

4.4.6 – NF-κB and anoïkis resistance

Recent evidences have highlighted the role of NF-kB signaling pathway in anoïkis resistance. First, it has been reported that Akt, frequently activated in cases of anoïkis resistance, can triggers NF-κB signaling pathway by phosphorylating and inhibiting the IκB inhibitory subunit (Romashkova and Makarov, 1999). In addition, it has been reported that NF-κB was activated in rat intestinal epithelial cells cultured in suspension, blocking anoïkis (Toruner et al., 2006). The authors reported that activation of NF-κB, after loss of extracellular matrix attachment, required the phosphorylation of FAK (focal adhesion kinase) on its Tyr397, leading to DNA binding of the RelA/p65 NF-κB complex, and thus, the transcription of osteoprotegerin, BCL-2, and IAP-1 anti-apoptotic proteins. NF-κB is an important redox-sensitive transcription factor and has been defined to strongly contributes to activate and maintain cancer cells in a mesenchymal state through engagement of EMT (Xia et al., 2004).

In addition, it has been reported that STK38 potentiates NF-κB activation though its kinase activity (Shi et al., 2012). The authors showed that overexpression of STK38 potentiates NF-κB activation induced by TNFα, whereas knockdown of STK38 inhibits NF-κB activation induced by TNFα. They also reported, by co-immunoprecipitation assays, direct interaction of STK38 with multiple signal components (except p65) of the NF-κB signaling pathway.

5 – XPO1 and nuclear export

5.1 – Nuclear export: introduction

Eukaryotic cells are characterized by a physical separation between the cytoplasm and the nucleus by the nuclear envelop. In terms of evolution, one can wonder about the *primum movens* of this separation: to fabricate a "bag" for DNA where DNA metabolic processes (duplication, transcription) will occur and/or a place for specific parts of machineries occurring in the cytoplasm. The control of this supply allows a quick response (faster than triggering transcription/translation) of these missing parts, the former function of DNA metabolism being quite efficient in prokaryotes made this physical barrier unnecessary in these organisms. The latter function allows a more flexible/efficient response, especially in case of stress when specific cellular biological processes are mobilized.

Proper cellular homeostasis rely on distinct spatiotemporal distribution of molecules in these two compartments by a bidirectional transport system though the nuclear pore complex (NPC). Small molecules (< 40 kDa) diffuse passively through the NPC when larger molecules, including RNAs and almost all proteins, rely on a receptor and energy-dependent process (Tran et al., 2014). Receptors responsible for the shuttling of large molecules are referred as importins and exportins (collectively mentioned as karyopherins, a family of 20 human proteins) that bind to cognate sequences on their transported cargoes (Görlich and Kutay, 1999).

The most documented nucleo/cytoplasmic transport signals consist of the nuclear localization signal (NLS), required for importin-mediated entry into the nucleus and the leucine-rich nuclear export signal (NES), required for exportin-mediated exit of the nucleus (Kutay and Güttinger, 2005; Lange et al., 2007). Among nuclear export receptors, XPO1 (for Exportin-1, aka CRM1 for chromosome maintenance 1) has been well characterized and defined as the major nuclear export receptor having a broad substrate range. Because XPO1 has intrinsically week cargo-binding, the loading and unloading of cargoes molecules is supposedly mediated by the small GTPase Ran (for Ras-related nuclear protein), which binds with karyopherins in its GTP-bound form in the nucleus, being an integral component of the transport complex (Fried and Kutay, 2003).

5.2 – XPO1: major nuclear export receptor

5.2.1 – Characteristics and structure of XPO1

XPO1 was first characterized in *S. pombe* in 1989, were mutagenesis conferred deformed nuclear chromosome domains (Adachi and Yanagida, 1989), resulting in its now well-established function of major nuclear export receptor. Human XPO1 protein is a 120 kDa protein composed of

1071 amino acids organized in 20 tandem HEAT repeats (Andrade and Bork, 1995). 3D structure of small fragments of XPO1 were reported in 2004 but the first full-length XPO1 structures were reported in 2009, followed by structures of XPO1-cargo and XPO1-cargo-RanGTP complexes (Dong et al., 2009). Each HEAT repeats forms a hairpin of helices denoted A and B, defining a ring-shaped solenoid, whose outer and inner surfaces comprise the A and B helices, respectively (see figure 26A).

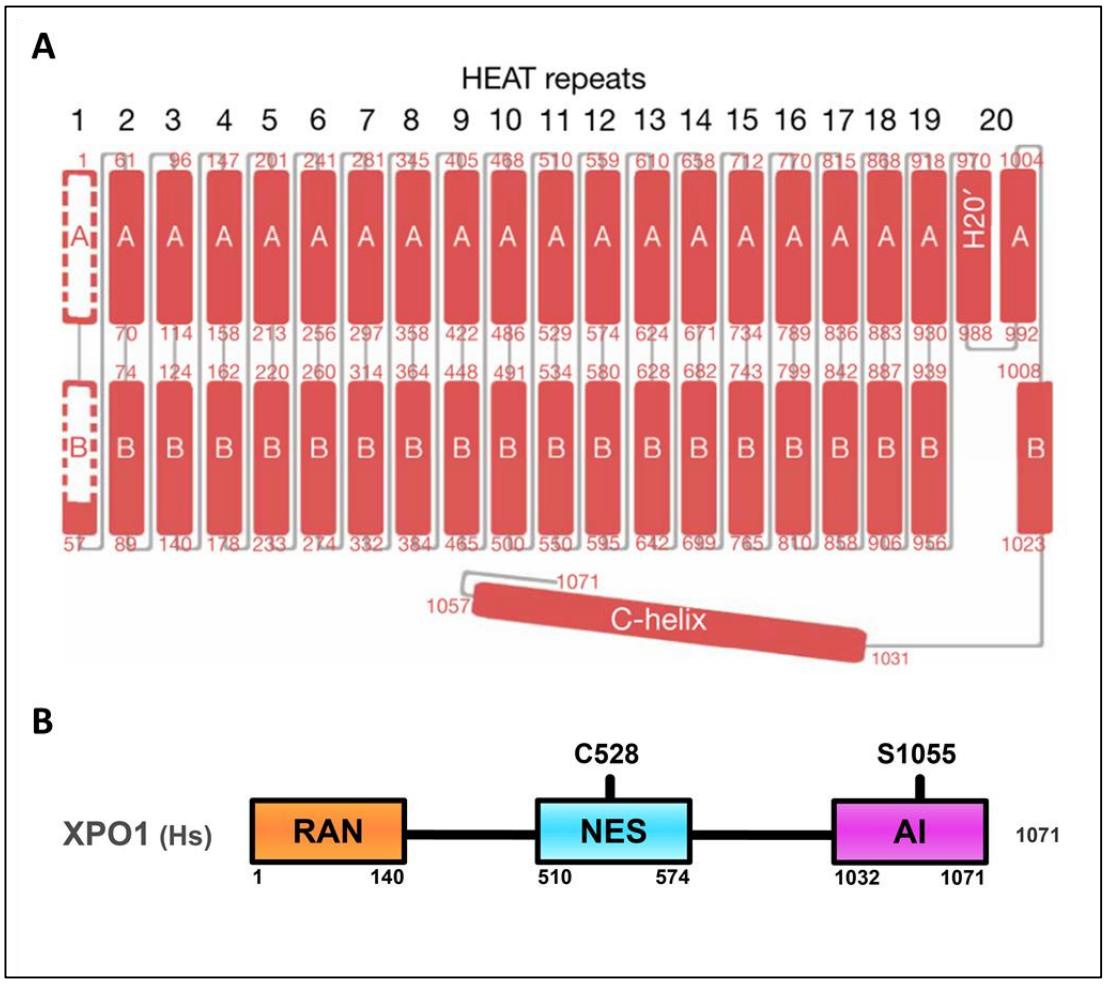

Figure 26 - XPO1 protein structure.
(A) HEAT repeat organization of XPO1. Most of H1 is disordered and not modelled in the structure. From Dong et al., 2009
(B) XPO1 protein domains. Graphical representation that highlights the 3 most important XPO1 domains for this study: the Ran binding domain (RAN), the NES binding domain (NES) and the auto-inhibitory domain (AI). Mutation of Cystein 528 into Serine makes XPO1 insensitive to KPT inhibitors while Serine 1055 plays a central role in this study, see the Results section.

Three main domains for XPO1 can be distinguished for this study (see figure 26B). The first one, comprised of the helices of repeats 2 and 3, is the location of association with Ran-GTP for the export activity, association occurring inside this ring precisely. The second domain, comprised of the helices of repeats 11 and 12, forming a hydrophobic groove on the outer surface of XPO1, binds the NES peptide by forming a docking site (Güttler et al., 2010). The third main domain, comprised of the helix repeat 21 and the c-helix, has been reported as an auto-inhibitory region. In the ternary XPO1-cargo-

RanGTP complex, this auto-inhibitory region packs next to the helix 21A, while its packs to the helices repeats 9 and 10, covering the NES binding domain in the other conformation (Monecke et al., 2009). In addition, it has been reported that deletion of the 39 last amino acid of XPO1, mimicking the deletion of this auto-inhibitory region, enhanced drastically the NES-binding activity as well as the export activity of XPO1 (Dian et al., 2013).

5.2.2 – Protein/RNA export activity

As mentioned above, XPO1 recognizes leucine-rich NESs carried by a wide variety of proteins. Few years ago, a German team attempted to characterize XPO1 cargo-spectrum by deep proteomics relying on mass spectrometry detection (Kirli et al., 2015). Briefly, they identified more than 1050 proteins being under the dependency of XPO1 for their nuclear export in human cells. XPO1 cargos include many tumor suppressors and cell growth regulators such as p53, BRCA1/2, FOXO3, and IκBα (Fung and Chook, 2014), where many of these proteins/cargoes are misregulated and/or mislocalized into the cytoplasm in cancer cells (Turner et al., 2012). Beside the nuclear export of proteins, XPO1 is also responsible for export of rRNA (in ribosomal subunits) and several other, less abundant, RNA species (Hutten and Kehlenbach, 2007).

The export activity of XPO1 requires the action of the small GTPase Ran. To perform this export correctly, a RanGTP-RanGDP gradient is maintained across the nuclear membrane by compartmentalization of Ran regulators. In the nucleus, Ran is predominant in its GTP bound state. In contrast, cytoplasmic Ran is predominant in its GDP state because of the cytoplasmic localisation of the GTPase-activating protein RanGAP1 that catalyses the hydrolysis of RanGTP to RanGDP (Fung and Chook, 2014).

5.3 – XPO1-mediated nuclear export

The active transport of cargoes against concentration gradients depend on an intact nuclear envelope and a nuclear pore complex barrier for retaining already transported cargoes in the desired compartment. This mechanism requires an input of metabolic energy delivered by the RanGTPase system. The XPO1-mdiated nuclear export can be divided in three main steps, the first one consisting of the formation of the trimeric RanGTP-XPO1-cargo complex. The second one consist of the translocation of this trimeric complex across the nuclear pore complex (NPC) followed by the last one, consisting of the dissociation of the trimeric complex, leading to the release of the cargo in the cytoplasm and the recycling of both XPO1 and Ran into the nucleus (see figure 27 for an overview).

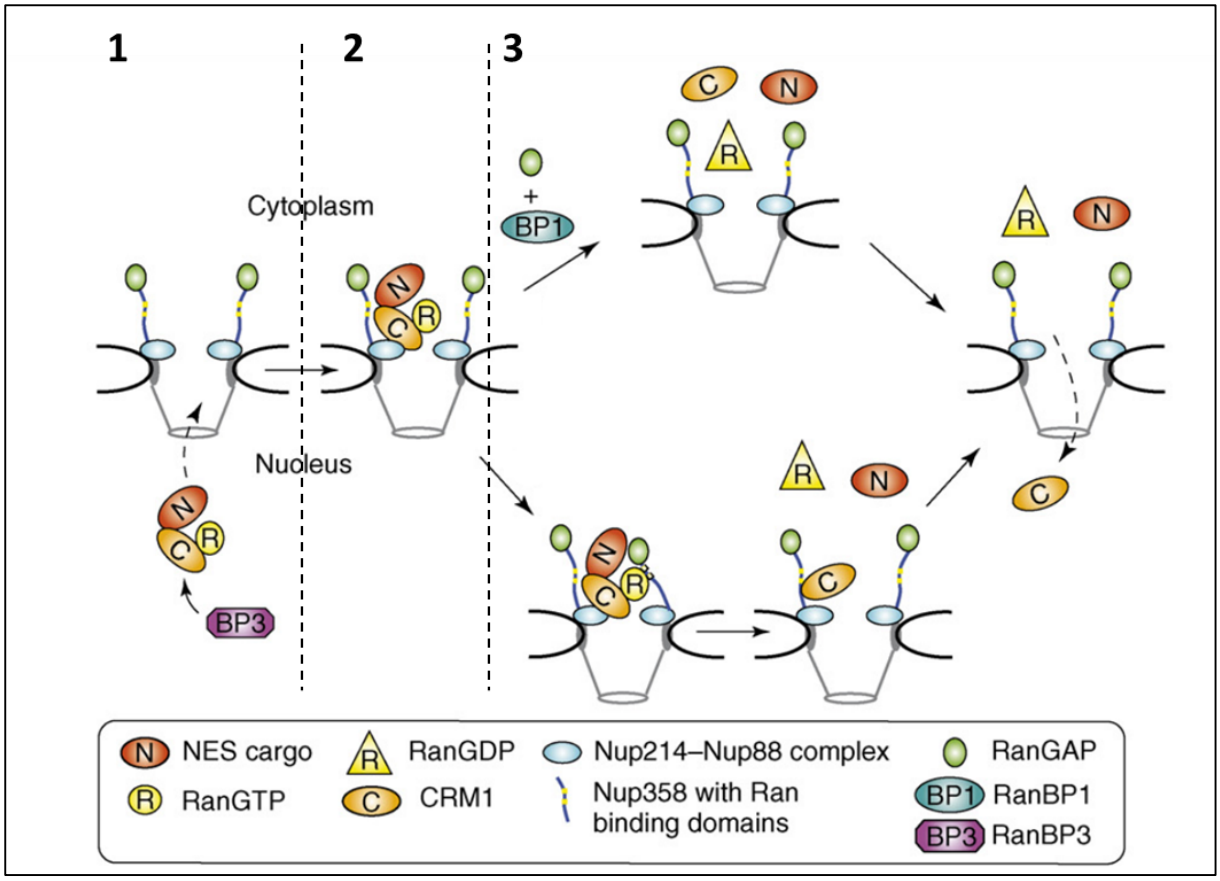

Figure 27 – Overview of the export pathway through the nuclear envelope.
(**1**) In the nucleus, RanBP3 can facilitate the formation of the export complex, containing XPO1 (aka CRM1), RanGTP and the export cargo. (**2**) The complex then translocates through the NPC and interacts with the Nup214–Nup88 complex on the cytoplasmic side of the NPC. (**3**) Hydrolysis of RanGTP to RanGDP by the concerted action of soluble RanGAP and soluble RanBP1 leads directly to the disassembly of the export complex and release of the NES cargo into the cytoplasm. Adapted from Hutten and Kehlenbach, 2007.

5.3.1 – Formation of the export complex

As said previously, XPO1 binds cooperatively to RanGTP and the cargo, leading to a nuclear trimeric transport complex (figure 27). It has been reported that the binding of NES-containing proteins with XPO1 could be either positively or negatively regulated by phosphorylation of the cargo. For example, phosphorylation of cyclin D1 promotes its export by XPO1 (Benzeno et al., 2006), while phosphorylation of c-Fos inhibits the nuclear export of this transcription factor (Sasaki et al., 2006). Two independent mechanisms mediated by the Ran-binding protein RanBP3 drive the formation of the export complex. First, RanBP3 tethers XPO1 to RCC1 and enhance the catalytic activity of RCC1, leading to the GDP-GTP exchange on Ran, increasing the RanGTP concentration in the vicinity of XPO1 (Nemergut et al., 2002). The second mechanism result in the increased affinity of XPO1 for NES containing cargoes caused by the binding of RanBP3 to XPO1 (figure 27 section 1). It has been suggested, by mutagenesis studies and molecular modelling, that RanBP3 stabilizes a XPO1 conformation that invites both cargo and RanGTP for binding, RanBP3 acting as a co-factor in XPO1-mediated export (Englmeier et al., 2001).

5.3.2 – Translocation through the nuclear pore complex

The directionality of transport is mainly imposed by the Ran GTP/GDP gradient, which favours the assembly of export complexes and the disassembly of import complexes in the nucleus though the cytoplasmic nucleoporins Nup proteins. XPO1 is known to interact with several nucleoporins such as Nup358 (aka RanBP2), Nup214, and Nup88. It has been found that NES cargoes increased the affinity of XPO1 to Nup214 (Hutten and Kehlenbach, 2006), giving a first insight of this translocation mechanism (figure 27, section 2). Nup358 is known to be the major component of the cytoplasmic filaments of the NPC and have a supportive role in XPO1-mediated export (Walther et al., 2002).

5.3.3 – Dissociation of the export complex

When the trimeric RanGTP-cargo-XPO1 complex has been transported to the cytoplasmic side of the NPC through the nucleoporins, the dissociation of the cargo from this complex, as well as the recycling of both XPO1 and Ran and their transport into the nucleus occurs. The RanGAP and RanBP1 have been reported to by soluble in the cytoplasm and suggested, with Nup358, to promote the dissociation of the export complex from its terminal binding site (Hutten and Kehlenbach, 2007) (figure 27, section 3). For the disassembly of the complex, RanGTP need to be hydrolysed. To do so, RanBP1 releases RanGTP to the trimeric complex, allowing RanGAP to hydrolyses GTP to GDP (Kehlenbach et al., 1999). The mechanism responsible for the reimport of XPO1 in the nucleus is even more elusive at this time than the nuclear export one, but Nup358 seems to be involved in this reimport by transient interaction with XPO1 (Hutten and Kehlenbach, 2007).

5.4 – Targeting XPO1: relevance in cancer therapy

The appropriate spatiotemporal localisation of molecules in the nucleus or the cytoplasm, regulated by the bidirectional transport system channel through the NPC, is crucial for cellular homeostasis. Defect in proper localisation of these molecules may alter their activities, thus disturbing the cell homeostasis and causing diseases such as cancer. It has been reported that nucleo/cytoplasmic shuttling dysregulation is involved in cancer cell survival, tumor progression, carcinogenesis, and drug resistance (Hung and Link, 2011). Many tumor suppressor proteins execute their antineoplastic functions into the nucleus, where upregulated nuclear export machinery could result in their functional inactivation (Gravina et al., 2014).

XPO1 has been found overexpressed in a large variety of tumors (see figure 28 for XPO1 alteration frequency in cancers), where its upregulation is associated with drug resistance and stands out as a poor prognosis factor in many malignancies (Sun et al., 2016), where the pathologic role of XPO1 and the underlying molecular mechanisms remain to be elucidated.

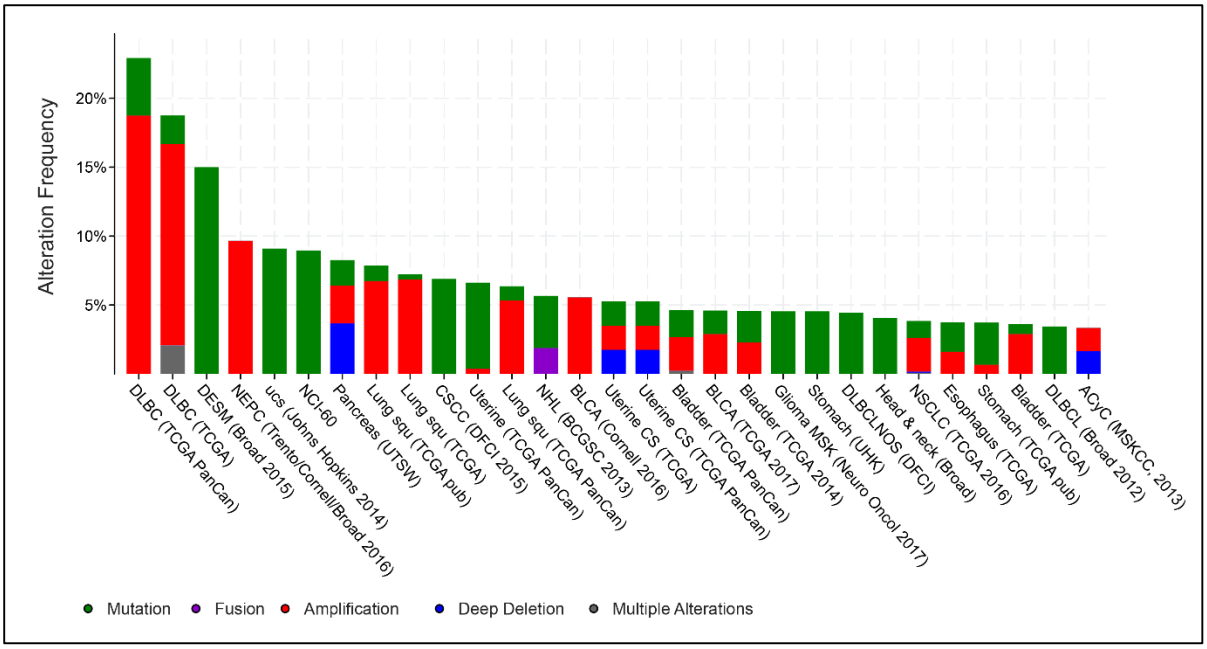

Figure 28 - XPO1 alteration frequency in cancer.
Graphical representation of XPO1 alteration frequency in several cancer types (only the 29 most important are shown). Source: cBioPortal.

Due to the critical role of XPO1 in nucleo/cytoplasmic shuttling and in tumor progression, its inhibition has emerged as a therapeutic strategy in cancer. The rational behind targeting XPO1 is very simple: increasing the nuclear concentration of tumor suppressor proteins using specific chemical inhibitors against XPO1 nuclear export activity, where one of them, Selinexor (KPT-330), is entering for phase II clinical studies. The first XPO1 inhibitor discovered was Leptomycin B (LMB), that covalently binds a cysteine residue (C528) in the cargo-binding domain of XPO1, preventing the cargo interaction with XPO1 (Kudo et al., 1999). Where LMB demonstrated efficient antitumor activity *in vitro*, it demonstrated severe toxicity attributed to off-target effects due to its binding to several cysteine proteases, in addition to the irreversible inhibition of XPO1, preventing its further clinical development (Lapalombella et al., 2012).

The atomic level understanding of CRM1 function has greatly facilitated recent drug discovery and development of CRM1 inhibitors to target a variety of malignancies. Thanks to these discoveries, a novel group of small molecule compounds, called selective inhibitors of nuclear export (SINE), have been developed. These SINEs, including KPT-115, KPT-127, KPT-185, KPT-251, KPT- 276, KPT-330 (Selinexor), and KPT-335 (Verdinexor), bind reversibly to the C528 residue of XPO1, with virtually no off-target effect (figure 29). These SINE compounds have been shown to inhibit the nuclear export of many tumor suppressor proteins harbouring key roles in genomic stability and DNA repair (TP53, TP73, and BRCA1), cell cycle progression (pRB1, CDKN1A, and CDKN1B), and apoptosis (FOXO, APC, and IκBα) in cancer cell lines and tumor biopsies (Conforti et al., 2015).

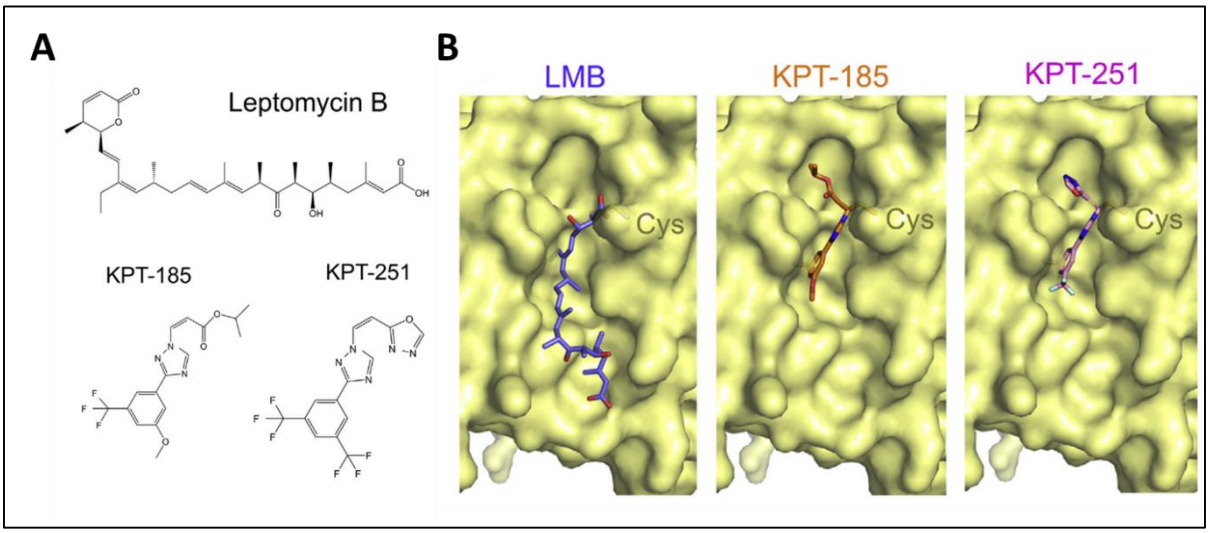

Figure 29 - Chemical inhibition of XPO1.
(A) Chemical structures of Leptomycin B (LMB), KPT-185 and KPT-251. (B) The XPO1 NES groove bound to LMB, KPT-185, and KPT-251. The reactive cysteine residue in the XPO1 NES groove which forms covalent bonds with the inhibitors is labelled. Adapted from Fung and Chook, 2014.

Defect in the nucleo/cytoplasmic shuttling may contribute to drug resistance, and in this regard, XPO1 inhibitors have shown synergistic anticancer activity when used in combination with targeted therapeutic agents or chemotherapy. It has been reported that XPO1 inhibition in myeloma cells reverted the resistance of these cells to doxorubicin and etoposide by inhibiting the nuclear export of topoisomerase II (Turner et al., 2012). In chronic myeloid leukemia cells, XPO1 inhibition leads to the nuclear sequestration of the BCR-ABL1 fusion oncoprotein, annihilating its mitogenic and antiapoptotic activities occurring in the cytoplasm. XPO1 inhibition and imatinib combination has been reported to induce death of imatinib-resistant cells (Turner et al., 2012).

At this time, KPT-330 (Selinexor) is the most represented XPO1 inhibitor in the phase I/II clinical trials with 64 on-going clinical trials registered at the ClinicalTrials.Gov database (http://clinicaltrials.gov/ct2/home). Other novel generated XPO1 inhibitors such as SL-801 and KPT-8602 are also registered under phase I/II clinical trials. Inhibition of XPO1 has been reported with promising preliminary results in hematologic malignancies and solid tumors where XPO1 inhibitors have been shown to preferentially supress or eliminate tumour cells, relatively sparing normal cells.

THESIS RATIONAL

This PhD project is part of the global work of Jacques Camonis laboratory whose main goal is to identify and understand the physio-pathological role of RalGTPases in normal and Ras-driven cancer cells and their underlying molecular mechanisms. One derived product would be to shine light on novel potential targeted therapies in Ras-driven cancers. Since the last decades, our team established the crucial role and implication of the Ras/Ral axis in several pro-tumorigenic mechanisms such as proliferation (O. Santos et al., 2016), cytokinesis (Cascone et al., 2008), autophagy (Bodemann et al., 2011), invasion and metastasis (Biondini et al., 2015; Zago et al., 2018), and migration (Biondini et al., 2016).

Most significantly, during its journey downstream of the Ras-RalGTPase-Exocyst complex axis, our team established a link between this previous cited complex and the Hippo tumor suppressor pathway. In order to define the Ral interactome, using Y2H screens, our team identified STK38 as a novel actor in Ral interactome. Digging into the relevance of this partnership in Ral-related functions, our team established that STK38 acts as a mediator of Ral signalling in stress management by reporting that under osmotic shock and apoptosis induction, MAP4K4, an effector of RalA via the Exocyst complex, activates STK38 though phosphorylation (Selimoglu et al., 2014).

Having discovered this novel link between the Ral-Exocyst complex axis and the Hippo pathway through the kinase STK38, our team discovered, using Y2H approach again, that STK38 interacts with the autophagy regulator Beclin1. Carine Joffre, a former post-doc of our team, investigated this link and discovered that STK38 is required for autophagy and that RalB acts upstream of STK38 (Joffre et al., 2015). The team went next to investigate the implication of this Ral-STK38 signaling axis regarding tumorigenesis, and more particularly in Ras-induced oncogenesis. Audrey Bettoun, a former PhD student of the team, discovered that Ras-induced transformation is regulated by RalGTPases through recruitment of STK38 (Bettoun et al., 2016). Furthermore, they uncovered the fact that STK38 is required for anchorage-independent growth in Ras driven oncogenesis, a hallmark of oncogenesis.

All these findings led to the elaboration of the main project of my thesis with two different specific goals aiming to characterize at the molecular level the required-implication of STK38 in two Ral-related functions supporting cancer cells survival: autophagy and anchorage-independent growth.

These aims are:

1) Identify and characterize STK38 interactome upon autophagy and anchorage-independent growth. As said previously, STK38 has been reported to be crucial for these mechanisms used by cancer cells to survive. Does STK38 modulates its interaction with specific proteins for its different tasks? Are these specific partners implicated in distinct cellular and molecular functions? Are they connected to, and so, does STK38 trigger, particular signaling pathways? The better understanding of STK38 partnership would let us to better understand the molecular mechanisms mobilized by STK38 in these two of its multifarious functions
2) Characterize at the molecular level the specific STK38-dependent event(s) occurring upon these pro-survival functions. The underlying biological question here is that STK38 is a kinase, with a unique discrete function: phosphorylating, and so, triggering activation of substrates. Does STK38 triggers specific numerous molecular events in these multifarious functions or are these unrelated functions regulated by a unique molecular mechanism triggered by STK38?

RESULTS

STK38 regulates the nuclear export of downstream partners by phosphorylating the auto-inhibitory domain of XPO1

Alexandre PJ Martin[1,2], Maarten Jacquemyn[3], Joanna Lipecka[4,8], Vassily N. Aushev[5], Brigitte Meunier[1,2], Manish K Singh[1,2], Nicolas Carpi[2,6], Matthieu Piel[2,6], Patrice Codogno[7,8], Alexander Hergovich[9], Maria-Carla Parrini[1,2], Gerard Zalcman[1,2], Ida Chiara Guerrera[8,10], Dirk Daelemans[3], Jacques H Camonis[1,2,11]

Manuscript under review

[1] ART group, Inserm U830
[2] Institut Curie, Centre de Recherche, Paris Sciences et Lettres Research University, 75005 Paris, France
[3] KU Leuven Department of Microbiology and Immunology, Laboratory of Virology and Chemotherapy, Rega Institute for Medical Research, KU Leuven, 3000 Leuven, Belgium
[4] Inserm U894, Center of Psychiatry and Neuroscience, Paris, France
[5] Icahn School of Medicine at Mount Sinai, 1 Gustave Levy Place, New York, NY 10029, USA
[6] CNRS, UMR 144
[7] Inserm U1151/CNRS UMR 8253, Institut Necker Enfants-Malades
[8] Université Paris Descartes, Sorbonne Paris Cité, Paris, France
[9] University College London, Cancer Institute, London, WC1E 6BT, United Kingdom
[10] Proteomics platform 3P5-Necker, Université Paris Descartes - Structure Fédérative de Recherche Necker, INSERM US24/CNRS UMS3633, Paris 75014, France.
[11] The Biophenics Project, Translational Biology Department, Institut Curie, 75005 Paris, France

Graphical Abstract

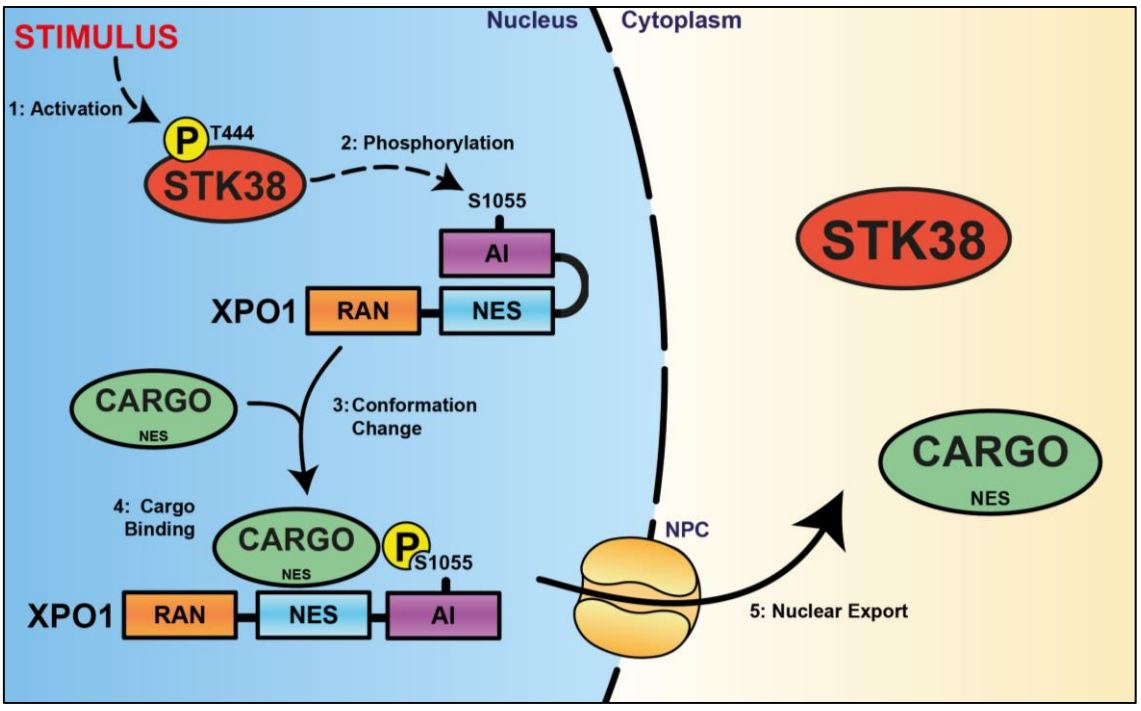

In Brief

- STK38 shuttles between the nucleus and the cytoplasm for its biological functions
- STK38 activates XPO1 by phosphorylation on serine 1055 within XPO1 autoinhibitory domain
- STK38 regulates its own nuclear exit by phosphorylating XPO1
- STK38 controls the nuclear exit of downstream regulators such as Beclin1, YAP1, and Centrin

Background of the project

As mentioned in the "Thesis rational" part of this thesis, my PhD project comes on top of two previous publications of our team. The first one recapitulates the work of Carine Joffre, a former post-doc of the team. She characterized the permissive role of STK38 for autophagy induced by nutrient starvation (Joffre et al., 2015). The molecular basis of its action can be counted, or not, by its binding to the autophagy essential protein Beclin1. The second publication summarize the work of a former PhD student of the team, Audrey Bettoun. She showed that STK38 is required for anchorage-independent growth survival of Ras-driven cancer cells. These two publications, that defined new and unsuspected STK38's biological functions in cancer cells, had opened the master plan of my future work.

Summary of the results

STK38 associates with cytoplasmic partners upon starvation and with nuclear proteins upon suspension (figure 1 of the manuscript)

The first objective of this work was to identify and characterize the proteins that interact with STK38 in two processes supporting cancer cell survival (Bettoun et al., 2016; Joffre et al., 2015).

To achieve this goal, we took advantage of a rather novel proteomic approach: the proximity biotinylation assay coupled to mass spectrometry detection (Rhee et al., 2013), composed of two distinct parts: the proximity labelling and purification of proteins of interest and then the protein identification by mass spectrometry. Briefly, this assay relies on one protein, APEX2, that transfer a biotin group on electron-rich amino acids (Tyr, Trp, His, and Cys) of all proteins within a 20 nm radius when cells are grown in presence of phenol-biotin and hydrogen peroxide (figure 30).

We engineered cell lines stably expressing STK38 fused with APEX2: HeLa cells for the autophagy condition and HekRasV12 cells for suspension conditions. These are the cell lines in which Joffre et al. and Bettoun et al. had firmly established the necessity of STK38 for autophagy induction upon starvation and anoïkis survival, respectively (Bettoun et al., 2016; Joffre et al., 2015). We applied a SILAC method in each condition to have reliable quantitative proteomic data and then be able to evaluate the dynamic of association of each STK38 interactor upon each experimental condition (see Fig. S1 of the manuscript for an illustrated example).

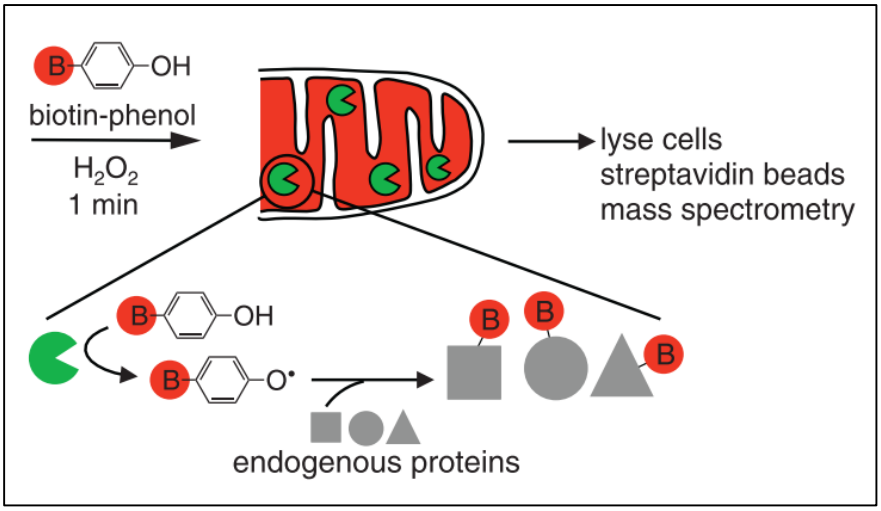

Figure 30 – The proximity biotinylation assay.
Cell are transfected with APEX (normally fused to a protein of interest) and treated with biotin-phenol and H2O2 for 1 minute. This incubation allow APEX2 to transfer the biotin group to all proteins in a 20 nm radius. Cells are then lysed and biotinylated proteins purified before mass spectrometry detection. Adapted from Rhee et al, 2013.

We identified 97 binding partners for STK38 in the context of nutrient starvation-induced autophagy and 221 for the suspension condition. Among all these newly identified partners, 50 were identified in both nutrient starvation-induced autophagy and suspension conditions, displaying a differential pattern of association with STK38, depending on the context. By interrogating Gene Ontology databases for the most enriched terms as "cellular component", we found that STK38 increases its association with cytoplasmic proteins upon nutrient starvation-induced autophagy. On the other hand, we found that STK38 decreases its association with these cytoplasmic proteins in favor of nuclear partners when cells are cultured in suspension.

STK38 accumulates in the cytoplasm upon starvation in a XPO1-dependent manner (figure 2 of the manuscript)

This different localizations of partners imply that STK38 has to shuttle between the nucleus and the cytoplasm in order to establish these partnerships for its different functions. One protein, that we identified in our proteomic screen, could be the key element of this hypothesis: the major nuclear export receptor, XPO1. Another reinforcing element put influence on the potential role of XPO1: a publication from 2015 identified STK38 as a XPO1 cargo (Kirli et al., 2015).

I first validated by co-immunoprecipitation that STK38 binds to XPO1, supporting the results obtained from our proteomic screen. Next, to test my STK38 nucleo/cytoplasmic shuttling hypothesis, I followed STK38 subcellular localization in HeLa cells by immunofluorescence. Because of the lack of specificity of commercially available antibodies against STK38 for immunofluorescence, I transfected cells with an exogenous STK38 fused to myc epitope.

The figure 2 of the manuscript prove that STK38 indeed exit the nucleus and accumulates in the cytoplasm upon nutrient starvation. Furthermore, using specific chemical inhibitors of XPO1 (see chapter 5.4 of the thesis introduction), I demonstrated that this STK38 nuclear export is under the dependency of XPO1. Finally, I showed that XPO1 export activity is not only required for STK38 nuclear exit upon nutrient starvation, but is also required for the resulting autophagic flux.

STK38 kinase activity is required and sufficient for its nuclear exit and autophagy upon starvation (figure 3 of the manuscript)

The next question ensued from the nature of STK38 itself: does STK38 kinase activity required for its nuclear exit?

I assessed the subcellular localization of different exogenous variants of STK38 in HeLa cells upon starvation. I found that the kinase dead version of STK38 wasn't able to exit the nucleus upon starvation whereas an hyper-active mutant accumulated in the cytoplasm even in nutrient rich conditions, demonstrating that STK38 kinase activity is required and sufficient for STK38 nuclear exit. I also investigated whether STK38 kinase activity is also required for the resulting autophagic process upon nutrient starvation, in addition to its role in STK38 nuclear exit. I found, also using exogenous variants of STK38 in the same condition as described above, that STK38 kinase activity is required and sufficient for the autophagy process.

STK38 phosphorylates XPO1 on serine 1055 (figure 4 of the manuscript)

XPO1 amino acid sequence harbors a STK38 phosphorylation motif embedded into the auto-inhibitory domain of XPO1 where the target amino acid is the serine 1055. This serine has been reported in a mass spectrometry phospho-proteomic paper to be indeed phosphorylated (Beausoleil et al., 2004). My hypothesis was now that STK38 is the kinase responsible for this phosphorylation. I challenged this hypothesis using a newly engineered specific antibody against phosphorylated XPO1_S1055.

I discovered that XPO1_S1055 was phosphorylated when cells were treated with okadaic acid, a potent inhibitor of protein phosphatase type 2A. Knockdown of endogenous STK38 using two independent siRNA abolished the phosphorylation of XPO1 on S1055, demonstrating that STK38 phosphorylates XPO1.

XPO1_S1055 phosphorylation is instructive and permissive for STK38 nuclear exit and autophagy upon starvation (figure 5 of the manuscript)

We next wondered whether S1055 phosphorylation by STK38 is important for XPO1-dependent STK38 nuclear export and, more globally, for XPO1 export activity, whatever the cargo. I undertook a two step strategy:

1. In order to get rid of endogenous XPO1 activity, I used the powerful and specific XPO1 inhibitor KPT-185
2. I transfected XPO1 variants harboring two mutations:
    a. Mutations on serine 1055, in order to appreciate its phosphorylation impact on XPO1 export activity
    b. A C528 to S mutation in all XPO1 variants used conferring resistance to KPT-185 inhibitor

This pharmaco-genomic approach allowed to question the functionality of the transfected XPO1 variants, without any parasitic confusion generated by endogenous wt XPO1. In this context, I tracked STK38 subcellular distribution in HeLa cells, questioning XPO1 variants for S1055. I tested a S1055A mutant that cannot be phosphorylated by any kinase and two phosphomimetic mutants (S1055D and S1055E).

The results were beyond our hope. I discovered that a S1055A mutant prevented all nuclear export of STK38 upon nutrient starvation: thus phosphorylation of S1055 is necessary for the export function of XPO1. On the other hand, phosphomimetics variants of XPO1 induced a cytoplasmic accumulation of STK38 in both well fed and starved cells, as well as a variant lacking the C-terminal auto-inhibitory domain of XPO1. These results revealed two important points. The first one is that S1055 phosphorylation of XPO1 is required and sufficient for the nuclear export of STK38. The second one point toward the auto-inhibitory domain of XPO1 where S1055 phosphorylation releases XPO1 auto-inhibitory activity, opening up the cargo binding site (see chapter 5.2.1 of the thesis introduction for XPO1 structure). These results highlight the fact that STK38 is its own gatekeeper, controlling its own subcellular distribution by phosphorylation the serine 1055 of XPO1.

In addition to the contribution of S1055 phosphorylation impact on XPO1-dependent nuclear exit of STK38, I investigated its role in the autophagic process. I observed, using genome edited cell lines, that XPO1's S1055 phosphorylation was required for the autophagic flux upon nutrient starvation. On the other hand, phosphomimetics variants of XPO1 were able to induce an autophagic flux even in complete growth conditions, indicating that phosphorylation of XPO1 S1055 is not only required for nutrient starvation-inducted autophagy, but also sufficient to induce autophagy.

Beclin1, YAP1, and Centrin subcellular localizations are also regulated by XPO1_S1055 phosphorylation by STK38 (figure 6, 7, and S9 of the manuscript)

The need of S1055 phosphorylation by STK38 for the sake of its own export is interesting but could remain anecdotic. Or is it? Are other cargoes of XPO1 also dependent on S1055 phosphorylation by STK38 for their nuclear export?

To extend our findings to a more general model, I investigated the contribution of the STK38-dependent phosphorylation of XPO1 to other XPO1 cargoes related to STK38 biological functions. I discovered that the subcellular distribution of both Beclin1, a major autophagy regulator (see section 3.2.2 of the introduction), and YAP1, the Hippo terminal effector (see section 2.1 of the introduction) are controlled by the STK38-dependent phosphorylation of XPO1 on serine 1055. I also found that centrosome duplication, and more specifically Centrin subcellular localization, is under the dependency of both STK38 and XPO1, suggesting here that the STK38-dependent phosphorylation of XPO1 could be the main regulator of this additional function. The impact of XPO1 serine 1055 phosphorylation on Centrin subcellular localization and on centrosome duplication couldn't be further analyzed due to a lack of compatibility of the required tools.

These results indicate that STK38 not only regulates its own subcellular localization that is important for its biological functions, but also controls the nuclear export of other downstream partners, everything by a same molecular mechanism on a unique substrate.

Significance for the field

As a general remark, this work provides as example that multifarious and unrelated functions, conferred to a single actor, can be attributed to a unique mechanism help by this single actor. I succeeded in the identification of STK38 interactors in two different of its biological functions by implanting the proximity biotinylation assay in the lab. Furthermore, I went beyond the establishment of an elementary interaction map of STK38 by adding the dimension of the dynamic, allowing the characterization of the association of STK38 with different sets of partners depending on the context, and the resulting biological relevance of these interactions. This conceptual model “multiple functions, a unique substrate” works when the substrate is the limiting factor for the accomplishment of the multiple functions.

Using this assay in order to determine the precise dynamic of association of one protein in different contexts has never been done before, this assay having been used for interactors identification or the characterization of proteins embedded in specific subcellular organelles. By demonstrating that the assay is enough powerful and sensitive at the same time, this work should provide new conceptual view on interactors identification with the incorporation of the dynamic dimension.

More specifically, this work provides new insight on the biological role of STK38 in cellular homeostasis by characterizing it as a major mediator of nuclear export. Going further, we can claim that STK38 is a cofactor of XPO1. This role can be seen as new for this kinase, among all the others multifarious and unrelated biological functions enumerated in section 2.2.3 of the introduction of this thesis. On the other hand, we can see this new nuclear export mediator role as the major upstream function of STK38, regulating in fact the previous reported biological functions. Finally, this work identified the first known activator of XPO1, the major nuclear export receptor: STK38.

MANUSCRIPT

STK38 regulates the nuclear export of downstream partners by phosphorylating the auto-inhibitory domain of XPO1

Alexandre PJ Martin[1,2], Maarten Jacquemyn[3], Joanna Lipecka[4,8], Vassily N. Aushev[5], Brigitte Meunier[1,2], Manish K Singh[1,2], Nicolas Carpi[2,6], Matthieu Piel[2,6], Patrice Codogno[7,8], Alexander Hergovich[9], Maria Carla Parrini[1,2], Gerard Zalcman[1,2,10], Ida Chiara Guerrera[8,11], Dirk Daelemans[3], Jacques H Camonis[1,2,12]

[1] ART group, Inserm U830
[2] Institut Curie, Centre de Recherche, Paris Sciences et Lettres Research University, 75005 Paris, France
[3] KU Leuven Department of Microbiology and Immunology, Laboratory of Virology and Chemotherapy, Rega Institute for Medical Research, KU Leuven, 3000 Leuven, Belgium
[4] Inserm U894, Center of Psychiatry and Neuroscience, Paris, France
[5] Icahn School of Medicine at Mount Sinai, 1 Gustave Levy Place, New York, NY 10029, USA
[6] CNRS, UMR 144
[7] Inserm U1151/CNRS UMR 8253, Institut Necker Enfants-Malades
[8] Université Paris Descartes, Sorbonne Paris Cité, Paris, France
[9] University College London, Cancer Institute, London, WC1E 6BT, United Kingdom
[10] Université Paris Diderot, Sorbonne Paris Cité, Paris, France
[11] Proteomics platform 3P5-Necker, Université Paris Descartes - Structure Fédérative de Recherche Necker, INSERM US24/CNRS UMS3633, Paris 75014, France.
[12] The Biophenics Project, Translational Biology Department, Institut Curie, 75005 Paris, France

Correspondence
Jacques H Camonis
Mail: JCamonis.Institut.Curie@gmail.com
Phone
Off.: +33 (0)1 56 24 66 54
Secr.: +33 (0)1 56 24 66 49
Fax: +33 (0)1 56 24 66 50
Mob.: +33 (0)6 63 83 14 67
26 rue d'Ulm, 75248 Paris cedex 05, France

Key words:
STK38, XPO1, Autophagy, Hippo pathway, YAP1, Proximity Labelling, APEX2

SUMMARY

STK38 (also known as NDR1) is a Hippo pathway serine/threonine protein kinase with multifarious functions in normal and cancer cells. Using a context-dependent proximity-labelling assay, we discovered that STK38 modulates its interaction with more than 250 different proteins depending on the subcellular context. STK38 associates with nuclear related partners upon ECM detachment and with cytoplasmic related proteins upon autophagy. This differential localisation-dependent activity relies on the XPO1 (aka Exportin-1, CRM1) mediated nuclear export of STK38. We further uncovered that the XPO1-mediated export of STK38 is dependent on XPO1 phosphorylation serine 1055 by STK38 itself. Thus, in addition to regulating its own nuclear export, STK38 also controls the subcellular distribution of Beclin1, a key regulator of autophagy. Moreover, the regulation of XPO1 by STK38 mediates the nuclear exclusion of YAP1, the Hippo pathway terminal transcriptional effector. Collectively, our results reveal that functions of STK38 are linked to the XPO1-mediated subcellular distribution of STK38 and key regulators. These observations show that apparently unrelated cellular functions could be regulated the same molecular mechanism, controlled by a single kinase, and establish a novel mechanism of XPO1-dependent cargo export regulation by phosphorylation of XPO1's C-terminal auto-inhibitory domain.

INTRODUCTION

The serine/threonine kinase 38 STK38, also known as NDR1, is important in diverse biological functions, playing roles in cell cycle progression (Cornils et al., 2011a, 2011b), apoptosis (Vichalkovski et al., 2008) and centrosome duplication (Hergovich et al., 2007, 2009). As a member of the Hippo core signalling, STK38 can directly phosphorylate the Hippo effector YAP1 on S127, resulting in YAP1 inactivation by cytoplasmic sequestration (Zhang et al., 2015). In addition, STK38 has pro-cancer cell survival functions in stress response and adaptation. On the other hand, STK38 can respond to osmotic shock and to the expression of RASSF1A, a Hippo pathway regulator (Selimoglu et al., 2014). Moreover, STK38 kinase activity is required for autophagy induction in response to starvation by regulating Beclin1 (Joffre et al., 2015). Finally, STK38 was also reported to be involved in resistance to anoïkis (ECM detachment-induced apoptosis) of cancer cells (Bettoun et al., 2016).

To understand how STK38 can perform these crucial, but clearly distinct functions, we performed a proximity-dependent biotinylation to map STK38 protein-protein interactions in different cellular contexts. This revealed that STK38 interacts mainly with cytoplasmic proteins upon starvation-induced autophagy, and with nuclear proteins after ECM detachment, suggesting that the subcellular localisation of STK38 may play a regulatory role in response to these diverse stimuli. Moreover, we discovered that STK38 phosphorylates the serine 1055 in the auto-inhibitory domain of XPO1 (Exportin-1, aka CRM1), thereby triggering the nuclear export of STK38 itself, as well as known XPO1 substrates such as Beclin1 and YAP1. These results suggest that STK38 regulates the subcellular localisation and thereby the function of central cellular components by modulating their nuclear export via phosphorylation of XPO1.

RESULTS

STK38 interacts with different sets of partners depending on the cellular context

To identify the proteins that interact with STK38 upon nutrient starvation-induced autophagy, or when cells resist to anoïkis in suspension, we applied a context-dependent proteomic approach (Rhee et al., 2013) by establishing cell lines stably expressing APEX2 N-terminally fused to STK38 (Fig. S1). HeLa cells were used for nutrient-starvation condition and HEK-HT-HRasG12V cells (hereafter referred as HekRasV12) (Counter et al., 1998; Hahn et al., 1999) for anoïkis resistance condition, to match with previous studies of STK38's roles in autophagy (Joffre et al., 2015) and survival upon ECM detachment (Bettoun et al., 2016), respectively. To discriminate between STK38's basal interactors context-dependent ones, we applied a quantitative SILAC proteomic methodology. Briefly, a referential condition was performed in parallel to the studied ones: complete medium incubation vs. nutrient starvation-induced autophagy (see Fig. S1 for this example), and attached growth vs. suspension growth. Validation of autophagy process (Fig. S2A and S2B) and biotinylation efficiency in both contexts (Fig. S2C and S2D) was performed before mass spectrometry (MS) identification. Each replicate displayed a good correlation between experiments (Fig. S2E), indicating a high reproducibility between biological triplicate samples.

A total of 97 binding partners of STK38 were identified in the context of nutrient starvation-induced autophagy and 221 partners were identified upon suspension condition (Fig. 1A) (Table S1 for the complete list). Several known interactors of STK38 were identified such as MAP4K4 (Selimoglu et al., 2014), HIST2H2AC (Campos et al., 2015), EWSR1 (Elzi et al., 2014), NPM1 (Chen et al., 2013), YWHAZ (Jin et al., 2004) and MAGOH (Singh et al., 2012). Among the 97 interactors identified upon nutrient starvation, 32 displayed an interaction with STK38 that was significantly increased as compared to rich medium, while interaction with only one protein was decreased in this condition. Upon ECM detachment, 44 proteins displayed an increased interaction with STK38, while for 72 proteins the interaction with STK38 was decreased. Interestingly, 50 partners were common to both nutrient starvation-induced autophagy and ECM detachment conditions, but displayed a differential association status with STK38, depending on the context (Fig. 1A). These 50 common partners were assessed for unsupervised hierarchical clustering, based on their association status with STK38, resulting in two main clusters as highlighted in orange and purple in Fig. 1B. The orange cluster is mainly composed of 31 proteins displaying increased association with STK38 upon nutrient starvation-induced autophagy, but decreased binding upon ECM detachment. The purple cluster consist of 19 proteins showing an increased interaction with STK38 in suspension, while being unaffected upon nutrient starvation-induced autophagy. Gene Ontology analysis of these two groups of interactors revealed a striking difference (Fig. 1C): the most enriched terms of the interactors under nutrient starvation-induced autophagy are proteins localized into the cytoplasm, while the cluster enriched upon ECM detachment contains nucleus-associated functions. These results suggest that upon autophagy induction, STK38 associates with cytoplasmic partners while, upon ECM detachment, STK38 appears to preferentially interact with nuclear proteins.

STK38 interacts with XPO1

The above observations imply that STK38 shuttles between the nucleus and the cytoplasm. Exportin-1 (XPO1), also known as the chromosomal region maintenance protein 1 (CRM1), the main nuclear export factor (karyopherin) that transports a wide diversity of proteins from the nucleus to the cytoplasm (Fornerod et al., 1997; Nishida et al., 1997; Ossareh-Nazari et al.,

1997; Stade et al., 1997), was identified in our screen as a novel STK38 interactor (Table S1). To investigate whether STK38 interacts with XPO1, we performed a pull-down experiment. Myc tagged STK38 was transiently co-expressed with Flag-XPO1 or Flag-Sirt3 as a control. Upon pull-down using Flag antibody, STK38 co-immunoprecipitated with XPO1 but not with Flag-Sirt3 (Fig. 2A), suggesting that STK38 interacts with XPO1. In addition, inhibiting protein phosphatase type 2A (PP2A) with Okadaic Acid (OA) did not modify the binding of STK38 and XPO1, indicating that increased STK38 phosphorylation is not required for its association with XPO1.

STK38 accumulates in the cytoplasm upon nutrient starvation-induced autophagy in a XPO1-dependent manner

Our proximity labelling experiment demonstrated that STK38 interacts mainly with cytoplasmic proteins upon nutrient starvation, suggesting that in this condition, STK38 is localized to the cytoplasm. Due to the lack of specific and sensitive antibodies to follow endogenous STK38 subcellular localisation using immunofluorescence (IF), HeLa cells were transfected with a plasmid expressing myc-tagged STK38. Immunostaining of STK38 in nutrient starved cells (EBSS medium) demonstrated that STK38 localizes mainly to the cytoplasm, while in nutrient rich medium (complete, DMEM) STK38 is mainly localised in the nucleus (Fig. 2B and 2C). Interestingly, the highly selective XPO1 inhibitors KPT-185 and KPT-330 (Lapalombella et al., 2012; Neggers et al., 2015) inhibited STK38's exit form the nucleus. XPO1 inhibition by KPT-185 and KPT-330 was validated in parallel by monitoring the nucleo/cytoplasmic localisation of a well-known cargo of XPO1: IκBα (Fig. S3A and S3B). Together, these results indicate that STK38 shuttles from nucleus to the cytoplasm upon nutrient starvation in a XPO1-dependent manner.

To study whether the XPO1-dependent transport of STK38 contributes to STK38's function in autophagy (Joffre et al., 2015, 2016), we monitored the p62/SQSTM1 levels, a well-known autophagy substrate. As expected, p62 levels decreased upon starvation (Fig. 2B). However, inhibition of STK38 cytoplasmic localisation by XPO1 inhibition prevented p62 degradation (Fig. 2B), indicating a defect in autophagy flux. As a complementary approach, we generated a stable cell line expressing the autophagic flux probe GFP-LC3-RFP-LC3Δ (Kaizuka et al., 2016). HeLa GFP-LC3-RFP-LC3Δ cells were authenticated by silencing autophagy regulators such as ATG5 and Beclin1 followed by measuring the GFP/RFP ratio by FACS (Fig. S3). Similar to the silencing of ATG5 or Beclin1, knockdown of STK38 significantly impaired the reduction of the GFP/RFP ratio observed in control condition upon EBSS treatment, indicating a defect in autophagy in these conditions (Fig. S3C and S3D). The same method was then used to examine XPO1's contribution to nutrient starvation-induced autophagy (Fig. 2E). Significantly, XPO1 inhibition by KPT-185 and KPT-330 significantly impaired autophagy, as measured by the GFP/RFP ratios (left panel of Fig. 2.E) and by calculating the Δ autophagy upon starvation (right panel of Fig. 2E). Taken together, these data indicate that STK38 is exported to the cytoplasm by XPO1, which is important for autophagy induction upon nutrient starvation

STK38 kinase activity is necessary and sufficient to induce its own cytoplasmic re-localisation and autophagy

To investigate whether STK38's kinase activity is required for its nuclear/cytoplasmic shuttling, HeLa cells were transiently transfected wild-type STK38 (wt), kinase-dead (K118R) (Vichalkovski et al., 2008) or constitutively-active (PIF) STK38 (Cook et al., 2014). Transfected

cells were subsequently cultured in nutrient rich or starvation conditions and stained for STK38 localisation (Fig. 3A and 3B). As expected, STK38(wt) accumulated in the cytoplasm of nutrient-starved cells (Fig. 3A and 3B). However, kinase-dead STK38(K118R) remained nuclear upon starvation while constitutively active version of STK38(PIF) accumulated in the cytoplasm, irrespective of culture conditions (Fig. 3A and 3B). These results indicate that STK38 kinase activity is required and sufficient to induce its export to the cytoplasm.

To further investigate whether STK38 kinase activity is also involved in nutrient starvation-induced autophagy, we knocked-down endogenous STK38 in HeLa GFP-LC3-RFP-LC3ΔG cells, then complemented these cells with RNAi-resistant STK38(wt), K118R or PIF variants (Fig. S4), and then measured the autophagic flux (Fig. 3C and 3D). As expected (Joffre et al., 2015), STK38 depletion significantly impaired autophagy upon nutrient starvation, which was restored by reintroducing wild-type STK38 (Fig. 3C). In stark contrast, expression of kinase-dead version of STK38(K118R) failed to restore nutrient starvation-induced autophagy, while constitutively active STK38(PIF) supported autophagy like STK38(wt) (Fig. 3C).

Next, we asked whether constitutively active STK38 is sufficient to promote autophagy irrespective of culturing conditions. Therefore, the autophagic flux was measured in STK38-depleted cells reconstituted with our RNAi-resistant STK38 variants of interest under nutrient-rich condition only (Fig. 3D). This revealed that expression of constitutively active STK38(PIF) is sufficient to promote a substantial increase of the autophagic flux in nutrient-rich conditions (Fig. 3D). In conclusion, these experiments support that the kinase activity of STK38 is important for its subcellular localisation and autophagy.

STK38 phosphorylates XPO1 on Serine 1055

The link between STK38 kinase activity and its XPO1-dependent cytoplasmic localisation upon nutrient starvation-induced autophagy prompted us to further investigate whether STK38 could phosphorylate XPO1. Therefore, we bioinformatically scanned XPO1 for an STK38 HxRxxS/T phosphorylation motif (Hergovich, 2016), and found that serine 1055 (S1055) of XPO1 represents a putative STK38 phosphorylation site. In this regard, it is noteworthy that S1055 phosphorylation of XPO1 has already been documented previously (Beausoleil et al., 2004; Mertins et al., 2014, 2016; Sharma et al., 2014), although the biological significance of this phosphorylation event is yet to be defined. We first generated a phospho-specific anti-S1055-P antibody that was validated using wt or phosphor-acceptor (S1055A) mutant of XPO1 (Fig. S5A). The anti-XPO1-S1055-P antibody exhibited a strong specificity for XPO1(wt) upon okadaic acid (OA) incubation, a potent inhibitor of protein phosphatase type 2A (PP2A) leading to XPO1 serine phosphorylation. Concurrently, as expected, the XPO1(S1055A) mutant was not detected with this antibody in both whole cell lysates and after pulling-down Flag-XPO1 variants (Fig. S5A).

Using this new and specific anti XPO1-S1055-P antibody, we investigated whether STK38 can phosphorylate serine 1055 of XPO1. Knockdown of endogenous STK38 (Fig. S5B) significantly reduced the phosphorylation of XPO1 on S1055 (Fig. 4A and 4B). As expected, this was paralleled by a reduction of T444 phosphorylation of STK38, a reliable readout for STK38 activity (Hergovich et al., 2005). Taken together, these results demonstrate that endogenous STK38 is required for phosphorylation of XPO1 serine 1055, revealing a kinase-substrate relationship between STK38 and XPO1.

Phosphorylation of XPO1 on S1055 induces nuclear export of STK38 and autophagy

Considering that S1055 of XPO1 is located within the auto-inhibitory domain of XPO1 (Dian et al., 2013), we wondered whether S1055 phosphorylation of XPO1 is important for XPO1-dependent STK38 nuclear export. To address this point, we analysed the localisation of STK38 in HeLa cells transiently transfected with XPO1 mutants that are either insensitive to phosphorylation (S1055A) or that mimic constitutive phosphorylation (S1055D and S1055E) (Fig. S6A). In order to inhibit endogenous wild-type XPO1 activity, cells were treated with the XPO1 inhibitor KPT-185. Selected S1055 mutants of XPO1 also contained a C528S mutation which renders XPO1 insensitive to pharmacological inhibition by KPT-185 (Neggers et al., 2015) (Fig. 5A). As expected, STK38 remained nuclear in both nutrient-rich and nutrient-deprived medium conditions when XPO1(wt) was expressed, since KPT-185 inhibited XPO1-mediated nuclear export (Fig. 5B and 5C). Conversely, STK38 localised to the cytoplasm upon starvation when XPO1(C528S) was expressed (Fig. 5B and 5C), further supporting the findings described in Fig. 2. However, upon XPO1(C528S/S1055A) expression, STK38 remained nuclear in starvation condition, suggesting that S1055 phosphorylation of XPO1 is required for the nuclear export of STK38. Reversely, expression of XPO1(C528S/S1055D) or XPO1(C528S/S1055E) resulted in a cytoplasmic accumulation of STK38 irrespective of the culturing conditions, further supporting the notion that XPO1 phosphorylation on S1055 is important for the nuclear export of STK38 (Fig. 5B and 5C).

The localisation of the serine 1055 residue within the C-terminal auto-inhibitory domain of XPO1 (highlighted in purple in Fig. 5A) (Dian et al., 2013), also prompted us to analyse the effect of a XPO1(C528S) mutant containing a 39 amino acid C-terminal deletion. Transfection of this C-terminal deletion mutant indeed resulted in a cytoplasmic accumulation of STK38 irrespective of the culturing conditions (Fig. 5B and 5C), supporting that the C-terminal auto-inhibitory region of XPO1 regulates STK38 export according to the phosphorylation status of the S1055. These results point towards a mechanism where phosphorylation of S1055 releases XPO1 auto-inhibitory activity to open up the cargo binding site.

To independently probe these results, we created S1055 XPO1 mutants in the endogenous genomic locus of haploid HAP1 cells using CRISPR/Cas9 genome editing (Fig. S6B). HAP1 cells carrying a XPO1S1055A mutant failed to undergo autophagy when starved of nutrient, as shown by the lack of degradation of the p62 autophagy marker compared to wild-type cells (Fig. 5D). Conversely, both phosphomimetic XPO1 mutants (XPO1S1055D and XPO1S1055E) induced p62 degradation irrespective of culturing conditions (Fig. 5D). These results indicate that phosphorylation of XPO1 S1055 is not only required for nutrient starvation-inducted autophagy, but also sufficient to induce autophagy.

STK38 controls Beclin1 subcellular distribution through XPO1 phosphorylation

In agreement with a previous report (Liang et al., 2001), we found that Beclin1 shuttles from the nucleus to the cytoplasm of starved HeLa cells in a XPO1-dependent manner (Fig. 6A and 6B). This shuttling was regulated by STK38, since Beclin1 failed to exit the nucleus when STK38 was silenced (see Fig. S7 for STK38 silencing verification) (Fig. 6A and 6B). This finding confirmed by immunostaining of endogenous Beclin1 in our genome-edited HAP1 cell lines. While Beclin1 exited the nucleus from wild-type HAP1 cell lines upon starvation (Fig. 6C and 6D), Beclin1 remained nuclear in cells containing the mutant XPO1(S1055A). Conversely, in cells expressing the phospho-mimetic S1055D or S1055E mutants, the nuclear exit of Beclin1 was promoted even in nutrient-rich medium (Fig. 6C and 6D). These results suggest that

STK38, in addition to regulating its own subcellular fate, also controls the subcellular distribution of Beclin1 through XPO1 phosphorylation, thereby revealing how STK38 through Beclin1 can regulate autophagy.

The subcellular localisation of the Hippo pathway terminal effector YAP1 is modulated by STK38-mediated phosphorylation of XPO1

The Hippo pathway effector YAP1 has been reported as a XPO1 cargo (Kirli et al., 2015) but also as a STK38 substrate (Zhang et al., 2015): STK38 phosphorylates YAP1 S127, resulting in YAP1 cytoplasmic accumulation, a way for the Hippo pathway to inactivate YAP1-dependent transcriptional activity regulation. In addition, nuclear/cytoplasmic shuttling of YAP1 has been reported to depend on the cell density (Zhao et al., 2007), while its nuclear export has been shown to depend on XPO1 in human cells (Dupont et al., 2011; Ege et al., 2018; Wei et al., 2015) and in Drosophila (Ren et al., 2010).

To investigate whether STK38 can regulate YAP1 subcellular localisation, we examined the subcellular localisation of YAP1 in A549 cells where RASSF1 promoter gene is methylated with loss of the remaining allele on 3p chromosome, leading to the absence of the RASSF1A protein which reduces YAP1 nuclear accumulation (Dubois et al., 2016). Consistent with reports (Das et al., 2016), we found that YAP1 is excluded from the nucleus at high cell density (Fig. 7A and 7B), while total YAP1 protein levels remained unchanged (Fig. S8B), and that XPO1 inhibition prevented YAP1 nuclear exclusion at high cell density. Interestingly, STK38 silencing (Fig. S8A) phenocopied XPO1 inhibition on YAP1 subcellular localisation at high cell density (Fig. 7A and 7B), indicating that the nuclear exit of YAP1 is under the control of STK38 and XPO1.

As an independent approach, we analysed YAP1 localisation in our modified HAP1 cells. YAP1 was excluded from the nucleus in confluent wild-type HAP1 cells (Fig. 7C and Fig. 7D), while YAP1 protein level remained the same between experimental conditions (Fig. S8C). However, cells expressing XPO1(S1055A) failed to induce YAP1 nuclear exclusion at high cell density whereas cells expressing phospho-mimetic S1055 mutants (S1055D or S1055E) induced YAP1 nuclear exclusion, even at low cell density. These results suggest that the subcellular localisation of YAP1 can be regulated by phosphorylation of XPO1 by STK38.

DISCUSSION

STK38 is a serine/threonine kinase belonging to the Hippo growth control pathway; however STK38 exerts also Hippo-independent functions such as autophagy (Joffre et al., 2015), centrosome duplication (Hergovich et al., 2007), stress response downstream of the Ral GTPases (Selimoglu et al., 2014), cell cycle progression (Cornils et al., 2011b), and NF-kB activation upon different contexts (Paul et al., 2017; Shi et al., 2012). Seeking to identify the substrates of STK38 in autophagy and anoïkis survival, we found that XPO1 is a permissive substrate for these functions. Phosphorylation of XPO1 by STK38 on S1055 is important for the nuclear export of crucial intracellular signal transducers such as Beclin1, YAP1, and, to a lesser extent, for centrosome duplication (Fig. S9). In this regard, we hypothesize that phosphorylation of S1055 by STK38 assists in STK38 itself, Beclin1 or YAP binding to the NES-binding pocket of XPO1, by inducing a change of conformation, revealing the cargo binding domain of XPO1 (Fig. S10).

Phosphorylation of XPO1 on S1055 by STK38 is important for the nuclear export of XPO1 cargoes implicated in STK38-related functions. This allows subtle cellular responses in a context-dependent manner by modulating the nuclear export of crucial regulators. Although, we demonstrate here that Beclin1 and YAP1 are important STK38-regulated XPO1 cargoes, it remains to be determined how many cargoes are regulated by this mechanism, if it is strictly circumscribed to STK38-related functions or if this activation mechanism can be generalized.

The C-terminal end of XPO1 protein sequence is highly conserved among all chordates (Fig. S11), including the S1055 site. However, the proper STK38 HxRxxS/T phosphorylation motif appears only in simians, non-simian primates and all other vertebrates (including all the usual model organisms like mouse, xenopus, zebrafish, etc.) carrying a HxLxxS/T motif. The question raised by this observation is whether in these organisms the response to these contexts is regulated by a STK38-like kinase or another post-translational modification.

The phenomena revealed by this work suggest also that the autoinhibition embedded within the structure of XPO1 is not anecdotic but necessary for its proper function and responsiveness to physiological clues. Once XPO1 gets inappropriately activated, it starts an improperly behaviour disconnected of cell physiology. In rich medium, it triggers early events of autophagy, that are supposed to take place only upon starvation. In contrast, in cells with the capacity to proliferate, XPO1 kicks YAP1 out of the nucleus while nuclear YAP1 is an important pro-proliferative regulator, as suggested by the YAP1 addiction of cancer cells (Han et al., 2018).

MATERIALS AND METHODS

Key Resources table

Reagent or Resource	Source	Identifier
Antibodies		
STK38	Abnova	Cat# H00011329-M11; RRID: AB_566001
XPO1	Santa Cruz	Cat# sc-374124; RRID: AB_10917075
Flag	Cell Signaling	Cat# 14793; RRID: AB_2572291
Myc	Cell Signaling	Cat# 2272; RRID: AB_10692100
HA	Roche	Cat# 11583816001; RRID: AB_514505
GAPDH	Merk Millipore	Cat# MAB374; RRID: AB_2107445
Actin	Sigma	Cat# A2228; RRID: AB_476697
p62/SQSTM1	MBL	Cat# M162-3; RRID: AB_1279299
LC3b	Cell Signaling	Cat# 2775; RRID: AB_915950
pT444-STK38	(Hergovich et al., 2005)	N/A
pS1055-XPO1	This study (Davids Biotechnologie)	N/A
Streptavidin-HRP	Life Technologies	Cat# 21126; RRID: N/A
IκBα	Cell Signaling	Cat# 4814; RRID: AB_390781
ATG5	Cell Signaling	Cat# 2630; RRID: AB_2062340
Beclin1 (WB)	Cell signaling	Cat# 3738; RRID: AB_490837
Beclin1 (IF)	Santa Cruz	Cat# sc-10086; RRID: AB_2259076
YAP1	Santa Cruz	Cat# sc-101199; RRID: AB_1131430
Chemicals & Reagents		
KPT-185	Selleckchem	Cat# S7125; RRID: N/A
KPT-330	Selleckchem	Cat# S7252; RRID: N/A
Okadaic Acid	Santa Cruz	Cat# 78111-17-8; RRID: N/A
Chloroquine	Sigma	Cat# C6628; RRID: N/A
Phenol-biotin	Iris Biotech	Cat# LS-3500 0250; RRID: N/A
H_2O_2	Sigma	Cat# H1009; RRID: N/A
Streptavidin mag. beads	Thermo	Cat# 88817; RRID: N/A
Protein A-mag. beads	Thermo	Cat# 10001D; RRID: N/A
Flag M2 mag. beads	Sigma	Cat# M8823; RRID: N/A
Biotin	Sigma	Cat# B4501; RRID: N/A
Cell Lines		
HeLa	(Joffre et al., 2015)	N/A
Hek-HT-HRas^{G12V}	(Hahn et al., 1999)	N/A
HAP1 (wt)	Horizon Discovery	Cat# C631; RRID: N/A
HAP1 k-I XPO1	This study	N/A
A549	ATCC	Cat# CCL-185; RRID: CVCL_0023
Hek293T	ATCC	Cat# CRL-3216; RRID: CVCL_0063
Oligonucleotides		
siControl On-Targetplus Non-Targeting siRNA	Dharmacon	Cat# D-001810-01-50; RRID: N/A
Recombinant DNA		
pWZL-APEX2-STK38	This study	N/A
pMRX-IP-GFP-LC3-RFP-LC3ΔG	Addgene	Cat# 84572; RRID: N/A
pcDNA3-Myc-STK38(wt/K118R)	(Hergovich et al., 2005)	N/A
pcDNA3-HA-STK38(PIF)	(Hergovich et al., 2005)	N/A
pCIG3-3xFlag-XPO1 (wt/mutants)	This study	N/A

Cell Culture and drug treatments

Cells were cultured in humidified chambers at 37°C and 5% CO2. HeLa and A549 (ATCC) cell lines were grown in DMEM (Gibco) supplemented with 10% FBS (Biosera), 1% penicillin/streptomycin (Gibco) and with 1% L-Glutamine (Gibco). Hek293T cells (ATCC) were grown in same medium as described above without antibiotics. Hek-HT-HRasG12V (HekRasV12) cells were provided by Christopher Counter (Counter et al., 1998; Hahn et al., 1999) and cultured in DMEM supplemented with 100 µg/mL Hygromycin, 400 µg/mL Geneticin and 300 µg/µL Zeocin. Cells stably expressing APEX-STK38 were cultured in appropriate medium supplemented with 10 µg/mL Blasticidin. Cells stably expressing the GFP-LC3-RFP-LC3ΔG autophagic flux probe were cultured in the appropriate medium supplemented with 1 µg/mL Puromycin. HAP1 cell lines were obtained from Horizon Discovery and grown in IMDM (Gibco) supplemented with 10% FBS (Biosera), 1% penicillin/streptomycin (Gibco) and with 1% L-Glutamine (Gibco). Knock-in HAP1 cell lines expressing XPO1 mutants were cultured with the same media described above supplemented with 1 µg/mL Puromycin. All antibiotics were from Invivogen.

For Okadaic Acid (OA) treatments, cells were cultured for 1 hour in the appropriate culture media supplemented with 1 µm okadaic acid purchased from Santa Cruz. For EBSS-induced autophagy, cells were growth in order to reach a maximum of 70% confluency. The day of the experiment, cells were washed once with PBS followed by incubation with growth medium (GM) or EBSS (24010-43, Gibco) for 4 hours as indicated. For chemical XPO1 inhibition, cells were cultured as indicated in the specific sections with media supplemented with 1 µM of KPT-185 or KPT-330 (Selleckchem). Chloroquine (Cq) was purchased from Sigma.

siRNA and DNA transfections

Cells were reversely transfected with siRNAs using Lipofectamine RNAiMax (Invitrogen according to manufacturer's instructions. 72h post-transfection cells were harvested as defined in the specific sections. For transient DNA transfection, cells were seeded and then transfected the next day with a total amount of 2 µg of DNA using JetPrime reagent (Polyplus Transfection) according to manufacturer's instructions. 48h post-transfection cells were harvested as defined in the specific sections. If both methods were used, the cells were reversely transfected with siRNA as described above the first day and then transfected with DNA as described above the next day. Cells were harvested 24h after DNA transfection as defined in the specific sections. siControl On-Targetplus Non-Targeting siRNA (referred as siNT) was purchased from Dharmacon (D-001810-01-50, Dharmacon). The remaining siRNAs were purchased from Eurogentec:

- STK38#3: 5'-GAGCAGGUUGGCCACAUUCdTT-3'
- STK38#206: 5'-CGUCGGCCAUAAACAGCUAdTT-3'
- ATG5: 5'-AACCUUUGGCCUAAGAAGAAAdTT-3'
- Beclin1: 5'-ACCGACUUGUUCCUUACGGAAdTT-3'

Generation of stable cell lines

HeLa and HekRasV12 cell lines stably expressing the APEX2-STK38 N-terminal fusion protein as well as the HeLa cells stably expressing the GFP-LC3-RFP-LC3ΔG autophagic flux reporter probe (Kaizuka et al., 2016) were generated by retroviral transduction. For retroviral production, HEK293T packaging cells were transfected with the retroviral vector pWZL-APEX2-STK38 or with the pMRX-IP-GFP-LC3-RFP-LC3ΔG retroviral vector (84572, Addgene) and the packaging plasmid pcl10A1 (NBP2-29542, Novus) using Fugene 6 (E2691, Promega) according

to manufacturer's instructions. 48 hours after transfection, supernatants were harvested, filtered through a 0.45 µm filter and added to the recipient cells in the presence of 4µg/mL polybrene (Sigma). 24 hours post-transduction, cells were harvested and seeded in fresh culture dishes and subsequently selected with appropriate antibiotics for one week.

Following antibiotic selection, HeLa cells stably expressing the GFP-LC3-RFP-LC3ΔG autophagic probe were subjected to clonal selection. Briefly, cells were washed twice with PBS and incubated with TrypL©Express (Gibco) according to manufacturer instructions and then resuspended in PBS supplemented with 25 mM Hepes (Gibco), 1 mM EDTA (Invitrogen) and 1% BSA (Euromedex) previously filtered through a 0.45 µm filter. Cells positive both for GFP and RFP were then sorted individually on a BD FACS ARIAIII in a 96 well plate and incubated several weeks with DMEM supplemented with antibiotic selection (1 µg/mL Puromycin). One clone was chosen according to GFP and RFP expression and cultured under antibiotic selection in order to use it for experiments.

CRISPR/Cas9 genome editing, DNA extraction and sequencing

Gene edited HAP1 cell lines were generated using the CRISPaint principle (Schmid-Burgk et al., 2016) and similarly as described before (Vercruysse et al., 2017). Briefly, cells were transfected using TurboFectin 8.0 (Origene) according to the manufacturer's instructions with a plasmid encoding an sgRNA targeting the C-terminus of XPO1 (5'-GAGAGAAATAGCCCTACGGC-3'), a plasmid encoding SpCas9 and an sgRNA targeting the donor plasmid (5'-GCCAGTACCCAAAAAGCGCC-3') and a repair donor plasmid. This repair plasmid contains the targeting site, the sequence to restore the C-terminus of XPO1 with a silent mutation upstream of the endogenous C-terminal PAM sequence, the desired S1055 mutation and 3xFLAG followed by a P2A-coupled puromycin resistance gene to stably integrate the mutation in the last exon of Xpo1 at its endogenous locus. Following transfection, cells were incubated for 2 days and then selected over a period of 1 week with 1 µg/mL puromycin. Cells were harvested and plated at a density of 0.5 cells/well in 96-well plates in 20% FBS containing medium to obtain single cell derived colonies. Colonies were grown for 2-4 weeks and were regularly screened.

When single cell derived colonies were sufficiently grown, cells were washed and then lysed in Bradley lysis buffer at 56°C (10 mM Tris-HCl (pH 7.5), 10 mM EDTA, 0.5% SDS, 10 mM NaCl and 1 µg/mL proteinase K). The genomic DNA was extracted from the lysate using ethanol-salt precipitation and centrifugation. The C-terminus of XPO1, was amplified by in-out PCR with the following primers: fwd: 5'- CTCAAGTAAAGCTCTTTGTGACAGGGC-3', rv: 5'-CAGCCATTCTCGGGCCGATC-3'. The PCR product was sequenced with reverse primer 5'-GGAACGTCGTCTCTTGTAGC-3' by Sanger Sequencing for correct integration of the mutation (Macrogen).

SILAC

HeLa and HekRasV12 cell lines stably expressing the APEX2-STK38 construct were metabolically labelled with light or heavy isotopes of arginine and lysine. Early passage of each cells were split on day 0 into two T25 flasks (Falcon). One flask was cultured in light SILAC media consisting of DMEM deficient in L-lysine and L-arginine (#89985, Thermo) that we supplemented with L-lysine (Lys0) and L-arginine (Arg0) (L8662 and A8094 respectively, Sigma) at 146 mg/L and 84 mg/L respectively, 10% FBS (Biosera), 1% pen/strep (Gibco) and 1% glutamine (Gibco). The other flask was cultured in heavy SILAC media as above except Lys0 and Arg0 that were replaced by L-lysine-13C6,15N2 (Lys8), and L-arginine-13C6,15N4 (Arg10)

(88209 and 89990 respectively, Thermo). Every, four days, before cells reached confluency, the heavy and light SILAC cultures were split into fresh SILAC heavy and light media respectively. After 8 passages, the heavy and light SILAC cultures were expanded in 10 cm petri dishes and cultured for two more passages. When heavy and light SILAC HeLa and HekRasV12 cells reached passage n° 10, a fraction of each condition was sent to mass-spectrometry analysis to confirm that amino acids have been well substituted by the heavy or light ones.

Context-dependent proximity biotinylation assay

For the context-dependent proximity biotinylation assay (PBA), we first induced the context in both heavy and light isotopic cell lines stably expressing the APEX2-STK38 construct (autophagy for Hela cells and suspension for HekRasV12 cells), then to proceed to the proximity labelling and finally to purify biotinylated proteins.

Light and heavy SILAC HeLa APEX2-STK38 cells were seeded in 10 cm petri dishes in order to obtain 80% confluence. The day of the experiment, cells were washed twice with PBS (Gibco) and then incubated in the presence of DMEM for the light SILAC condition or in the presence of EBSS (24010-043, Life Technologies) for the heavy SILAC condition during 4 hours. Light and heavy SILAC HekRasV12 APEX2-STK38 cells were seeded to obtain 80% confluence the next day in attached (normal 10 cm petri dish growth condition) for the light SILAC condition or in suspension (see below) for the heavy SILAC condition and cultured overnight. For suspension culture, cells were grown overnight in Ultra Low Attachment Surface 6-well plates or 10 cm dishes (Greiner) that were previously incubated in 0.02% pluronic acid-coated for 1 hour at 37°C followed by two washes with PBS.

The day of the PBA, cells were pre-incubated 30 minutes with phenol-biotin (LS-3500 0250, Iris Biotech) at a concentration of 500 µM at 37°C before addition of 1mM of H2O2 (H1009, Sigma) during 1 minute at room temperature. The cells were immediately quenched by two following washes of PBS supplemented with 10 mM sodium azide (S2002, Sigma), 10 mM sodium ascorbate (A7631, Sigma) and 5 mM Trolox (238813, Sigma) followed by two washes of PBS (10 mL at each time) allowing the removal of the phenol-biotin/H2O2 solution. Attached cells were then collected using TrypL©Express (Gibco) as indicated by manufacturer instructions followed by centrifugation at 1000 rpm during 5 minutes. Cell pellets were then lysed on ice by adding 1 mL of freshly-prepared RIPA lysis buffer (50 mM Tris, 150 mM NaCL, 0.1% SDS, 0.5% sodium deoxycholate, 1% Triton X-100, 1x cOmplete EDTA-free protease inhibitor cocktail (05892791001, Roche) supplemented with 1 mM PMSF, 10 mM sodium azide, 10 mM sodium ascorbate and 5 mM Trolox. Lysates were then incubated on tube rotator for 20 minutes at 4 °C followed by centrifugation at 13 000 rpm for 10 minutes at 4 °C. Supernatants were separated from pellets and then directly flash-frozen in liquid nitrogen been before stored at -80 °C. Protein concentration was measured using the Pierce BCA protein assay kit according to the manufacturer instructions (23225, Thermo) with bovine serum albumin as standard and absorbance at 262 nm was recorded on a Fluostar Optima plate reader (BMG Labtech).

Samples from the lysed SILAC cells were combined in a 1:1 ratio (2 mg of total protein) as indicated in the Fig. S1 for the autophagy condition and incubated 1 hour at 4 °C in the presence of Protein A-magnetic beads (10001D, Thermo) on a tube rotor in order to perform a pre-clear. Non-bound fractions were then incubated in the presence 500 µL of streptavidin-magnetic beads (88817, thermo) previously washed as for the protein A-magnetic beads and then incubated 1 hour at 4 °C on a tube rotor. Streptavidin beads were then washed two times

with 1 mL of the same lysis buffer described above, one time with 1 mL of KCl 1 M, one time with 1 mL of Na2CO3 0.1 M, one time with 1 mL of 2 M urea in 10 mM Tris-HCl pH 8.0, and then two times with lysis buffer. Biotinylated proteins were then eluted by incubating the beads with 60 µL of 1x Laemmli sample buffer (1610747, Biorad) supplemented with 50 mM DTT and 2 mM biotin (B4501, Sigma) and by heating them at 95 °C for 5 minutes.

Sample preparation and digestion

Immunoprecipitates were prepared as described above. After the final elution in 1X reducing Laemmli buffer, the samples were proceeded for digestion using filter-assisted sample preparation (FASP) method, performed essentially as described (Lipecka et al., 2016; Wiśniewski et al., 2009). Briefly, protein extracts were applied to 30kDa MWCO centrifugal filter units (Microcon, Millipore), mixed with UA buffer (8M urea, 100mM Tris-HCl pH 8.9) and centrifuged. Alkylation was carried out by incubation for 20min in the dark with UA buffer containing 50mM iodoacetamide. Filters were then washed twice with UA buffer followed by two washes with ABC buffer (50 mM ammonium bicarbonate). Finally, 1µg of trypsin (Promega, France) was added and digestion was achieved by overnight incubation at 37°C.

After recovery, peptides were subjected to detergent removal procedure using HiPPR (High Protein and Peptide Recovery) Detergent Removal Resin from Thermo Fisher Scientific, as recommended by manufacturer. Briefly, the spin columns containing detergent removal resin were centrifuged at 1500g for 1 min to remove the storage buffer. The resin was washed three times by adding ABC buffer and centrifuging at 1500g for 1 min. Samples were then added to resin in a vol:vol ratio and incubated for 10 min at room temperature. The spin columns were placed in a collection tube and centrifuged at 1500g for 2 min to collect the detergent-free sample. Peptides were vacuum dried and resuspended in 10% acetonitrile, 0.1% formic acid for LC-MS/MS.

Mass spectrometry

For each run, 1 µL were injected in a nanoRSLC-Q Exactive PLUS (Dionex RSLC Ultimate 3000, Thermo Scientific, Waltham, MA, USA). Extracted peptides were resuspended in 0.1% (v/v) trifluoroacetic acid, 10% acetonitrile, and were loaded onto a µ-precolumn (Acclaim PepMap 100 C18, cartridge, 300 µm i.d.×5 mm, 5 µm, Dionex), followed by separation on the analytical 50 cm nano column (0.075 mm ID, Acclaim PepMap 100, C18, 2 µm, Dionex). Chromatography solvents were (A) 0.1% formic acid in water, and (B) 80% acetonitrile, 0.08% formic acid. Peptides were eluted from the column using a gradient from 5% to 40% B over 38 min and were analyzed by data dependent MS/MS, using top-10 acquisition method. Briefly, the instrument settings were as follows: resolution was set to 70,000 for MS scans and 17,500 for the data dependent MS/MS scans in order to increase speed. The MS AGC target was set to 3.106 counts with a maximum injection time of 200 ms, while MS/MS AGC target was set to 1.105 with a maximum injection time of 120 ms. Dynamic exclusion was set to 30 sec. Each sample was analyzed in three to five biological replicates. The mass spectrometry proteomics data have been deposited to the ProteomeXchange Consortium via the PRIDE (Vizcaíno et al., 2016) partner repository with the dataset identifier PXD011968.

Data Processing Following LC-MS/MS acquisition

Raw MS files were processed with the MaxQuant software version 1.5.3.30 and searched with Andromeda search engine against the Homo Sapiens Uniprot KB/Swiss-Prot v.06/2016. To search parent mass and fragment ions, we set an initial mass deviation of 4.5 ppm and 20 ppm

respectively. The minimum peptide length was set to 7 aminoacids and strict specificity for trypsin cleavage was required, allowing up to two missed cleavage sites. Carbamidomethylation (Cys) was set as fixed modification, whereas oxidation (Met) and N-term acetylation were set as variable modifications. The false discovery rates (FDRs) at the protein and peptide level were set to 1%. Scores were calculated in MaxQuant as described previously (Cox and Mann, 2008). The reverse and common contaminants hits were removed from MaxQuant output. Proteins were quantified on parent ions, selecting multiplicity "2" for standard quantification in SILAC; the heavy label was Arg10 and Lys8, while the light labelled corresponded to non-labelled Arg and Lys. Maximum labelled aminoacids per peptide was set to 3. Protein quantification was obtained using at least 2 peptides ration counts per protein.

Three biological replicates were analysed for each condition studied. Statistical analysis was performed with Perseus software (version 1.5.5.3) freely available at www.perseus-framework.org. The matrix was filtered to keep proteins quantified at least three times in at least one condition. Statistical analysis was performed on each condition (group of three biological replicates) by one sample test against the value 1, and we retained the proteins significative according to t-test (S0=1, p value<0.05). Subsequently, we applied a personalized priority scoring in order to highlight the proteins who were changing the most and more significantly priority score=(1⁄p-value × (<ratio>-1)2)).

Western-Blot

After indicated treatments, cells were washed with ice-cold PBS and lysed at 4°C in freshly made lysis buffer (20 mM Tris-HCl pH=8, 150 mM NaCl, 10% glycerol, 1% Triton X100, 1 mM EDTA, 1 mM PMSF, 50 mM NaF, 1mM DTT, 1 mM Na3VO4, protease inhibitor cocktail). Lysate were incubated 20 minutes at 4°C on a rotary wheel and then subjected to a 13,000g centrifugation for 10 minutes at 4°C. Sample supernatants were resuspended in Laemmli buffer (2% SDS, 60 mM Tris-HCl pH=6.8, 10 % Glycerol, 100 mM DTT and 0.005% Bromophenol blue) followed by boiling at 95°C for 5 minutes. An equal amount of protein were run on NuPage precast gradient SDS-PAGE gels (Life technologies). After protein separation by electrophoresis, proteins were transferred on a 0.2 µm nitrocellulose transfer membrane (GE Healthcare). Non-specific sites were blocked 1 hour in TBS-Tween (TBST) 0.2 % with 5% BSA at room temperature. Membranes were then incubated over-night à 4°C under gentle agitation with appropriate primary antibodies diluted in TBST-BSA 5%. The next day, membranes were washed 3 times with TBST at room temperature (RT) and incubated with appropriate secondary antibodies for 1 hour at RT under gentle agitation prior to washes as described before. Luminescent signal was visualized and recorded with enhanced chemiluminescence method (Western Lightning Plus-ECL, PerkinElmer) using horseradish peroxidase (HRP)-conjugated secondary antibodies (Jackson Immuno Research) followed by image acquisition using a Chemidoc MP imaging system (Bio-Rad) or with the LICOR Odyssey Infrared Imaging System (LI-COR Biosciences) using IRDye-conjugated secondary antibodies. The anti pS1055_XPO1 antibody (Davids Biotechnologie) was generated in guinea pigs immunized with specific phospho-peptide mimicking phosphorylated XPO1 S1055. After purification of antibodies with the same phospho-peptide, non-specific antibodies were eliminated using non-phospho-peptide.

Immunoprecipitations

For immunoprecipitation experiments, cells were grown in 10 cm petri dishes in order to reach 80% confluency the day of the experiment. After indicated treatments, cells were washed with ice-cold PBS and lysed at 4°C using same lysis buffer as described in the Western-Blot section. Lysate were incubated 20 minutes at 4°C on a rotary wheel and then subjected to a 13,000g centrifugation for 10 minutes at 4°C. Supernatant was then incubated 1 hour at 4 °C in the presence of Protein A-magnetic beads (10001D, Thermo) on a tube rotor in order to perform a pre-clear. Non-bound fractions were then incubated in the presence of anti-Flag M2 magnetic beads (M8823, Sigma) for 1 hour at 4 °C on a tube rotor. Magnetic beads were then washed two times with the same lysis buffer, one time with high-salt lysis buffer (300 mM NaCl) and one time with normal lysis buffer. Magnetic beads were then resuspended in Laemmli buffer and then heated at 95 °C for 5 minutes for elution.

Flow cytometry

To determine the autophagic flux in HeLa GFP-LC3-RFP-LC3ΔG cells, cells were seeded in 96-well view-plate (Perkin-Elmer) in order to reach 80 % confluence the day of acquisition. Cells were subjected to treatment as indicated and described above. Cells were resuspended using phenol-red lacking Trypsin-EDTA (59418C, Sigma) prior to be quenched using Defined Trypsin Inhibitor (R007100, Thermo). All data were acquired on a CytoFlex (Beckman Coulter) and analyzed using FlowJo (LLC).

Immunofluorescence and image analysis

Cells were grown on coverslips, washed twice in PBS, fixed with 4% paraformaldehyde for 5 min at room temperature (RT) followed by 3 washes in PBS and then quenched with 50mM NH_4Cl in PBS for 15 min at RT. After 3 PBS washes, fixed cells were permeabilized in 0.1% Triton X-100 in PBS for 10 minutes at RT followed by 3 washes in PBS and then blocked in 5% BSA, 10 % FBS in PBS for 30 minutes at RT. Cells were subsequently incubated 1 hour at RT with primary antibodies diluted in blocking buffer. After 3 washes in PBS, cells were incubated with secondary antibodies diluted in blocking buffer for 1 hour at RT followed by 3 washes in PBS. Coverslips were dried and then mounted with ProLong™ Gold Antifade Mountant with DAPI (P36941, Thermo). Images were acquired on a Zeiss Axioplan 2 microscope through a CoolSnap HQ2 camera (Photometrics) under the control of MetaMorph software (Universal imaging). Cells were selected for acquisition if they were positive for all staining.

Image processing was performed using ImageJ software (NIH). For nucleo/cytoplasmic ratio, the fluorescent signal was quantified in the nuclear and the cytosolic compartments. The nucleus was identified by DAPI staining and the cell area by thresholding the background. The cytosolic area was determined by subtracting the nuclear compartment to the cell compartment. The ratio was obtained by dividing the mean of fluorescence in the cytosolic area by the mean of fluorescence in the nuclear one. For YAP1 nuclear intensity, the mean of fluorescence intensity was calculated only in the nuclear area identified by the DAPI staining.

Snapshots of live cells: centrosomes

For centrosomes experiment, HeLa cells stably expressing GFP-Centrin were cultured on glass-bottom 6 well plates (MatTek) and incubated with the siRNAs or drugs as indicated in the figure legend. The day of the experiment, the GFP signal was recorded using a Zeiss Z1 observer microscope through a Hamamatsu Flash4 camera under the control of MetaMorph software (Universal imaging). The number of centrosomes were counted manually on Z-stacks

images by counting the number of centrosomes (Centrin "spots") without differentiating unique separated centrioles in G1 phase from separated centrosomes (harbouring 2 centrioles each) in S/G2 phase. Image processing was performed using ImageJ software (NIH).

Bioinformatics & statistical analysis

Heatmap of STK38 interactors association fold was generated using the online tool Morpheus from the Broad Institute: https://software.broadinstitute.org/morpheus. Rows and columns were clustered using the hierarchal clustering tool in Morpheus by the one minus Pearson correlation matrix and the average linking method. Enrichment analysis was performed using Gene Ontology (David Bioinformatics) website: http://www.geneontology.org/ for enriched terms as cellular components in Homo sapiens. The 10 most enriched terms according to their adjusted p-value were plotted. Adjusted p-value was calculated using the Bonferroni correction for multiple testing. Correlogram was generated using the "corrplot" package in R.

Statistical significance was quantified by p-values using Graphpad Prism v5.0 software. Student's t test was used if data followed normal distribution otherwise Mann-Whitney test was used. All test performed were two-sided. For all tests, differences were considered statistically significant when p-values were below 0.05 (*), 0.01 (**), or 0.001 (***). In the figures, p-values are indicated as: *p<0.05; **p<0.01; ***p<0.001; ns, not significant. Graphs represent mean ± standard error of the mean (SEM).

Protein sequence alignment

Protein sequences were retrieved from UniProt (https://www.uniprot.org/) as FASTA files, aligned in msa R package {10.1093/bioinformatics/btv494} using ClustalOmega method {10.1038/msb.2011.75} with default parameters. The following sequences were used: Human: O14980 (Homo sapiens); Chimpanzee: H2R0K9 (Pan troglodytes); Gibbon: G1RF15 (Nomascus leucogenys); Cercocebus: A0A2K5LXU0 (Cercocebus atys); Drill: A0A2K5YJR1 (Mandrillus leucophaeus); Colobus: A0A2K5I3H1 (Colobus angolensis); Capuchin: A0A2K5SFU2 (Cebus capucinus); Saimiri: A0A2K6UYF0 (Saimiri boliviensis); Tarsier: A0A1U7TKR2 (Tarsius syrichta); Sifaka: A0A2K6G794 (Propithecus coquereli); Galago: H0WFU2 (Otolemur garnettii); Rabbit: G1SMY6 (Oryctolagus cuniculus); Beaver: A0A250Y6Q4 (Castor canadensis); Guinea_pig: A0A286XB55 (Cavia porcellus); Mole_rat: A0A0P6K7E8 (Heterocephalus glaber); Hamster: A0A1U7QPJ1 (Mesocricetus auratus); Mouse: Q6P5F9 (Mus musculus); Rat: Q80U96 (Rattus norvegicus); Ground_squirrel: A0A287CSQ9 (Ictidomys tridecemlineatus); Tupaia: L9KQ84 (Tupaia chinensis); Panda: D2HZX2 (Ailuropoda melanoleuca); Dog: E2R9K4 (Canis lupus); Horse: F6S8L9 (Equus caballus); Sheep: W5QG19 (Ovis aries); Pig: A0A218PI30 (Sus scrofa); Bat: G1PGH6 (Myotis lucifugus); Hedgehog: A0A1S3ARI2 (Erinaceus europaeus); Manatee: A0A2Y9RGB7 (Trichechus manatus); Elephant: G3TDG6 (Loxodonta africana); Tasman_devil: G3WCI2 (Sarcophilus harrisii); Opossum: F7EIW1 (Monodelphis domestica); Platypus: F7DTN5 (Ornithorhynchus anatinus); Chicken: A0A1D5P8H7 (Gallus gallus); Owl: A0A093FS26 (Tyto alba); Alligator: A0A1U7RM64 (Alligator sinensis); Green_turtle: M7B3V0 (Chelonia mydas); Copperhead: A0A1W7RHI2 (Agkistrodon contortrix); Anole_lizard: H9G6E3 (Anolis carolinensis); Xenopus: A0A1L8G775 (Xenopus laevis); Salmon: A0A1S3PKN6 (Salmo salar); Zebrafish: E7FBU7 (Danio rerio); Gar: W5NGS6 (Lepisosteus oculatus); Catfish: W5UJN6 (Ictalurus punctatus); Latimeria: H3BFQ8 (Latimeria chalumnae); Gostshark: V9K8G4 (Callorhinchus milii); Lamprey: S4R883 (Petromyzon marinus); Ascidia: A0A1W3JKJ9 (Ciona intestinalis); Octopus: A0A0L8GCW5 (Octopus bimaculoides); Sea_cucumber: A0A2G8LJC7 (Stichopus japonicus); Lingula: A0A1S3IRI2 (Lingula unguis); Slug: A0A0B7BCQ8 (Arion

vulgaris); Leech: T1FP79 (Helobdella robusta); C_elegans: Q23089 (Caenorhabditis elegans); Flour_beetle: D6X0Q6 (Tribolium castaneum); Black_ant: A0A0J7KFR1 (Lasius niger); Honeybee: A0A087ZMS1 (Apis mellifera); Drosophila: A0A0S0WNN6 (Drosophila melanogaster); Crab: A0A0P4WHK7 (Scylla olivacea); Ixodes: V5I1V1 (Ixodes ricinus); Dictyostelium: Q54EV7 (Dictyostelium discoideum); Arabidopsis: Q9SMV6 (Arabidopsis thaliana); Bakers_yeast: P30822 (Saccharomyces cerevisiae); Fission_yeast: P14068 (Schizosaccharomyces pombe)

Acknowledgments

A.PJ.M. was supported by funding from Paris Sciences et Lettres Research University and Institut Curie. M.K.S. was supported by fellowship from Institut national de la Santé et de la Recherche médicale (INSERM ITMO Plan Cancer 2014-2018, PC201530 to MCP, fellowship to M.K.S). This work was supported by institutional funding by INSERM and Institut Curie, Association pour la Recherche sur le Cancer (grant number 29928 to J.H.C), Ligue Contre le Cancer (grant number 24098 to J.H.C) and Association Christelle Bouillot. We thank the staff of the Flow Cytometry Core Facility of Institut Curie for their expert support and advise. We thank Alice Y. Ting (MIT) for her generous advices about APEX2 labelling system.

Author contributions

A.PJ.M. and J.H.C. designed the study and experiments. A.PJ.M. conducted experiments with the help of B.M. and N.C., and analyzed the data. J.L. prepared the proteomic samples and performed mass spectrometry. I.C.G. performed initial analysis on the proteomic data. A.PJ.M and M.K.S. designed ImageJ macro for nuclear/cytoplasmic IF quantifications. M.J. performed the CRISPR/Cas9 genome editing. V.N.A. performed the protein sequence alignment. M.P., P.C., A.H. and G.Z. assisted expertly centrosome, autophagy, STK38 and YAP1 data, respectively. MC.P. supervised biochemical experiments. D.D shed expert light on XPO1. A.PJ.M. designed the figures. A.PJ.M. and J.H.C., with the assistance of A.H. and D.D., wrote the manuscript with input from all authors. All authors approved the final manuscript.

Competing interest statement

The authors declare that they have no competing interest.

REFERENCES

Beausoleil, S.A., Jedrychowski, M., Schwartz, D., Elias, J.E., Villen, J., Li, J., Cohn, M.A., Cantley, L.C., and Gygi, S.P. (2004). Large-scale characterization of HeLa cell nuclear phosphoproteins. Proc. Natl. Acad. Sci. 101, 12130–12135.

Bettoun, A., Joffre, C., Parrini, M.C., Gundogdu, R., Ahmad, A.D., Gomez, M., Cascone, I., Meunier, B., White, M. a., Codogno, P., et al. (2016). Mitochondrial clearance by the STK38 kinase supports oncogenic Ras-induced cell transformation. Oncotarget 7, 44142–44160.

Campos, E.I., Smits, A.H., Kang, Y.-H., Landry, S., Escobar, T.M., Nayak, S., Ueberheide, B.M., Durocher, D., Vermeulen, M., Hurwitz, J., et al. (2015). Analysis of the Histone H3.1 Interactome: A Suitable Chaperone for the Right Event. Mol. Cell 60, 697–709.

Chen, R., Wang, Y., Liu, Y., Zhang, Q., Zhang, X., Zhang, F., Shieh, C.-H.P., Yang, D., and Zhang, N. (2013). Quantitative study of the interactome of PKCζ involved in the EGF-induced tumor cell chemotaxis. J. Proteome Res. 12, 1478–1486.

Cook, D., Hoa, L.Y., Gomez, V., Gomez, M., and Hergovich, A. (2014). Constitutively active NDR1-PIF kinase functions independent of MST1 and hMOB1 signalling. Cell. Signal. 26, 1657–1667.

Cornils, H., Kohler, R.S., Hergovich, A., and Hemmings, B. a. (2011a). Downstream of human NDR kinases: Impacting on c-myc and p21 protein stability to control cell cycle progression. Cell Cycle 10, 1897–1904.

Cornils, H., Kohler, R.S., Hergovich, A., and Hemmings, B. a (2011b). Human NDR kinases control G(1)/S cell cycle transition by directly regulating p21 stability. Mol. Cell. Biol. 31, 1382–1395.

Counter, C.M., Hahn, W.C., Wei, W., Caddle, S.D., Beijersbergen, R.L., Lansdorp, P.M., Sedivy, J.M., and Weinberg, R.A. (1998). Dissociation among in vitro telomerase activity, telomere maintenance, and cellular immortalization. Proc. Natl. Acad. Sci. U. S. A. 95, 14723–14728.

Cox, J., and Mann, M. (2008). MaxQuant enables high peptide identification rates, individualized p.p.b.-range mass accuracies and proteome-wide protein quantification. Nat. Biotechnol. 26, 1367–1372.

Das, A., Fischer, R.S., Pan, D., and Waterman, C.M. (2016). YAP Nuclear Localization in the Absence of Cell-Cell Contact Is Mediated by a Filamentous Actin-dependent, Myosin II- and Phospho-YAP-independent Pathway during Extracellular Matrix Mechanosensing. J. Biol. Chem. 291, 6096–6110.

Dian, C., Bernaudat, F., Langer, K., Oliva, M.F., Fornerod, M., Schoehn, G., Müller, C.W., and Petosa, C. (2013). Structure of a truncation mutant of the nuclear export factor CRM1 provides insights into the auto-inhibitory role of its C-terminal helix. Structure 21, 1338–1349.

Dubois, F., Keller, M., Calvayrac, O., Soncin, F., Hoa, L., Hergovich, A., Parrini, M.-C., Mazières, J., Vaisse-Lesteven, M., Camonis, J., et al. (2016). RASSF1A Suppresses the Invasion and Metastatic Potential of Human Non–Small Cell Lung Cancer Cells by Inhibiting YAP Activation through the GEF-H1/RhoB Pathway. Cancer Res. 76, 1627–1640.

Dupont, S., Morsut, L., Aragona, M., Enzo, E., Giulitti, S., Cordenonsi, M., Zanconato, F., Le Digabel, J., Forcato, M., Bicciato, S., et al. (2011). Role of YAP/TAZ in mechanotransduction. Nature 474, 179–184.

Ege, N., Dowbaj, A.M., Jiang, M., Howell, M., Hooper, S., Foster, C., Jenkins, R.P., and Sahai, E. (2018). Quantitative Analysis Reveals that Actin and Src-Family Kinases Regulate Nuclear YAP1 and Its Export. Cell Syst. 6, 692–708.e13.

Elzi, D.J., Song, M., Hakala, K., Weintraub, S.T., and Shiio, Y. (2014). Proteomic Analysis of the EWS-Fli-1 Interactome Reveals the Role of the Lysosome in EWS-Fli-1 Turnover. J. Proteome Res. 13, 3783–3791.

Fornerod, M., Ohno, M., Yoshida, M., and Mattaj, I.W. (1997). CRM1 is an export receptor for leucine-rich nuclear export signals. Cell 90, 1051–1060.

Hahn, W.C., Counter, C.M., Lundberg, A.S., Beijersbergen, R.L., Brooks, M.W., and Weinberg, R.A. (1999). Creation of human tumour cells with defined genetic elements. Nature 400, 464–468.

Han, H., Yang, B., Nakaoka, H.J., Yang, J., Zhao, Y., Le Nguyen, K., Bishara, A.T., Mandalia, T.K., and Wang, W. (2018). Hippo signaling dysfunction induces cancer cell addiction to YAP. Oncogene 2, 6414–6424.

Hergovich, A. (2016). The Roles of NDR Protein Kinases in Hippo Signalling. Genes (Basel). 7, 21.

Hergovich, A., Bichsel, S.J., and Hemmings, B. a (2005). Human NDR kinases are rapidly activated by MOB proteins through recruitment to the plasma membrane and phosphorylation. Mol. Cell. Biol. 25, 8259–8272.

Hergovich, A., Lamla, S., Nigg, E.A., and Hemmings, B.A. (2007). Centrosome-Associated NDR Kinase Regulates Centrosome Duplication. Mol. Cell 25, 625–634.

Hergovich, A., Kohler, R.S., Schmitz, D., Vichalkovski, A., Cornils, H., and Hemmings, B. a. (2009). The MST1 and hMOB1 Tumor Suppressors Control Human Centrosome Duplication by Regulating NDR Kinase Phosphorylation. Curr. Biol. 19, 1692–1702.

Hung, V., Udeshi, N.D., Lam, S.S., Loh, K.H., Cox, K.J., Pedram, K., Carr, S.A., and Ting, A.Y. (2016). Spatially resolved proteomic mapping in living cells with the engineered peroxidase APEX2. Nat. Protoc. 11, 456–475.

Jin, J., Smith, F.D., Stark, C., Wells, C.D., Fawcett, J.P., Kulkarni, S., Metalnikov, P., O'Donnell, P., Taylor, P., Taylor, L., et al. (2004). Proteomic, functional, and domain-based analysis of in vivo 14-3-3 binding proteins involved in cytoskeletal regulation and cellular organization. Curr. Biol. 14, 1436–1450.

Joffre, C., Dupont, N., Hoa, L., Gomez, V., Pardo, R., Gonçalves-Pimentel, C., Achard, P., Bettoun, A., Meunier, B., Bauvy, C., et al. (2015). The Pro-apoptotic STK38 Kinase Is a New Beclin1 Partner Positively Regulating Autophagy. Curr. Biol. 1–14.

Joffre, C., Codogno, P., Fanto, M., Hergovich, A., and Camonis, J. (2016). STK38 at the crossroad between autophagy and apoptosis. Autophagy 8627, 1–2.

Kaizuka, T., Morishita, H., Hama, Y., Tsukamoto, S., Matsui, T., Toyota, Y., Kodama, A., Ishihara, T., Mizushima, T., and Mizushima, N. (2016). An Autophagic Flux Probe that Releases an Internal Control. Mol. Cell 64, 835–849.

Kirli, K., Karaca, S., Dehne, H.J., Samwer, M., Pan, K.T., Lenz, C., Urlaub, H., and Gorlich, D. (2015). A deep proteomics perspective on CRM1-mediated nuclear export and nucleocytoplasmic partitioning. Elife 4, 1–28.

Lapalombella, R., Sun, Q., Williams, K., Tangeman, L., Jha, S., Zhong, Y., Goettl, V., Mahoney, E., Berglund, C., Gupta, S., et al. (2012). Selective inhibitors of nuclear export show that CRM1/XPO1 is a target in chronic lymphocytic leukemia. Blood 120, 4621–4634.

Liang, X.H., Yu, J., Brown, K., and Function, T.S. (2001). Beclin 1 Contains a Leucine-rich Nuclear Export Signal That Is Required for Its Autophagy and Tumor Suppressor Function Beclin 1 Contains a Leucine-rich Nuclear Export Signal That Is Required for Its. 3443–3449.

Lipecka, J., Chhuon, C., Bourderioux, M., Bessard, M.-A., van Endert, P., Edelman, A., and Guerrera, I.C. (2016). Sensitivity of mass spectrometry analysis depends on the shape of the filtration unit used for filter aided sample preparation (FASP). Proteomics 16, 1852–1857.

Mertins, P., Yang, F., Liu, T., Mani, D.R., Petyuk, V.A., Gillette, M.A., Clauser, K.R., Qiao, J.W., Gritsenko, M.A., Moore, R.J., et al. (2014). Ischemia in Tumors Induces Early and Sustained Phosphorylation Changes in Stress Kinase Pathways but Does Not Affect Global Protein Levels. Mol. Cell. Proteomics 13, 1690–1704.

Mertins, P., Mani, D.R., Ruggles, K. V., Gillette, M.A., Clauser, K.R., Wang, P., Wang, X., Qiao, J.W., Cao, S., Petralia, F., et al. (2016). Proteogenomics connects somatic mutations to signalling in breast cancer. Nature 534, 55–62.

Neggers, J.E., Vercruysse, T., Jacquemyn, M., Vanstreels, E., Baloglu, E., Shacham, S., Crochiere, M., Landesman, Y., and Daelemans, D. (2015). Identifying drug-target selectivity of small-molecule CRM1/XPO1 inhibitors by CRISPR/Cas9 genome editing. Chem. Biol. 22, 107–116.

Nishida, E., Fukuda, M., Asano, S., Nakamura, T., Adachi, M., Yoshida, M., and Yanagida, M. (1997). CRM1 is responsible for intracellular transport mediated by the nuclear export signal. Nature 390, 308–311.

Ossareh-Nazari, B., Bachelerie, F., and Dargemont, C. (1997). Evidence for a role of CRM1 in signal-mediated nuclear protein export. Science 278, 141–144.

Paul, I., Batth, T.S., Iglesias-gato, D., Al-araimi, A., Al-, I., Alkharusi, A., Norstedt, G., Olsen, J. V, and Zadjali, F. (2017). The ubiquitin ligase Cullin5 SOCS2 regulates NDR1 / STK38 stability and NF- κ B transactivation. Sci. Rep. 1–14.

Ren, F., Zhang, L., and Jiang, J. (2010). Hippo signaling regulates Yorkie nuclear localization and activity through 14-3-3 dependent and independent mechanisms. Dev. Biol. 337, 303–312.

Rhee, H.-W., Zou, P., Udeshi, N.D., Martell, J.D., Mootha, V.K., Carr, S. a, and Ting, A.Y. (2013). Proteomic Mapping of Mitochondria in Living Cells via Spatially Restricted Enzymatic Tagging. Science (80-.). 1328.

Schmid-Burgk, J.L., Höning, K., Ebert, T.S., and Hornung, V. (2016). CRISPaint allows modular base-specific gene tagging using a ligase-4-dependent mechanism. Nat. Commun. 7, 12338.

Selimoglu, R., Bettoun, A., Joffre, C., Meunier, B., Parrini, M.C., Fesquet, D., Formstecher, E., Cascone, I., Hergovich, A., and Camonis, J.H. (2014). RalA GTPase and MAP4K4 Function through NDR1 Activation in Stress Response and Apoptotic Signaling. HSOA J. Cell Biol. Cell Metab. 1, 1–11.

Sharma, K., D'Souza, R.C.J., Tyanova, S., Schaab, C., Wiśniewski, J.R., Cox, J., and Mann, M. (2014). Ultradeep Human Phosphoproteome Reveals a Distinct Regulatory Nature of Tyr and Ser/Thr-Based Signaling. Cell Rep. 8, 1583–1594.

Shi, D.D., Shi, H., Lu, D., Li, R., Zhang, Y., and Zhang, J. (2012). NDR1/STK38 potentiates NF-kB activation by its kinase activity. Cell Biochem. Funct. 30, 664–670.

Singh, G., Kucukural, A., Cenik, C., Leszyk, J.D., Shaffer, S.A., Weng, Z., and Moore, M.J. (2012). The cellular EJC interactome reveals higher-order mRNP structure and an EJC-SR protein nexus. Cell 151, 750–764.

Stade, K., Ford, C.S., Guthrie, C., and Weis, K. (1997). Exportin 1 (Crm1p) is an essential nuclear export factor. Cell 90, 1041–1050.

Vercruysse, T., De Bie, J., Neggers, J.E., Jacquemyn, M., Vanstreels, E., Schmid-Burgk, J.L., Hornung, V., Baloglu, E., Landesman, Y., Senapedis, W., et al. (2017). The second-generation exportin-1 inhibitor KPT-8602 demonstrates potent activity against acute lymphoblastic leukemia. Clin. Cancer Res. 23, 2528–2541.

Vichalkovski, A., Gresko, E., Cornils, H., Hergovich, A., Schmitz, D., and Hemmings, B.A. (2008). NDR Kinase Is Activated by RASSF1A/MST1 in Response to Fas Receptor Stimulation and Promotes Apoptosis. Curr. Biol. 18, 1889–1895.

Vizcaíno, J.A., Csordas, A., del-Toro, N., Dianes, J.A., Griss, J., Lavidas, I., Mayer, G., Perez-Riverol, Y., Reisinger, F., Ternent, T., et al. (2016). 2016 update of the PRIDE database and its related tools. Nucleic Acids Res. 44, D447–D456.

Wei, S.C., Fattet, L., Tsai, J.H., Guo, Y., Pai, V.H., Majeski, H.E., Chen, A.C., Sah, R.L., Taylor, S.S., Engler, A.J., et al. (2015). Matrix stiffness drives epithelial-mesenchymal transition and tumour metastasis through a TWIST1-G3BP2 mechanotransduction pathway. Nat. Cell Biol. 17, 678–688.

Wiśniewski, J.R., Zougman, A., Nagaraj, N., and Mann, M. (2009). Universal sample preparation method for proteome analysis. Nat. Methods 6, 359–362.

Zhang, L., Tang, F., Terracciano, L., Hynx, D., Kohler, R., Bichet, S., Hess, D., Cron, P., Hemmings, B.A., Hergovich, A., et al. (2015). NDR Functions as a Physiological YAP1 Kinase in the Intestinal Epithelium. Curr. Biol. 25, 296–305.

Zhao, B., Zhao, B., Wei, X., Wei, X., Li, W., Li, W., Udan, R.S., Udan, R.S., Yang, Q., Yang, Q., et al. (2007). Inactivation of YAP oncoprotein by the Hippo pathway is involved in cell contact inhibition and tissue growth control. Genes Dev. 21, 2747–2761.

GRAPHICAL ABSTRACT

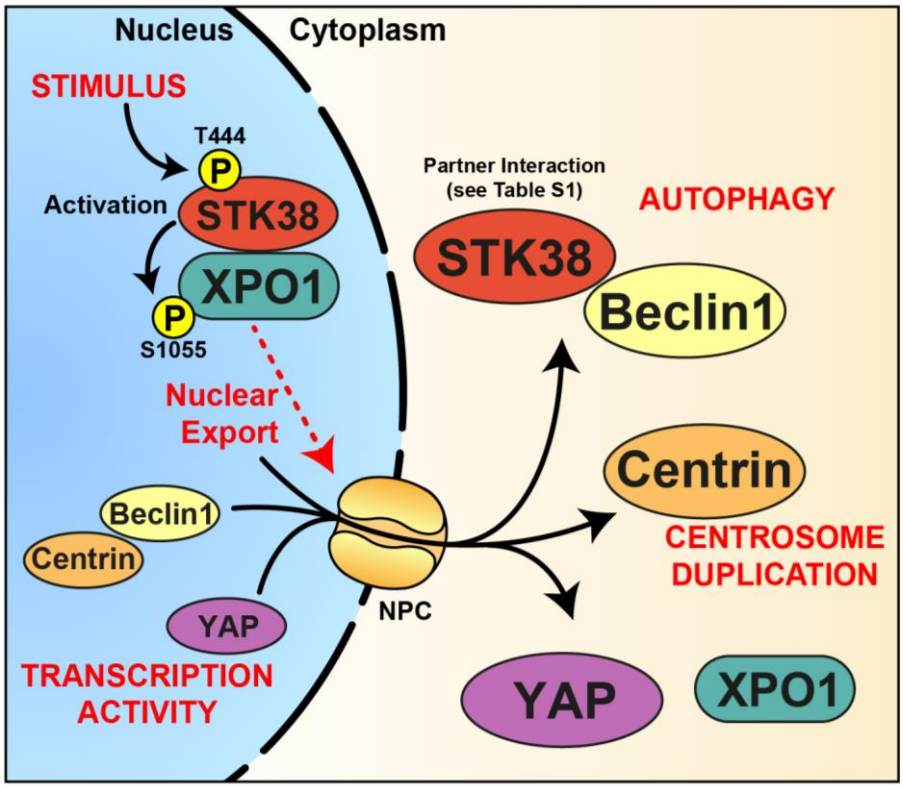

MAIN FIGURES

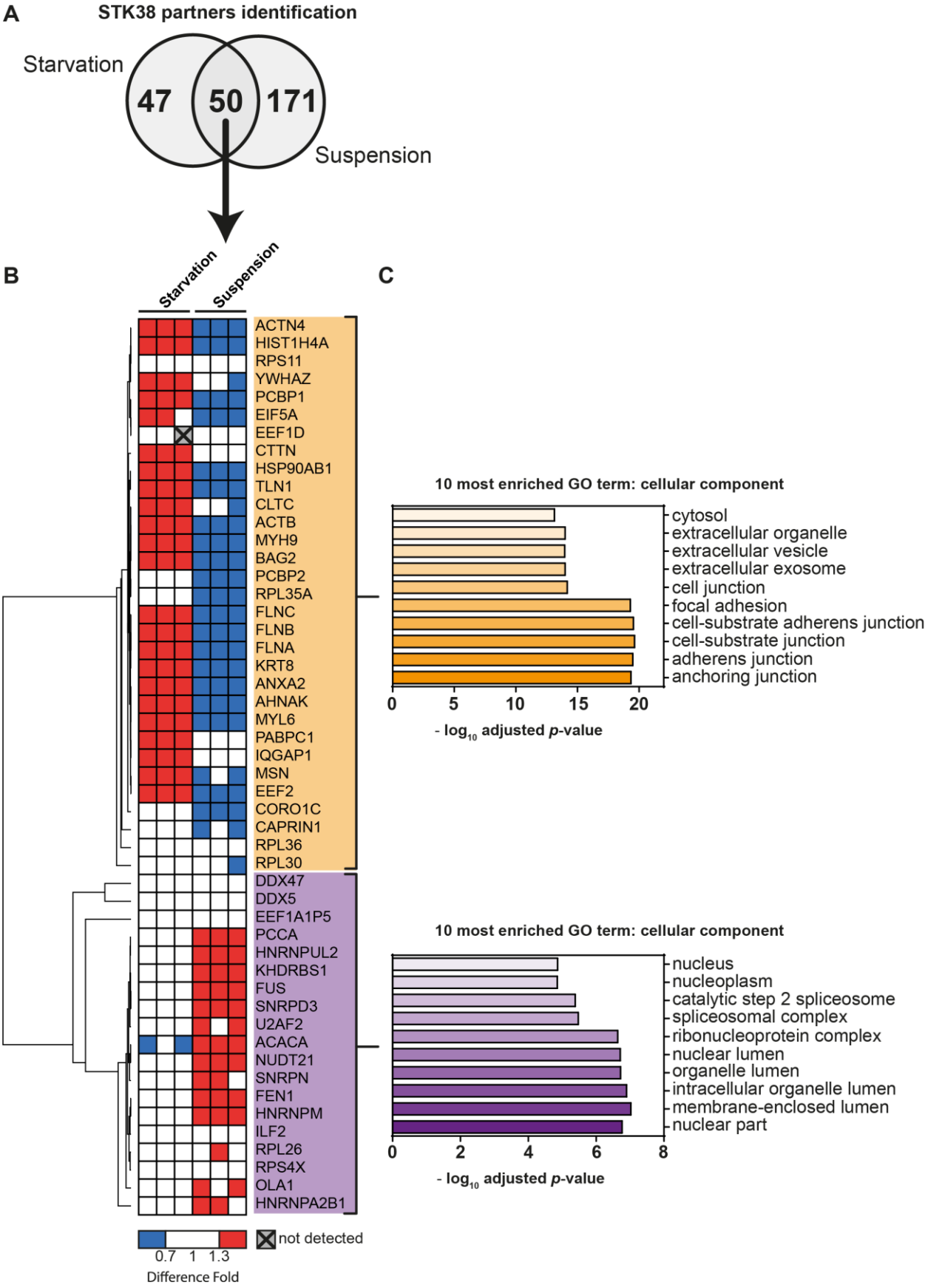

Figure 1. STK38 associates with cytoplasmic interactors upon nutrient starvation and with nuclear interactors upon suspension growth.

(**A**) Venn diagram of STK38 partners identified in both starvation and suspension conditions by proximity biotinylation assay coupled to mass spectrometry identification (see Table S1 for STK38 context-dependent interactors complete list and Fig S1-S2 for context-dependent protein labelling strategy). (**B**) Heatmap representation of common STK38 interactors identified in both starvation and suspension conditions according to their dynamic of association with STK38. Unsupervised hierarchical clustering was generated based on their association fold using Pearson correlation. (**C**) Representation of the 10 most cellular component enriched terms of the two clusters (assessed by using the Gene Ontology (GO) database: http://www.geneontology.org/).

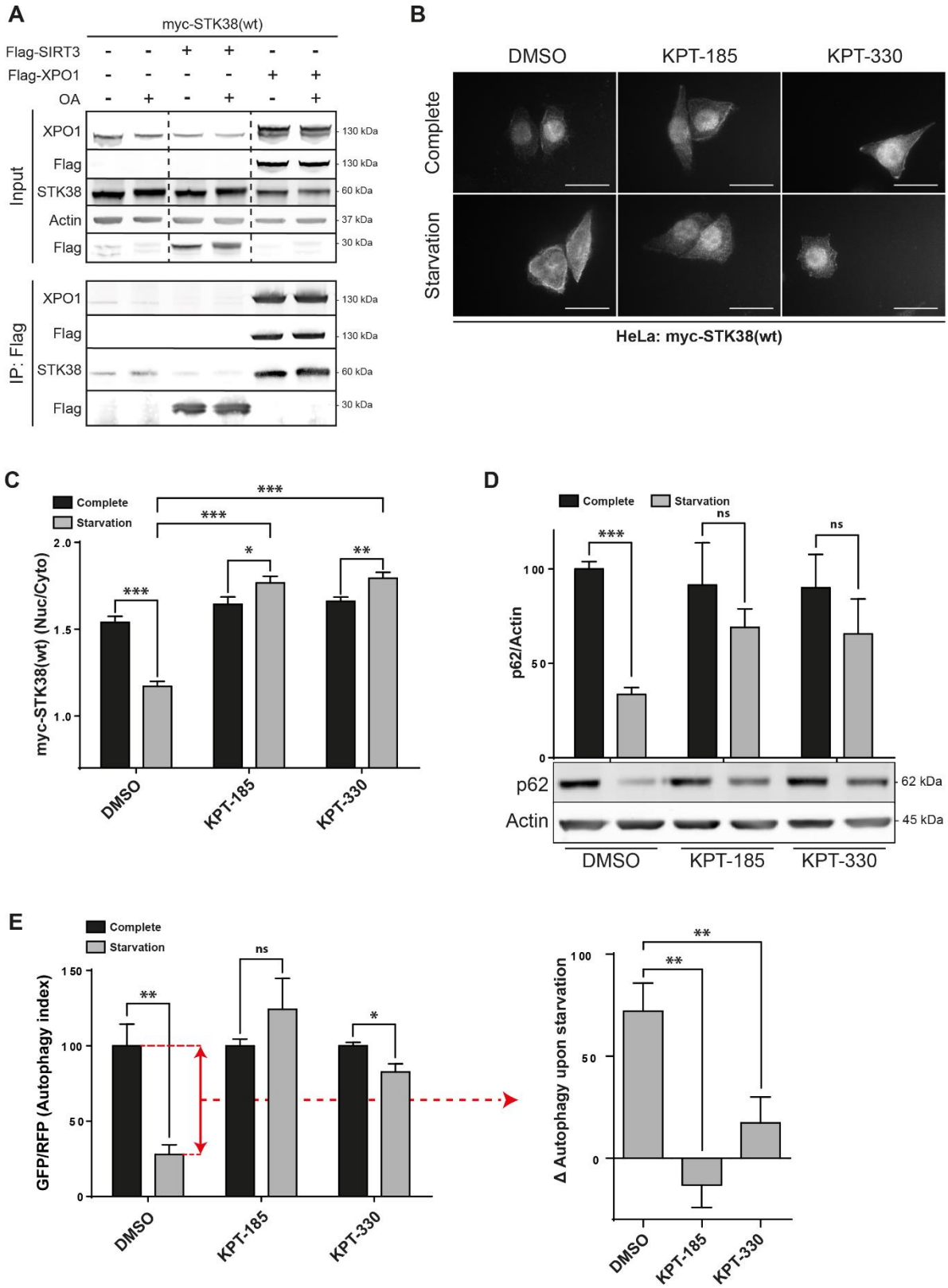
A
myc-STK38(wt)
Flag-SIRT3
Flag-XPO1
OA
Input
XPO1
Flag
STK38
Actin
Flag
IP: Flag
130 kDa
60 kDa
37 kDa
30 kDa
B
DMSO
KPT-185
KPT-330
Complete
Starvation
HeLa: myc-STK38(wt)
C
Complete
Starvation
myc-STK38(wt) (Nuc/Cyto)
D
p62/Actin
p62
Actin
62 kDa
45 kDa
ns
E
GFP/RFP (Autophagy index)
Δ Autophagy upon starvation

Figure 2. XPO1 activity is required for STK38 cytoplasmic accumulation and autophagy upon nutrient starvation.

(**A**) STK38 interacts with XPO1. HekRasV12 cells were transiently transfected with myc-STK38(wt) together with either Flag-XPO1(wt) plasmid, Flag-control (ctrl = Sirt3) plasmid or without DNA. 24h later, cells were incubated with Okadaic Acid (OA), (final concentration = 1µM) for 1 hour or with DMSO. Flag fusions were pulled-down and co-immunoprecipited proteins were analyzed by western blotting (WB). Upper panel displays whole cell lysates (WCL) and lower panel represents immunoprecipitated proteins. (**B-C**) STK38 accumulates in the cytoplasm upon nutrient starvation in a XPO1-dependant manner. (**B**) HeLa cells were transfected with myc-STK38(wt) plasmid. The next day, cells were incubated with DMEM or EBSS in the presence of XPO1 inhibitors KPT-185 or KPT-330 as indicated (final concentration = 1 µM) or DMSO for 4 hours. Cells were then fixed and stained for myc-tag. Representative images are shown and scale bars are 40 µm. (**C**) Quantification of myc-STK38(wt) nuclear/cytoplasmic staining (n > 30 cells from 3 independent experiments, Mann-Whitney test). (**D-E**) XPO1 activity is required for nutrient starvation-induced autophagy. (**D**) Immunoblotting with indicated antibodies of whole cell lysates of cells in (**B**) and (**C**) and its graphical representation (n = 3 independent experiments, Student's *t* test). As expected, p62 degradation in starvation conditions was inhibited in presence of XPO1 inhibitors. (**E**) HeLa cells stably expressing the GFP-LC3-RFP-LC3ΔG reporter autophagic probe (Kaizuka et al., 2016) were incubated with DMEM or EBSS in the presence of XPO1 inhibitors KPT-185 or KPT-330 (final concentration = 1 µM) or DMSO for 4 hours. On the left panel, the GFP and RFP signals were recorded by FACS analysis and then shown as a ratio recapitulating overall LC3 level (n=3 independent experiments, Student's *t* test). The right panel displays the difference of the GFP/RFP signal between DMEM and EBSS for each condition presented as in the left panel and is presented as a Δ Autophagy upon starvation (n=3 independent experiments, Student's *t* test). Here again, incubation with XPO1 inhibitors significantly impaired the autophagy process (see Fig. S3 for stable cell line validation).

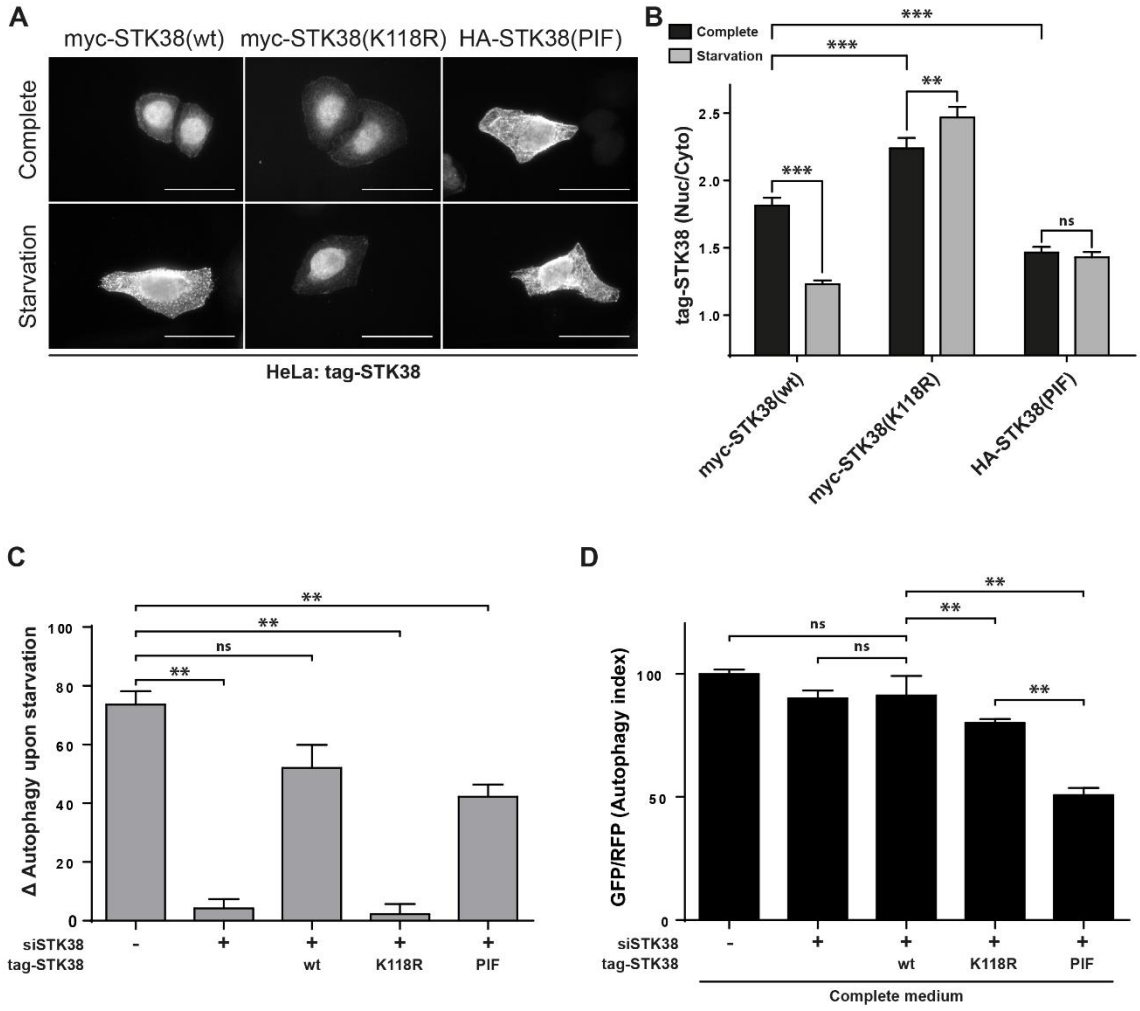

Figure 3. STK38 kinase activity is necessary and sufficient to induce its cytoplasmic relocalisation and autophagy.

(**A-B**) STK38 kinase activity is required and sufficient for its cytoplasmic accumulation upon nutrient starvation. (**A**) HeLa cells were transfected with myc-STK38(wt) expressing plasmid, myc-STK38(K118R) (STK38 kinase-dead version) plasmid or with HA-STK38(PIF) (STK38 constitutively active version) plasmid. 24 hours later, cells were incubated with DMEM or EBSS for 4 hours, fixed and stained for myc-tag or HA-tag. Representative images are shown and scale bars are 40 µm. (**B**) Graphical representation of tag-STK38 variants nuclear staining/cytoplasmic staining (n > 30 cells from 3 independent experiments, Mann-Whitney test). (**C-D**) STK38 kinase activity is required and sufficient for nutrient-starvation induced autophagy. (**C**) HeLa cells stably expressing the GFP-LC3-RFP-LC3ΔG autophagic probe (Kaizuka et al., 2016) were transiently transfected with siRNA targeting the 3'UTR region of endogenous STK38 (or with non-targeting siRNA (siNT)). The next day, cells were transiently transfected with the indicated STK38 mutants expressing plasmids (identical to (**A-B**)). 24 hours after plasmid transfection, cells were incubated with DMEM or EBSS for 4 hours. The GFP and RFP signals were recorded by FACS analysis and then shown as a Δ Autophagy upon starvation (n= 4 independent experiments, Mann-Whitney test). As published (Joffre et al., 2015), depleting STK38 prevents autophagy to take place. This effect was partially reversed by expressing the wt ORF as well as constitutively active STK38 whereas kinase-dead version failed to reproduce endogenous STK38 effect. (**D**) Same cells as used in (**C**) were assessed for autophagy induction but in nutrient rich condition only (DMEM incubation) by plotting the GFP/RFP signal ratio (n=4 independent experiments, Mann-Whitney test). Here, the result indicates that expression of constitutively active STK38 is sufficient to induce a substantial change in the autophagic flux upon nutrient rich conditions (see Fig. S4 for STK38 replacement).

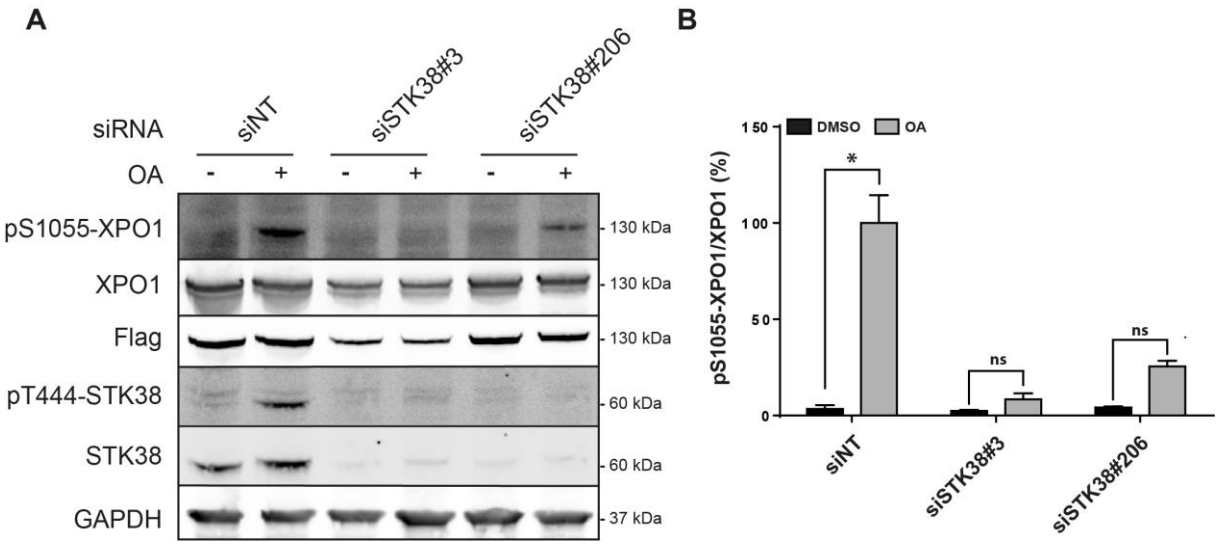

Figure 4. STK38 is required for phosphorylation of XPO1 on its Ser1055.
STK38 is required for XPO1 S1055 phosphorylation. (**A**) HeLa cells were transiently transfected with the indicated siRNA and subjected to Flag-XPO1(wt) transient transfection the following day. 48 hours later, cells were incubated with Okadaic Acid (OA, final concentration = 1 µM) for 1 hour or with DMSO. Immunoblotting was performed on whole cell lysates with indicated antibodies. (**B**) Graphical representation of the phospho S1055-XPO1 signal on total XPO1 (n = 3 independent experiments, Mann-Whitney test). As expected, XPO1 is phosphorylated on its Ser1055 upon OA treatment but not when STK38 is silenced (see Fig. S5 for antibody validation and STK38 silencing quantification).

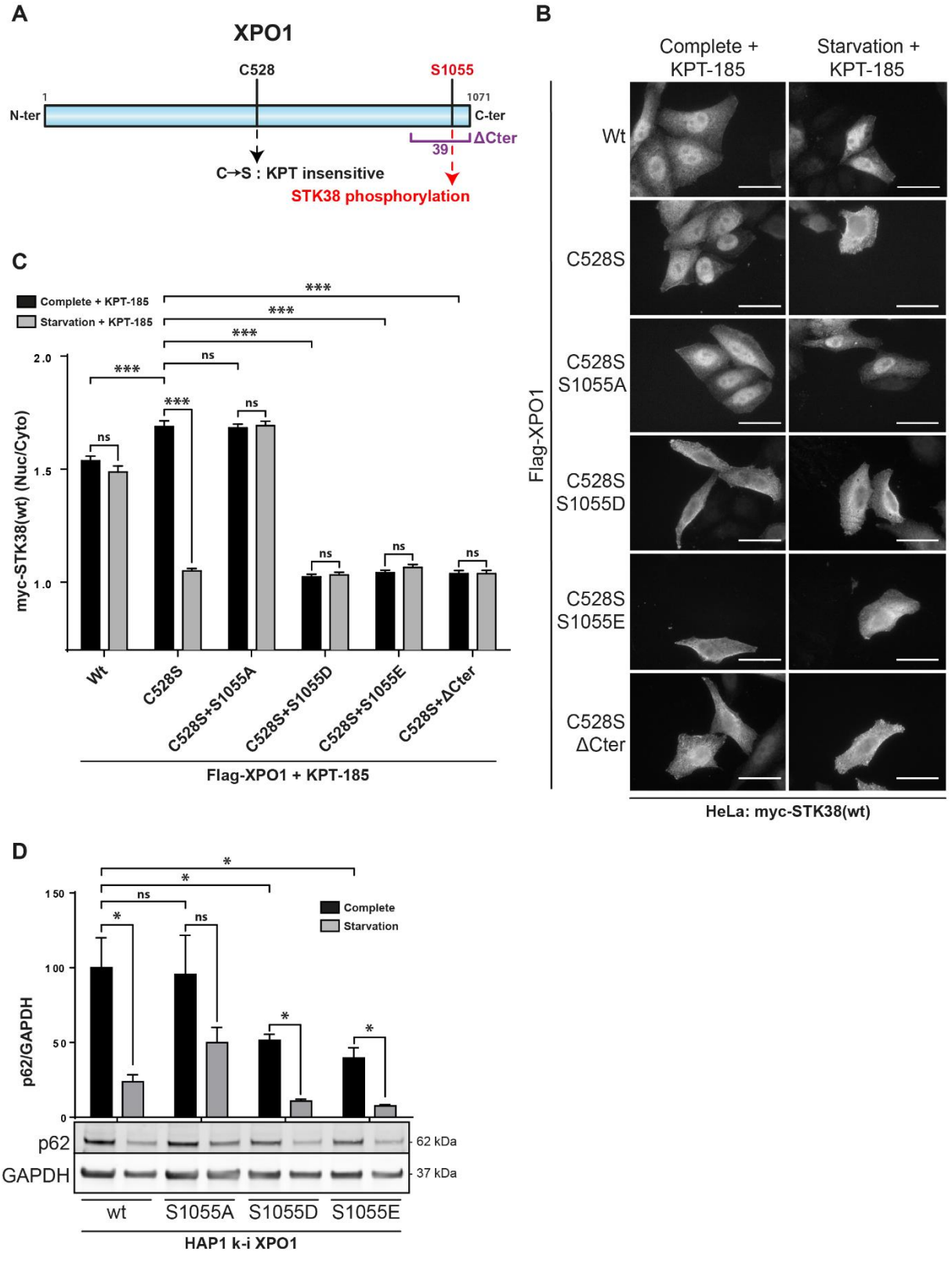
A
XPO1
C528
S1055
1
1071
N-ter
C-ter
ΔCter
39
C→S : KPT insensitive
STK38 phosphorylation
B
Complete + KPT-185
Starvation + KPT-185
Wt
C528S
C528S S1055A
C528S S1055D
C528S S1055E
C528S ΔCter
Flag-XPO1
HeLa: myc-STK38(wt)
C
Complete + KPT-185
Starvation + KPT-185
myc-STK38(wt) (Nuc/Cyto)
2.0
1.5
1.0
***
ns
Wt
C528S
C528S+S1055A
C528S+S1055D
C528S+S1055E
C528S+ΔCter
Flag-XPO1 + KPT-185
D
p62/GAPDH
150
100
50
0
*
ns
Complete
Starvation
p62
GAPDH
62 kDa
37 kDa
wt
S1055A
S1055D
S1055E
HAP1 k-i XPO1

Figure 5. XPO1_S1055 phosphorylation is required and sufficient for STK38 nuclear exit and autophagy upon nutrient starvation.

(**A**) Graphical representation of XPO1 protein. C528 to S amino acid mutation confers XPO1 resistance to both KPT-185 and KPT-330 chemical inhibitors (Neggers et al., 2015). S1055 amino acid correspond to the phosphorylation target of the STK38. Finally, the ΔCter region is also highlighted corresponding to a XPO1 construct lacking the 39 C-terminal residues (Dian et al., 2013). (**B-C**) XPO1_S1055 phosphorylation is required and sufficient for STK38 nuclear exit upon nutrient starvation. (**B**) HeLa cells were transiently transfected with myc-STK38(wt) in addition to indicated Flag-XPO1 mutants plasmids. 24 hours later, cells were incubated with DMEM or EBSS for 4 hours both supplemented with KPT-185 (final concentration = 1 µM) in order to inhibit endogenous XPO1 activity. Cells were then fixed and stained for Flag and myc tags. Only cells positives for both Flag-XPO1 and myc-STK38(wt) were captured. Representative images are shown and scale bars are 40 µm. (**C**) Graphical representation of myc-STK38(wt) nuclear staining/cytoplasmic staining (n > 30 cells from 3 independent experiments, Mann-Whitney test). Expression of wt XPO1 failed to induce cytoplasmic localisation of STK38 upon nutrient starvation in presence of KPT-185 where C528S mutant recapitulates results described in Fig.2B-C. Expression of phosphonegative XPO1 (S1055A) failed to induces STK38 cytoplasmic localisation upon EBSS treatment while phosphomimetics XPO1 (S1055D and S1055E) were sufficient to promote STK38 cytoplasmic localisation without autophagic stimuli. Finally, expression of XPO1 lacking in its 39 C-terminal residues mimicked phosphomimetics variants. (**D**) HAP1 cells carrying genomic XPO1 mutations of S1055 were subjected for IMDM (nutrient rich medium) or EBSS incubation for 4 hours followed by western-blot analysis for p62 level measurement. This result indicates that p62 degradation in starvation conditions was inhibited in XPO1_S1055A HAP1 cells whereas p62 degradation was potentiated in both phosphomimetics variant (S1055D & S1055E) (n = 4 independent experiments, Mann-Whitney test; see Fig. S6B for HAP1 genome edited cell lines).

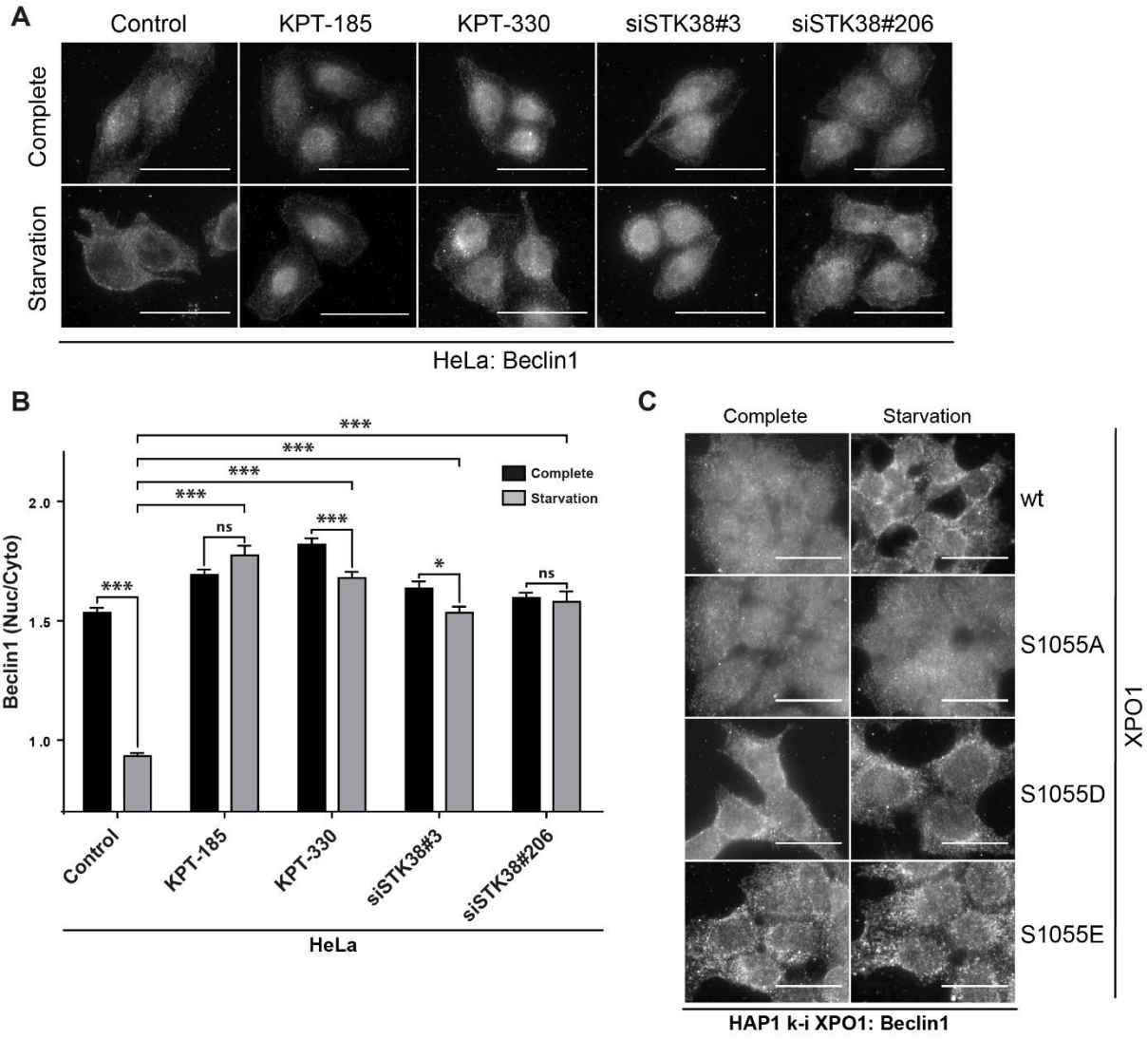
A
Control
KPT-185
KPT-330
siSTK38#3
siSTK38#206
Complete
Starvation
HeLa: Beclin1
B
Beclin1 (Nuc/Cyto)
Complete
Starvation
***
ns
*
Control
KPT-185
KPT-330
siSTK38#3
siSTK38#206
HeLa
C
Complete
Starvation
wt
S1055A
S1055D
S1055E
XPO1
HAP1 k-i XPO1: Beclin1
D
Complete
Starvation
Beclin1 (Nuc/Cyto)
wt
S1055A
S1055D
S1055E
HAP1 k-i XPO1

Figure 6. XPO1_S1055 phosphorylation is required and sufficient for Beclin1 nuclear exit upon nutrient starvation.

(**A-B**) XPO1 and STK38 are required for Beclin1 cytoplasmic accumulation upon nutrient starvation-induced autophagy. (**A**) HeLa cells were transiently transfected with the indicated siRNA (control condition = siNT). 72 hours later, cells were incubated with XPO1 inhibitors KPT-185 or KPT-330 as indicated (final concentration = 1 µM) or with DMSO for all other conditions for 2 hours prior incubation with DMEM or EBSS supplemented (or not) with inhibitors for 2 hours. Cells were fixed and stained for endogenous Beclin1. Representative images are shown and scale bars are 40 µm. (**B**) Graphical representation of endogenous Beclin1 nuclear staining/cytoplasmic staining (n > 30 cells from 3 independent experiments, Mann-Whitney test). XPO1 activity inhibition by both KPT-185 and KPT-330 as well as STK38 silencing failed to induce Beclin1 cytoplasmic accumulation upon nutrient starvation (see Fig. S7A for STK38 silencing validation). (**C-D**) XPO1_S1055 phosphorylation is required and sufficient for Beclin1 nuclear exit upon nutrient starvation. (**C**) Genome edited XPO1 mutant HAP1 cells were incubated with IMDM (nutrient-rich medium) or EBSS for 2 hours. Cells were then fixed and stained for endogenous Beclin1. Representative images are shown and scale bars are 20 µm. (**D**) Graphical representation of endogenous Beclin1 nuclear staining/cytoplasmic staining (n > 30 cells from 3 independent experiments, Mann-Whitney test). Here, phosphonegative XPO1 failed to induce Beclin1 cytoplasmic accumulation upon nutrient starvation whereas phosphomimetics variant (S1055D & S1055E) potentiated Beclin1 cytoplasmic accumulation.

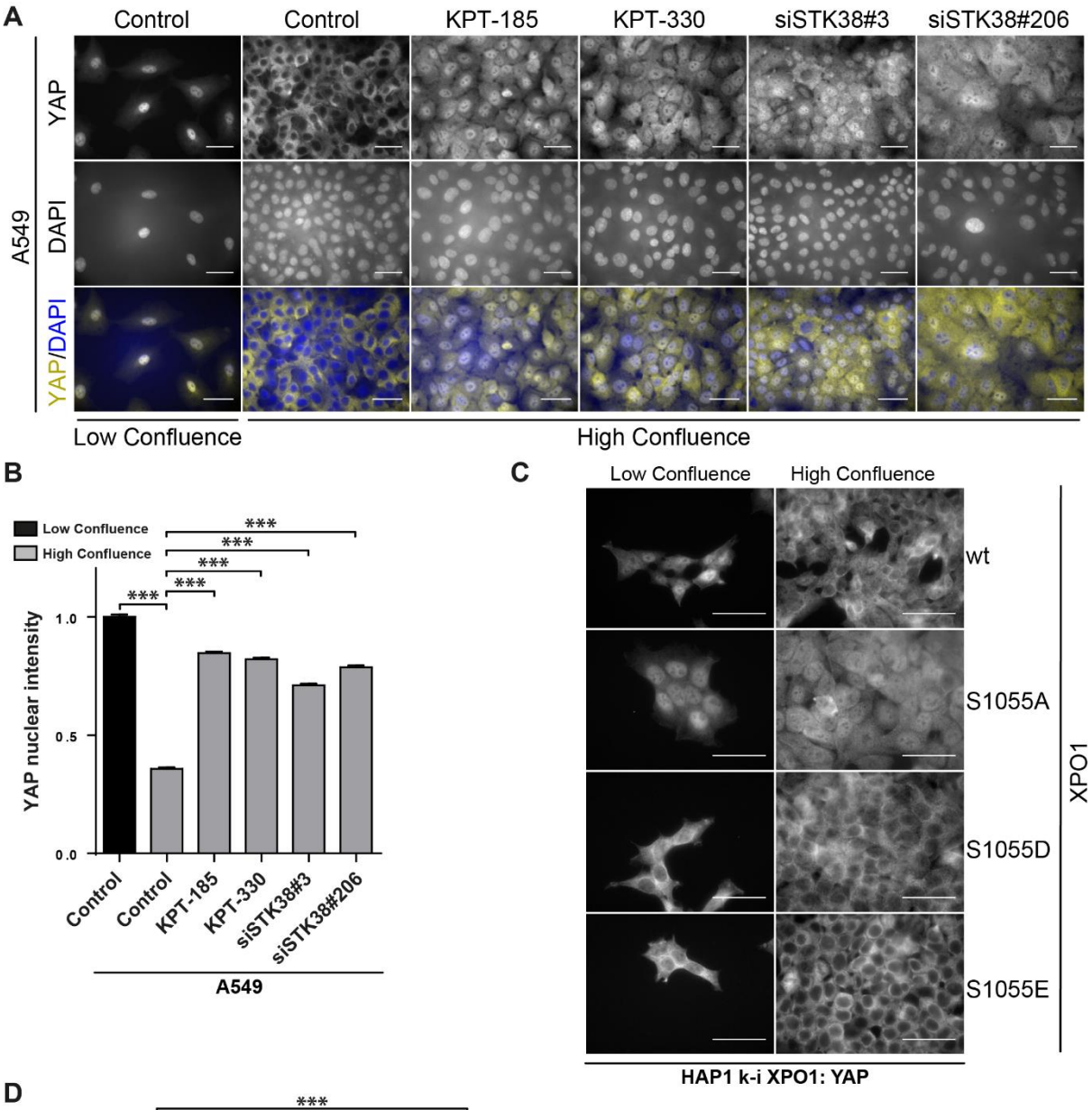
A
Control
Control
KPT-185
KPT-330
siSTK38#3
siSTK38#206
A549
YAP
DAPI
YAP/DAPI
Low Confluence
High Confluence
B
Low Confluence
High Confluence
YAP nuclear intensity
1.0
0.5
0.0
***
Control
Control
KPT-185
KPT-330
siSTK38#3
siSTK38#206
A549
C
Low Confluence
High Confluence
wt
S1055A
S1055D
S1055E
XPO1
HAP1 k-i XPO1: YAP
D
Low Confluence
High Confluence
YAP nuclear intensity
1.0
0.5
0.0
***
wt
S1055A
S1055D
S1055E
HAP1 k-i XPO1

Figure 7. XPO1_S1055 phosphorylation is required and sufficient for YAP nuclear exit at high confluency.

(**A-B**) XPO1 and STK38 are required for YAP1 nuclear export at high confluency. (**A**) A549 cells were transiently transfected with the indicated siRNA (control conditions = siNT) at low or high confluency. 48 hours later, cells were incubated overnight in the presence of XPO1 inhibitors KPT-185 and KPT-330 (final concentration = 1 µM) or with DMSO for all other conditions. The next day, cells were fixed and stained for endogenous YAP1. Representative images are shown and scale bars are 40 µm. (**B**) Quantitative representation of YAP1 nuclear fluorescence intensity (n > 300 cells from 3 independent experiments, Mann-Whitney test). XPO1 activity inhibition by both KPT-185 and KPT-330 as well as STK38 silencing failed to induce YAP1 nuclear exit at high confluency (see Fig. S8A for STK38 silencing levels). (**C-D**) XPO1_S1055 phosphorylation is required and sufficient for YAP nuclear exit. (**C**) Genome edited XPO1 HAP1 cells were cultured for two days at low versus high confluency. Cells were then fixed and stained for endogenous YAP1. Representative images are shown and scale bars are 40 µm. (**D**) Quantitative representation of YAP1 nuclear fluorescence intensity (n > 300 cells from 3 independent experiments, Mann-Whitney test). Here, phosphonegative XPO1 failed to induce YAP nuclear exit at high confluency whereas phosphomimetics variant (S1055D & S1055E) potentiated YAP nuclear exit.

SUPPLEMENTARY FIGURES

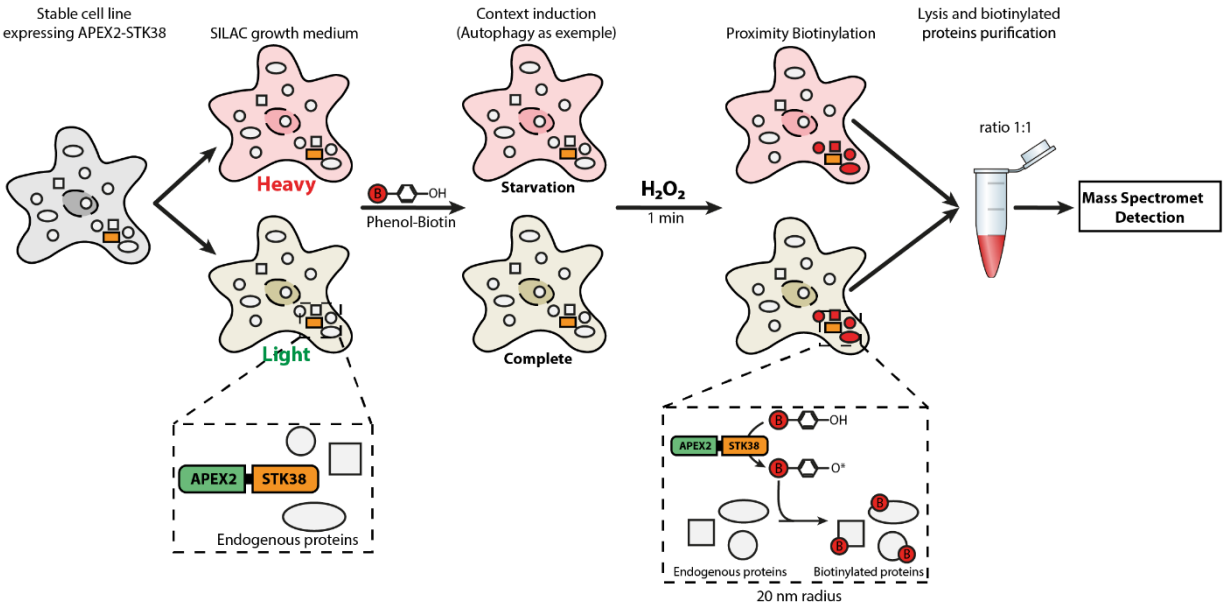

Figure S1 (in support of figure 1). STK38 partners identification strategy.
Figure indicating the strategy used to identify STK38 partners association dynamic depending on the context (example is shown for autophagy condition here). Stable cell lines expressing the fusion construct APEX2-STK38 was generated and then subdivided for amino acid replacement (SILAC). Context was then induced (4 hours EBSS incubation for autophagy induction and suspension growth) as well as a control condition (nutrient rich medium incubation and attached growth, respectively). Proximity labelling of STK38 partners was performed as described (Hung et al., 2016): briefly, cells were incubated with phenol-biotin for a minimum of 30 minutes followed by H_20_2 incubation for 1 minute precisely. Finally, biotinylated proteins (=STK38 partners) were purified from whole cell lysates using streptavidin-coated magnetic beads and subjected to mass spectrometry identification.

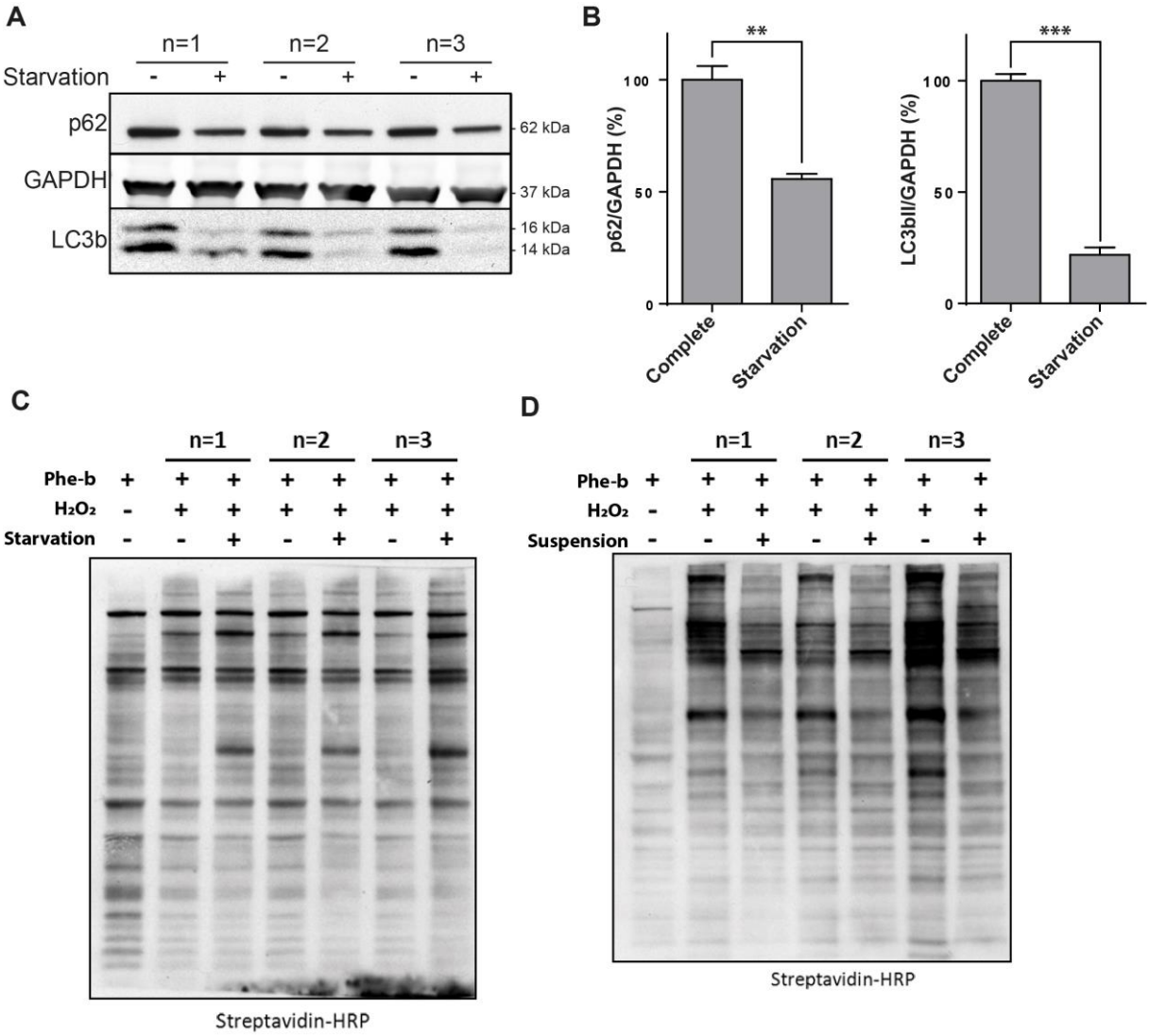
A
n=1
n=2
n=3
Starvation
- + - + - +
p62
GAPDH
LC3b
62 kDa
37 kDa
16 kDa
14 kDa
B
**
***
p62/GAPDH (%)
LC3bII/GAPDH (%)
100
50
0
Complete
Starvation
C
n=1
n=2
n=3
Phe-b + + + + + + +
H2O2 - + + + + + +
Starvation - - + - + - +
Streptavidin-HRP
D
n=1
n=2
n=3
Phe-b + + + + + + +
H2O2 - + + + + + +
Suspension - - + - + - +
Streptavidin-HRP
E
Starvation #1
Starvation #2
Starvation #3
Suspension #1
Suspension #2
Suspension #3
1
0.8
0.6
0.4
0.2
0
-0.2
-0.4
-0.6
-0.8
-1
Pearson Correlation

Figure S2 (in support of figure 1). Validation of nutrient starvation-induced autophagy and biotinylation.

(**A**) Western Blots show protein level for both autophagic markers p62 and LC3 from cell lysates identical to the ones used for mass spectrometry identification. (**B**) Graphical representations show a significant decrease of both autophagic markers p62 and LC3 upon EBSS incubation indicating a good autophagy induction (n = 3 independent experiment, Mann-Whitney test). (**C**) Western blot revealing biotinylation pattern of whole cell lysates identical to the ones used in mass spectrometry for the nutrient starvation-induced autophagy condition. (**D**) Western blot revealing biotinylation pattern of whole cell lysates identical to the ones sent to mass spectrometry for the suspension condition. (**E**) Correlation matrix of the three replicates for both nutrient starvation-induced autophagy and ECM detachment conditions based on the association fold of STK38 newly identified partners using Pearson correlation indicating good reproducibility between each replicate. Circles size and colour represent the correlation coefficient (blue for positive, red for negative).

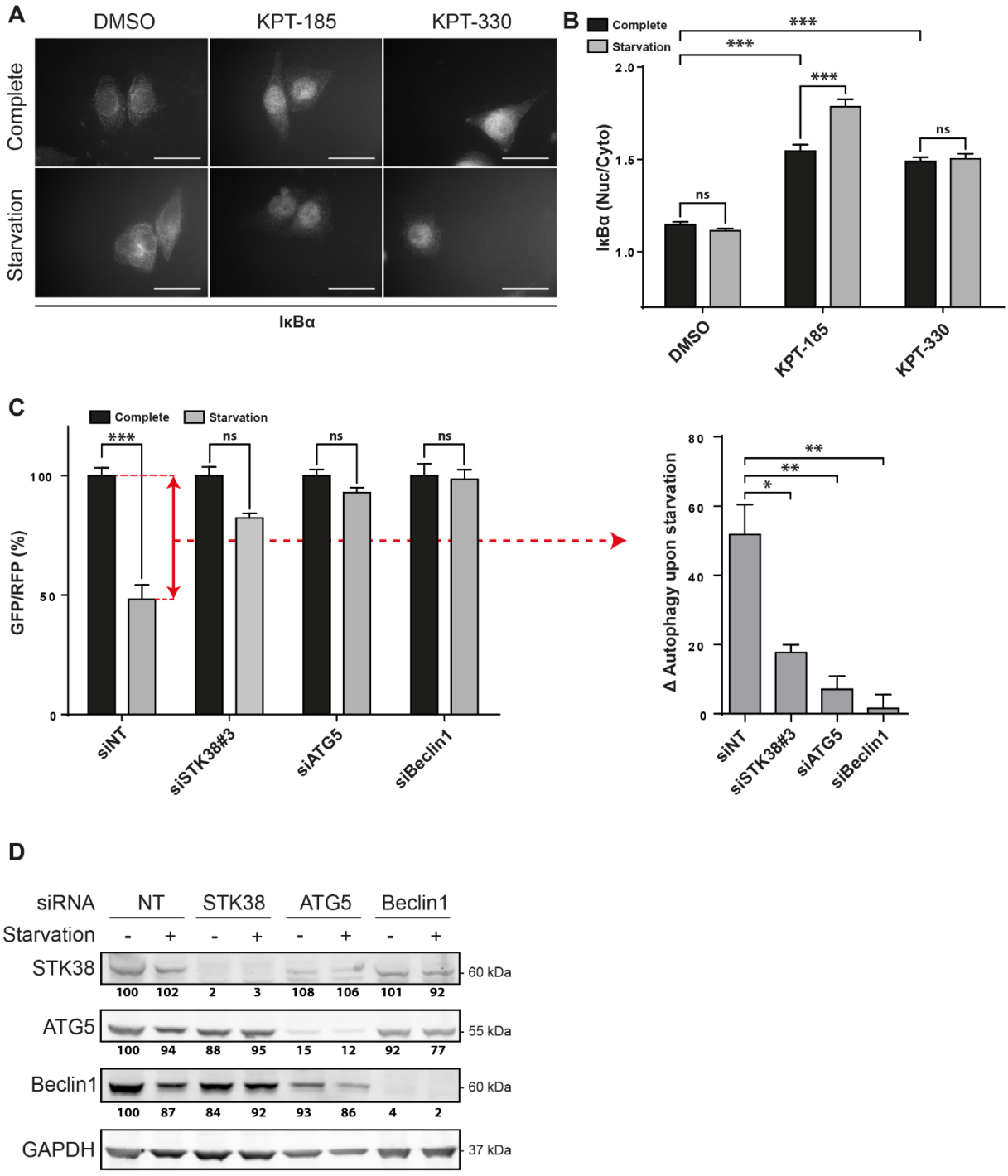

Figure S3 (in support of figure 2). Validation of XPO1 inhibition and autophagy monitoring cell line. (**A**) Validation of XPO1 activity inhibition as shown in Fig. 2. HeLa cells were incubated with DMEM or EBSS in the presence of XPO1 inhibitors KPT-185 or KPT-330 as indicated (final concentration = 1 µM) or DMSO for 4 hours. Cells were then fixed and stained for endogenous IκBα, a well known XPO1 cargo. Representative images are shown and scale bars are 40 µm. (**B**) Graphical representation of IκBα nuclear staining/cytoplasmic staining (n > 30 cells from 3 independent experiments, Mann-Whitney test). As anticipated, XPO1 activity inhibition by KPT-185 or KPT-330 induced a nuclear retention of IκBα. (**C-D**) Validation of autophagy monitoring cell line. (**C**) HeLa cells stably expressing the GFP-LC3-RFP-LC3ΔG reporter autophagic probe (Kaizuka et al., 2016) were incubated with the indicated siRNA. 72h later, cells were incubated with DMEM or EBSS for 4 hours and the GFP and RFP signals were

recorded by FACS analysis and then shown as a GFP/RFP ratio (%) as presented on the left panel (n=4 independent experiments, Mann-Whitney test). As expected, nutrient starvation incubation induced a significant decrease of the GFP/RFP ratio that is stopped when the pro autophagic proteins ATG5 and Beclin1 are silenced. As expected also, STK38 silencing inhibited (partially) the autophagic process. The right panel displays the difference of the GFP/RFP signal between DMEM and EBSS for each condition presented as in the left panel and is presented as a Δ Autophagy upon starvation (n=4 independent experiments, Mann-Whitney test). (**D**) Validation of silencing of proteins indicated in (**C**). Western blot indicates good silencing of STK38, ATG5 and Beclin1 proteins when associated with their respective siRNA (numbers indicate the average protein level normalized on GAPDH level for the 4 replicates).

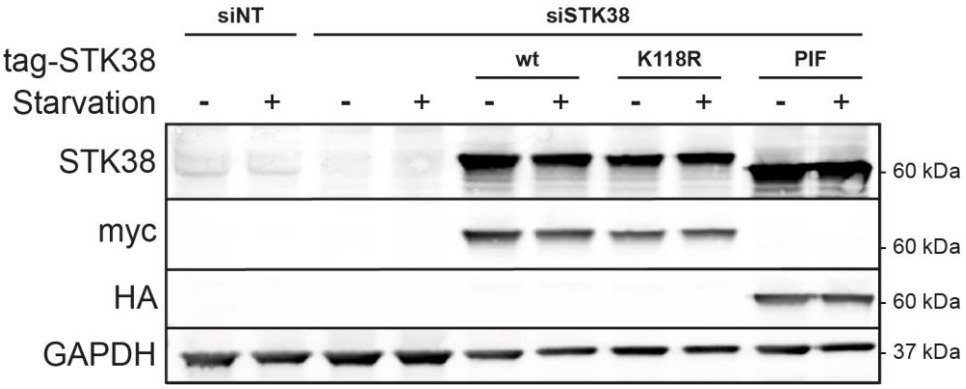

Figure S4 (in support of figure 3). Validation of STK38 replacement.
HeLa cells stably expressing the GFP-LC3-RFP-LC3ΔG reporter autophagic probe (same as presented as in Fig. 3C&D) were transiently transfected with siRNA targeting the 3'UTR region of endogenous STK38 (or with non-targeting siRNA (siNT)). The next day, cells were transiently transfected with the indicated STK38 mutants expressing plasmids. 24 hours after, cells were incubated with DMEM or EBSS for 4 hours and then subjected to lysis and western blotting analysis (here, only one replicate of the experiments presented in Fig. 3C&D is presented). This indicates a good replacement of STK38 in all conditions.

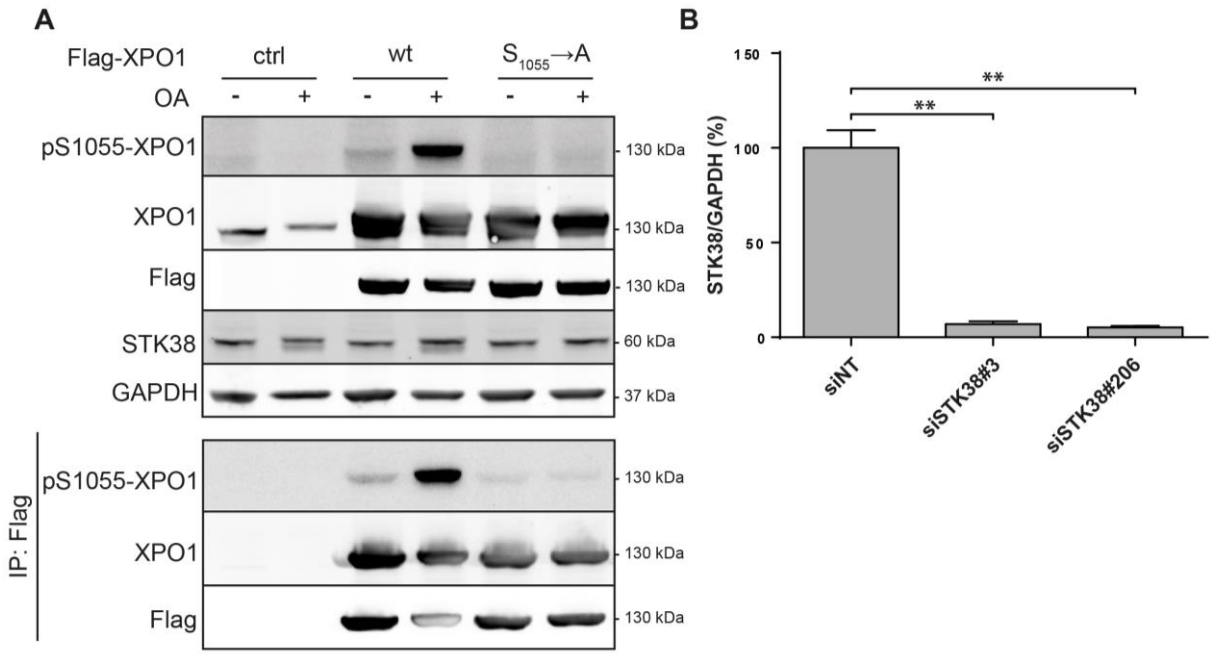

Figure S5 (in support of figure 4). Validation of pS1055_XPO1 antibody.
(**A**) HeLa cells were transiently transfected with the indicated Flag-XPO1 mutants expressing plasmids (wt or S1055A mutation) or without DNA. The next day, cells were treated with 1 µM OA or with vehicle (DMSO) for 1 hour. Flag fusions were immunoprecipited and pulled-down proteins were analyzed by western blotting. Upper panel displays whole cell lysates and lower panel represents immunoprecipited proteins. (**B**) Graphical representation of STK38 protein level for experiment presented in Fig. 4A&B (n=3 independent experiments, Mann-Whitney test).

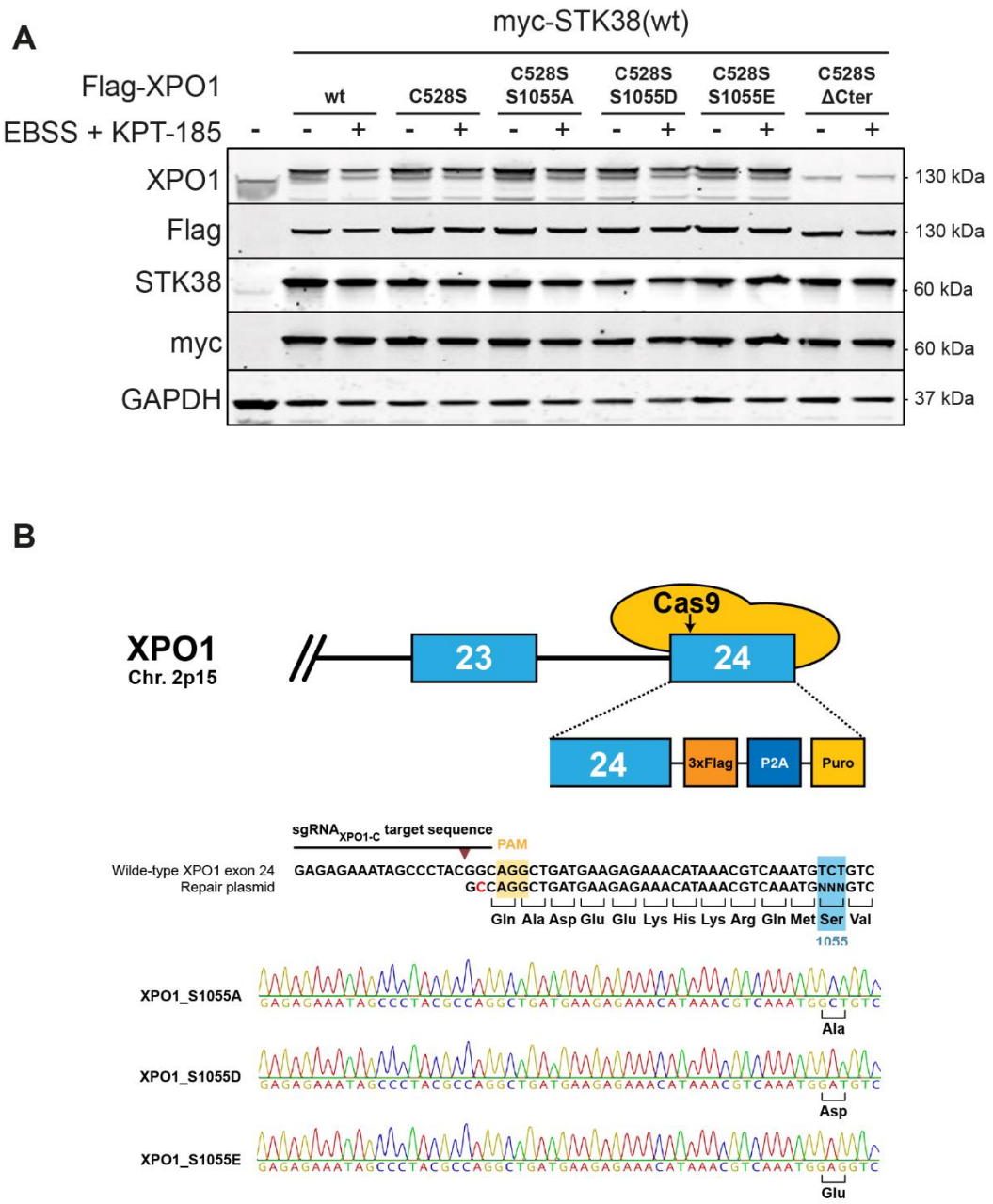

Figure S6 (in support of figure 5). XPO1 mutants transfection validation & CRISPR/Cas9 knock-in HAP1 cell lines.

(**A**) Same cells used as in Fig. 5B&C were subjected to whole cell lysis and western blotting analysis (here, only one replicate of the three is presented). This figure indicates a cells used are well transfected for myc-STK38(wt) and for Flag-XPO1 variants plasmids. Exogenous signal for XPO1 in C528S_ΔCter is absent (compared to the others) because the targeted amino acid sequence of the anti-XPO1 antibody is included in the Cter region deleted in this construct. (**B**) Schematic overview of CRISPR/Cas9 genome editing of XPO1 in HAP1 cell lines. Exons are shown as blue boxes and introns are visualized as a thick black line, while Cas9 is represented by the yellow oval shapes. The DNA sequence and corresponding amino acid of the region around the Ser1055 residue are enlarged. The Cas9 PAM sequence is indicated in yellow, the sgRNA sequence is highlighted by a black line above the DNA sequence and the Cas9 cutting site is indicated by the brown arrowhead. The wild-type sequence is shown together with the sequence of the donor repair plasmid used to generate the S1055 mutations and the additional silent mutation to prevent recutting of the mutagenized gene is marked in red. Sanger sequencing chromatograms of the generated XPO1 S1055 mutant cell lines are shown with the desired mutations highlighted in bold.

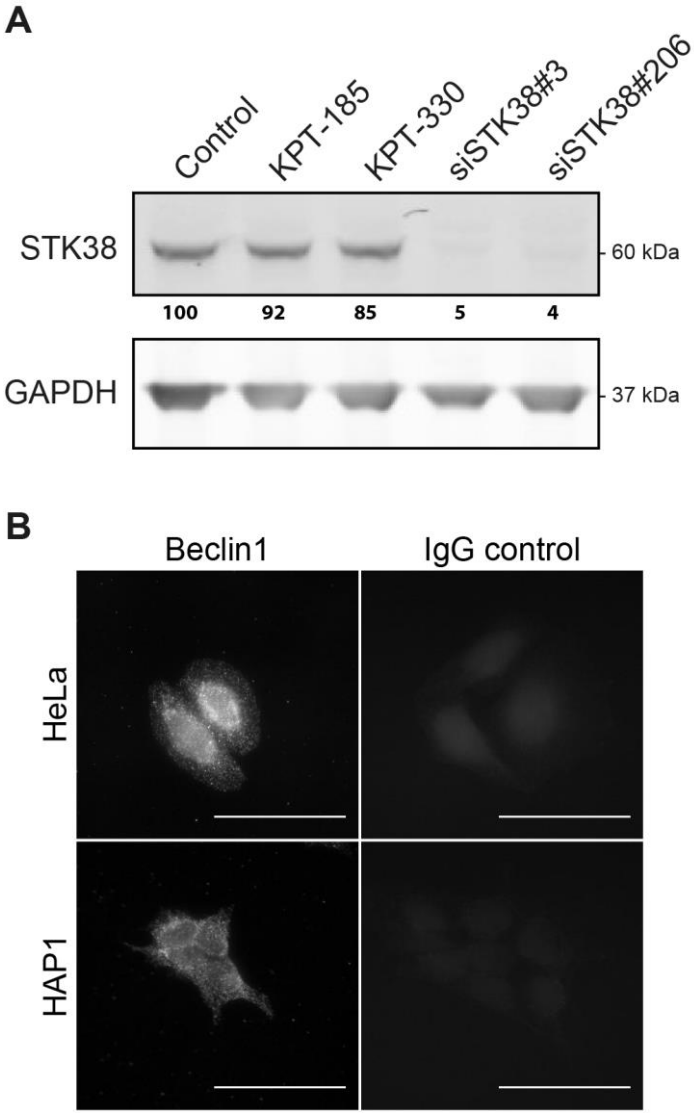

Figure S7 (in support of figure 6). Validation of STK38 silencing and Beclin1 antibody.
(**A**) STK38 silencing. Same cells as used in Fig. 6A&B were subjected for whole cell lysis and western blotting analysis in order confirm STK38 silencing (numbers indicate the average STK38 protein level normalized on GAPDH level for the 3 replicates of the experiment). Results indicates here an efficient silencing of endogenous STK38. (**B**) Validation of anti Beclin1 antibody used in Fig. 6A-D. HeLa and HAP1 wt cells were subjected to IF using anti Beclin1 or IgG control antibodies. The Ifs with IgG control were black, demonstrating the specificity of the anti Beclin1 antibody, scale bars are 40 µm.

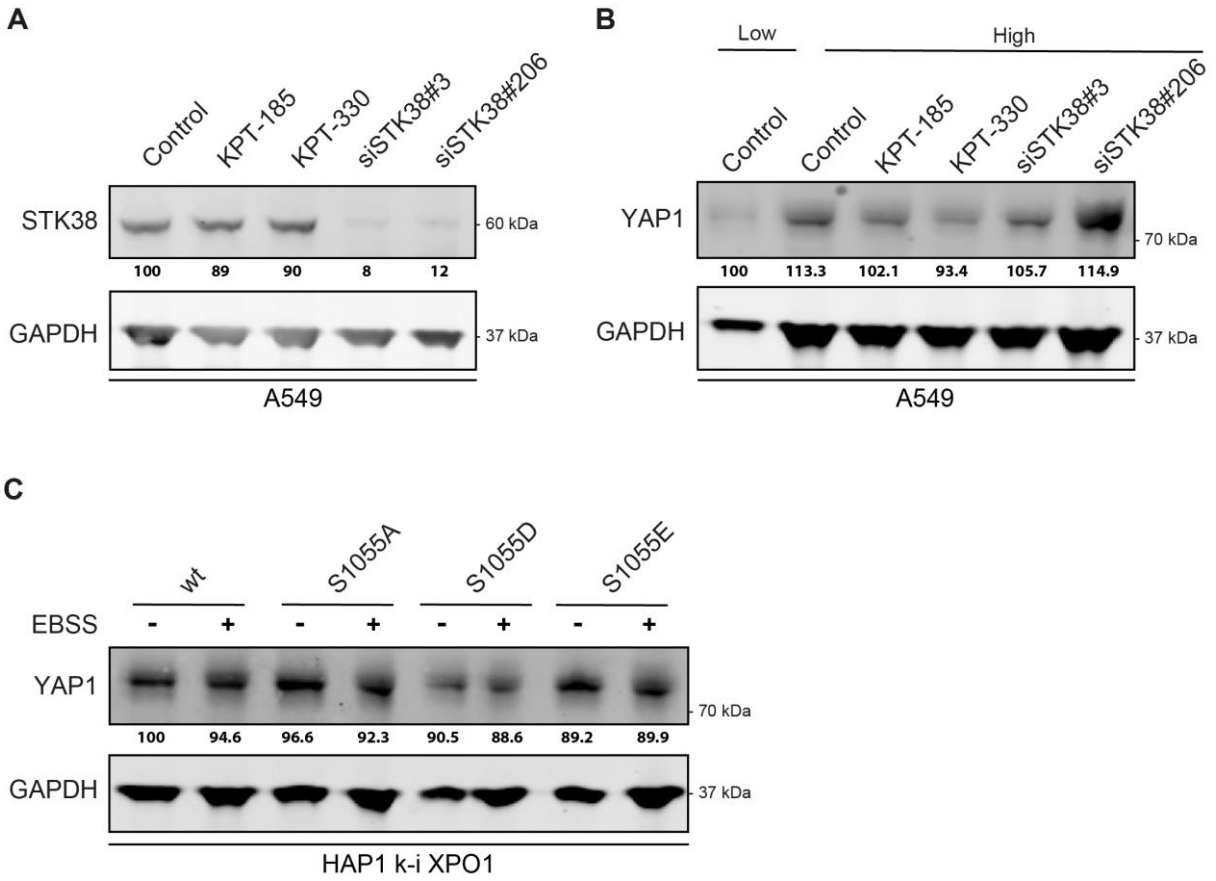

Figure S8 (in support of figure 7). Validation of STK38 silencing and YAP1 protein level.
(**A**) Same cells as used in Fig. 7A&B were subjected for whole cell lysis and western blotting analysis in order to confirm STK38 silencing (numbers indicate STK38 protein level normalized on GAPDH level for the 3 replicates of the experiment). Results indicates here an efficient silencing of endogenous STK38. (**B**) Same cells as used in Fig. 7A&B were subjected for whole cell lysis and western blotting analysis in order to check for YAP1 global protein level (numbers indicate the average YAP1 protein level normalized on GAPDH level for the 3 replicates of the experiment). Blots indicate that YAP1 protein level remain approximatively identical between each conditions, indicating that YAP1 nuclear exclusion observed in Fig. 7A&B is due to nuclear/cytoplasmic shuttling and not to protein degradation. (**C**) Same cells as used in Fig. 7C&D were subjected for whole cell lysis and western blotting analysis in order to check for YAP1 global protein level (numbers indicate the average YAP1 protein level normalized on GAPDH level for the 3 replicates of the experiment). Blots indicate that YAP1 protein level remain approximatively identical between each conditions, indicating that YAP1 nuclear exclusion observed in Fig. 7A&B is due to nuclear/cytoplasmic shuttling and not to protein degradation.

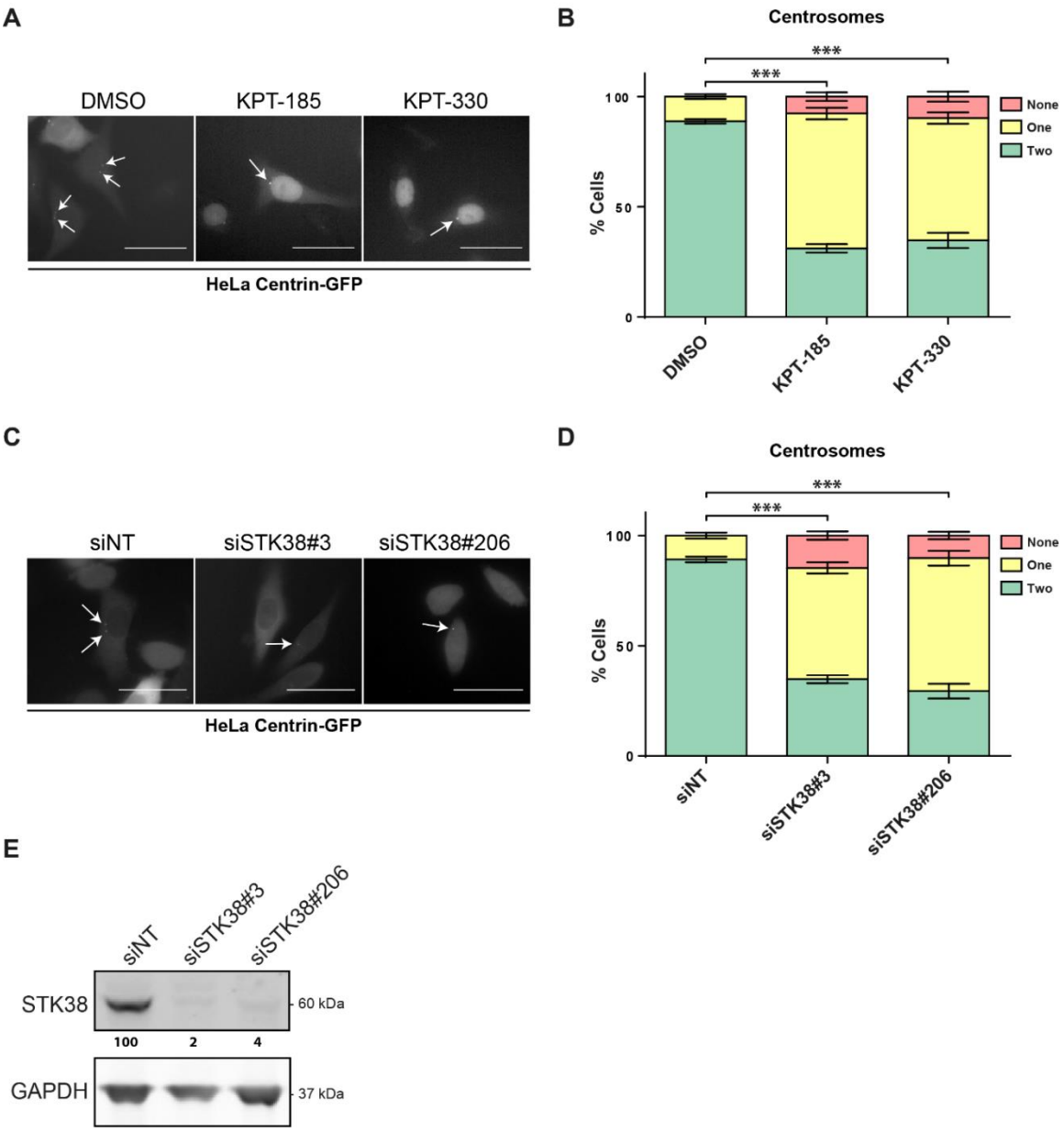

Figure S9. XPO1 blockage phenocopies STK38 silencing for proper centrosome distribution.
(**A-B**) XPO1 is required for centrosome distribution. (**A**) HeLa cells stably expressing GFP-Centrin were cultured on glass-bottom 6 well plates for two days in order to each 50% confluency the day of the experiment. GFP signal was then recorded on live microscopy and centrosomes (centrin "spots") were counted on Z-stacks images without differentiating unique separated centrioles in G1 phase from separated centrosomes (harbouring 2 centrioles each) in S/G2 phase. Representative images are shown and scale bars are 40 µm. (**B**) Graphical representation of cell population harbouring one, two, or no centrosomes. (n> 300 cells from 13 different fields from 3 experiments, Mann-Whitney test). Here, XPO1 blockage sgnifically impaired proper centrosomal distribution. (**C-E**) STK38 is required for centrosome distribution. (**C**) HeLa cells stably expressing GFP-Centrin were transiently transfected with the indicated siRNA for two days. GFP signal was then recorded on live microscopy and centrosomes (centrin "spots") were counted on Z-stacks images as described above. Representative images are shown and scale bars are 40 µm. (**D**) Graphical representation of cell population harbouring one, two, or no centrosomes. (n> 200 cells from 15 different fields from 3 experiments, Mann-Whitney test). Here, STK38 silencing sgnifically impaired proper centrosome distribution. (**E**) STK38 protein level of cells shown in **C**, numbers indicate the average STK38 protein level normalized on GAPDH level for the 3 replicates of the experiment. Results indicates here an efficient silencing of endogenous STK38.

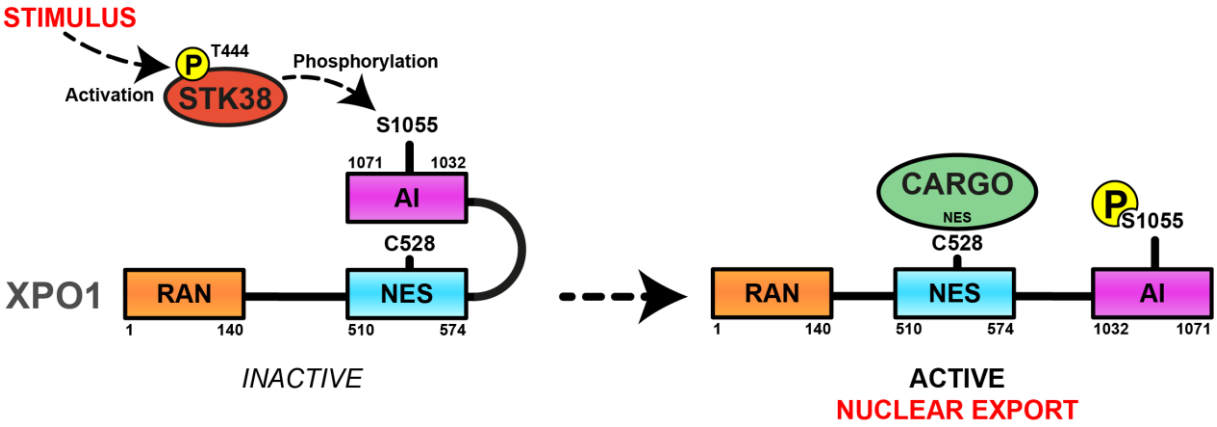

Figure S10. Diagram of the mechanism of activation of XPO1 by STK38.
Activated STK38 (triggered by T444 phosphorylation) phosphorylates inactivated XPO1 on S1055 within the auto-inhibitory domain (AI) resulting in a change of conformation of XPO1 and exposing its cargo binding region (NES, for Nuclear Export Signal recognition domain). Supposedly, the binding of Ran-GTP to its association domain (RAN) finalize this process leading to the nuclear export of the cargo.

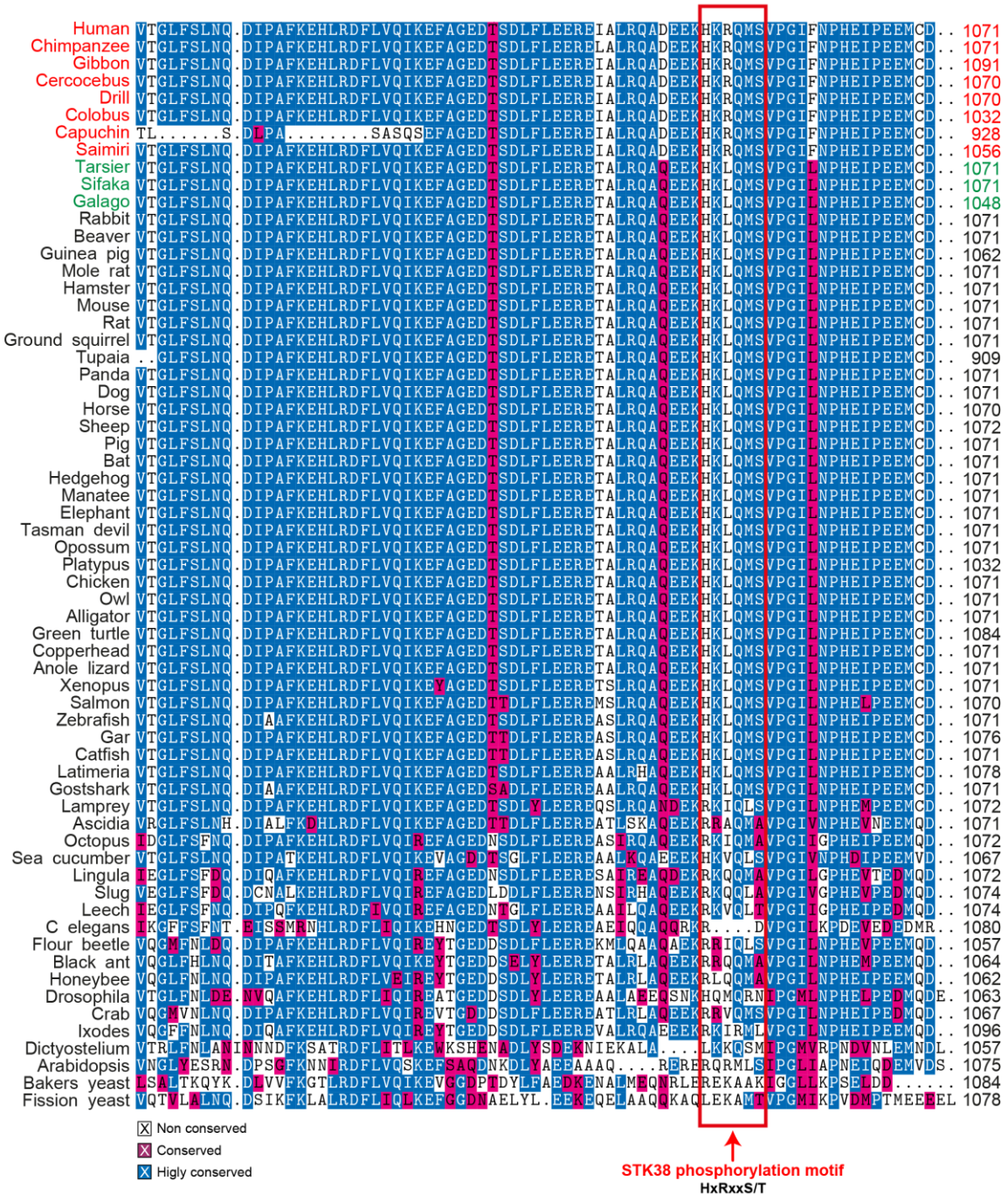

Figure S11. STK38 phosphorylation motif in XPO1 is conserved in simians.
XPO1 protein sequences among different systematic groups were aligned (only the C-terminal domain is shown). Amino acids highly conserved among all species are marked with blue color, less conserved are marked with pink color where non conserved are marked without color. Simians are highlighted in red and non-simian primates are highlighted in green. Red frame denotes location of the STK38 phosphorylation motif HxRxxS/T.

Table S1. STK38 interactors identification.

Mass spectrometry results of the APEX2 labelling experiment coupled to SILAC amino acid replacement according to the experiment represented in Fig. S1. In the table, we report in the columns “1,2 and 3” the isotopic ratio of the heavy (starvation or suspension growth) and the light (complete medium or adherent growth) labelled proteins in three independent biological replicates for the two conditions tested (nutrient starvation-induced autophagy and suspension growth). The “Ratio H/L count” reports the number of redundant peptides used for quantitation. We performed one sample-T test for determining if the mean is significantly different from the fixed value=1 (a ratio of 1 is expected if the interactor is present in the same amounts in the non-treated and in the autophagy induced condition). We report the “T-Test p-value”, and the “T-test difference” between the “mean of the ratios” in columns 1,2,3 and the fixed value=1. We also transformed this difference in fold change. In addition, there is a categorical column added in which it is indicated by a '+' when the row is significant. The scoring takes into account the p-value and the fold change, as described in material and methods. The tab “Starvation significant” and “Suspension significant” contain the interactors of STK38 who are significantly detected in the respective condition. We also report in the “STK38 phosphorylation motif” column the interactors harbouring a STK38 phosphorylation motif (HxRxxS/T).

DISCUSSION

Elucidating the role of the Hippo pathway STK38 kinase in the context Ras-Ral tumorigenesis has been extensively carried out in the team and by collaborators since few years. The first insight from the team came in 2014 when they found that STK38 interacts with MAP4K4 downstream of the RalA-Exocyst signaling axis. Moreover, they found that upon oxidative stress, STK38 is phosphorylated and activated by MAP4K4. The second hint came one year after, when the team identified the autophagic Beclin1 protein as an interactor of STK38, characterizing later STK38 as a pro-autophagic protein. The last evidence came in 2016 when the team found that STK38 is required for cancer cells anchorage-independent growth, downstream of Ras. In this context, our work has helped to better understand the specific contribution of STK38 in these mechanisms that contribute to chemotherapy resistance and cancer cell dissemination.

STK38 interactors

Taking advantage of the proximity biotinylation assay allowed us to dress a map of interaction of STK38 depending on the context. In this regard, we found that STK38 associates with a broad range of proteins: some of them were already known interactors, but the majority has never been qualified as interactor of STK38. Interestingly, a different number of interactors were retrieved in the two cell lines used for our study: 97 in HeLa cells against 221 for HekRasV12. This difference of partners, at basal level, can be either explained by the intrinsic differences between the two cell lines or by a better biotinylation efficiency in the latter one. However, applying a SILAC methodology to our proteomic screen allowed us to encompass this difference of basal interactors depending on the cellular background. Unlike in our research article manuscript where we focused our analysis on the common partners for both studied context (nutrient starvation-induced autophagy and anoïkis resistance), we will here concentrate on these two contexts independently.

Regarding the context of autophagy, we found that STK38 interacts with a total of 97 partners in HeLa cells (figure 31). In addition to the difference of subcellular localization already detailed in the results section of this manuscript, new informations can be extracted regarding the biological processes. At basal level, STK38 interacts with three major sets of partners, where two of them, highly connected, are involved in mRNA splicing, suggesting here a novel function for STK38 as a potential regulator/organizer of RNA processing and/or protein synthesis. The association status of STK38 with these two sets of partners remains globally unchanged upon nutrient starvation, suggesting that the specific role of STK38 for the autophagy process that we were looking for is not here.

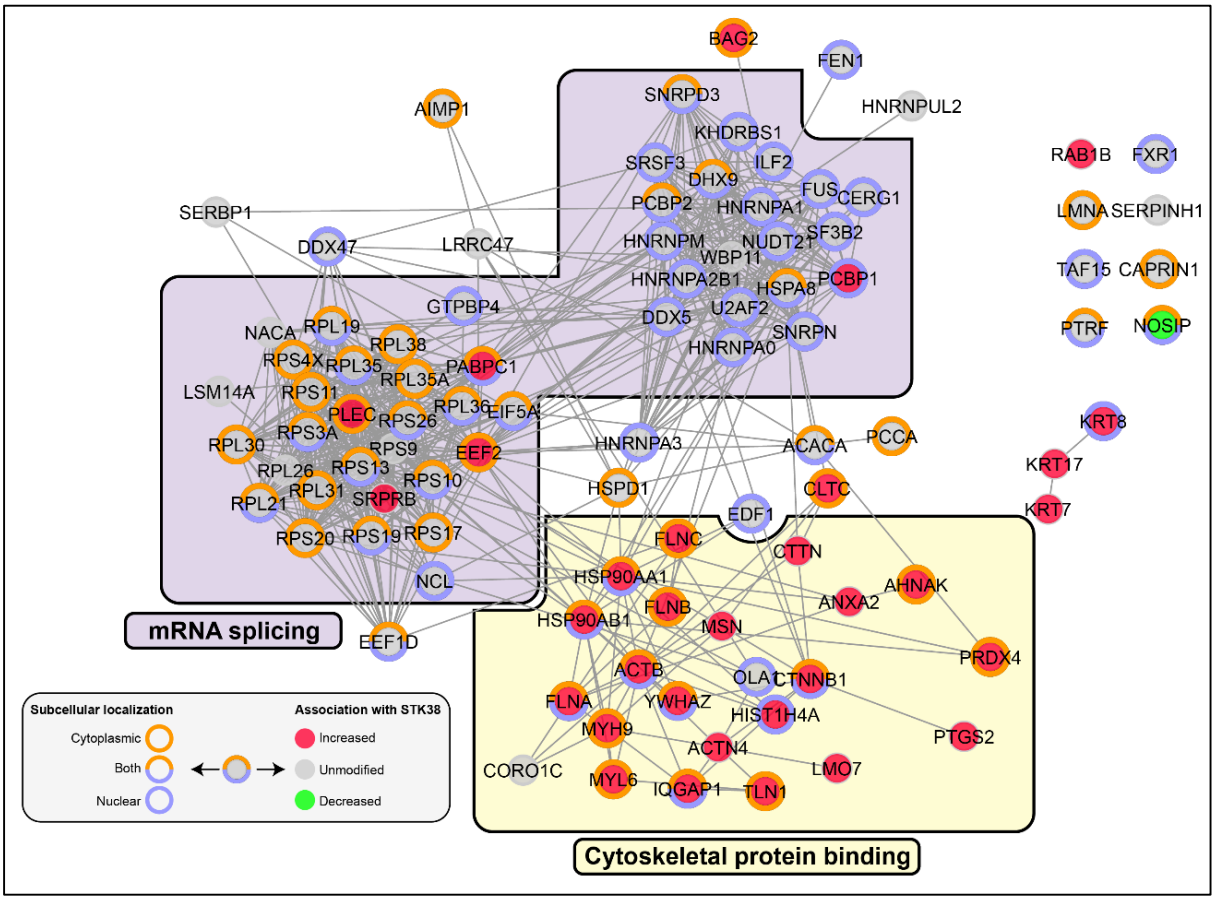

Figure 31 - STK38 interactors for nutrient starvation-induced autophagy.
Network of STK38 interactors identified for the context of autophagy. Network was build using Cytoscape (https://cytoscape.org/) by compiling interrogations to the STRING (protein association network), the GO: cellular component (subcellular localization), and the GO: biological process (relevant biological processes) human databases. Colour code is explained in the encapsulated legend.

On the other hand, STK38 increases its association with partners implicated in cytoskeleton protein binding (the third major set of proteins) when autophagy is going on. The association of STK38 with these cytoplasmic proteins can simply due to the nuclear export of STK38 upon nutrient starvation, cytoplasmic STK38 has more chances to run into cytoplasmic proteins than nuclear ones. One possible other explanation points toward the cytoskeleton-autophagy connection. Evidences indicate that actin cytoskeleton dynamics play an essential role in autophagy (Kast and Dominguez, 2017). During autophagy, STK38 increases its interaction with the cytoskeleton-related proteins Actin (ACTB), Myosin 9 (MYH9), Alpha actinin 4 (ACTN4), Filamin A/B/C (FLNA/FLNB/FLNC), and Moesin (MSN) (figure 31). Both Actin cytoskeleton and Myosins-dependent transport have been reported to be crucial for the autophagy machinery (Kruppa et al., 2016). The importance of the Actin cytoskeleton for autophagy was demonstrated using depolymerizing drugs, inhibiting the autophagosome formation (Aguilera et al., 2012; Aplin et al., 1992). Myosins rely on the actin cytoskeleton in order to transport, sort, and distribute protein complexes, membranes and other specific cargoes to specific

subcellular locations. The transport of crucial components regulating autophagy by this actin-myosin dynamic process seems to occur in all steps of autophagy (Kruppa et al., 2016).

Another interesting point concerns the source of membranes participating in phagophores formation. Many subcellular structures have been shown to be lipid sources for autophagosome formation: endoplasmic reticulum, Golgi, nucleus, mitochondria, and the plasma membrane (Puri et al., 2013). Numerous plasma membrane related proteins see their association with STK38 increased upon autophagy: Clathrin heavy chain 1 (CLTC), Plectin (PLEC), Annexin A2 (ANXA2), and Src substrate cortactin (CTTN) (figure 31). It has been shown that autophagosome biogenesis is partly due to clathrin-dependent endocytosis and membrane-associated ATG16L1 traffic (Pavel and Rubinsztein, 2016). In addition, it has been shown that starvation induced an increase of mobility of vesicles emerging from the plasma membrane (Puri et al., 2013; Vizcaíno et al., 2016). In addition of its nuclear export role, is would be very interesting to study the possible requirement of STK38 for autophagosome formation at plasma membrane as well as for the trafficking of these organelles alongside the actin-myosin cytoskeleton.

Regarding the context of anoïkis resistance, we found a total of 221 binding partners of STK38 in HekRasV12 cells (see figure 32; for the clarity of the figure, only the 126 partners that modify the most their association with STK38 are displayed). Here again, we identified some specific clusters of interactors, found to be implicated in various cellular processes after interrogating Gene Ontology databases. In the context of anoïkis resistance, upon anchorage-independent growth, STK38 increases its association with two set of partners implicated in mRNA splicing and mitochondrial-related metabolic processes, while it decreases its association with cytoplasmic proteins implicated in organelles organization. A distinct comparison can be performed taking into account the results obtained for the autophagy context. The hypothesis would be that, in addition of its nuclear/cytoplasmic shuttling regulatory role largely detailed in the results section of this thesis manuscript, upon autophagy, STK38 would be implicated in cytoplasmic reorganization while, upon anoïkis resistance during anchorage-independent growth, STK38 would be implicated in metabolic activity changes as well as protein synthesis. Interestingly, one recent publication studied the metabolic and proteomic changes in cells after suspension growth. They found that the breast cancer MDA-MB-468 cells endure a complete change of metabolic and transcriptomic profiling. When cultured in suspension, these cells reduce drastically their amount of amino acids, except for glutamic acid and leucine, and increase the expression of genes implicated in metabolic and biosynthetic processes of sterols, steroids, and lipids (Park et al., 2018).

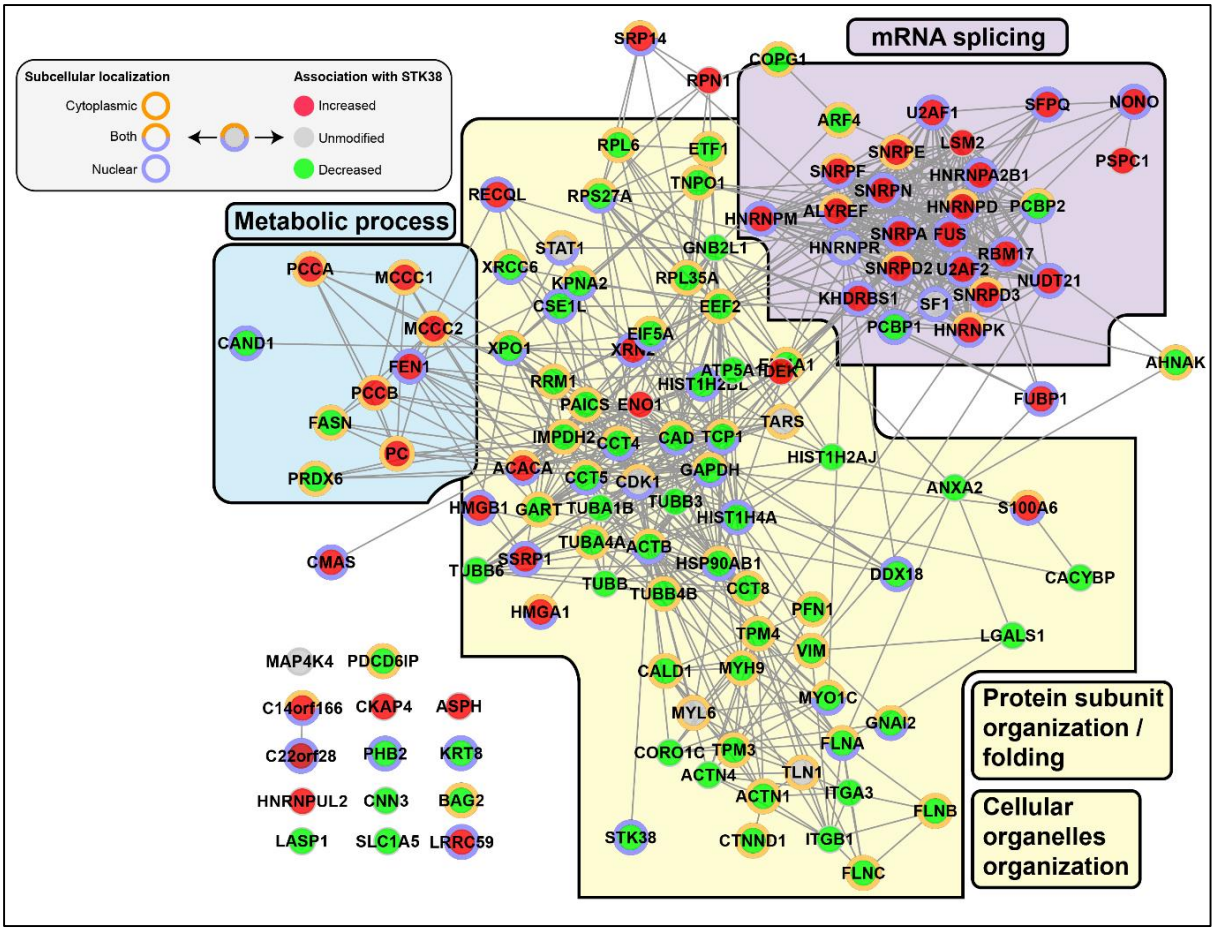

Figure 32 - STK38 interactors for anchorage-independent growth.
Network of STK38 interactors identified for the context of anoïkis resistance. Network was build using Cytoscape (https://cytoscape.org/) by compiling interrogations to the STRING (protein association network), the GO: cellular component (subcellular localization), and the GO: biological process (relevant biological processes) human databases. Colour code is explained in the encapsulated legend. For the clarity of the figure, only the 126 most representative interactors are displayed, based on the modulation of their association status with STK38

Many efforts remain to be undertaken in order to completely understand the relevant functionality of the dynamic of association of STK38 with these specific sets of partners implicated in specific cellular processes. For the autophagy context, the results point toward a cytoskeleton remodelling, a concept showed to have essential role in autophagy for specific mechanisms such as vesicle formation and transport (Zhang et al., 2018). A way to know if the unique contribution of STK38 to autophagy is the subcellular distribution of autophagy regulators through XPO1 activation, is to test the dependency of our XPO1 phosphomimetics HAP1 cells (S1055D & S1055E) regarding STK38. If these cells, harbouring a constitutively activated XPO1, are still able to drive autophagy without STK38 (siRNA technology), that would mean that STK38 implication to autophagy goes through this unique and molecular function: regulating XPO1 activity through phosphorylation. On the other hand, if these cells are not able to triggers autophagy in the absence of STK38, this means that STK38 is required for other specific functions. In this regard, STK38 precise subcellular localization should be evaluated using high

magnification microscope, as well as its localization at specific cellular compartments implicated in autophagy such as plasma membrane, endosomes (early and recycling), autophagosomes and mitochondria. The possible implication of STK38 to autophagosome biogenesis (see above) should also be functionally evaluated.

Concerning the context of anoïkis resistance, two points should be elucidated. The first one concern the increase of STK38 association with partners implicated in protein synthesis. It would be interesting to evaluate the possible changes of protein levels between attached cells and cells going into anoïkis resistance upon suspension growth. This question could be assessed by proteomic analysis using mass spectrometry coupled to a SILAC approach. The second point involves the set of partners related to generic metabolic process. In this regard, evaluating the changes of cell metabolism and their dependency to STK38 could be very interesting by targeting general metabolic activities such as oxygen consumption, glycolysis, fatty acid metabolism as well as mitochondrial functions and oxidative stress.

STK38 nucleo/cytoplasmic shuttling and XPO1 activation

The main outcome resulting from our work is the regulation of proteins nuclear exit by STK38 through XPO1 phosphorylation. By characterizing that STK38 phosphorylates XPO1 on its serine 1055 embedded within its auto-inhibitory domain, we identified STK38 as the first activator of XPO1. Regarding the literature on XPO1 3D structure (Dong et al., 2009) and activation mechanisms (Cautain et al., 2015), we are able to propose a general activation mechanism of XPO1 by STK38.

In its inactivated state, the auto-inhibitory domain of XPO1, including the serine 1055, covers the NES-binding domain of XPO1, avoiding the cargoes to bind to XPO1, even if this latter is loaded with Ran-GTP. The next step starts from a stimulus that phosphorylates STK38 on T444, resulting in its activation, followed by nuclear STK38 phosphorylating inactive XPO1 on serine 1055. This phosphorylation induces a change of conformation of XPO1, where the auto-inhibitory domain does not hide the NES-binding domain of XPO1 anymore. The consequence is very simple; the cargo can bind to XPO1 and be exported into the cytoplasm (figure 33).

This mechanism can be viewed as a system that we generally use everyday: a car. Let us imagine that a person wants to travel from a point A to a point B, or rather to a point N to a point C. This person (let's call him a Cargo) wants to go from N(ucleus) to C(ytoplasm). To do this, this passenger needs a transport method, a car, where the brand new model is called XPO1. We know that in order to work, a car needs two crucial elements: the gas (that can be seen as Ran-GTP) and the key to activate it (STK38 here). To correlates with the biological meaning of this "simplified" view, we know that a car needs both gas and the key to be functional. However, we also know that a car fully loaded with gas

will not move if it's not activated with the key, and reciprocally. We know, from literature, that a balance of RanGTP-RanGDP is maintained across the nuclear membrane, RanGTP being predominant in the nucleus. In details, Ran is efficiently loaded with GTP in the nucleus by its guanidine nucleotide exchange factor RCC1, which is tethered to chromatin through interactions with histones H2A and H2B (Fung and Chook, 2014). In view of the elements given above, it seems that the amount of RanGTP is not the limiting factor for the XPO1-dependent export of distinct cargoes.

These observations bring us back to the car metaphor: who is the driver? Who decides to drive this specific passenger and not another one at this particular time? The two other possible limiting factors concern XPO1 activation by STK38 and the cargo presentation to XPO1. Regarding the first hypothesis and in order to completely understand the molecular machinery implicated in the activation of STK38-dependent nuclear export, it would be very interesting to identify the upstream regulators of STK38 in this context, starting with the "dogmatic" ones. As detailed in the introduction of this thesis manuscript, several activators of STK38 have been already identified, such as the Ste20-like kinases MAST1/2/3 that phosphorylate and activate STK38 (Hergovich, 2013) as well as MAP4K4 (Selimoglu et al., 2014), and also the co-activators MOBs proteins. The contribution of each of the above-mentioned STK38 regulators could be easily tested by silencing them before following the subcellular distribution of distinct XPO1 cargoes such as Beclin1 or YAP1 in the respective contexts triggering their nuclear export. Others screen, relying on proximity labelling assays such as APEX2 can also be used in order to identify the possible activators/interactors of STK38 in this mechanism.

The second hypothesis rely on the cargoes presentation to XPO1. This raises the question of whether a second control mechanism, in addition of the XPO1 activation by STK38, takes place, controlling the ability of cargoes to present themselves to XPO1. As explained in the nuclear export part of the introduction, the XPO1-dependent nuclear export rely on the presentation of a nuclear export signal (NES) sequence of the cargoes to XPO1 (figure 33). It is well known that p53 is exported by XPO1, this is even one of the main reasons of XPO1-dependent nuclear export inhibition in cancer: keeping p53 in the nucleus for its anti-tumorigenic activity. For this example, it has been reported that p53 nuclear export rely on its ubiquitination by MDM2, exposing the NES embedded in its C-terminal region. Other proteins rely on the masking/unmasking of their NES for their proper subcellular localization (Poon and Jans, 2005) such as the INI1/hSNF5 integrase interactor 1 component of the SWI/SNF complex (Craig et al., 2002) and the FOXO1 transcription factor that requires multiple phosphorylation on specific amino acids for the presentation of its NES (Zhao et al., 2004).

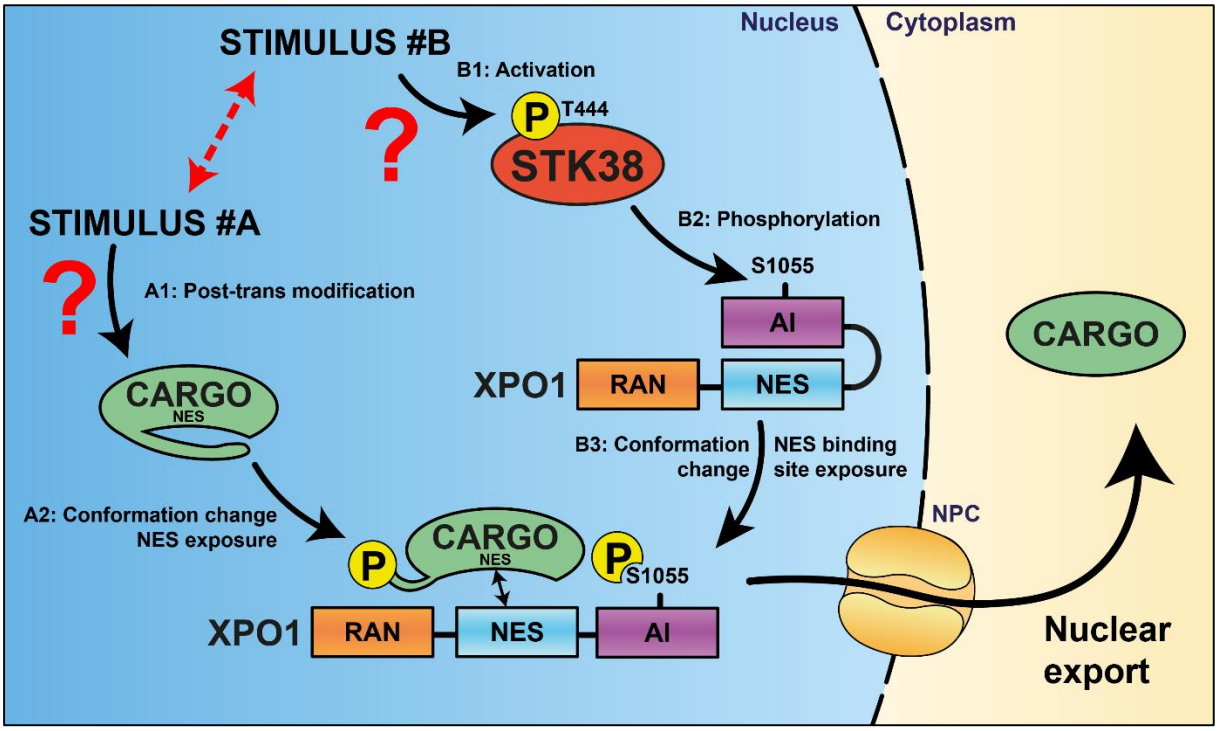

Figure 33 - Control of XPO1-dependent nuclear export by convergent mechanisms.
The XPO1-dependent nuclear export of a cargo is mediated by, at least, two distinct mechanisms. For stimulus #A, the cargo is post-translationally modified by distinct actors, inducing a change of conformation and the exposure of its NES. On the other side (stimulus #B), STK38 is activated, phosphorylates XPO1 on serine 1055, inducing a change of conformation and the exposure of its cargo binding site. The complex is then exported across the nuclear pore complex into the cytoplasm.

A general model of the XPO1-dependent nuclear export of cargoes is presented in the figure 33. However, some elements need to be characterized, such as the activator(s) of STK38 in the context of nuclear export as well as the identification of activators of all XPO1-dependent cargoes, although the final list start to take shape (Poon and Jans, 2005). A final element needs to be also characterized, the possible crosstalk between the activation of the two branches of the activation process (i.e. the cargo conformation change and STK38 activation).

Additionally, one question can be assessed on the nuclear export function of STK38 regarding its effectors. In our work, we demonstrated that STK38 induces the nuclear export of Beclin1 upon nutrient starvation and the nuclear export of YAP1 in confluent cells. The question aims to know if STK38 can bypass the selective activation of some cargoes. In order to answer this question, it would be interesting to analyse the subcellular localization of YAP1 upon nutrient starvation, does it goes out of the nucleus as Beclin1 does? Does Beclin1 goes out of the nucleus in confluent cells as YAP1 does?

STK38: a unique molecular function for multiple biological processes?

Our work brings two main questions regarding the STK38-XPO1 relationship with respect to the literature. The first one tends to know if some of the previous reported biological functions of STK38 (e.g. centrosome duplication, autophagy, cell cycle progression, etc…) are "artefacts" of its nuclear export role. An example comes from one of our previous studies that characterized a direct binding of Beclin1 with STK38 by *in vitro* co-immunoprecipitations (Joffre et al., 2015). However, our work demonstrated that the nuclear exit of Beclin1 is under the dependency of the XPO1-STK38 complex upon nutrient starvation. The STK38-Beclin1 binding previously characterized could simply be the product of Beclin1 nuclear export under the mediation of STK38 and XPO1. Simple tests can be carried out in order to test this hypothesis: assessing the binding capacity of STK38 with interactors in presence of XPO1 inhibitors such as KPT-330. If the previously seen association disappear in the presence of XPO1 inhibitor, that would mean that this interactor is actually a XPO1 cargo under the dependency of STK38.

The second question aims to know if all XPO1 cargoes are under the dependency of STK38 activation of XPO1 for their nuclear export. Is the XPO1 activation by STK38 a general mechanism of protein subcellular localization or is specific to STK38-related biological functions? In order to decipher this important point the subcellular distribution of the proteome could be carried using mass spectrometry. This proteomic experiment, comparing the nuclear vs cytoplasmic fraction of proteins according to XPO1 activity (addition of chemical inhibitors) and STK38 (silencing with siRNA) would clarify this ambiguous point.

STK38 as a potential therapeutic drug target

Inhibiting STK38 could be beneficial for patients in some cancers such as breast, lung, and ovarian cancer where high expression level of STK38 correlates with poor survival outcome (figure 15). Previous work demonstrated that STK38 inhibition abolishes the resistance to anoïkis of Ras-driven cancer cells upon anchorage-independent growth. In addition, STK38-depleted tumors (HekRasV12 cells) display significant decreased growth when injected in mice (Bettoun et al., 2016). Moreover, inhibiting STK38 would also impair autophagy, a process that can contribute to tumor progression by helping cells to survive to poor environmental growth conditions.

Targeting STK38 for cancer treatment will require tight assessment taking into account all the previous reported cellular functions related to STK38. Moreover, loss of STK38 in mice is functionally compensated by an elevation of its isoform, STK38L, protein level where the complete loss of both STK38 and STK38L is lethal (Schmitz-Rohmer et al., 2015). In addition, STK38-deficient mice are more

disposed to the development of T-cell lymphoma and myeloproliferative diseases in old animals (Cornils et al., 2010).

For now, there is no effective drug that target STK38 and inhibits its kinase activity. However, a recent publication shined light on one possible way to target specifically STK38 activity without modifying the genetic background of the cells. Three dimensional structure of the kinase domain of human STK38 protein revealed an atypically long activation segment including the Ser281 and acting as an auto-inhibitory region (figure 34) (Xiong et al., 2018). This serine 281 phosphorylation has been reported to be crucial for STK38 activity (Millward et al., 1999). The hypothesis is that serine 281 phosphorylation could induce a change of conformation of STK38, resulting in its activation. We are actually into the process of targeting this mechanism of activation by a stapled peptide approach. Our next steps will be to appreciate the incorporation of our new potential drug in different cell types and to analyse its capacity to inhibit STK38 supportive role in pro-tumoral processes such as autophagy, anoïkis resistance of Ras-driven cancer cells, and in a broader way, to the nuclear export.

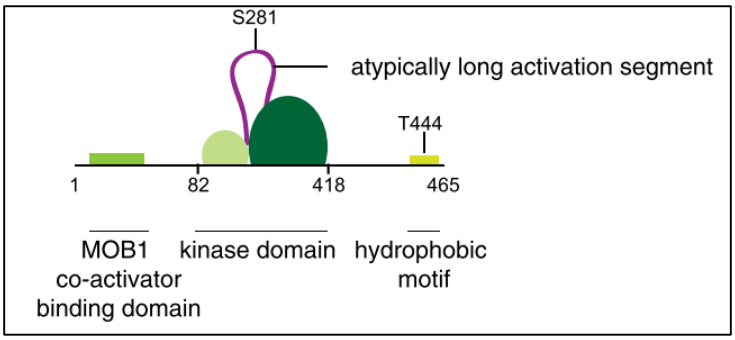

Figure 34 - Domain architecture of STK38.
Domain architecture of STK38 kinase highlighting an atypically long activation segment and two phosphoregulatory sites: S281 and T444. From Xiong et al., 2018.

REFERENCES

Adachi, Y., and Yanagida, M. (1989). Higher order chromosome structure is affected by cold-sensitive mutations in a Schizosaccharomyces pombe gene crm1+ which encodes a 115-kD protein preferentially localized in the nucleus and its periphery. J. Cell Biol. *108*, 1195–1207.

Adhikary, S., and Eilers, M. (2005). Transcriptional regulation and transformation by Myc proteins. Nat. Rev. Mol. Cell Biol. *6*, 635–645.

Aguilera, M.O., Berón, W., and Colombo, M.I. (2012). The actin cytoskeleton participates in the early events of autophagosome formation upon starvation induced autophagy. Autophagy *8*, 1590–1603.

Albright, C.F., Giddings, B.W., Liu, J., Vito, M., and Weinberg, R.A. (1993). Characterization of a guanine nucleotide dissociation stimulator for a ras-related GTPase. EMBO J. *12*, 339–347.

Altomare, D.A., and Testa, J.R. (2005). Perturbations of the AKT signaling pathway in human cancer. Oncogene *24*, 7455–7464.

Andrade, M.A., and Bork, P. (1995). HEAT repeats in the Huntington's disease protein. Nat. Genet. *11*, 115–116.

Aoudjit, F., and Vuori, K. (2001). Matrix attachment regulates Fas-induced apoptosis in endothelial cells: a role for c-flip and implications for anoikis. J. Cell Biol. *152*, 633–643.

Aplin, A., Jasionowski, T., Tuttle, D.L., Lenk, S.E., and Dunn, W.A. (1992). Cytoskeletal elements are required for the formation and maturation of autophagic vacuoles. J. Cell. Physiol. *152*, 458–466.

Atkins, C., Evans, C.W., Nordin, B., Patricelli, M.P., Reynolds, R., Wennerberg, K., and Noah, J.W. (2014). Global Human-Kinase Screening Identifies Therapeutic Host Targets against Influenza. J. Biomol. Screen. *19*, 936–946.

Avivar-Valderas, A., Salas, E., Bobrovnikova-Marjon, E., Diehl, J.A., Nagi, C., Debnath, J., and Aguirre-Ghiso, J.A. (2011). PERK integrates autophagy and oxidative stress responses to promote survival during extracellular matrix detachment. Mol. Cell. Biol. *31*, 3616–3629.

Azad, M.B., Chen, Y., Henson, E.S., Cizeau, J., McMillan-Ward, E., Israels, S.J., and Gibson, S.B. (2008). Hypoxia induces autophagic cell death in apoptosis-competent cells through a mechanism involving BNIP3. Autophagy *4*, 195–204.

Balakireva, M., Rossé, C., Langevin, J., Chien, Y., Gho, M., Gonzy-Treboul, G., Voegeling-Lemaire, S., Aresta, S., Lepesant, J.-A., Bellaiche, Y., et al. (2006). The Ral/exocyst effector complex counters c-Jun N-terminal kinase-dependent apoptosis in Drosophila melanogaster. Mol. Cell. Biol. *26*, 8953–8963.

Barrallo-Gimeno, A., and Nieto, M.A. (2005). The Snail genes as inducers of cell movement and survival: implications in development and cancer. Development *132*, 3151–3161.

Beausoleil, S.A., Jedrychowski, M., Schwartz, D., Elias, J.E., Villen, J., Li, J., Cohn, M.A., Cantley, L.C., and Gygi, S.P. (2004). Large-scale characterization of HeLa cell nuclear phosphoproteins. Proc. Natl. Acad. Sci. *101*, 12130–12135.

Belaiche, Y., Belaiche, Y., Camonis, J., and Balakireva, M. (2014). RalGTPase Controls Cell Polarity Organization during Epithelial Tissue Remodeling. Cell Dev. Biol. *03*, 1–7.

Benzeno, S., Lu, F., Guo, M., Barbash, O., Zhang, F., Herman, J.G., Klein, P.S., Rustgi, A., and Diehl, J.A. (2006). Identification of mutations that disrupt phosphorylation-dependent nuclear export of cyclin D1. Oncogene *25*, 6291–6303.

Bernales, S., McDonald, K.L., and Walter, P. (2006). Autophagy Counterbalances Endoplasmic Reticulum Expansion during the Unfolded Protein Response. PLoS Biol. *4*, e423.

Bettoun, A., Joffre, C., Parrini, M.C., Gundogdu, R., Ahmad, A.D., Gomez, M., Cascone, I., Meunier, B., White, M. a., Codogno, P., et al. (2016). Mitochondrial clearance by the STK38 kinase supports oncogenic Ras-induced cell transformation. Oncotarget *7*, 44142–44160.

Bichsel, S.J., Tamaskovic, R., Stegert, M.R., and Hemmings, B.A. (2004). Mechanism of activation of NDR (nuclear Dbf2-related) protein kinase by the hMOB1 protein. J. Biol. Chem. *279*, 35228–35235.

Biondini, M., Duclos, G., Meyer-Schaller, N., Silberzan, P., Camonis, J., and Carla Parrini, M. (2015). RalB regulates contractility-driven cancer dissemination upon TGFβ stimulation via the RhoGEF GEF-H1. Sci. Rep. *5*, 11759.

Biondini, M., Sadou-Dubourgnoux, A., Paul-Gilloteaux, P., Zago, G., Arslanhan, M.D., Waharte, F., Formstecher, E., Hertzog, M., Yu, J., Guerois, R., et al. (2016). Direct interaction between Exocyst and Wave complexes promotes cell protrusions and motility. J. Cell Sci. 3756–3769.

Bisikirska, B.C., Adam, S.J., Alvarez, M.J., Rajbhandari, P., Cox, R., Lefebvre, C., Wang, K., Rieckhof, G.E., Felsher,

D.W., and Califano, a (2013). STK38 is a critical upstream regulator of MYC's oncogenic activity in human B-cell lymphoma. Oncogene *32*, 5283–5291.

Blanco, M.J., Moreno-Bueno, G., Sarrio, D., Locascio, A., Cano, A., Palacios, J., and Nieto, M.A. (2002). Correlation of Snail expression with histological grade and lymph node status in breast carcinomas. Oncogene *21*, 3241–3246.

Blommaart, E.F., Krause, U., Schellens, J.P., Vreeling-Sindelárová, H., and Meijer, A.J. (1997). The phosphatidylinositol 3-kinase inhibitors wortmannin and LY294002 inhibit autophagy in isolated rat hepatocytes. Eur. J. Biochem. *243*, 240–246.

Bodemann, B.O., Orvedahl, A., Cheng, T., Ram, R.R., Ou, Y.H., Formstecher, E., Maiti, M., Hazelett, C.C., Wauson, E.M., Balakireva, M., et al. (2011). RalB and the exocyst mediate the cellular starvation response by direct activation of autophagosome assembly. Cell *144*, 253–267.

Bon, G., Folgiero, V., Bossi, G., Felicioni, L., Marchetti, A., Sacchi, A., and Falcioni, R. (2006). Loss of beta4 integrin subunit reduces the tumorigenicity of MCF7 mammary cells and causes apoptosis upon hormone deprivation. Clin. Cancer Res. *12*, 3280–3287.

Bonten, E.J., Annunziata, I., and d'Azzo, A. (2014). Lysosomal multienzyme complex: pros and cons of working together. Cell. Mol. Life Sci. *71*, 2017–2032.

Bouchard, V., Demers, M.-J., Thibodeau, S., Laquerre, V., Fujita, N., Tsuruo, T., Beaulieu, J.-F., Gauthier, R., Vézina, A., Villeneuve, L., et al. (2007). Fak/Src signaling in human intestinal epithelial cell survival and anoikis: differentiation state-specific uncoupling with the PI3-K/Akt-1 and MEK/Erk pathways. J. Cell. Physiol. *212*, 717–728.

Boudreau, N.J., and Jones, P.L. (1999). Extracellular matrix and integrin signalling: the shape of things to come. Biochem. J. *339 (Pt 3)*, 481–488.

Budovskaya, Y. V, Stephan, J.S., Reggiori, F., Klionsky, D.J., and Herman, P.K. (2004). The Ras/cAMP-dependent protein kinase signaling pathway regulates an early step of the autophagy process in Saccharomyces cerevisiae. J. Biol. Chem. *279*, 20663–20671.

Cantor, S.B., Urano, T., and Feig, L.A. (1995). Identification and characterization of Ral-binding protein 1, a potential downstream target of Ral GTPases. Mol. Cell. Biol. *15*, 4578–4584.

Cascone, I., Selimoglu, R., Ozdemir, C., Del Nery, E., Yeaman, C., White, M., and Camonis, J. (2008). Distinct roles of RalA and RalB in the progression of cytokinesis are supported by distinct RalGEFs. EMBO J. *27*, 2375–2387.

Cautain, B., Hill, R., De Pedro, N., and Link, W. (2015). Components and regulation of nuclear transport processes. FEBS J. *282*, 445–462.

Chan, E.Y.W., Longatti, A., McKnight, N.C., and Tooze, S.A. (2009). Kinase-inactivated ULK proteins inhibit autophagy via their conserved C-terminal domains using an Atg13-independent mechanism. Mol. Cell. Biol. *29*, 157–171.

Chardin, P., and Tavitian, a (1986). The ral gene: a new ras related gene isolated by the use of a synthetic probe. EMBO J. *5*, 2203–2208.

Chen, J.L., David, J., Cook-spaeth, D., Casey, S., Cohen, D., Selvendiran, K., Bekaii-saab, T., and Hays, J.L. (2017). Autophagy Induction Results in Enhanced Anoikis Resistance in Models of Peritoneal Disease. Mol. Cancer Res. *15*, 26–35.

Chen, N., Eritja, N., Lock, R., and Debnath, J. (2013). Autophagy restricts proliferation driven by oncogenic phosphatidylinositol 3-kinase in three-dimensional culture. Oncogene *32*, 2543–2554.

Chen, Y., McMillan-Ward, E., Kong, J., Israels, S.J., and Gibson, S.B. (2008). Oxidative stress induces autophagic cell death independent of apoptosis in transformed and cancer cells. Cell Death Differ. *15*, 171–182.

Cheng, E.H., Wei, M.C., Weiler, S., Flavell, R.A., Mak, T.W., Lindsten, T., and Korsmeyer, S.J. (2001). BCL-2, BCL-X(L) sequester BH3 domain-only molecules preventing BAX- and BAK-mediated mitochondrial apoptosis. Mol. Cell *8*, 705–711.

Chiba, S., Ikeda, M., Katsunuma, K., Ohashi, K., and Mizuno, K. (2009). MST2- and Furry-mediated activation of NDR1 kinase is critical for precise alignment of mitotic chromosomes. Curr. Biol. *19*, 675–681.

Chien, Y., and White, M. a (2003). RAL GTPases are linchpin modulators of human tumour-cell proliferation and survival. EMBO Rep. *4*, 800–806.

Chien, Y., Kim, S., Bumeister, R., Loo, Y.M., Kwon, S.W., Johnson, C.L., Balakireva, M.G., Romeo, Y., Kopelovich, L., Gale, M., et al. (2006). RalB GTPase-Mediated Activation of the IkB Family Kinase TBK1 Couples Innate Immune Signaling to Tumor Cell Survival. Cell *127*, 157–170.

Conforti, F., Wang, Y., Rodriguez, J.A., Alberobello, A.T., Zhang, Y.W., and Giaccone, G. (2015). Molecular pathways: Anticancer activity by inhibition of nucleocytoplasmic shuttling. Clin. Cancer Res. *21*, 4508–4513.

Cook, D., Hoa, L.Y., Gomez, V., Gomez, M., and Hergovich, A. (2014). Constitutively active NDR1-PIF kinase functions independent of MST1 and hMOB1 signalling. Cell. Signal. *26*, 1657–1667.

Cornils, H., Stegert, M.R., Hergovich, A., Hynx, D., Schmitz, D., Dirnhofer, S., and Hemmings, B.A. (2010). Ablation of the Kinase NDR1 Predisposes Mice to the Development of T Cell Lymphoma. Sci. Signal. *3*, ra47-ra47.

Cornils, H., Kohler, R.S., Hergovich, A., and Hemmings, B. a. (2011a). Downstream of human NDR kinases: Impacting on c-myc and p21 protein stability to control cell cycle progression. Cell Cycle *10*, 1897–1904.

Cornils, H., Kohler, R.S., Hergovich, A., and Hemmings, B. a (2011b). Human NDR kinases control G(1)/S cell cycle transition by directly regulating p21 stability. Mol. Cell. Biol. *31*, 1382–1395.

Cosse, J.-P., Sermeus, A., Vannuvel, K., Ninane, N., Raes, M., and Michiels, C. (2007). Differential effects of hypoxia on etoposide-induced apoptosis according to the cancer cell lines. Mol. Cancer *6*, 61.

Craig, E., Zhang, Z.-K., Davies, K.P., and Kalpana, G. V (2002). A masked NES in INI1/hSNF5 mediates hCRM1-dependent nuclear export: implications for tumorigenesis. EMBO J. *21*, 31–42.

Cuervo, A.M., and Wong, E. (2014). Chaperone-mediated autophagy: Roles in disease and aging. Cell Res. *24*, 92–104.

van Dam, E.M., and Robinson, P.J. (2006). Ral: Mediator of membrane trafficking. Int. J. Biochem. Cell Biol. *38*, 1841–1847.

van Dam, T.J.P., Bos, J., and Snel, B. (2011). Evolution of the Ras-like small GTPases and their regulators. Small GTPases *2*, 4–16.

Dan, I., Watanabe, N.M., and Kusumi, A. (2001). The Ste20 group kinases as regulators of MAP kinase cascades. Trends Cell Biol. *11*, 220–230.

Davies, M.A., Koul, D., Dhesi, H., Berman, R., McDonnell, T.J., McConkey, D., Yung, W.K., and Steck, P.A. (1999). Regulation of Akt/PKB activity, cellular growth, and apoptosis in prostate carcinoma cells by MMAC/PTEN. Cancer Res. *59*, 2551–2556.

Debnath, J., Muthuswamy, S.K., and Brugge, J.S. (2003). Morphogenesis and oncogenesis of MCF-10A mammary epithelial acini grown in three-dimensional basement membrane cultures. Methods *30*, 256–268.

Degenhardt, K., Mathew, R., Beaudoin, B., Bray, K., Anderson, D., Chen, G., Mukherjee, C., Shi, Y., Gélinas, C., Fan, Y., et al. (2006). Autophagy promotes tumor cell survival and restricts necrosis, inflammation, and tumorigenesis. Cancer Cell *10*, 51–64.

Devroe, E., Silver, P.A., and Engelman, A. (2005). HIV-1 incorporates and proteolytically processes human NDR1 and NDR2 serine-threonine kinases. Virology *331*, 181–189.

Dian, C., Bernaudat, F., Langer, K., Oliva, M.F., Fornerod, M., Schoehn, G., Müller, C.W., and Petosa, C. (2013). Structure of a truncation mutant of the nuclear export factor CRM1 provides insights into the auto-inhibitory role of its C-terminal helix. Structure *21*, 1338–1349.

Diao, J., Liu, R., Rong, Y., Zhao, M., Zhang, J., Lai, Y., Zhou, Q., Wilz, L.M., Li, J., Vivona, S., et al. (2015). ATG14 promotes membrane tethering and fusion of autophagosomes to endolysosomes. Nature *520*, 563–566.

Ding, Z.-B., Shi, Y.-H., Zhou, J., Qiu, S.-J., Xu, Y., Dai, Z., Shi, G.-M., Wang, X.-Y., Ke, A.-W., Wu, B., et al. (2008). Association of autophagy defect with a malignant phenotype and poor prognosis of hepatocellular carcinoma. Cancer Res. *68*, 9167–9175.

Dong, X., Biswas, A., Süel, K.E., Jackson, L.K., Martinez, R., Gu, H., and Chook, Y.M. (2009). Structural basis for leucine-rich nuclear export signal recognition by CRM1. Nature *458*, 1136–1141.

Du, Z., Tong, X., and Ye, X. (2013). Cyclin D1 promotes cell cycle progression through enhancing NDR1/2 kinase activity independent of cyclin-dependent kinase. J. Biol. Chem. *288*, 26678–26687.

Dubois, F., Keller, M., Calvayrac, O., Soncin, F., Hoa, L., Hergovich, A., Parrini, M.-C., Mazières, J., Vaisse-Lesteven, M., Camonis, J., et al. (2016). RASSF1A Suppresses the Invasion and Metastatic Potential of Human Non–Small Cell Lung Cancer Cells by Inhibiting YAP Activation through the GEF-H1/RhoB Pathway. Cancer Res. *76*, 1627–

1640.

EauClaire, S., and Guo, W. (2003). Conservation and specialization. The role of the exocyst in neuronal exocytosis. Neuron *37*, 369–370.

Emkey, R., Freedman, S., and Feig, L.A. (1991). Characterization of a GTPase-activating protein for the Ras-related Ral protein. J. Biol. Chem. *266*, 9703–9706.

Englmeier, L., Fornerod, M., Bischoff, F.R., Petosa, C., Mattaj, I.W., and Kutay, U. (2001). RanBP3 influences interactions between CRM1 and its nuclear protein export substrates. EMBO Rep. *2*, 926–932.

Falsetti, S.C., Wang, D., Peng, H., Carrico, D., Cox, A.D., Der, C.J., Hamilton, A.D., and Sebti, S.M. (2007). Geranylgeranyltransferase I inhibitors target RalB to inhibit anchorage-dependent growth and induce apoptosis and RalA to inhibit anchorage-independent growth. Mol. Cell. Biol. *27*, 8003–8014.

Fenwick, R.B., Prasannan, S., Campbell, L.J., Nietlispach, D., Evetts, K.A., Camonis, J., Mott, H.R., and Owen, D. (2009). Solution structure and dynamics of the small GTPase RalB in its active conformation: significance for effector protein binding. Biochemistry *48*, 2192–2206.

Frankel, P., Aronheim, A., Kavanagh, E., Balda, M.S., Matter, K., Bunney, T.D., and Marshall, C.J. (2005). RalA interacts with ZONAB in a cell density-dependent manner and regulates its transcriptional activity. EMBO J. *24*, 54–62.

Fried, H., and Kutay, U. (2003). Nucleocytoplasmic transport: taking an inventory. Cell. Mol. Life Sci. *60*, 1659–1688.

Frisch, S.M., and Francis, H. (1994). Disruption of epithelial cell-matrix interactions induces apoptosis. J. Cell Biol. *124*, 619–626.

Frisch, S.M., and Screaton, R.A. (2001). Anoikis mechanisms. Curr. Opin. Cell Biol. *13*, 555–562.

Fukai, S., Matern, H.T., Jagath, J.R., Scheller, R.H., and Brunger, A.T. (2003). Structural basis of the interaction between RalA and Sec5, a subunit of the sec6/8 complex. EMBO J. *22*, 3267–3278.

Fukasawa, T., Enomoto, A., and Miyagawa, K. (2015). Serine-Threonine Kinase 38 regulates CDC25A stability and the DNA damage-induced G2/M checkpoint. Cell. Signal. *27*, 1569–1575.

Fung, H.Y.J., and Chook, Y.M. (2014). Atomic basis of CRM1-cargo recognition, release and inhibition. Semin. Cancer Biol. *27*, 52–61.

Fung, C., Lock, R., Gao, S., Salas, E., and Debnath, J. (2008). Induction of autophagy during extracellular matrix detachment promotes cell survival. Mol. Biol. Cell *19*, 797–806.

Gallegos, M.E., and Bargmann, C.I. (2004). Mechanosensory neurite termination and tiling depend on SAX-2 and the SAX-1 kinase. Neuron *44*, 239–249.

Gazaryan, I.G., and Brown, A.M. (2007). Intersection between mitochondrial permeability pores and mitochondrial fusion/fission. Neurochem. Res. *32*, 917–929.

Gehlsen, K.R., Davis, G.E., and Sriramarao, P. (1992). Integrin expression in human melanoma cells with differing invasive and metastatic properties. Clin. Exp. Metastasis *10*, 111–120.

Geiger, T.R., and Peeper, D.S. (2007). Critical role for TrkB kinase function in anoikis suppression, tumorigenesis, and metastasis. Cancer Res. *67*, 6221–6229.

Gentry, L.R., Martin, T.D., Reiner, D.J., and Der, C.J. (2014). Ral small GTPase signaling and oncogenesis: More than just 15minutes of fame. Biochim. Biophys. Acta - Mol. Cell Res. *1843*, 2976–2988.

Gewirtz, D.A. (2009). Autophagy, senescence and tumor dormancy in cancer therapy. Autophagy *5*, 1232–1234.

Gheldof, A., and Berx, G. (2013). Cadherins and Epithelial-to-Mesenchymal Transition. Prog. Mol. Biol. Transl. Sci. *116*, 317–336.

Giannoni, E., Parri, M., and Chiarugi, P. (2012). EMT and oxidative stress: a bidirectional interplay affecting tumor malignancy. Antioxid. Redox Signal. *16*, 1248–1263.

Gilmore, A.P. (2005). Anoikis. Cell Death Differ. *12*, 1473–1477.

Gomez, V., Gundogdu, R., Gomez, M., Hoa, L., Panchal, N., O'Driscoll, M., and Hergovich, A. (2015). Regulation of DNA damage responses and cell cycle progression by hMOB2. Cell. Signal. *27*, 326–339.

Görlich, D., and Kutay, U. (1999). Transport Between the Cell Nucleus and the Cytoplasm. Annu. Rev. Cell Dev. Biol. *15*, 607–660.

Gravina, G.L., Senapedis, W., McCauley, D., Baloglu, E., Shacham, S., and Festuccia, C. (2014). Nucleo-cytoplasmic transport as a therapeutic target of cancer. J. Hematol. Oncol. *7*, 85.

Grindstaff, K.K., Yeaman, C., Anandasabapathy, N., Hsu, S.C., Rodriguez-Boulan, E., Scheller, R.H., and Nelson, W.J. (1998). Sec6/8 complex is recruited to cell-cell contacts and specifies transport vesicle delivery to the basal-lateral membrane in epithelial cells. Cell *93*, 731–740.

Grossmann, J. (2002). Molecular mechanisms of "detachment-induced apoptosis—Anoikis." APOPTOSIS *7*, 247–260.

Guadamillas, M.C., Cerezo, a., and del Pozo, M. a. (2011). Overcoming anoikis - pathways to anchorage-independent growth in cancer. J. Cell Sci. *124*, 3189–3197.

Güttler, T., Madl, T., Neumann, P., Deichsel, D., Corsini, L., Monecke, T., Ficner, R., Sattler, M., and Görlich, D. (2010). NES consensus redefined by structures of PKI-type and Rev-type nuclear export signals bound to CRM1. Nat. Struct. Mol. Biol. *17*, 1367–1376.

Gysin, S., Salt, M., Young, A., and McCormick, F. (2011). Therapeutic Strategies for Targeting Ras Proteins. Genes Cancer *2*, 359–372.

Hanahan, D., and Weinberg, R. a (2000). The Hallmarks of Cancer. Cell *100*, 57–70.

Hanahan, D., and Weinberg, R. a (2011). Hallmarks of cancer: the next generation. Cell *144*, 646–674.

Hannigan, G., Troussard, A.A., and Dedhar, S. (2005). Integrin-linked kinase: a cancer therapeutic target unique among its ILK. Nat. Rev. Cancer *5*, 51–63.

Harris, A.L. (2002). Hypoxia — a key regulatory factor in tumour growth. Nat. Rev. Cancer *2*, 38–47.

Hazelett, C.C., Sheff, D., and Yeaman, C. (2011). RalA and RalB differentially regulate development of epithelial tight junctions. Mol. Biol. Cell *22*, 4787–4800.

He, C., and Levine, B. (2010). The Beclin 1 interactome. Curr. Opin. Cell Biol. *22*, 140–149.

Vander Heiden, M.G., Chandel, N.S., Williamson, E.K., Schumacker, P.T., and Thompson, C.B. (1997). Bcl-xL regulates the membrane potential and volume homeostasis of mitochondria. Cell *91*, 627–637.

Hergovich, A. (2011). MOB control: Reviewing a conserved family of kinase regulators. Cell. Signal. *23*, 1433–1440.

Hergovich, A. (2013). Regulation and functions of mammalian LATS/NDR kinases: looking beyond canonical Hippo signalling. Cell Biosci. *3*, 32.

Hergovich, A., Bichsel, S.J., and Hemmings, B. a (2005). Human NDR kinases are rapidly activated by MOB proteins through recruitment to the plasma membrane and phosphorylation. Mol. Cell. Biol. *25*, 8259–8272.

Hergovich, A., Stegert, M.R., Schmitz, D., and Hemmings, B. a (2006). NDR kinases regulate essential cell processes from yeast to humans. Nat. Rev. Mol. Cell Biol. *7*, 253–264.

Hergovich, A., Lamla, S., Nigg, E.A., and Hemmings, B.A. (2007). Centrosome-Associated NDR Kinase Regulates Centrosome Duplication. Mol. Cell *25*, 625–634.

Hergovich, A., Cornils, H., and Hemmings, B. a. (2008). Mammalian NDR protein kinases: From regulation to a role in centrosome duplication. Biochim. Biophys. Acta - Proteins Proteomics *1784*, 3–15.

Hergovich, A., Kohler, R.S., Schmitz, D., Vichalkovski, A., Cornils, H., and Hemmings, B. a. (2009). The MST1 and hMOB1 Tumor Suppressors Control Human Centrosome Duplication by Regulating NDR Kinase Phosphorylation. Curr. Biol. *19*, 1692–1702.

Hoa, L., Kulaberoglu, Y., Gundogdu, R., Cook, D., Mavis, M., Gomez, M., Gomez, V., and Hergovich, A. (2016). The characterisation of LATS2 kinase regulation in Hippo-YAP signalling. Cell. Signal. *28*, 488–497.

Hong, W., and Guan, K.-L. (2012). The YAP and TAZ transcription co-activators: Key downstream effectors of the mammalian Hippo pathway. Semin. Cell Dev. Biol. *23*, 785–793.

Hung, M.-C., and Link, W. (2011). Protein localization in disease and therapy. J. Cell Sci. *124*, 3381–3392.

Hutten, S., and Kehlenbach, R.H. (2006). Nup214 Is Required for CRM1-Dependent Nuclear Protein Export In Vivo. Mol. Cell. Biol. *26*, 6772–6785.

Hutten, S., and Kehlenbach, R.H. (2007). CRM1-mediated nuclear export: to the pore and beyond. Trends Cell Biol. *17*, 193–201.

Inami, Y., Waguri, S., Sakamoto, A., Kouno, T., Nakada, K., Hino, O., Watanabe, S., Ando, J., Iwadate, M.,

Yamamoto, M., et al. (2011). Persistent activation of Nrf2 through p62 in hepatocellular carcinoma cells. J. Cell Biol. *193*, 275–284.

Inoki, K., Zhu, T., and Guan, K.-L. (2003). TSC2 mediates cellular energy response to control cell growth and survival. Cell *115*, 577–590.

Itakura, E., Kishi-Itakura, C., and Mizushima, N. (2012). The hairpin-type tail-anchored SNARE syntaxin 17 targets to autophagosomes for fusion with endosomes/lysosomes. Cell *151*, 1256–1269.

Izuishi, K., Kato, K., Ogura, T., Kinoshita, T., and Esumi, H. (2000). Remarkable tolerance of tumor cells to nutrient deprivation: possible new biochemical target for cancer therapy. Cancer Res. *60*, 6201–6207.

Janes, S.M., and Watt, F.M. (2004). Switch from alphavbeta5 to alphavbeta6 integrin expression protects squamous cell carcinomas from anoikis. J. Cell Biol. *166*, 419–431.

Jin, S., DiPaola, R.S., Mathew, R., and White, E. (2007). Metabolic catastrophe as a means to cancer cell death. J. Cell Sci. *120*, 379–383.

Joffre, C., Dupont, N., Hoa, L., Gomez, V., Pardo, R., Gonçalves-Pimentel, C., Achard, P., Bettoun, A., Meunier, B., Bauvy, C., et al. (2015). The Pro-apoptotic STK38 Kinase Is a New Beclin1 Partner Positively Regulating Autophagy. Curr. Biol. 1–14.

Joffre, C., Codogno, P., Fanto, M., Hergovich, A., and Camonis, J. (2016). STK38 at the crossroad between autophagy and apoptosis. Autophagy *8627*, 1–2.

Johnson, L.N., Noble, M.E., and Owen, D.J. (1996). Active and inactive protein kinases: structural basis for regulation. Cell *85*, 149–158.

Juhász, G., Hill, J.H., Yan, Y., Sass, M., Baehrecke, E.H., Backer, J.M., and Neufeld, T.P. (2008). The class III PI(3)K Vps34 promotes autophagy and endocytosis but not TOR signaling in Drosophila. J. Cell Biol. *181*, 655–666.

Jullien-Flores, V., Dorseuil, O., Romero, F., Letourneur, F., Saragosti, S., Berger, R., Tavitian, A., Gacon, G., and Camonis, J.H. (1995). Bridging Ral GTPase to Rho pathways. RLIP76, a Ral effector with CDC42/Rac GTPase-activating protein activity. J. Biol. Chem. *270*, 22473–22477.

Kamada, Y., Yoshino, K., Kondo, C., Kawamata, T., Oshiro, N., Yonezawa, K., and Ohsumi, Y. (2010). Tor directly controls the Atg1 kinase complex to regulate autophagy. Mol. Cell. Biol. *30*, 1049–1058.

Kang, M.R., Kim, M.S., Oh, J.E., Kim, Y.R., Song, S.Y., Kim, S.S., Ahn, C.H., Yoo, N.J., and Lee, S.H. (2009). Frameshift mutations of autophagy-related genes *ATG2B, ATG5, ATG9B* and *ATG12* in gastric and colorectal cancers with microsatellite instability. J. Pathol. *217*, 702–706.

Kast, D.J., and Dominguez, R. (2017). The Cytoskeleton–Autophagy Connection. Curr. Biol. *27*, R318–R326.

Ke, B., Tian, M., Li, J., Liu, B., and He, G. (2016). Targeting Programmed Cell Death Using Small-Molecule Compounds to Improve Potential Cancer Therapy. Med. Res. Rev. *36*, 983–1035.

Kehlenbach, R.H., Dickmanns, A., Kehlenbach, A., Guan, T., and Gerace, L. (1999). A role for RanBP1 in the release of CRM1 from the nuclear pore complex in a terminal step of nuclear export. J. Cell Biol. *145*, 645–657.

Khan, A.Q., Kuttikrishnan, S., Siveen, K.S., Prabhu, K.S., Shanmugakonar, M., Al Naemi, H., Haris, M., Dermime, S., and Uddin, S. (2018). RAS-mediated oncogenic signaling pathways in human malignancies. Semin. Cancer Biol. 0–1.

Kim, M.H., and Kim, J. (2017). Role of YAP/TAZ transcriptional regulators in resistance to anti-cancer therapies. Cell. Mol. Life Sci. *74*, 1457–1474.

Kim, J.-H., Kim, H.Y., Lee, Y.-K., Yoon, Y.-S., Xu, W.G., Yoon, J.-K., Choi, S.-E., Ko, Y.-G., Kim, M.-J., Lee, S.-J., et al. (2011a). Involvement of mitophagy in oncogenic K-Ras-induced transformation: overcoming a cellular energy deficit from glucose deficiency. Autophagy *7*, 1187–1198.

Kim, J.H., Lee, S. Do, Han, J.M., Lee, T.G., Kim, Y., Park, J.B., Lambeth, J.D., Suh, P.-G., and Ryu, S.H. (1998). Activation of phospholipase D1 by direct interaction with ADP-ribosylation factor 1 and RalA. FEBS Lett. *430*, 231–235.

Kim, M.J., Woo, S.J., Yoon, C.H., Lee, J.S., An, S., Choi, Y.H., Hwang, S.G., Yoon, G., and Lee, S.J. (2011b). Involvement of autophagy in oncogenic K-Ras-induced malignant cell transformation. J. Biol. Chem. *286*, 12924–12932.

Kirli, K., Karaca, S., Dehne, H.J., Samwer, M., Pan, K.T., Lenz, C., Urlaub, H., and Gorlich, D. (2015). A deep proteomics perspective on CRM1-mediated nuclear export and nucleocytoplasmic partitioning. Elife *4*, 1–28.

Klionsky, D.J. (2008). Autophagy revisited: a conversation with Christian de Duve. Autophagy *4*, 740–743.

Klionsky, D.J., Abdelmohsen, K., Abe, A., Abedin, M.J., Abeliovich, H., Acevedo Arozena, A., Adachi, H., Adams, C.M., Adams, P.D., Adeli, K., et al. (2016). Guidelines for the use and interpretation of assays for monitoring autophagy (3rd edition). Autophagy *12*, 1–222.

Komarnitsky, S.I., Chiang, Y.C., Luca, F.C., Chen, J., Toyn, J.H., Winey, M., Johnston, L.H., and Denis, C.L. (1998). DBF2 protein kinase binds to and acts through the cell cycle-regulated MOB1 protein. Mol. Cell. Biol. *18*, 2100–2107.

Kroemer, G., Galluzzi, L., and Brenner, C. (2007). Mitochondrial Membrane Permeabilization in Cell Death. Physiol. Rev. *87*, 99–163.

Kruppa, A.J., Kendrick-Jones, J., and Buss, F. (2016). Myosins, Actin and Autophagy. Traffic *17*, 878–890.

Ktistakis, N.T. (2017). In praise of M. Anselmier who first used the term "autophagie" in 1859. Autophagy *13*, 2015–2017.

Kudo, N., Matsumori, N., Taoka, H., Fujiwara, D., Schreiner, E.P., Wolff, B., Yoshida, M., and Horinouchi, S. (1999). Leptomycin B inactivates CRM1/exportin 1 by covalent modification at a cysteine residue in the central conserved region. Proc. Natl. Acad. Sci. U. S. A. *96*, 9112–9117.

Kutay, U., and Güttinger, S. (2005). Leucine-rich nuclear-export signals: born to be weak. Trends Cell Biol. *15*, 121–124.

Kuwana, T., Bouchier-Hayes, L., Chipuk, J.E., Bonzon, C., Sullivan, B.A., Green, D.R., and Newmeyer, D.D. (2005). BH3 domains of BH3-only proteins differentially regulate Bax-mediated mitochondrial membrane permeabilization both directly and indirectly. Mol. Cell *17*, 525–535.

Lange, A., Mills, R.E., Lange, C.J., Stewart, M., Devine, S.E., and Corbett, A.H. (2007). Classical nuclear localization signals: definition, function, and interaction with importin alpha. J. Biol. Chem. *282*, 5101–5105.

Lapalombella, R., Sun, Q., Williams, K., Tangeman, L., Jha, S., Zhong, Y., Goettl, V., Mahoney, E., Berglund, C., Gupta, S., et al. (2012). Selective inhibitors of nuclear export show that CRM1/XPO1 is a target in chronic lymphocytic leukemia. Blood *120*, 4621–4634.

Lebleu, V.S., Taduri, G., Connell, J.O., Teng, Y., Cooke, V.G., Woda, C., Sugimoto, H., and Kalluri, R. (2013). Origin and function of myofibroblasts in kidney fibrosis. Nat. Med. *19*.

Lee, H.-Y., You, H.-J., Won, J.-Y., Youn, S.-W., Cho, H.-J., Park, K.-W., Park, W.-Y., Seo, J.-S., Park, Y.-B., Walsh, K., et al. (2008). Forkhead factor, FOXO3a, induces apoptosis of endothelial cells through activation of matrix metalloproteinases. Arterioscler. Thromb. Vasc. Biol. *28*, 302–308.

Leevers, S.J., Paterson, H.F., and Marshall, C.J. (1994). Requirement for Ras in Raf activation is overcome by targeting Raf to the plasma membrane. Nature *369*, 411–414.

Lester, R.D., Jo, M., Montel, V., Takimoto, S., and Gonias, S.L. (2007). uPAR induces epithelial–mesenchymal transition in hypoxic breast cancer cells. J. Cell Biol. *178*, 425–436.

Li, W.W., Li, J., and Bao, J.K. (2012a). Microautophagy: Lesser-known self-eating. Cell. Mol. Life Sci. *69*, 1125–1136.

Li, Y., Paonessa, J.D., and Zhang, Y. (2012b). Mechanism of Chemical Activation of Nrf2. PLoS One *7*, e35122.

Liang, J., Shao, S.H., Xu, Z.-X., Hennessy, B., Ding, Z., Larrea, M., Kondo, S., Dumont, D.J., Gutterman, J.U., Walker, C.L., et al. (2007). The energy sensing LKB1–AMPK pathway regulates p27kip1 phosphorylation mediating the decision to enter autophagy or apoptosis. Nat. Cell Biol. *9*, 218–224.

Liang, X.H., Jackson, S., Seaman, M., Brown, K., Kempkes, B., Hibshoosh, H., and Levine, B. (1999). Induction of autophagy and inhibition of tumorigenesis by beclin 1. Nature *402*, 672–676.

Liu, B., Zheng, Y., Yin, F., Yu, J., Silverman, N., and Pan, D. (2016). Toll Receptor-Mediated Hippo Signaling Controls Innate Immunity in Drosophila. Cell *164*, 406–419.

Liu, X., Wang, X., Zhang, J., Lam, E.K.Y., Shin, V.Y., Cheng, A.S.L., Yu, J., Chan, F.K.L., Sung, J.J.Y., and Jin, H.C. (2010). Warburg effect revisited: an epigenetic link between glycolysis and gastric carcinogenesis. Oncogene *29*, 442–450.

Lock, R., Roy, S., Kenific, C.M., Su, J.S., Salas, E., Ronen, S.M., and Debnath, J. (2011). Autophagy facilitates glycolysis during Ras-mediated oncogenic transformation. Mol. Biol. Cell *22*, 165–178.

Long, X., Ortiz-Vega, S., Lin, Y., and Avruch, J. (2005a). Rheb Binding to Mammalian Target of Rapamycin (mTOR)

Is Regulated by Amino Acid Sufficiency. J. Biol. Chem. *280*, 23433–23436.

Long, X., Lin, Y., Ortiz-Vega, S., Yonezawa, K., and Avruch, J. (2005b). Rheb Binds and Regulates the mTOR Kinase. Curr. Biol. *15*, 702–713.

Lu, Z., Luo, R.Z., Lu, Y., Zhang, X., Yu, Q., Khare, S., Kondo, S., Kondo, Y., Yu, Y., Mills, G.B., et al. (2008). The tumor suppressor gene ARHI regulates autophagy and tumor dormancy in human ovarian cancer cells. J. Clin. Invest. *118*, 3917–3929.

Lum, J.J., Bauer, D.E., Kong, M., Harris, M.H., Li, C., Lindsten, T., and Thompson, C.B. (2005). Growth Factor Regulation of Autophagy and Cell Survival in the Absence of Apoptosis. Cell *120*, 237–248.

Mah, A.S., Jang, J., and Deshaies, R.J. (2001). Protein kinase Cdc15 activates the Dbf2-Mob1 kinase complex. Proc. Natl. Acad. Sci. U. S. A. *98*, 7325–7330.

Manning, G., Whyte, D.B., Martinez, R., Hunter, T., and Sudarsanam, S. (2002). The Protein Kinase Complement of the Human Genome. Science (80-.). *298*, 1912–1934.

Marinkovi, M., Matilda, Š., Buljuba, M., and Novak, I. (2018). Autophagy Modulation in Cancer : Current Knowledge on Action and Therapy. Oxid. Med. Cell. Longev. *2018*.

Martin, T.D., Mitin, N., Cox, A.D., Yeh, J.J., and Der, C.J. (2012). Phosphorylation by protein kinase Cα regulates RalB small GTPase protein activation, subcellular localization, and effector utilization. J. Biol. Chem. *287*, 14827–14836.

Martin, T.D., Chen, X.-W., Kaplan, R.E.W., Saltiel, A.R., Walker, C.L., Reiner, D.J., and Der, C.J. (2014). Ral and Rheb GTPase Activating Proteins Integrate mTOR and GTPase Signaling in Aging, Autophagy, and Tumor Cell Invasion. Mol. Cell *53*, 209–220.

Mathew, R., Kongara, S., Beaudoin, B., Karp, C.M., Bray, K., Degenhardt, K., Chen, G., Jin, S., and White, E. (2007a). Autophagy suppresses tumor progression by limiting chromosomal instability. Genes Dev. *21*, 1367–1381.

Mathew, R., Karantza-Wadsworth, V., and White, E. (2007b). Role of autophagy in cancer. Nat. Rev. Cancer *7*, 961–967.

McFall, A., Ulkü, A., Lambert, Q.T., Kusa, A., Rogers-Graham, K., and Der, C.J. (2001). Oncogenic Ras blocks anoikis by activation of a novel effector pathway independent of phosphatidylinositol 3-kinase. Mol. Cell. Biol. *21*, 5488–5499.

McKnight, N.C., and Zhenyu, Y. (2013). Beclin 1, an Essential Component and Master Regulator of PI3K-III in Health and Disease. Curr. Pathobiol. Rep. *1*, 231–238.

Meng, Z., Moroishi, T., Mottier-Pavie, V., Plouffe, S.W., Hansen, C.G., Hong, A.W., Park, H.W., Mo, J.-S., Lu, W., Lu, S., et al. (2015a). MAP4K family kinases act in parallel to MST1/2 to activate LATS1/2 in the Hippo pathway. Nat. Commun. *6*, 8357.

Meng, Z., Moroishi, T., Mottier-Pavie, V., Plouffe, S.W., Hansen, C.G., Hong, A.W., Park, H.W., Mo, J.-S., Lu, W., Lu, S., et al. (2015b). MAP4K family kinases act in parallel to MST1/2 to activate LATS1/2 in the Hippo pathway. Nat. Commun. *6*, 8357.

Meng, Z., Moroishi, T., and Guan, K.-L. (2016). Mechanisms of Hippo pathway regulation. Genes Dev. *30*, 1–17.

Michel, J.-B. (2003). Anoikis in the cardiovascular system: known and unknown extracellular mediators. Arterioscler. Thromb. Vasc. Biol. *23*, 2146–2154.

Milburn, M. V, Tong, L., deVos, A.M., Brünger, A., Yamaizumi, Z., Nishimura, S., and Kim, S.H. (1990). Molecular switch for signal transduction: structural differences between active and inactive forms of protooncogenic ras proteins. Science *247*, 939–945.

Millward, T.A., Heizmann, C.W., Schäfer, B.W., and Hemmings, B.A. (1998). Calcium regulation of Ndr protein kinase mediated by S100 calcium-binding proteins. EMBO J. *17*, 5913–5922.

Millward, T.A., Hess, D., and Hemmings, B.A. (1999). Ndr protein kinase is regulated by phosphorylation on two conserved sequence motifs. J. Biol. Chem. *274*, 33847–33850.

Mizushima, N., and Klionsky, D.J. (2007). Protein Turnover Via Autophagy: Implications for Metabolism. Annu. Rev. Nutr. *27*, 19–40.

Mizushima, N., and Komatsu, M. (2011). Autophagy: Renovation of Cells and Tissues. Cell *147*, 728–741.

Mizushima, N., and Levine, B. (2010). Autophagy in mammalian development and differentiation. Nat. Cell Biol. *12*, 823–830.

Monecke, T., Güttler, T., Neumann, P., Dickmanns, A., Görlich, D., and Ficner, R. (2009). Crystal structure of the nuclear export receptor CRM1 in complex with Snurportin1 and RanGTP. Science *324*, 1087–1091.

Montgomery, A.M., Reisfeld, R.A., and Cheresh, D.A. (1994). Integrin alpha v beta 3 rescues melanoma cells from apoptosis in three-dimensional dermal collagen. Proc. Natl. Acad. Sci. U. S. A. *91*, 8856–8860.

Moon, S., Yeon Park, S., and Woo Park, H. (2018). Regulation of the Hippo pathway in cancer biology. Cell. Mol. Life Sci. 1–17.

Moroishi, T., Hansen, C.G., and Guan, K.-L. (2015). The emerging roles of YAP and TAZ in cancer. Nat. Rev. Cancer *15*, 73–79.

Morozevich, G.E., Kozlova, N.I., Chubukina, A.N., and Berman, A.E. (2003). Role of Integrin αvβ3 in Substrate-Dependent Apoptosis of Human Intestinal Carcinoma Cells. Biochemistry *68*, 416–423.

Morselli, E., Tasdemir, E., Chiara Maiuri, M., Galluzzi, L., Kepp, O., Criollo, A., Vicencio, J.M., Soussi, T., and Kroemer, G. (2008). Mutant p53 protein localized in the cytoplasm inhibits autophagy. Cell Cycle *7*, 3056–3061.

Moscat, J., and Diaz-Meco, M.T. (2009). p62 at the crossroads of autophagy, apoptosis, and cancer. Cell *137*, 1001–1004.

Moskalenko, S., Henry, D.O., Rosse, C., Mirey, G., Camonis, J.H., and White, M. a (2002). The exocyst is a Ral effector complex. Nat. Cell Biol. *4*, 66–72.

Moskalenko, S., Tong, C., Rosse, C., Mirey, G., Formstecher, E., Daviet, L., Camonis, J., and White, M.A. (2003). Ral GTPases Regulate Exocyst Assembly through Dual Subunit Interactions. J. Biol. Chem. *278*, 51743–51748.

Neel, N.F., Martin, T.D., Stratford, J.K., Zand, T.P., Reiner, D.J., and Der, C.J. (2011). The RalGEF-Ral Effector Signaling Network: The Road Less Traveled for Anti-Ras Drug Discovery. Genes Cancer *2*, 275–287.

Nemergut, M.E., Lindsay, M.E., Brownawell, A.M., and Macara, I.G. (2002). Ran-binding protein 3 links Crm1 to the Ran guanine nucleotide exchange factor. J. Biol. Chem. *277*, 17385–17388.

Neyraud, V., Aushev, V.N., Hatzoglou, a., Meunier, B., Cascone, I., and Camonis, J. (2012). RalA and RalB Proteins Are Ubiquitinated GTPases, and Ubiquitinated RalA Increases Lipid Raft Exposure at the Plasma Membrane. J. Biol. Chem. *287*, 29397–29405.

Ngsee, J.K., Elferink, L.A., and Scheller, R.H. (1991). A family of ras-like GTP-binding proteins expressed in electromotor neurons. J. Biol. Chem. *266*, 2675–2680.

Nicely, N.I., Kosak, J., de Serrano, V., and Mattos, C. (2004). Crystal structures of Ral-GppNHp and Ral-GDP reveal two binding sites that are also present in Ras and Rap. Structure *12*, 2025–2036.

Novick, P., and Schekman, R. (1979). Secretion and cell-surface growth are blocked in a temperature-sensitive mutant of Saccharomyces cerevisiae. Proc. Natl. Acad. Sci. U. S. A. *76*, 1858–1862.

O. Santos, A., Parrini, M.C., and Camonis, J. (2016). RalGPS2 Is Essential for Survival and Cell Cycle Progression of Lung Cancer Cells Independently of Its Established Substrates Ral GTPases. PLoS One *11*, e0154840.

Ohta, Y., Suzuki, N., Nakamura, S., Hartwig, J.H., and Stossel, T.P. (1999). The small GTPase RalA targets filamin to induce filopodia. Proc. Natl. Acad. Sci. U. S. A. *96*, 2122–2128.

Opferman, J.T., Letai, A., Beard, C., Sorcinelli, M.D., Ong, C.C., and Korsmeyer, S.J. (2003). Development and maintenance of B and T lymphocytes requires antiapoptotic MCL-1. Nature *426*, 671–676.

Paoli, P., Giannoni, E., and Chiarugi, P. (2013). Anoikis molecular pathways and its role in cancer progression. Biochim. Biophys. Acta - Mol. Cell Res. *1833*, 3481–3498.

Park, J.M., Choi, J.Y., Yi, J.M., Chung, J.W., Leem, S.H., Koh, S.S., and Kang, T.H. (2015). NDR1 modulates the UV-induced DNA-damage checkpoint and nucleotide excision repair. Biochem. Biophys. Res. Commun. *461*, 543–548.

Park, J.Y., Jeong, A.L., Joo, H.J., Han, S., Kim, S.-H., Kim, H.-Y., Lim, J.-S., Lee, M.-S., Choi, H.-K., and Yang, Y. (2018). Development of suspension cell culture model to mimic circulating tumor cells. Oncotarget *9*, 622–640.

Parri, M., and Chiarugi, P. (2013). Redox molecular machines involved in tumor progression. Antioxid. Redox Signal. *19*, 1828–1845.

Parrini, M.C., Sadou-Dubourgnoux, A., Aoki, K., Kunida, K., Biondini, M., Hatzoglou, A., Poullet, P., Formstecher, E., Yeaman, C., Matsuda, M., et al. (2011). SH3BP1, an exocyst-associated RhoGAP, inactivates Rac1 at the front to drive cell motility. Mol. Cell *42*, 650–661.

Pattingre, S., Bauvy, C., and Codogno, P. (2003). Amino acids interfere with the ERK1/2-dependent control of macroautophagy by controlling the activation of Raf-1 in human colon cancer HT-29 cells. J. Biol. Chem. *278*, 16667–16674.

Paul, I., Batth, T.S., Iglesias-gato, D., Al-araimi, A., Al-, I., Alkharusi, A., Norstedt, G., Olsen, J. V, and Zadjali, F. (2017). The ubiquitin ligase Cullin5 SOCS2 regulates NDR1 / STK38 stability and NF- κ B transactivation. Sci. Rep. 1–14.

Pavel, M., and Rubinsztein, D.C. (2016). Mammalian autophagy and the plasma membrane. FEBS J. *284*, 672–679.

Pimkina, J., Humbey, O., Zilfou, J.T., Jarnik, M., and Murphy, M.E. (2009). ARF induces autophagy by virtue of interaction with Bcl-xl. J. Biol. Chem. *284*, 2803–2810.

Poon, I.K.H., and Jans, D.A. (2005). Regulation of nuclear transport: Central role in development and transformation? Traffic *6*, 173–186.

Pulciani, S., Santos, E., Lauver, A. V, Long, L.K., Robbins, K.C., and Barbacid, M. (1982). Oncogenes in human tumor cell lines: molecular cloning of a transforming gene from human bladder carcinoma cells. Proc. Natl. Acad. Sci. U. S. A. *79*, 2845–2849.

Puri, C., Renna, M., Bento, C.F., Moreau, K., and Rubinsztein, D.C. (2013). Diverse autophagosome membrane sources coalesce in recycling endosomes. Cell *154*, 1285–1299.

Qu, X., Yu, J., Bhagat, G., Furuya, N., Hibshoosh, H., Troxel, A., Rosen, J., Eskelinen, E.-L., Mizushima, N., Ohsumi, Y., et al. (2003). Promotion of tumorigenesis by heterozygous disruption of the beclin 1 autophagy gene. J. Clin. Invest. *112*, 1809–1820.

Qu, X., Zou, Z., Sun, Q., Luby-Phelps, K., Cheng, P., Hogan, R.N., Gilpin, C., and Levine, B. (2007). Autophagy gene-dependent clearance of apoptotic cells during embryonic development. Cell *128*, 931–946.

Ragusa, M.J., Stanley, R.E., and Hurley, J.H. (2012). Architecture of the Atg17 complex as a scaffold for autophagosome biogenesis. Cell *151*, 1501–1512.

Ramos, D.M., But, M., Regezi, J., Schmidt, B.L., Atakilit, A., Dang, D., Ellis, D., Jordan, R., and Li, X. (2002). Expression of integrin β6 enhances invasive behavior in oral squamous cell carcinoma. Matrix Biol. *21*, 297–307.

Rhee, H.-W., Zou, P., Udeshi, N.D., Martell, J.D., Mootha, V.K., Carr, S. a, and Ting, A.Y. (2013). Proteomic Mapping of Mitochondria in Living Cells via Spatially Restricted Enzymatic Tagging. Science (80-.). *1328*.

Rigbolt, K.T.G., Prokhorova, T.A., Akimov, V., Henningsen, J., Johansen, P.T., Kratchmarova, I., Kassem, M., Mann, M., Olsen, J. V., and Blagoev, B. (2011). System-wide temporal characterization of the proteome and phosphoproteome of human embryonic stem cell differentiation. Sci. Signal. *4*, 1–18.

Rojas, A.M., Fuentes, G., Rausell, A., and Valencia, A. (2012). The Ras protein superfamily: Evolutionary tree and role of conserved amino acids. J. Cell Biol. *196*, 189–201.

Romashkova, J.A., and Makarov, S.S. (1999). NF-κB is a target of AKT in anti-apoptotic PDGF signalling. Nature *401*, 86–90.

Rossé, C., Hatzoglou, A., Parrini, M.-C., White, M.A., Chavrier, P., and Camonis, J. (2006). RalB mobilizes the exocyst to drive cell migration. Mol. Cell. Biol. *26*, 727–734.

Rowland, B.D., and Peeper, D.S. (2006). KLF4, p21 and context-dependent opposing forces in cancer. Nat. Rev. Cancer *6*, 11–23.

Sancak, Y., Peterson, T.R., Shaul, Y.D., Lindquist, R.A., Thoreen, C.C., Bar-Peled, L., and Sabatini, D.M. (2008). The Rag GTPases bind raptor and mediate amino acid signaling to mTORC1. Science *320*, 1496–1501.

Sasaki, T., Kojima, H., Kishimoto, R., Ikeda, A., Kunimoto, H., and Nakajima, K. (2006). Spatiotemporal regulation of c-Fos by ERK5 and the E3 ubiquitin ligase UBR1, and its biological role. Mol. Cell *24*, 63–75.

Scherz-Shouval, R., Shvets, E., Fass, E., Shorer, H., Gil, L., and Elazar, Z. (2007). Reactive oxygen species are essential for autophagy and specifically regulate the activity of Atg4. EMBO J. *26*, 1749–1760.

Schlegelmilch, K., Mohseni, M., Kirak, O., Pruszak, J., Rodriguez, J.R., Zhou, D., Kreger, B.T., Vasioukhin, V., Avruch, J., Brummelkamp, T.R., et al. (2011). Yap1 Acts Downstream of α-Catenin to Control Epidermal Proliferation. Cell *144*, 782–795.

Schmalhofer, O., Brabletz, S., and Brabletz, T. (2009). E-cadherin, β-catenin, and ZEB1 in malignant progression of cancer. Cancer Metastasis Rev. *28*, 151–166.

Schmitz-Rohmer, D., Probst, S., Yang, Z.-Z., Laurent, F., Stadler, M.B., Zuniga, A., Zeller, R., Hynx, D., Hemmings, B. a., and Hergovich, A. (2015). NDR Kinases Are Essential for Somitogenesis and Cardiac Looping during Mouse Embryonic Development. PLoS One *10*, e0136566.

Selimoglu, R., Bettoun, A., Joffre, C., Meunier, B., Parrini, M.C., Fesquet, D., Formstecher, E., Cascone, I., Hergovich, A., and Camonis, J.H. (2014). RalA GTPase and MAP4K4 Function through NDR1 Activation in Stress Response and Apoptotic Signaling. HSOA J. Cell Biol. Cell Metab. *1*, 1–11.

Sharif, A.A.D., and Hergovich, A. (2017). The NDR/LATS protein kinases in immunology and cancer biology. Semin. Cancer Biol. 0–1.

Sheridan, C., and Downward, J. (2013). Inhibiting the RAS–PI3K Pathway in Cancer Therapy. Enzym. *34*, 107–136.

Sheridan, D.L., Kong, Y., Parker, S.A., Dalby, K.N., and Turk, B.E. (2008). Substrate discrimination among mitogen-activated protein kinases through distinct docking sequence motifs. J. Biol. Chem. *283*, 19511–19520.

Shi, D.D., Shi, H., Lu, D., Li, R., Zhang, Y., and Zhang, J. (2012). NDR1/STK38 potentiates NF-kB activation by its kinase activity. Cell Biochem. Funct. *30*, 664–670.

Shimizu, K., Goldfarb, M., Suard, Y., Perucho, M., Li, Y., Kamata, T., Feramisco, J., Stavnezer, E., Fogh, J., and Wigler, M.H. (1983). Three human transforming genes are related to the viral ras oncogenes. Proc. Natl. Acad. Sci. U. S. A. *80*, 2112–2116.

Shirakawa, R., Fukai, S., Kawato, M., Higashi, T., Kondo, H., Ikeda, T., Nakayama, E., Okawa, K., Nureki, O., Kimura, T., et al. (2009). Tuberous sclerosis tumor suppressor complex-like complexes act as GTPase-activating proteins for Ral GTPases. J. Biol. Chem. *284*, 21580–21588.

Simicek, M., Lievens, S., Laga, M., Guzenko, D., Aushev, V.N., Kalev, P., Baietti, M.F., Strelkov, S. V, Gevaert, K., Tavernier, J., et al. (2013). The deubiquitylase USP33 discriminates between RALB functions in autophagy and innate immune response. Nat. Cell Biol. *15*, 1220–1230.

Singhal, S.S., Singhal, J., Yadav, S., Dwivedi, S., Boor, P.J., Awasthi, Y.C., and Awasthi, S. (2007). Regression of lung and colon cancer xenografts by depleting or inhibiting RLIP76 (Ral-binding protein 1). Cancer Res. *67*, 4382–4389.

Srivastava, S.K., Di Donato, A., and Lacal, J.C. (1989). H-ras mutants lacking the epitope for the neutralizing monoclonal antibody Y13-259 show decreased biological activity and are deficient in GTPase-activating protein interaction. Mol. Cell. Biol. *9*, 1779–1783.

Stegert, M.R., Tamaskovic, R., Bichsel, S.J., Hergovich, A., and Hemmings, B.A. (2004). Regulation of NDR2 protein kinase by multi-site phosphorylation and the S100B calcium-binding protein. J. Biol. Chem. *279*, 23806–23812.

Stegert, M.R., Hergovich, A., Tamaskovic, R., Bichsel, S.J., and Hemmings, B.A. (2005a). Regulation of NDR protein kinase by hydrophobic motif phosphorylation mediated by the mammalian Ste20-like kinase MST3. Mol. Cell. Biol. *25*, 11019–11029.

Stegert, M.R., Hergovich, A., Tamaskovic, R., Bichsel, S.J., and Hemmings, B.A. (2005b). Regulation of NDR protein kinase by hydrophobic motif phosphorylation mediated by the mammalian Ste20-like kinase MST3. Mol. Cell. Biol. *25*, 11019–11029.

Stupack, D.G., Puente, X.S., Boutsaboualoy, S., Storgard, C.M., and Cheresh, D.A. (2001). Apoptosis of adherent cells by recruitment of caspase-8 to unligated integrins. J. Cell Biol. *155*, 459–470.

Sun, Q., Chen, X., Zhou, Q., Burstein, E., Yang, S., and Jia, D. (2016). Inhibiting cancer cell hallmark features through nuclear export inhibition. Signal Transduct. Target. Ther. *1*, 16010.

Takahashi, Y., Coppola, D., Matsushita, N., Cualing, H.D., Sun, M., Sato, Y., Liang, C., Jung, J.U., Cheng, J.Q., Mul, J.J., et al. (2007). Bif-1 interacts with Beclin 1 through UVRAG and regulates autophagy and tumorigenesis. Nat. Cell Biol. *9*, 1142–1151.

Takaya, A., Kamio, T., Masuda, M., Mochizuki, N., Sawa, H., Sato, M., Nagashima, K., Mizutani, A., Matsuno, A., Kiyokawa, E., et al. (2007). R-Ras Regulates Exocytosis by Rgl2/Rlf-mediated Activation of RalA on Endosomes. Mol. Biol. Cell *18*, 1850–1860.

Takeuchi, T., Inoue, S., and Yokosawa, H. (2006). Identification and Herc5-mediated ISGylation of novel target proteins. Biochem. Biophys. Res. Commun. *348*, 473–477.

Takeyama, Y., Sato, M., Horio, M., Hase, T., Yoshida, K., Yokoyama, T., Nakashima, H., Hashimoto, N., Sekido, Y., Gazdar, A.F., et al. (2010). Knockdown of ZEB1, a master epithelial-to-mesenchymal transition (EMT) gene, suppresses anchorage-independent cell growth of lung cancer cells. Cancer Lett. *296*, 216–224.

Tanaka, K., Mohri, Y., Nishioka, J., Kobayashi, M., Ohi, M., Miki, C., Tonouchi, H., Nobori, T., and Kusunoki, M. (2009). Neurotrophic receptor, tropomyosin-related kinase B as an independent prognostic marker in gastric cancer patients. J. Surg. Oncol. *99*, 307–310.

Tang, F., Gill, J., Ficht, X., Barthlott, T., Cornils, H., Schmitz-Rohmer, D., Hynx, D., Zhou, D., Zhang, L., Xue, G., et al. (2015). The kinases NDR1/2 act downstream of the Hippo homolog MST1 to mediate both egress of thymocytes from the thymus and lymphocyte motility. Sci. Signal. *8*, ra100.

Tanida, I., Ueno, T., and Kominami, E. (2004a). LC3 conjugation system in mammalian autophagy. Int. J. Biochem. Cell Biol. *36*, 2503–2518.

Tanida, I., Sou, Y., Ezaki, J., Minematsu-Ikeguchi, N., Ueno, T., and Kominami, E. (2004b). HsAtg4B/HsApg4B/autophagin-1 cleaves the carboxyl termini of three human Atg8 homologues and delipidates microtubule-associated protein light chain 3- and GABAA receptor-associated protein-phospholipid conjugates. J. Biol. Chem. *279*, 36268–36276.

Taylor, R.C., Cullen, S.P., and Martin, S.J. (2008a). Apoptosis: controlled demolition at the cellular level. Nat. Rev. Mol. Cell Biol. *9*, 231–241.

Taylor, R.C., Cullen, S.P., and Martin, S.J. (2008b). Apoptosis: controlled demolition at the cellular level. Nat. Rev. Mol. Cell Biol. *9*, 231–241.

Tazat, K., Harsat, M., Goldshmid-Shagal, A., Ehrlich, M., and Henis, Y.I. (2013). Dual effects of Ral-activated pathways on p27 localization and TGF-β signaling. Mol. Biol. Cell *24*, 1812–1824.

Thomas, J.C., Cooper, J.M., Clayton, N.S., Wang, C., White, M.A., Abell, C., Owen, D., and Mott, H.R. (2016). Inhibition of Ral GTPases Using a Stapled Peptide Approach. J. Biol. Chem. jbc.M116.720243.

Thornberry, N.A. (1998). Caspases: key mediators of apoptosis. Chem. Biol. *5*, R97-103.

Toruner, M., Fernandez-zapico, M., Sha, J.J., Pham, L., Urrutia, R., and Egan, L.J. (2006). Antianoikis Effect of Nuclear Factor-B through Up-regulated Expression of Osteoprotegerin, BCL-2, and IAP-1. J. Biol. Chem. *281*, 8686–8696.

Trachootham, D., Lu, W., Ogasawara, M.A., Valle, N.R.-D., and Huang, P. (2008). Redox Regulation of Cell Survival. Antioxid. Redox Signal. *10*, 1343–1374.

Tran, E.J., King, M.C., and Corbett, A.H. (2014). Macromolecular transport between the nucleus and the cytoplasm: Advances in mechanism and emerging links to disease. Biochim. Biophys. Acta *1843*, 2784–2795.

Turner, J.G., Dawson, J., and Sullivan, D.M. (2012). Nuclear export of proteins and drug resistance in cancer. Biochem. Pharmacol. *83*, 1021–1032.

Urano, T., Emkey, R., and Feig, L.A. (1996). Ral-GTPases mediate a distinct downstream signaling pathway from Ras that facilitates cellular transformation. EMBO J. *15*, 810–816.

Valentijn, A.J., and Gilmore, A.P. (2004). Translocation of full-length Bid to mitochondria during anoikis. J. Biol. Chem. *279*, 32848–32857.

Veeriah, S., Taylor, B.S., Meng, S., Fang, F., Yilmaz, E., Vivanco, I., Janakiraman, M., Schultz, N., Hanrahan, A.J., Pao, W., et al. (2010). Somatic mutations of the Parkinson's disease–associated gene PARK2 in glioblastoma and other human malignancies. Nat. Genet. *42*, 77–82.

Visintin, R., and Amon, A. (2001). Regulation of the mitotic exit protein kinases Cdc15 and Dbf2. Mol. Biol. Cell *12*, 2961–2974.

Vizcaíno, J.A., Csordas, A., del-Toro, N., Dianes, J.A., Griss, J., Lavidas, I., Mayer, G., Perez-Riverol, Y., Reisinger, F., Ternent, T., et al. (2016). 2016 update of the PRIDE database and its related tools. Nucleic Acids Res. *44*, D447–D456.

Wajant, H. (2002). The Fas signaling pathway: more than a paradigm. Science (80-.). *296*, 1635–1636.

Walther, T.C., Pickersgill, H.S., Cordes, V.C., Goldberg, M.W., Allen, T.D., Mattaj, I.W., and Fornerod, M. (2002). The cytoplasmic filaments of the nuclear pore complex are dispensable for selective nuclear protein import. J. Cell Biol. *158*, 63–77.

Wang, H., Owens, C., Chandra, N., Conaway, M.R., Brautigan, D.L., and Theodorescu, D. (2010). Phosphorylation of RalB is important for bladder cancer cell growth and metastasis. Cancer Res. *70*, 8760–8769.

Wang, W., Xiao, Z.-D., Li, X., Aziz, K.E., Gan, B., Johnson, R.L., and Chen, J. (2015). AMPK modulates Hippo pathway activity to regulate energy homeostasis. Nat. Cell Biol. *17*, 490–499.

Wang, Z., Wu, Y., Wang, H., Zhang, Y., Mei, L., Fang, X., Zhang, X., Zhang, F., Chen, H., Liu, Y., et al. (2014). Interplay of mevalonate and Hippo pathways regulates RHAMM transcription via YAP to modulate breast cancer cell motility. Proc. Natl. Acad. Sci. *111*, E89–E98.

Warburg, O. (1956). On the origin of cancer cells. Science *123*, 309–314.

Wen, M., Ma, X., Cheng, H., Jiang, W., Xu, X., Zhang, Y., Zhang, Y., Guo, Z., Yu, Y., Xu, H., et al. (2015). Stk38 protein kinase preferentially inhibits TLR9-activated inflammatory responses by promoting MEKK2 ubiquitination in macrophages. Nat. Commun. *6*, 7167.

Wennerberg, K., Rossman, K.L., and Der, C.J. (2005). The Ras superfamily at a glance. J. Cell Sci. *118*, 843–846.

Whelan, K.A., Caldwell, S.A., Shahriari, K.S., Jackson, S.R., Franchetti, L.D., Johannes, G.J., and Reginato, M.J. (2010). Hypoxia Suppression of Bim and Bmf Blocks Anoikis and Luminal Clearing during Mammary Morphogenesis. Mol. Biol. Cell *21*, 3829–3837.

Wu, Y., and Zhou, B.P. (2010). Snail: More than EMT. Cell Adh. Migr. *4*, 199–203.

Wu, Z., Sawada, T., Shiba, K., Wu, Z., Sawada, T., Shiba, K., Liu, S., Kanao, T., and Takahashi, R. (2013). Tricornered / NDR kinase signaling mediates PINK1-directed mitochondrial quality control and tissue maintenance. Genes Dev. 157–162.

Xia, H., Nho, R.S., Kahm, J., Kleidon, J., and Henke, C.A. (2004). Focal adhesion kinase is upstream of phosphatidylinositol 3-kinase/Akt in regulating fibroblast survival in response to contraction of type I collagen matrices via a beta 1 integrin viability signaling pathway. J. Biol. Chem. *279*, 33024–33034.

Xie, Z., and Klionsky, D.J. (2007). Autophagosome formation: core machinery and adaptations. Nat. Cell Biol. *9*, 1102–1109.

Xiong, S., Lorenzen, K., Couzens, A.L., Templeton, C.M., Rajendran, D., Mao, D.Y.L., Juang, Y.C., Chiovitti, D., Kurinov, I., Guettler, S., et al. (2018). Structural Basis for Auto-Inhibition of the NDR1 Kinase Domain by an Atypically Long Activation Segment. Structure *26*, 1101–1115.e6.

Xu, L., Salloum, D., Medlin, P.S., Saqcena, M., Yellen, P., Perrella, B., and Foster, D.A. (2011). Phospholipase D mediates nutrient input to mammalian target of rapamycin complex 1 (mTORC1). J. Biol. Chem. *286*, 25477–25486.

Yan, C., and Theodorescu, D. (2018). RAL GTPases: Biology and Potential as Therapeutic Targets in Cancer. Pharmacol. Rev. *70*, 1–11.

Yan, C., Liu, D., Li, L., Wempe, M.F., Guin, S., Khanna, M., Meier, J., Hoffman, B., Owens, C., Wysoczynski, C.L., et al. (2014). Discovery and characterization of small molecules that target the GTPase Ral. Nature *515*, 443–447.

Yang, S., Wang, X., Contino, G., Liesa, M., Sahin, E., Ying, H., Bause, A., Li, Y., Stommel, J.M., Dell'antonio, G., et al. (2011). Pancreatic cancers require autophagy for tumor growth. Genes Dev. *25*, 717–729.

Yordy, J.S., and Muise-Helmericks, R.C. (2000). Signal transduction and the Ets family of transcription factors. Oncogene *19*, 6503–6513.

Young, A.R.J., Chan, E.Y.W., Hu, X.W., Köchl, R., Crawshaw, S.G., High, S., Hailey, D.W., Lippincott-Schwartz, J., and Tooze, S.A. (2006). Starvation and ULK1-dependent cycling of mammalian Atg9 between the TGN and endosomes. J. Cell Sci. *119*, 3888–3900.

Young, A.R.J., Narita, M., Ferreira, M., Kirschner, K., Sadaie, M., Darot, J.F.J., Tavaré, S., Arakawa, S., Shimizu, S., Watt, F.M., et al. (2009). Autophagy mediates the mitotic senescence transition. Genes Dev. *23*, 798–803.

Yu, F.-X., and Guan, K.-L. (2013). The Hippo pathway: regulators and regulations. Genes Dev. *27*, 355–371.

Zago, G., Veith, I., Singh, M.K., Fuhrmann, L., De Beco, S., Remorino, A., Takaoka, S., Palmeri, M., Berger, F., Brandon, N., et al. (2018). RalB directly triggers invasion downstream Ras by mobilizing the Wave complex. Elife *7*, 1–23.

Zhang, J., Wang, G., Zhou, Y., Chen, Y., Ouyang, L., and Liu, B. (2018). Mechanisms of autophagy and relevant small-molecule compounds for targeted cancer therapy. Cell. Mol. Life Sci. 1–24.

Zhang, L., Tang, F., Terracciano, L., Hynx, D., Kohler, R., Bichet, S., Hess, D., Cron, P., Hemmings, B.A., Hergovich, A., et al. (2015). NDR Functions as a Physiological YAP1 Kinase in the Intestinal Epithelium. Curr. Biol. *25*, 296–305.

Zhao, B., Li, L., Lu, Q., Wang, L.H., Liu, C.-Y., Lei, Q., and Guan, K.-L. (2011). Angiomotin is a novel Hippo pathway component that inhibits YAP oncoprotein. Genes Dev. *25*, 51–63.

Zhao, X., Gan, L., Pan, H., Kan, D., Majeski, M., Adam, S.A., and Unterman, T.G. (2004). Multiple elements regulate nuclear/cytoplasmic shuttling of FOXO1: characterization of phosphorylation- and 14-3-3-dependent and -independent mechanisms. Biochem. J. *378*, 839–849.

Zou, H., Henzel, W.J., Liu, X., Lutschg, A., and Wang, X. (1997). Apaf-1, a Human Protein Homologous to C. elegans CED-4, Participates in Cytochrome c–Dependent Activation of Caspase-3. Cell *90*, 405–413.

APPENDIX

Localization of the RGL2-RalB signaling axis at endomembrane compartments and its modulation by autophagy

Manish Kumar Singh[1,2], **Alexandre PJ Martin**[1,2], Carine Joffre[3], Giulia Zago[1,2], Jacques Camonis[1,2], Mathieu Coppey[1,4], Maria Carla Parrini[1,2,#]

Manuscript submitted

[#] Corresponding author: maria-carla.parrini@curie.fr
[1] Institut Curie, Centre de Recherche, Paris Sciences et Lettres Research University, 75005 Paris, France;
[2] ART group, Inserm U830, 75005 Paris, France;
[3] Centre de Recherches en Cancérologie de Toulouse (CRCT), Inserm UMR1037, Toulouse, France;
[4] LOCCO group, UMR168, 75005 Paris, France.

Background of the project

One of the historical interests of our lab is to decipher and functionally characterize the role of Ral proteins in the whole spectrum of oncogenesis, including cell motility. Despite their 81% identity and common activators, RalA and RalB have distinct cellular functions. Since decades, our team, and collaborators, reported a specific role for RalB in regulating cell motility/invasion (Biondini et al., 2015; Rossé et al., 2006; Zago et al., 2018) and autophagy (Bodemann et al., 2011; Simicek et al., 2013). This project, entrusted to a former post-doc of the team, Manish Singh, aimed to understand how RalB coordinates these two distinct processes.

Summary of the results

The Rgl2 to RalB signaling axis is required for autophagy (figure 1 of the manuscript)

This work started by a screen performed by a former post-doc of the lab, Carine Joffre, using siRNA targeting each of the six RalGEFs in order to identify the required ones for autophagy. She founds that three of them, RalGDS, Rgl1, and Rgl2 severely impaired autophagy when silenced in HeLa cells (figure 1A). Then, we tested the contribution of RalGEFs to autophagy in Ras-driven cancer cells (HekRasV12), in order to match with previous observation reporting the crucial role of RalB acting downstream of activated Ras in motility (Rossé et al., 2006). We focused our efforts on the Rgl2-RalB axis rather than the one implicating Rgl2 because of the strongest impact of Rgl2 on autophagy and because Rgl2 has been previously reported to endosomes (Takaya et al., 2007). RalGDS was excluded for this work because not acting downstream of Ras (see part 1.3.1.2 of the thesis introduction). We confirmed the crucial role of Rgl2 for autophagy in the Hek-HT cell line (figure 1C), demonstrating that the contribution of the Rgl2-RalB axis on and autophagy can be analyzed in this model and in the tumorigenic, invasive and metastatic one: Hek-HT-H-RasV12.

Application of a novel automated image analysis to quantify proteins of interests at endomembranes

The core of this article consists of the development of a novel image analysis methodology that aims to quantify the localization of proteins of interest within subcellular structures, such as endomembranes. This automated method relies on the analysis, through Image J software, of images captured by microscopy of, at least, two different fluorescent channels. The first one consist of the fluorescent signal of the protein of interest, labelled with fluorescent antibodies or fused with a fluorescent protein. The second one defines the endomembrane compartment, also labelled with fluorescent antibody of fused protein. As a control, the method also draws randomized cellular compartments, having the same characteristics (number, size, etc…) than the real ones studied, and compare the proportion of localization of the protein of interest within the real to the randomized compartments. The assumption is that the protein of interest is certainly localized at the studied compartment if there is a significant difference as compared to the randomized compartments (figure 2).

Rgl2 and RalB localize at early endosomes, recycling endosomes, and autophagosomes

Equipped with this new algorithm, we found that both RalB (figure 4) and its activator, Rgl2 (figure 3), localize at discrete endomembranes in both normal and Ras-transformed cell lines, namely at early endosomes (EEA1 marker), recycling endosomes (Rab11 marker), and autophagosomes (LC3 marker). Only Rgl2 decreased its specific localization at both recycling endosomes and autophagosomes in Ras-transformed cell lines, as compared to the normal ones (figure 3), suggesting the existence of an active Rgl2-RalB signaling axis at these subcellular compartments.

The active Ras itself could explain the decrease of Rgl2 at the above-cited endomembranes in Ras-transformed cells. Indeed, Rgl2 molecules could be diverted from these endomembranes compartments to the plasma membrane, where the active Ras-GTP is localized.

Autophagy impact on Rgl2/RalB localization

Because both Rgl2 and RalB localize at endomembranes compartments, we analyzed if autophagy, induced by nutrient starvation, could promote a reorganization of Rgl2 and RalB endomembranes localization. As expected, we observed a reduction of early and recycling endosomes in favor of autophagosomes biosynthesis upon nutrient starvation in both normal and Ras-transformed cell lines (figure 5A).

Only two noticeable consequences of autophagy induction on Rgl2 and RalB subcellular localization were observed. Autophagy induction stimulated Rgl2 localization to recycling endosomes in normal cells only (figure 5B) and decreased RalB localization at early endosomes in normal cells only

(figure 5C). The results exhibit that autophagy induces an evident reorganization of endomembranes and changes in Rgl2 and RalB localizations, that may contribute to the autophagy process.

Autophagy impact on RalB activity

We nest used a FRET-based RalB biosensor (Martin et al., 2014) in order to characterize RalB specific activity (figure 6A). We found that RalB was more activated at autophagosomes in Ras-transformed cells as compared to normal cells at basal conditions, without autophagy induction, suggesting that the Rgl2-RalB signaling axis is more active at autophagosomes in Ras-transformed cell lines. Autophagy induction, by nutrient starvation, induced an important increase of RalB activity at autophagosomes in normal cells but not in Ras-transformed ones, probably because RalB activity is already saturated in these constitutively active Ras cell lines, even saturated (figure 6C).

Discussion

This work suggests, using a novel automated quantification method, the existence of an active Ras-Rgl2-RalB signaling axis at the above-described endomembranes. We showed that Rgl2, activator of RalB, is crucial for RalB activation upon autophagy, where the autophagosome number is found increased to the detriment of early and recycling endosomes, in line with the idea that the latter contribute to the former. Going beyond the dogma establishing RalB localization at the plasma membrane, we demonstrated here that RalB signaling occurs also at endomembranes. However, the role of RalB activation by Rgl2 at endomembrane for the autophagy process, as well as for other biological processes, still remains elusive and warrants more investigations.

My specific contribution to this project

When I took part to this project, it was already at an advanced stage and Manish Singh, who was in charge of it, already reported a link between Rgl2-RalB localization at different endomembranes and autophagy. As reported previously, this project started from a screen performed by Carine Joffre that identified the crucial role of Rgl2 for autophagy process in HeLa cells. However, the experimental procedure about the link between the Rgl2-RalB subcellular localization and autophagy held by Manish Singh was being performed in Hek-HT and the derived Hek-HT-RasV12, a link was missing. My contribution consisted to test the requirement of Rgl2 for the autophagy process in Hek-HT cells.

To do so, I transfected Hek-HT cells with two independent siRNA targeting endogenous Rgl2 in addition to a control siRNA. Autophagy was induced by incubating these cells with EBSS (nutrient starvation) and LC3-II degradation was blocked by the addition of chloroquine (Klionsky et al., 2016). After four hours of incubation, I lysed the cells and performed a Western-blotting to evaluate the level of Rgl2 (figure S1B) and the resulting autophagy process (figure 1C and figure S1B). I found, as expected, that Rgl2 silencing, using two independent siRNA, severely impaired starvation-induced autophagy in this cell line, as assessed by LC3 conversion assay (Klionsky et al., 2016).

Localization of the RGL2-RalB signaling axis at endomembrane compartments and its modulation by autophagy

Manish Kumar Singh[1,2], Alexandre PJ Martin[1,2], Carine Joffre[3], Giulia Zago[1,2], Jacques Camonis[1,2], Mathieu Coppey[1,4], Maria Carla Parrini[1,2,#]

[#] Corresponding author: maria-carla.parrini@curie.fr

[1] Institut Curie, Centre de Recherche, Paris Sciences et Lettres Research University, 75005 Paris, France;

[2] ART group, Inserm U830, 75005 Paris, France;

[3] Centre de Recherches en Cancérologie de Toulouse (CRCT), Inserm UMR1037, Toulouse, France;

[4] LOCCO group, UMR168, 75005 Paris, France.

Key words: RalB, RGL2, Endomembranes, Co-localization, Autophagy

ABSTRACT
The monomeric GTPase RalB controls crucial physiological processes, including autophagy and invasion, but it is still unclear how its multifunctionality is achieved. We previously reported that the RalGEF (Guanine nucleotide Exchange Factor) RGL2 binds and activates RalB to promote invasion. We show here that RGL2 is also a major activator of RalB required for autophagy.
Using a novel automated image analysis method (Protein at Endomembrane compartments "Pro@EMC") we spatially mapped the RGL2-RalB signaling axis in an isogenic normal and Ras-transformed cell model by quantifying the endogenous localization of the RGL2 activator and of its substrate RalB at different endomembrane compartments. We found that, in both normal and Ras-transformed cells, RGL2 and RalB substantially localize at early and recycling endosomes, and to less extent at autophagosomes, but not at trans-Golgi. Interestingly the use of a FRET-based RalB bionsensor indicated that the RGL2-RalB signaling axis is active at these endomembrane compartments at basal level in rich medium. Induction of autophagy by nutrient starvation led to a considerable reduction of early and recycling endosomes, as opposed to the expected increase of autophagosomes, in both normal and Ras-transformed cells. However, autophagy mildly affected relative abundances of both RGL2 and RalB at early and recycling endosomes, and at autophagosomes. Moreover, RalB activity increased at autophagosomes upon starvation in normal cells. These results suggest that the contribution of endosome membranes (carrying RGL2 and RalB molecules) increases RGL2- RalB total pool at autophagosome forming compartments and might contribute to amplify RalB signaling to support autophagy.

INTRODUCTION

The two human Ral proteins (RalA and RalB) are monomeric GTPases which are activated by RalGEFs (Guanine Nucleotide Exchange Factors) [1,2]. Among the six identified RalGEFs, four do contain a Ras-association (RA) domain (RGL1, RGL2, RGL3, RalGDS) and are direct effectors of Ras GTPases oncogene proteins (K-Ras, H-Ras, N-Ras). The Ral pathway is permissive if not instructive per se for Ras induced oncogenesis [3].

One of the most frequent oncogenic events in human cancers is the activation by constitutive mutations of Ras oncoproteins [4]. Targeting the Ral signaling is a potential, yet not exploited anti- cancer therapeutic strategy [5]. The studies on Ral signaling network led to the discovery of an impressive variety of cellular functions under the control of Ral proteins, such as motility and invasion [6–11], membrane trafficking [12–14], autophagy [15–18], apoptosis [19,20], and cell division [21,22]. Intriguingly, even though in some cellular contexts RalA and RalB seem to have overlapping effects, a distinct role for RalB activity was reported in specifically regulating two important cellular processes: motility/invasion [6–8,10,23–25] and autophagy [26,27]. How RalB coordinates the interplay between invasion and autophagy, particularly in the context of cancer cells with Ras mutations, is unknown.

One possible explanation for this functional versatility could be that RalB is activated at specific sub-cellular locations [28,29], by distinct RalGEFs, with specific temporal features. The notion that activated GTP-bound Ras recruits RalGEFs at the plasma-membrane, triggering the activation of RalB by GDP/GTP exchange, is supported by experimental evidences [25,30], but the possibility that the Ras to Ral signaling could occur also at endomembranes has been very poorly explored, partially because of simple technical difficulties.

When studying protein localizations at endomembrane compartments (such as endosomes, autophagosomes, Golgi apparatus), the existing analysis approaches present several drawbacks. The most common approach is to compose an overlay image of dual color images (e.g. green and red): the presence of both green and red biomolecule at same pixels results in yellow spots [31,32]. However, since the subsequent yellow spots totally depend on the signal strength measured in green and red channels, the approach is reliable only if both channels show similar grey level dynamics. Another commonly used approach is based on the cross-correlation analysis of grey value of dual channel images (e.g. Pearson correlation coefficient and the Mander's overlap coefficient) [33,34]. But, these coefficients rely on signal proportionality of two probes, which can be misleading if the probe ratio varies widely [32]. Moreover, in addition to localization, it is also important to measure the local activities of the proteins of interest. For this work, we developed a robust automated method in order to quantify the endomembrane compartments that are positive for proteins of interest. We named this method "Pro@EMC", for Protein at EndoMembrane Compartments. This method is independent of probe signal strength or its proportionality because its uses one channel to segment endomembrane compartments and another to measure protein intensity. We applied the Pro@EMC method to the study of RalB localization and activity at endomembranes, specifically at early endosomes (identified by EEA1 and Rab5 makers), recycling endosomes (identified by Rab11 marker), autophagosomes (identified by LC3 marker), and trans-Golgi (identified by Rab6 marker). Thanks to this approach we found the existence of a RGL2 to RalB signaling axis at early and recycling endosomes, and at to a less extent at autophagosomes, at basal level in rich medium. Moreover, we characterized the effects of starvation-induced autophagy on this RGL2-RalB endomembrane signaling.

RESULTS

RGL1 and RGL2 are key activators of RalB for both invasion and autophagy

We previously reported that, among the six RalGEFs, RGL1 and RGL2 are required to activate RalB for promoting invasion down-stream oncogenic Ras [25]. Since autophagy is another process regulated by RalB [26,27], we aimed at identifying the specific RalGEF(s) required for autophagy. We silenced by siRNAs each one among the six RalGEFs in Hela cells and we followed autophagy by LC3 conversion assay [35]. The depletion of RGL2 and RalGDS substantially impaired autophagy; the depletion of RGL1 as well had a significant inhibitory effect (Figure 1A, Figure S1A). Thus RGL1 and RGL2, which act down-stream Ras since they have a Ras-association domain (RA), are key activators of RalB for both invasion and autophagy (Figure 1B). We focused our attention on the RGL2-RalB rather than RGL1-RalB signaling axis because of the strong effect of RGL2 silencing on autophagy and because a function for RGL2 had been previously reported at endosomes [36].

To evaluate the contribution of oncogenic Ras in the activation of RGL2-RalB signaling, we used for the rest of the study a genetically controlled cell model: the HEK-HT cells, which are immortalized but not transformed, and become tumorigenic, invasive and metastatic upon expression of constitutive active H-RasV12 [37,38]. Moreover, because of their flat morphology, these cells are very suitable for imaging studies. Importantly, we confirmed the requirement of RGL2 for autophagy in this cell model: RGL2 silencing with two independent siRNAs impaired starvation-induced autophagy in HEK-HT cells, as assessed by LC3 conversion assay (Figure 1C, Figure S1B).

An automated image analysis method to quantify localization of proteins of interest at endomembrane compartments

In order to quantify the localization of RGL2 and RalB at endomembranes (Figure 2A), we developed a novel automated image analysis method, named Pro@EMC (Figure 2B).
In a first step, Pro@EMC uses one channel to identify specific endomembrane compartments (for example early endosomes, using EEA1 marker) and another channel to measure the mean intensity of the protein of interest (for example RalB, using specific anti-RalB antibodies) within these compartments. In a second step, in order to correct for co-localization by chance, Pro@EMC creates "randomized" pseudo-compartments whose number and size can be modulated by user. For example we used n=1000 and area=1.2 μm^2 for endosomes and autophagosomes, and n=10 and area=9.2 μm^2 for trans-Golgi, to mimic the properties of the specific compartments under investigation. Since the localization of the pseudo-compartments is random, they could colocalize by chance with the real endomembrane compartments. The assumption is that a protein of interest is really localized at particular endomembrane compartments only if there is a significant difference between the measurements at the specific compartments as compared to the measurements at the pseudo-compartments. The region of interested for the analysis is defined by the user in a way to restrict the analysis to cell areas where the specific compartments are present.
We tested various thresholds to identify a good compromise between specificity and sensitivity (Figure S3). We chose to consider an endomembrane compartment positive for a protein of interest only if its mean intensity was above the sum of mean intensity (of all compartments) and standard deviation (mean+1 fold SD) within the region of interest. As benchmark, we assessed this Pro@EMC method by quantifying the co-localization of two different markers for the same compartment: the EEA1 and Rab5 markers of early endosomes. Almost 100% of EEA1 compartments were positive for Rab5, both in normal

and Ras-transformed cells (Figure S4), demonstrating that the method is efficient and robust.
Pro@EMC was also useful to simply count the number of specific endomembrane compartments per cell (Figure 2C). There was no difference in the counts per cell of early endosomes, recycling endosomes and Trans-Golgi compartments in HEK-HT versus HEK-HT-H-RasV12 cells, indicating that oncogenic Ras does not globally impact on the organization of these endomembranes at basal level. On the contrary, we observed 2.3 fold more autophagosomes (LC3-positive compartments) in Ras-transformed cells than in isogenic normal cells, in agreement with previous reports on increased autophagy in Ras-driven cancer cells [39,40].

RGL2 and RalB localization at early endosomes, recycling endosomes, and autophagosomes

The Pro@EMC method revealed that a very substantial fraction of early endosomes (EEA1 compartments) and recycling endosomes (Rab11 compartments) is positive for endogenous RGL2 staining (~80% and ~60%, respectively). RGL2 is also found at ~30% of autophagosomes (LC3 compartments). In contrast, RGL2 is not present at Trans-Golgi (Rab6 compartments) since no significant difference was found between the measurements at Rab6 specific compartments as compared to the measurements at the pseudo-compartments (Figure 3). There were no differences between normal and transformed cells, except a significant decrease of RGL2 at recycling endosomes and autophagosomes in Ras-transformed cells as compared to normal cells. One possible explanation is that RGL2 molecules are diverted by Ras-GTP from endomembranes to plasma-membrane during Ras-dependent transformation [25].
The localization of endogenous RalB was very similar to that of RGL2. A very substantial fraction of early endosomes (EEA1 compartments) and recycling endosomes (Rab11 compartments) is positive for endogenous RalB staining (~75% and ~40%, respectively). RalB is also found at ~20% of autophagosomes (LC3 compartments). In contrast, RalB is not present at Trans-Golgi (Rab6 compartments) (Figure 4). There were no detectable differences between normal and transformed cells concerning the RalB localization at endomembrane compartments.
In conclusion, both RGL2 and RalB localize at early and recycling endosomes, and to less extent at basal autophagosomes (in rich medium), suggesting the existence of an active RGL2-RalB signaling axis at these subcellular localizations.

Modulation of endomembrane compartments and RGL2/RalB localization upon autophagy

To characterize the impact of starvation-induced autophagy on RGL2/RalB localization at endomembranes, normal HEK-HT cells and transformed HEK-HT-H-RasV12 cells were grown in basal rich (DMEM) medium or starvation (EBSS) medium for 4 hours to induce autophagy. The counts of the compartments (Figure 5A) showed an increase of autophagosomes, as expected since autophagy was induced, in both normal and transformed cells. Interestingly, a substantial reduction of early and recycling endosomes was observed upon starvation, supporting the notion that maturation of autophagosomes involves fusion with endosomes to contribute to form amphisomes which eventually will fuse with lysosomes [41].
However, percent distributions of both RGL2 (Figure 5B) and RalB (Figure 5C) within compartments were overall mildly affected by autophagy, with only two noticeable effects: autophagy induction stimulated RGL2 association to recycling endosomes in normal cells, but not in Ras-transformed cells; RalB dissociated from early endosomes during autophagy

in normal cells, but not in Ras-transformed cells. As consequence, upon autophagy, when comparing normal and transformed cells, RGL2 and RalB were more present at early endosomes, and RGL2 was less present at recycling endosomes and autophagosomes, in HEK- HT-H-RasV12 cells as compared to normal HEK-HT cells. Taken together, these observations show that autophagy induces a profound reorganization of endomembranes, as expected, and subtle changes in RGL2 and RalB localizations which might contribute to the autophagy process.

RalB activation at endomembranes and its modulation by autophagy

In order to assess the activation status of RalB molecules at endomembranes, we used a FRET- based RalB biosensor [42] that monitors the balance of RalGEF (Guanine Nucleotide Exchange Factor) and RalGAP (GTPase Activating Proteins) activities. We measured RalB activity in the entire cell and at selected cellular localizations: at cell edge (5μm-wide band, mainly reflecting activity at plasma-membrane), at early endosomes, recycling endosomes, and autophagosomes, segmented as previously with specific markers (RFP-Rab5A, mCherry-Rab11, and mCherry- LC3) (Figure 6).

Interestingly, in rich basal medium, RalB was equally activated at cell edge (i.e. plasma-membrane) and at endosomes, but less activated at autophagosomes, in normal cells, while in transformed cells RalB was also activated at autophagosomes (Figure 6B), indicating that the axis RGL2-RalB is more active at autophagosomes in transformed as compared to normal cells. Ras-transformed HEK-HT-H-RasV12 cells have been previously reported to have higher RalB- GTP levels than parental HEK-HT cells by biochemical pull-down assay [43]. Consistently, the FRET-based RalB biosensor monitored higher RalB activity in entire HEK-HT-H-RasV12 cells, and also at cell edges and at autophagosomes, but not at endosomes, as compared with HEK-HT cells (Figure 6C).

When autophagy was induced by starvation (in EBSS medium), we observed a substantial increase of RalB activity at autophagosomes in normal HEK-HT cells, but not in transformed HEK-HT-H-RasV12 cells, probably because in these cells RalB activity was already high at basal level, maybe saturated. No significant changes were observed in normal cells for the other subcellular localizations. In transformed cells, upon autophagy, a slight decrease of RalB activity was detected in all locations except autophagosomes (Figure 6C). Taken together, these results support the relevance of keeping RalB active, specifically at autophagosomes, for the autophagy process.

DISCUSSION

This study reveals that, beyond the expected signaling at the plasma-membrane, a signaling path goes from Ras to RalB via RGL2 at endomembranes. A detailed spatial quantification of this intracellular signaling was possible by exploiting a novel method (Pro@EMC) to evaluate protein localizations at endomembrane compartments. The main advantage of Pro@EMC over the existing methods is that it quantifies the localization of a protein of interest at specific compartments with respect to randomly generated pseudo-compartments, correcting for co- localization occurring by chance and thus allowing robust statistics even on not obvious images. Moreover, the analysis task is fully automated by the use of a biologist-friendly free-access plugin in the ImageJ environment.

Our finding that both RGL2 and RalB substantially localize at early endosomes, recycling endosomes, and autophagosomes, supports the notion of the existence of an active RGL2-RalB signaling axis at these subcellular localizations. A previous study showed that exogenous RGL2 localized at endosomes, where it could activate RalA to promote exocytosis [36]; however, the implication of RalB was not explored. Taking into account the established role of RalB in promoting autophagy [26,27], the presence of RGL2 at autophagosomes was particularly interesting. Indeed, by a RNAi approach, we found that RGL2 was required for efficient starvation-induced autophagy in Hela and HEK-HT cells, indicating that RGL2 is a key RalGEF for activation of RalB during autophagy.

We observed that starvation-induced autophagy leads to a detectable increase of RalB activity at autophagosomes in normal HEK-HT cells, as assessed by a FRET-based biosensor. On the other hand, the increase of autophagosomes number upon starvation was associated with a considerable reduction of early and recycling endosomes, while the association of both RGL2 and RalB to the various endomembranes was only mildly affected. The biogenesis of autophagosomes is very complex and clearly involves contributions from several membrane compartments [44,45]. We speculate that the fusion of endosomes (carrying RGL2 and RalB molecules) with autophagosome forming compartments might be sufficient to locally increase RGL2-RalB pool at autophagosomes and might contribute to amplify RalB signaling to support autophagy.

In conclusion, this works shows that RalB signaling occurs not only at the plasma-membrane but also at endomembranes. We previously demonstrated that activation of RalB by RGL2 at plasma-membrane leads to protrusions and invasiveness [25]. Here, we provide evidences suggesting that activation of RalB by RGL2 at autophagosomes might contribute to autophagy. Activation of RalB by RGL2 at endosomes might participate to other functions that will need to be further investigated. The spatial control of RalB localization and activity is very likely the key to understand its functional versatility.

MATERIALS AND METHOD

List of plasmids

pCherry-Rab6 (Bruno Goud lab, Institut Curie)
pRFP-Rab5A (Bruno Goud lab, Institut Curie)
pEGFP-Rab11A (Clontech pEGFP-C1 vector backbone) (Bruno Goud lab, Institut Curie)
pCDNA3- RalB FRET Biosensor [34]
pLVXW-mCherry-LC3
pCherry-Rab11 (Clontech pEGFP-C1 vector backbone) (Bruno Goud lab, Institut Curie)

List of siRNAs

siRNA name	Target sense sequence
siControl	ON-TARGET plus Non-targeting siRNA #1 (Dharmacon)
siRalGDS_utr	5'-AACCAGAGGACUAGCUGACUU-3'
siRGL1_300	5'-CCAUAAUACAGCUCCUAAATT-3'
siRGL2_2296	5'-GGAUGGAGCUUCACACGAUTT-3'
siRGL2_2272	5’-GCUAAUGUAUUCUACGCCATT-3’
siRGL2_2333	5'-CGAAGGUCCUCUACUGCUATT-3'
siRGL3_1354	5'- ACACAGCCCUGCCGGAUAU -3'
siGPS1_ups1	5'-GAACAAAGAUCCAAUCAGA-3'
siRalGPS2_231	5'-GAUUCAGCAUACCCAUCAA-3'
siRalB_107	5'-UGACGAGUUUGUAGAAGAC-3'

List of reagents

Reagent	Manufacturer	Catalogue #
Dulbecco’s modified Eagle’s medium	GE Healthcare	SH30081.01
Earle's Balanced Salt Solution	Gibco- Life technologies	24010043
Phosphate-buffered saline	Gibco- Life technologies	10010015
L-Glutamine	Gibco- Life technologies	25030024
Penicillin-Streptomycin	Gibco- Life technologies	15140122
Fetal Bovine Serum	Biosera	FB-1003/500
Sodium Pyruvate	Gibco- Life technologies	11360070
Hygromycin B Gold	InvivoGen	ant-hg
Zeocin	InvivoGen	ant-zn

Geneticin	Gibco- Life technologies	10131035
Puromycin	InvivoGen	ant-pr
Paraformaldehyde	Electron Microscopy Sciences	15710
Glycine	Invitrogen	15527013
Triton X-100	Euromedex	2000-C
Bovine Serum Albumin	Euromedex	04-100-812-C
jetPRIME transfection buffer	Polyplus	712-60
jetPRIME transfection reagent	Polyplus	114-07
Fluoromount-G	Southern biotech	0100-01
Lipofectamine™ RNAiMAX transfection reagent	Thermo Fisher Scientific	13778150
Opti-MEM	Gibco	31985062
Protease inhibitor cocktail	Roche	0589291001

List of antibodies

Antibody	**Manufacturer**	**Catalogue #**	**Dilution**
Mouse monoclonal anti-RalB antibody (clone 4D1)	Sigma-Aldrich	WH0005899M4	1:200 (IF) 1:1000 (WB)
Mouse monoclonal anti-RGL2 antibody (clone 4D10)	Novus biologicals	H00005863-M02	1:200 (IF) 1:1000 (WB)
Rabbit polyclonal anti-EEA1 antibody	Calbiochem	324610	1:200 (IF)
Goat anti-mouse secondary antibody AF488	Life technologies	A-11029	1:500 (IF)
Goat anti-mouse secondary antibody AF546	Life technologies	A-11030	1:500 (IF)
Goat anti-rabbit secondary antibody FITC	Invitrogen	F-2765	1:500 (IF)
Rabbit polyclonal anti-LC3B antibody	Cell Signaling	2775	1:1000 (WB)
Mouse monoclonal anti-β-Actin antibody (clone AC-74)	Sigma-Aldrich	A2228	1:10000 (WB)
Goat anti-mouse HRP-conjugated secondary antibody	Jackson immuno research laboratories	115-035-003	1:12000 (WB)
Goat anti-rabbit HRP-conjugated secondary antibody	Jackson immuno research laboratories	111-035-114	1:12000 (WB)
IRDye-conjugated secondary antibodies	LI-COR Biosciences	NA	1:12000 (WB)

Cell culture, transfections, RT-qPCR

HEK-HT and HEK-HT-H-RasV12 cells [32, 33] were obtained from Chris Counter laboratory. Cells were cultured at 37°C with 5% CO2 in DMEM media containing 10% FBS, 1% Sodium Pyruvate, 1% Penicillin-Streptomycin and 1% L-Glutamine. Hygromycin (100 μg/mL) and Geneticin (400 μg/mL) were added in HEK-HT cell culture media. Hygromycin, Geneticin, and Zeocin (300 μg/μL) were added in HEK-HT-H-RasV12 cell culture media. Puromycin (0.5 μg/mL) was added in culture media of cells stably expressing iRFP-LC3 constructed via lentivirus infection. To induce autophagy, cells were starved for 4 hrs in EBSS serum and amino acid free media.

Cells were transfected with DNAs using jetPRIME transfection reagent according to manufacturer's protocol. Cells were seeded in 6-well plates at 0.5 x 10^6 cells per well; 24 hrs later, transfection mix containing 2 μg plasmid DNA, 200 μL of jetPRIME buffer, and 4 μL of jetPRIME reagent were added dropwise to the cells; media were changed 4 hrs later. Cells were used for experiments 24 hrs after DNA transfection.

Cells were transfected with siRNAs using Lipofectamine™ RNAiMAX transfection reagent according to manufacturer's protocol. Typically cells were seeded in 6-well plate at 2.5 x 10^5 cells per well; 24 hrs later, the transfection mix containing 3 uL Lipofectamine™ RNAiMAX, and 10 nM of siRNA, in 500 μl opti-MEM, was prepared, incubated 20 min at room temperature, and added to each well, followed by 2 mL culture medium per well; medium was changed 24 hrs later and experiments were performed 48 or 72 hrs after siRNA transfection.

RT-qPCR protocols and primers for the six RalGEFs have been described previously [46].

Western blotting

Cell were lysed at 4°C in lysis buffer (50 mM Tris-HCl pH 8.0, 150 mM NaCl, 0.5% sodium deoxycholate, 0.1% SDS, 0.5% Triton X-100, freshly supplemented with 1 mM DTT and protease inhibitor cocktail). Laemmli buffer was then added to the whole cell lysate and boiled at 95°C for 10 min. Whole cell lysate was loaded on Novex NuPAGE 10% Bis-Tris (# NP0301BOX) and transferred on 0.45 μm nitrocellulose membranes. Blocking was done with 5% BSA in TBS-tween for 30 min at RT. Membranes were incubated with primary antibodiesovernight at 4°C and, after washes, with secondary antibodies for 1hr at RT. Detection was performed alternatively with enhanced chemiluminescence method (Western Lightning Plus- ECL, PerkinElmer) when using HRP-conjugated secondary antibodies or with the LICOR Odyssey Infrared Imaging System (LI-COR Biosciences) when using RDye-conjugated secondary antibodies.

Immunofluorescence

Cells were cultured on coverslips for 24 hours, washed trice with Phosphate-buffered saline (PBS), and then fixed using 4% paraformaldehyde in PBS at room temperature (RT) for 10 minutes followed by 3 washes in PBS. Cells were incubated for 3 minutes at RT in 1M Glycine solution to avoid quenching followed by 3 washes in PBS. Cells were permeabilized using 0.1% of Triton-100X in PBS for 10 min at RT and washed trice with PBS. To block not-specific binding sites, cells were incubated at RT for 45 min in PBS with 4% FBS and 1% BSA (blocking buffer). Cells were incubated with primary antibody diluted in blocking buffer for 1 hr at RT. Cells were washed with PBS and incubated with secondary antibody diluted in blocking buffer for 1 hr at RT followed by 3 washes in PBS. Coverslips were dried and then mounted on slide using Fluoromount-G mounting media.

Immunofluorescent samples were imaged using a laser scanning confocal microscope LSM 710 NLO (Zeiss, Jena, Germany) equipped with 63×/1.4NA oil-immersion objective (Zeiss). An Argon 488 laser 40mW (Green), DPSS laser 561 20mW (Red), and Helium-Neon 633 (Far red) were used to excite Alexa Fluor 488, Alexa Fluor 561, and iRFP fluorophores respectively. Samples were visualized on standard photomultiplier tube (PMT) detector.

FRET measurements

Cells were plated on 35-mm glass bottom dishes (Mattek, Cat. No. # P35G-0.170-14-C) and were transiently transfected with a plasmid expressing a RalB FRET biosensor [34]. Images were acquired using a Leica DMIRE2 inverted microscope equipped with 63x objective with 1.32 NA. Samples were excited in CFP channel (430 nm) and both CFP emission (480 nm) and FRET emission (530 nm) were recorded. Binning of 2x2 for early endosomes, recycling endosomes and 3x3 binning for autophagosomes were used. FRET analysis was carried out using ImageJ software. First, the background was subtracted using a region outside the cell. Then the image was segmented manually and FRET/CFP ratio was depicted using ratiometric image with fire color code. Calibration bar represents the FRET ratio. Whole segmented cells were used to represent the FRET ratio in entire cell. A 5 μm-wide band from the cell periphery was segmented to measure the FRET ratio at the cell edges. To measure FRET in endomembrane compartments, the endomembrane compartments were first segmented using co-transfected specific markers (RFP-Rab5A, mCherry-Rab11, and mCherry-LC3), then FRET ratio were measured in these regions.

Image Processing with Pro@EMC plugin

The Pro@EMC method was developed to be used with ImageJ software [47] (https://imagej.nih.gov/ij/). The plugin can be downloaded from: https://github.com/mformanu9/PROatEMC.git
The execution of Pro@EMC plugin pops up a window that asks user to enter some parameters such as pixel size, approximate size of endomembrane compartments, numbers of randomized compartments, input and out folder path. The input image for Pro@EMC is a dual channel image in which one channel corresponds to protein of interest and the other channel to endomembrane compartments. A region of interest (ROI) is manually selected by the user of dimension 300x300 pixel, aiming at including most of the endomembrane compartments. To segment the endomembrane compartments Gaussian blur filter is used followed by thresholding. Morphological operations such as fill holes and close are used to refine image. Subsequently, analyze particle tool is used to discard the unwanted objects with very small size. Once the endomembrane compartments are identified, the mean intensity in the ROI in the protein channel is measured. Then the mean intensity of the protein of interest is measured at each segmented compartment. The results of these measurements (area, mean intensity, standard deviation) are saved in a text file in the destination folder. In parallel, user defined number of randomized pseudo-compartments are created, with a size comparable to that of the endomembrane compartments under investigation. The results of these measurements (area, mean intensity, standard deviation) are saved in another text file in the destination folder. Finally, the mean intensity of the protein of interest at each endomembrane compartment is compared to its mean intensity in the entire ROI. To qualify as an endomembrane compartment positive for the protein of interest, the mean intensity of the endomembrane compartment must be higher than the sum of mean and standard deviation (mean+1 fold SD) of protein intensity in the entire ROI.

Statistical analysis

Results are shown as mean ± standard error of the mean (SEM). Graphs were created and statistical analysis was performed using Graphpad Prism (v5.0). All the tests were performed using Mann Whitney test. P value less than 0.05 or 0.01 were considered significant, depending on the experiments, as indicated in legends.

ACKNOWLEDGEMENTS

We thank the Cell and Tissue Imaging (PICT-IBiSA) platform, Institut Curie, member of the French National Research Infrastructure France-BioImaging (ANR10-INBS-04). This work was supported by Fondation ARC pour la Recherche sur le Cancer (PJA 20151203371), Institut national de la Santé et de la Recherche médicale (INSERM ITMO Plan Cancer 2014-2018, PC201530), and Association Christelle Bouillot.

REFERENCES

1. Gentry LR, Martin TD, Reiner DJ, Der CJ. Ral small GTPase signaling and oncogenesis: More than just 15minutes of fame. Biochim Biophys Acta 2014; 1843:2976–88.
2. Neel NF, Martin TD, Stratford JK, Zand TP, Reiner DJ, Der CJ. The RalGEF-Ral Effector Signaling Network: The Road Less Traveled for Anti-Ras Drug Discovery. Genes Cancer 2011; 2:275–87.
3. Hamad NM, Elconin JH, Karnoub AE, Bai W, Rich JN, Abraham RT, Der CJ, Counter CM. Distinct requirements for Ras oncogenesis in human versus mouse cells. Genes Dev 2002; 16:2045–57.
4. Simanshu DK, Nissley DV, McCormick F. RAS Proteins and Their Regulators in Human Disease. Cell 2017; 170:17–33.
5. Yan C, Theodorescu D. RAL GTPases: Biology and Potential as Therapeutic Targets in Cancer. Pharmacol Rev 2018; 70:1–11.
6. Rossé C, Hatzoglou A, Parrini M-C, White MA, Chavrier P, Camonis J. RalB mobilizes the exocyst to drive cell migration. Mol Cell Biol 2006; 26:727–34.
7. Oxford G, Owens CR, Titus BJ, Foreman TL, Herlevsen MC, Smith SC, Theodorescu D. RalA and RalB: antagonistic relatives in cancer cell migration. Cancer Res 2005; 65:7111– 20.
8. Lim K-H, O'Hayer K, Adam SJ, Kendall SD, Campbell PM, Der CJ, Counter CM. Divergent roles for RalA and RalB in malignant growth of human pancreatic carcinoma cells. Curr Biol CB 2006; 16:2385–94.
9. Parrini MC, Sadou-Dubourgnoux A, Aoki K, Kunida K, Biondini M, Hatzoglou A, Poullet P, Formstecher E, Yeaman C, Matsuda M, et al. SH3BP1, an exocyst-associated RhoGAP, inactivates Rac1 at the front to drive cell motility. Mol Cell 2011; 42:650–61.
10. Biondini M, Duclos G, Meyer-Schaller N, Silberzan P, Camonis J, Parrini MC. RalB regulates contractility-driven cancer dissemination upon TGFβ stimulation via the RhoGEF GEF-H1. Sci Rep 2015; 5:11759.
11. Biondini M, Sadou-Dubourgnoux A, Paul-Gilloteaux P, Zago G, Arslanhan MD, Waharte F, Formstecher E, Hertzog M, Yu J, Guerois R, et al. Direct interaction between exocyst and Wave complexes promotes cell protrusions and motility. J Cell Sci 2016; 129:3756–69.
12. Hyenne V, Apaydin A, Rodriguez D, Spiegelhalter C, Hoff-Yoessle S, Diem M, Tak S, Lefebvre O, Schwab Y, Goetz JG, et al. RAL-1 controls multivesicular body biogenesis and exosome secretion. J Cell Biol 2015; 211:27–37.
13. Mei K, Guo W. The exocyst complex. Curr Biol CB 2018; 28:R922–5.
14. Zago G, Biondini M, Camonis J, Parrini MC. A family affair: A Ral-exocyst-centered

network links Ras, Rac, Rho signaling to control cell migration. Small GTPases 2017; :1–8.
15. Bodemann BO, Orvedahl A, Cheng T, Ram RR, Ou Y-H, Formstecher E, Maiti M, Hazelett CC, Wauson EM, Balakireva M, et al. RalB and the exocyst mediate the cellular starvation response by direct activation of autophagosome assembly. Cell 2011; 144:253–67.
16. Martin TD, Chen X-W, Kaplan REW, Saltiel AR, Walker CL, Reiner DJ, Der CJ. Ral and Rheb GTPase activating proteins integrate mTOR and GTPase signaling in aging, autophagy, and tumor cell invasion. Mol Cell 2014; 53:209–20.
17. Joffre C, Dupont N, Hoa L, Gomez V, Pardo R, Gonçalves-Pimentel C, Achard P, Bettoun A, Meunier B, Bauvy C, et al. The Pro-apoptotic STK38 Kinase Is a New Beclin1 Partner Positively Regulating Autophagy. Curr Biol CB 2015; 25:2479–92.
18. Joffre C, Codogno P, Fanto M, Hergovich A, Camonis J. STK38 at the crossroad between autophagy and apoptosis. Autophagy 2016; 12:594–5.
19. Chien Y, Kim S, Bumeister R, Loo Y-M, Kwon SW, Johnson CL, Balakireva MG, Romeo Y, Kopelovich L, Gale M, et al. RalB GTPase-mediated activation of the IkappaB family kinase TBK1 couples innate immune signaling to tumor cell survival. Cell 2006; 127:157– 70.
20. Balakireva M, Rossé C, Langevin J, Chien Y, Gho M, Gonzy-Treboul G, Voegeling-Lemaire S, Aresta S, Lepesant J-A, Bellaiche Y, et al. The Ral/exocyst effector complex counters c- Jun N-terminal kinase-dependent apoptosis in Drosophila melanogaster. Mol Cell Biol 2006; 26:8953–63.
21. Cascone I, Selimoglu R, Ozdemir C, Del Nery E, Yeaman C, White M, Camonis J. Distinct roles of RalA and RalB in the progression of cytokinesis are supported by distinct RalGEFs. EMBO J 2008; 27:2375–87.
22. Kashatus DF, Lim K-H, Brady DC, Pershing NLK, Cox AD, Counter CM. RALA and RALBP1 regulate mitochondrial fission at mitosis. Nat Cell Biol 2011; 13:1108–15.
23. Neel NF, Rossman KL, Martin TD, Hayes TK, Yeh JJ, Der CJ. The RalB Small GTPase Mediates Formation of Invadopodia through a GTPase-Activating Protein-Independent Function of the RalBP1/RLIP76 Effector. Mol Cell Biol 2012; 32:1374–86.
24. Rybko VA, Knizhnik AV, Komelkov AV, Aushev VN, Trukhanova LS, Tchevkina EM. Different metastasis promotive potency of small G-proteins RalA and RalB in in vivo hamster tumor model. Cancer Cell Int 2011; 11:22.
25. Zago G, Veith I, Singh M, Fuhrmann L, De Beco S, Remorino A, Takaoka S, Palmeri M, Berger F, Brandon N, et al. RalB directly triggers invasion downstream Ras by mobilizing the Wave complex. eLife 2018; 7.
26. Bodemann BO, Orvedahl A, Cheng T, Ram RR, Ou Y-H, Formstecher E, Maiti M, Hazelett CC, Wauson EM, Balakireva M, et al. RalB and the exocyst mediate the cellular starvation response by direct activation of autophagosome assembly. Cell 2011; 144:253–67.
27. Simicek M, Lievens S, Laga M, Guzenko D, Aushev VN, Kalev P, Baietti MF, Strelkov SV, Gevaert K, Tavernier J, et al. The deubiquitylase USP33 discriminates between RALB functions in autophagy and innate immune response. Nat Cell Biol 2013; 15:1220–30.
28. Gentry LR, Nishimura A, Cox AD, Martin TD, Tsygankov D, Nishida M, Elston TC, Der CJ. Divergent roles of CAAX motif-signaled posttranslational modifications in the regulation and subcellular localization of Ral GTPases. J Biol Chem 2015; 290:22851–61.
29. Martin TD, Mitin N, Cox AD, Yeh JJ, Der CJ. Phosphorylation by protein kinase Cα regulates RalB small GTPase protein activation, subcellular localization, and effector

utilization. J Biol Chem 2012; 287:14827–36.
30. Vigil D, Martin TD, Williams F, Yeh JJ, Campbell SL, Der CJ. Aberrant overexpression of the Rgl2 Ral small GTPase-specific guanine nucleotide exchange factor promotes pancreatic cancer growth through Ral-dependent and Ral-independent mechanisms. J Biol Chem 2010; 285:34729–40.
31. Bolte S, Cordelières FP. A guided tour into subcellular colocalization analysis in light microscopy. J Microsc 2006; 224:213–32.
32. Dunn KW, Kamocka MM, McDonald JH. A practical guide to evaluating colocalization in biological microscopy. Am J Physiol Cell Physiol 2011; 300:C723-742.
33. Manders EMM, Verbeek FJ, Aten JA. Measurement of co-localization of objects in dual-colour confocal images. J Microsc 1993; 169:375–82.
34. Adler J, Parmryd I. Quantifying colocalization by correlation: The Pearson correlation coefficient is superior to the Mander's overlap coefficient. Cytometry A 2010; 77A:733–42.
35. Klionsky DJ, Abdelmohsen K, Abe A, Abedin MJ, Abeliovich H, Acevedo Arozena A, Adachi H, Adams CM, Adams PD, Adeli K, et al. Guidelines for the use and interpretation of assays for monitoring autophagy (3rd edition). Autophagy 2016; 12:1–222.
36. Takaya A, Kamio T, Masuda M, Mochizuki N, Sawa H, Sato M, Nagashima K, Mizutani A, Matsuno A, Kiyokawa E, et al. R-Ras regulates exocytosis by Rgl2/Rlf-mediated activation of RalA on endosomes. Mol Biol Cell 2007; 18:1850–60.
37. Hahn WC, Counter CM, Lundberg AS, Beijersbergen RL, Brooks MW, Weinberg RA. Creation of human tumour cells with defined genetic elements. Nature 1999; 400:464–8.
38. O'Hayer KM, Counter CM. A genetically defined normal human somatic cell system to study ras oncogenesis in vivo and in vitro. Methods Enzymol 2006; 407:637–47.
39. Guo JY, Chen H-Y, Mathew R, Fan J, Strohecker AM, Karsli-Uzunbas G, Kamphorst JJ, Chen G, Lemons JMS, Karantza V, et al. Activated Ras requires autophagy to maintain oxidative metabolism and tumorigenesis. Genes Dev 2011; 25:460–70.
40. Yang S, Wang X, Contino G, Liesa M, Sahin E, Ying H, Bause A, Li Y, Stommel JM, Dell'antonio G, et al. Pancreatic cancers require autophagy for tumor growth. Genes Dev 2011; 25:717–29.
41. Simonsen A, Tooze SA. Coordination of membrane events during autophagy by multiple class III PI3-kinase complexes. J Cell Biol 2009; 186:773–82.
42. Martin TD, Chen X-W, Kaplan REW, Saltiel AR, Walker CL, Reiner DJ, Der CJ. Ral and Rheb GTPase activating proteins integrate mTOR and GTPase signaling in aging, autophagy, and tumor cell invasion. Mol Cell 2014; 53:209–20.
43. Bettoun A, Joffre C, Zago G, Surdez D, Vallerand D, Gundogdu R, Sharif AAD, Gomez M, Cascone I, Meunier B, et al. Mitochondrial clearance by the STK38 kinase supports oncogenic Ras-induced cell transformation. Oncotarget 2016; 7:44142–60.
44. Lamb CA, Yoshimori T, Tooze SA. The autophagosome: origins unknown, biogenesis complex. Nat Rev Mol Cell Biol 2013; 14:759–74.
45. Nascimbeni AC, Giordano F, Dupont N, Grasso D, Vaccaro MI, Codogno P, Morel E. ER- plasma membrane contact sites contribute to autophagosome biogenesis by regulation of local PI3P synthesis. EMBO J 2017; 36:2018–33.
46. O Santos A, Parrini MC, Camonis J. RalGPS2 Is Essential for Survival and Cell Cycle Progression of Lung Cancer Cells Independently of Its Established Substrates Ral GTPases. PloS One 2016; 11:e0154840.
47. Rueden CT, Schindelin J, Hiner MC, DeZonia BE, Walter AE, Arena ET, Eliceiri KW. ImageJ2: ImageJ for the next generation of scientific image data. BMC Bioinformatics 2017; 18:529.

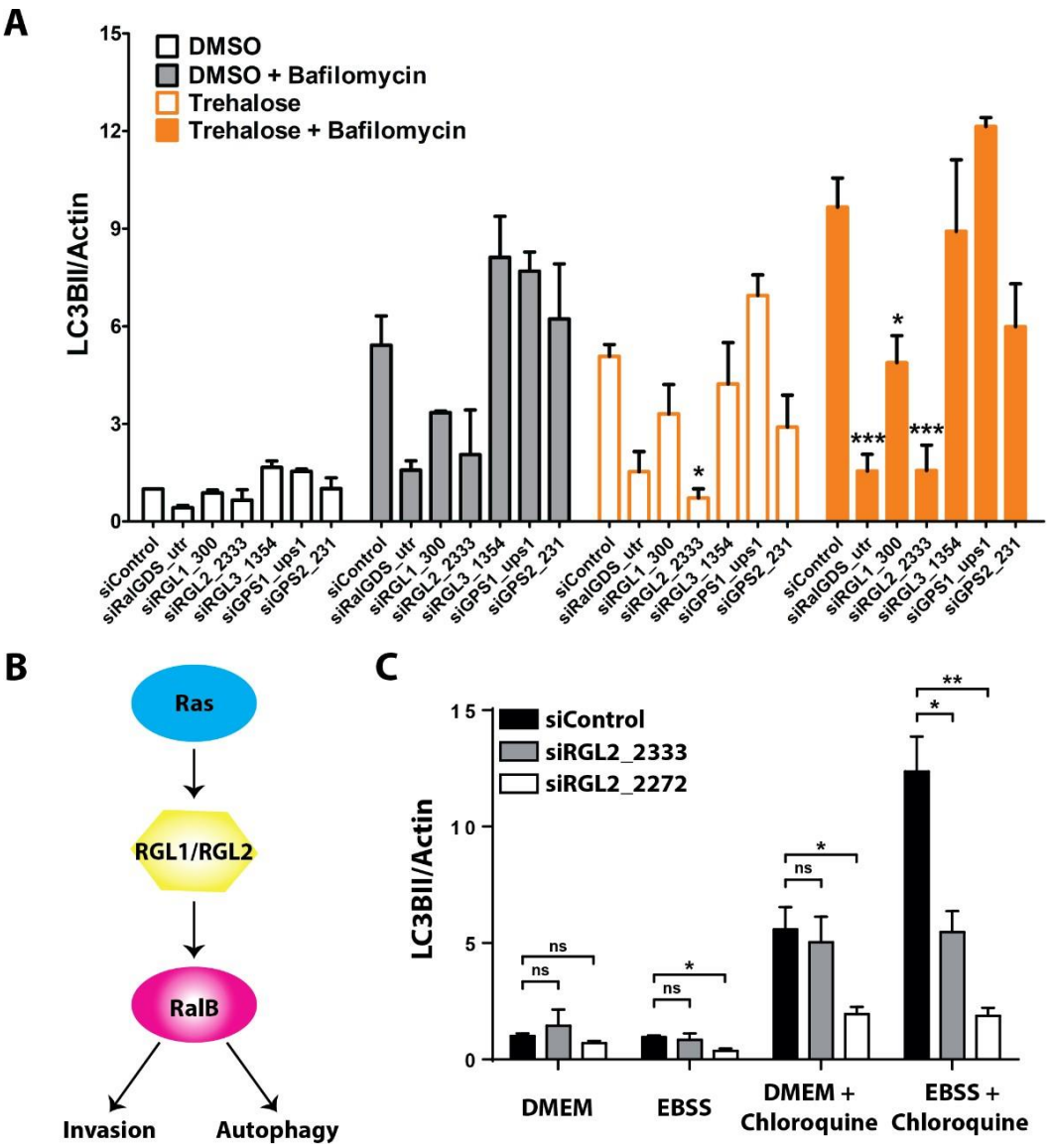

Figure 1. RGL2 to RalB signaling is required for autophagy.

(A) The RalGEFs' screen for autophagy. RalGDS, RGL1, and RGL2 are required for autophagy. Hela cells were depleted by siRNAs against each of the six RalGEFs. Trehalose (100mM for 16 hour) was used to induce autophagy. Bafilomycin (200 nM) was used to block autophagy flux. The LC3II/actin ratios were calculated and normalized for siControl condition. Graphs show the mean +/- SEM, from 2-3 experiments per condition. For statistics one-way ANOVA test was used to compare the siRNA RalGEF effects with the siControl of same culture condition. * $p<0.05$, ** $p<0.01$, *** $p<0.001$.

(B) RGL1 and RGL2 act down-stream Ras to activate RalB for both invasion and autophagy.

(C) RGL2 is required for autophagy in HEK-HT cells. HEK-HT cells were transiently transfected with indicated siRNAs. Nutrient-deprived medium (EBSS) for 4 hrs was used to induce autophagy. Chloroquine (50 µM) was used to block autophagy flux. Graphs show the mean +/- SEM, from 3 independent experiments per condition. For statistics Student's t test was used. * $p<0.05$, ** $p<0.01$, *** $p<0.001$, ns not-significant.

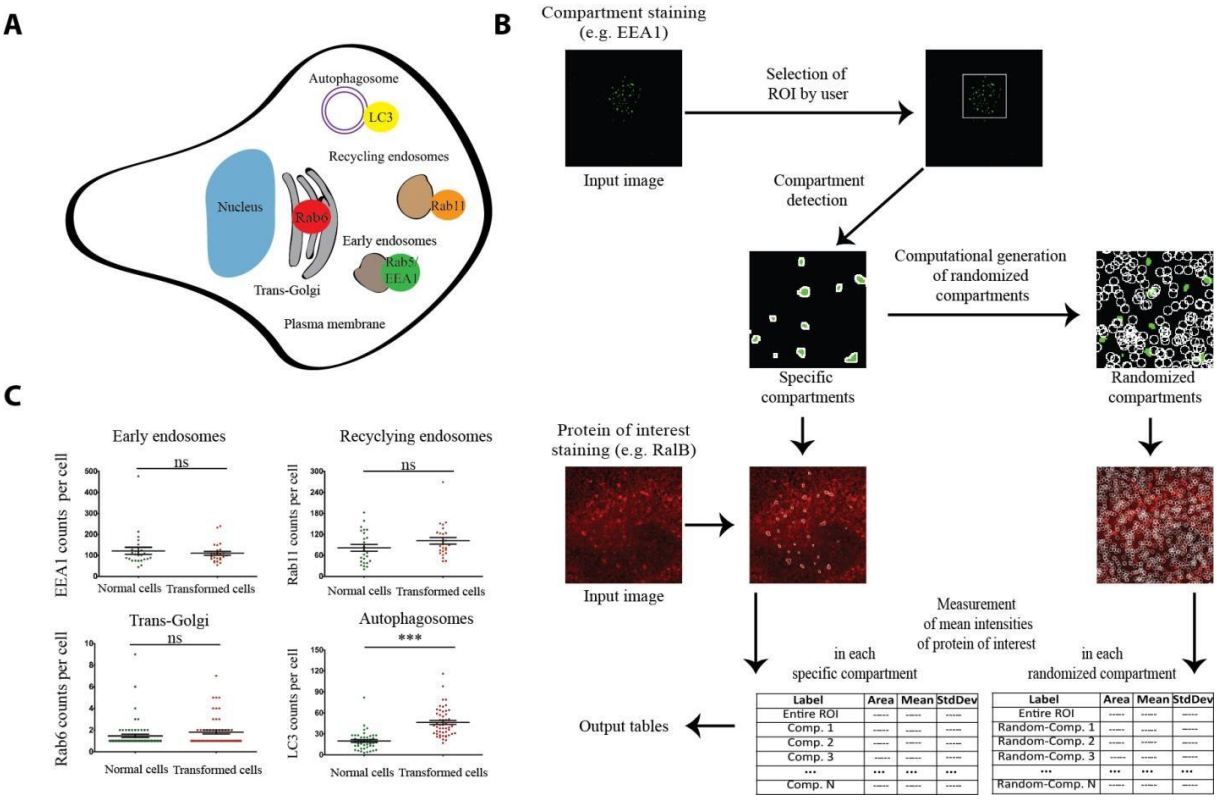

Figure 2. An automated image analysis method to quantify localization of proteins of interest at endomembrane compartments.

(A) The endomembrane compartments. Schematic representation of the different endomembrane compartments investigated in this study and their markers.

(B) Work-flow of the Pro@EMC ImageJ plug-in.

(C) Counts of different endomembrane compartments in HEK-HT (normal cells) and HEK-HT-H-RasV12 (transformed cells). Graph represents mean ± SEM of n > 35 cells from 4 independent experiments. Each dot corresponds to one cell. For statistics Mann Whitney test was used. ** p<0.01, *** p<0.001, ns not-significant.

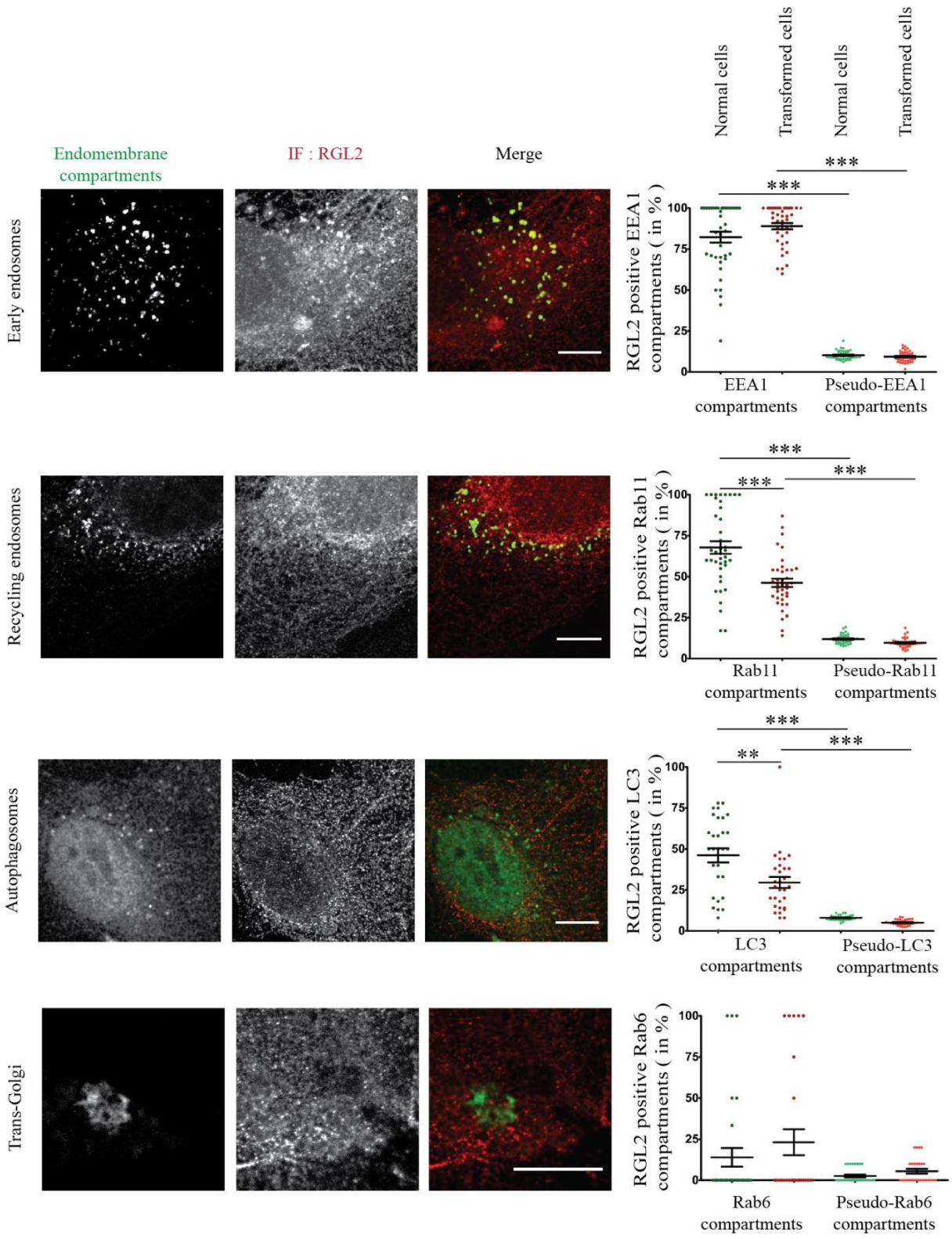

Figure 3. Localization of RGL2 at different endomembrane compartments.
HEK-HT (Normal cells) and HEK-HT-H-RasV12 (Transformed cells) cells were fixed and imaged for endogenous RGL2 (IF anti-RGL2, represented in red), together with EEA1 (early endosome marker, IF anti-EEA1, represented in green), GFP-Rab11 (recycling endosome marker, represented in green), GFP-Rab6 (Trans-Golgi marker, represented in green), or iRFP- LC3 (autophagosome marker, represented in green). Representative confocal cross sections of normal cells are shown (left). Quantifications

are reported for both normal and transformed cells (right). Localization was calculated as percentage (%) of the indicated endomembrane compartments positive for RGL2, as compared to the control pseudo-compartments. Each dot corresponds to one cell Graph represents mean ± SEM of 21 to 40 cells from 3-4 independent experiments. For statistics Mann Whitney test was used. ** p value <0.01, *** p value <0.001. Scale bars are 10 µm.

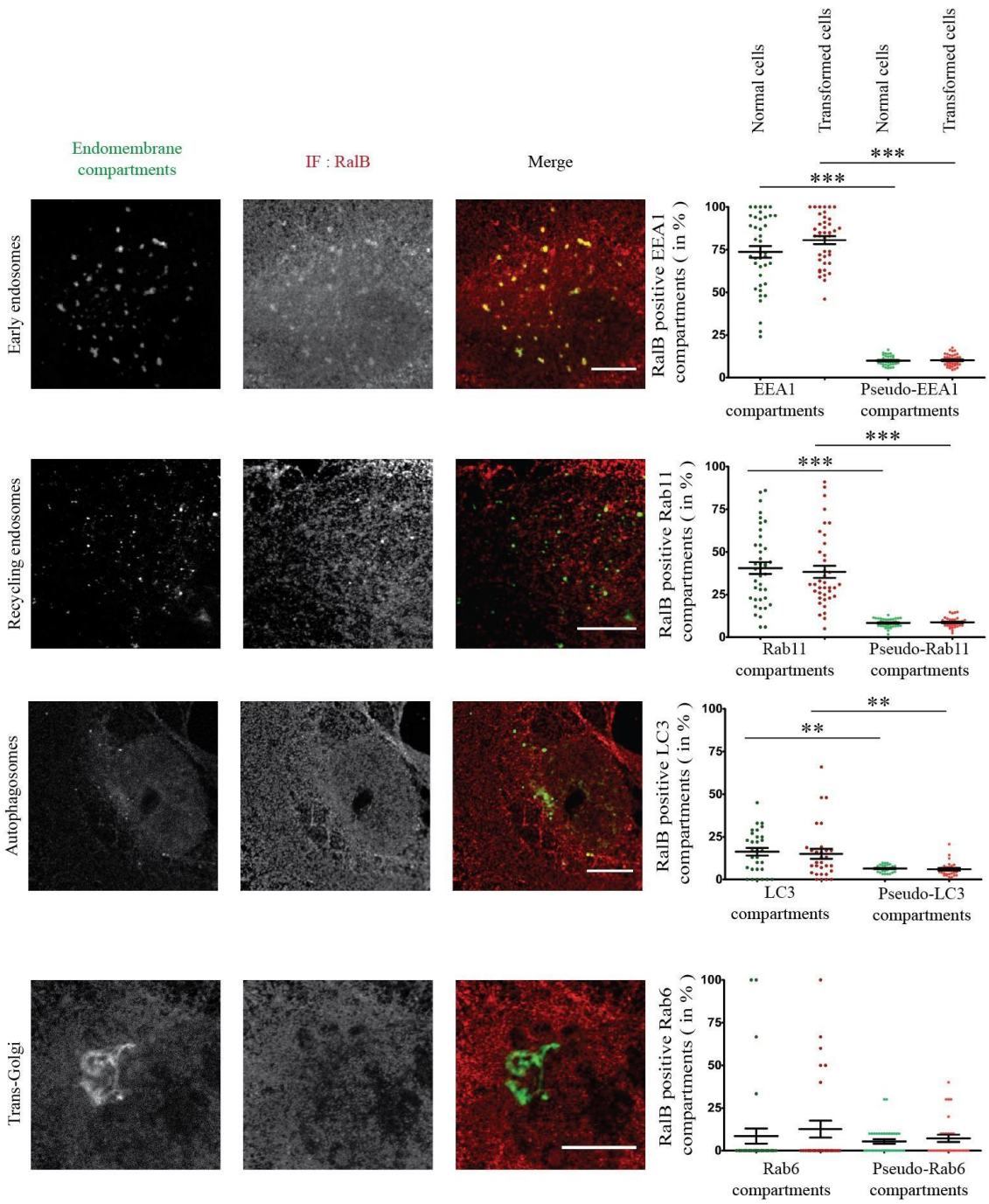

Figure 4. Localization of RalB at different endomembrane compartments.
HEK-HT (Normal cells) and HEK-HT-H-RasV12 (Transformed cells) cells were fixed and imaged for endogenous RalB (IF anti-RalB, represented in red in overlay images), together with EEA1 (early endosome marker, IF anti-EEA1, represented in green), GFP-Rab11 (recycling endosome marker, represented in green), GFP-Rab6 (Trans-Golgi marker, represented in green), or iRFP-LC3 (autophagosome marker, represented in green). Representative confocal cross sections of normal cells are shown (left). Quantifications are reported for both normal and transformed cells (right). Localization was calculated as percentage (%) of the indicated endomembrane compartments positive for RalB, as compared to control pseudo-compartments. Each dot corresponds to one cell. Graph represents mean ± SEM of 21 to 40 cells from 3-4 independent experiments. For statistics Mann Whitney test was used. ** p value <0.01, *** p value <0.001. Scale bars are 10 µm.

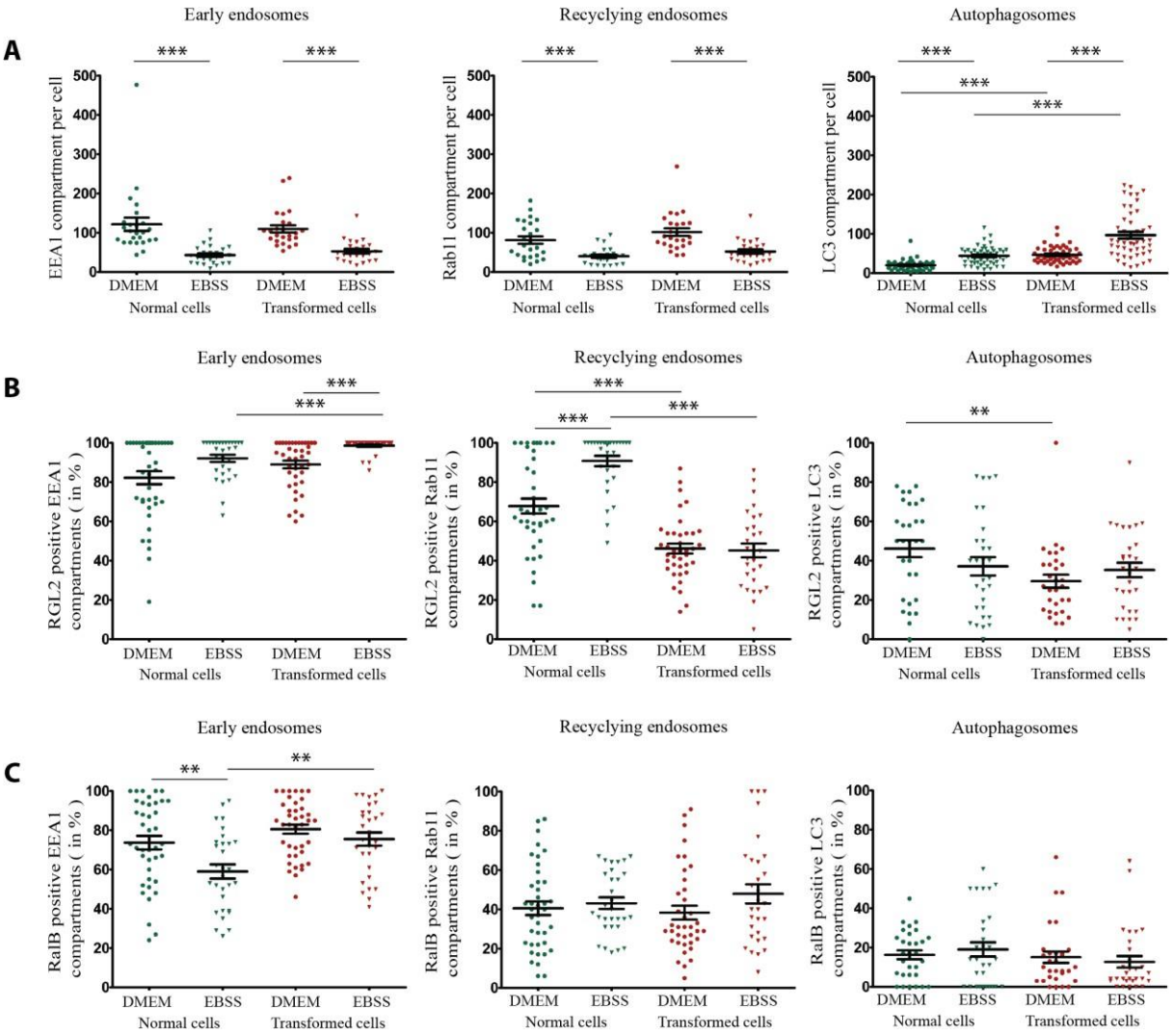

Figure 5. Modulation by autophagy of endomembrane compartments and of RGL2 and RalB localization.

(A) Modulation by autophagy of endomembrane compartments. The different endomembrane compartments were counted in HEK-HT (Normal cells) and HEK-HT-H-RasV12 (Transformed cells), in basal (DMEM) and starvation (EBSS) condition. To allow comparison DMEM versus EBSS, the same counts in basal conditions of Figure 2C were reported also here.

(B) Modulation by autophagy of RGL2 localization at endomembranes. Normal and transformed cells were incubated in either basal (DMEM) or starvation (EBSS) medium (4 hours) before fixation. To allow comparison DMEM versus EBSS, the same measurements in basal conditions of Figure 3 were reported also here.

(C) Modulation by autophagy of RalB localization at endomembranes. Normal and transformed cells were incubated in either basal (DMEM) or starvation (EBSS) medium (4 hours) before fixation. To allow comparison DMEM versus EBSS, the same measurements in basal conditions of Figure 4 were reported also here.

Graph represents mean ± SEM of 21 to 40 cells from 4 independent experiments. For statistics Mann Whitney test was used. ** p value <0.01, *** p value <0.001.

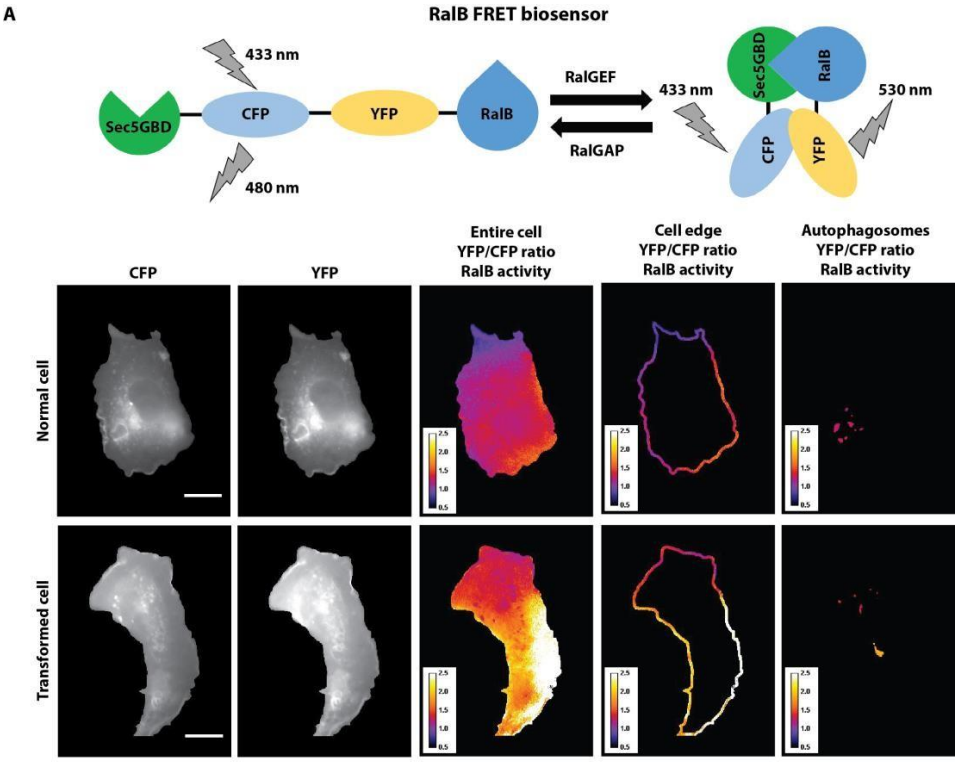
A
RalB FRET biosensor
433 nm
Sec5GBD
CFP
YFP
RalB
480 nm
RalGEF
RalGAP
433 nm
530 nm
CFP
YFP
Entire cell YFP/CFP ratio RalB activity
Cell edge YFP/CFP ratio RalB activity
Autophagosomes YFP/CFP ratio RalB activity
Normal cell
Transformed cell

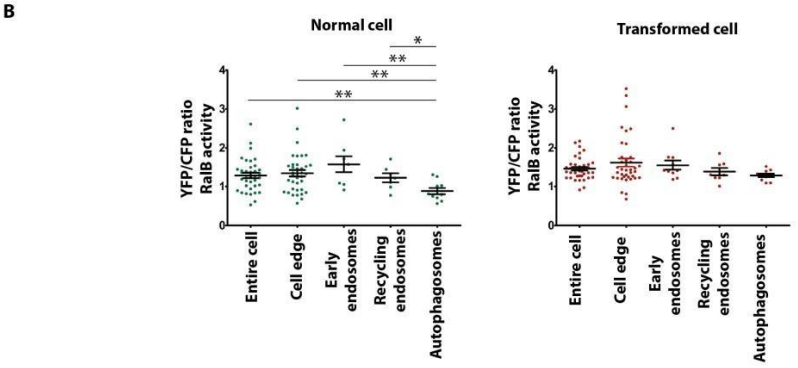
B
Normal cell
Transformed cell
YFP/CFP ratio RalB activity
Entire cell
Cell edge
Early endosomes
Recycling endosomes
Autophagosomes

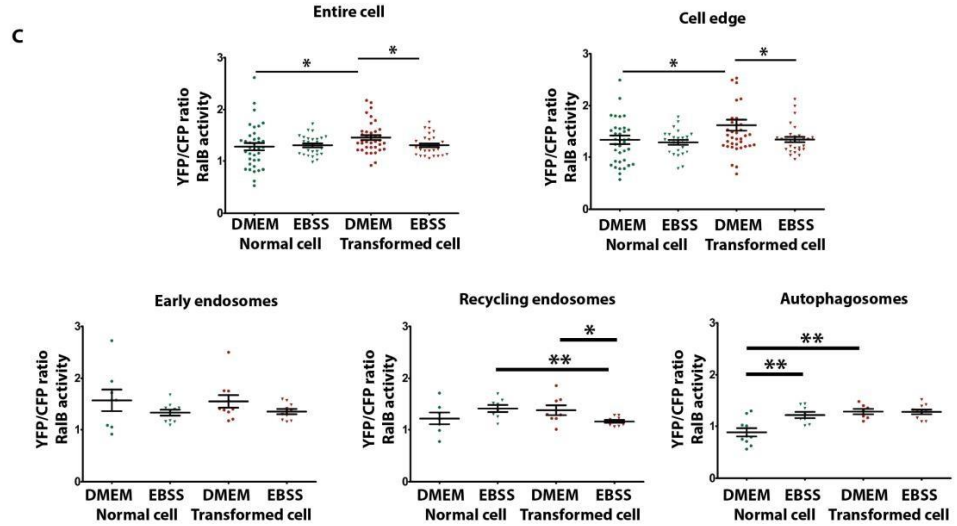
C
Entire cell
Cell edge
Early endosomes
Recycling endosomes
Autophagosomes
YFP/CFP ratio RalB activity
DMEM EBSS DMEM EBSS
Normal cell Transformed cell

Figure 6. Localization of RalB activity at different cellular compartments and its modulation by autophagy.

(A) Measurement of local RalB activities using a FRET-based biosensor. Representative HEK-HT and HEK-HT-H-RasV12 cells expressing a RalB FRET biosensor are shown in basal condition. FRET, measured by calculating the ratio of YFP to CFP intensity after subtracting background, is used as indicator of RalB activation at various subcellular locations. Representative ratiometric images (YFP/CFP) are represented with a color code for entire cell, cell edge (5µm–wide band) and autophagosomes.

(B) Comparison of RalB activity at various subcellular localizations, in HEK-HT cells and HEK-HT-H-RasV12 cells. Measurements of FRET ratio in normal HEK-HT and transformed HEK-HT-H-RasV12 cells in basal condition at different cellular compartments: entire cell, cell edges, early endosomes, recycling endosomes, and autophagosomes. Each dot corresponds to one cell.

(C) Modulation by autophagy of local RalB activities. Normal and transformed cells were incubated in either basal (DMEM) or starvation (EBSS) medium (4 hours) before fixation. To allow comparison DMEM versus EBSS, the same measurements in basal conditions of panel 6B were reported also here.

Graph represents mean ± SEM of n = 26 to 37 cells for entire cell and cell edges, and n= 7 to 10 cells for each endomembrane compartment, from 2 independent experiments. For statistics Mann Whitney test was used, * $p<0.05$, ** $p<0.01$, ***, and $p<0.001$. Scale bars are 20 µm.

SUPPLEMENTARY FIGURES

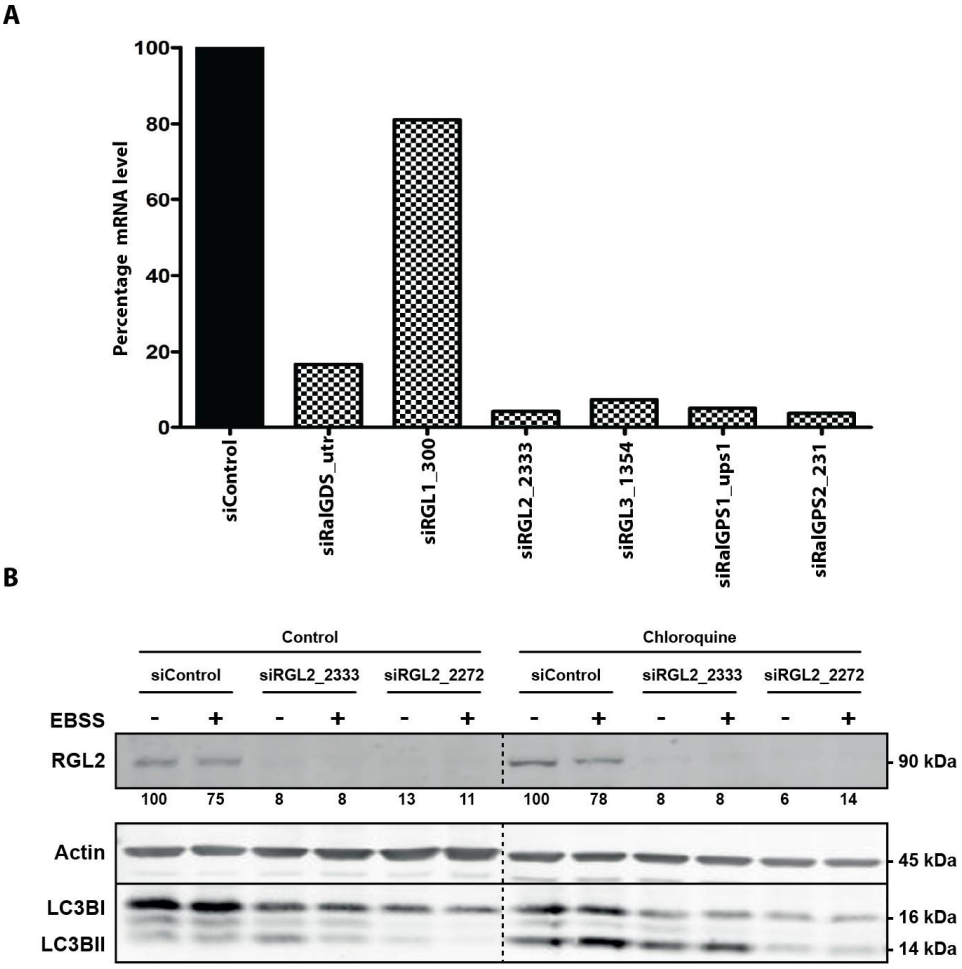

Figure S1. Validation of depletions by siRNAs.

(A) Validation of RalGEFs' depletion for autophagy screen in Hela cells. Depletion of mRNA levels is quantified by RT-qPCR for the six RALGEFs, in one experiment (n=1). Note that even if the depletion of RGL1 mRNA is modest, it is sufficient to impact on autophagy (Figure 1A). Depletions could not be validated by western-blots because specific, sensitive antibodies do not exist for RALGEFs (with the exception of RGL2).

(B) RGL2 depletions and LC3 conversion assay in HEK-HT cells. Representative western blots for RGL2, actin, LC3 from cell lysates of HEK-HT cells prepared 72 hrs after transfection with the indicated siRNAs. Quantifications of RGL2 protein depletion, normalized for siControl condition (=100), are shown below the WB.

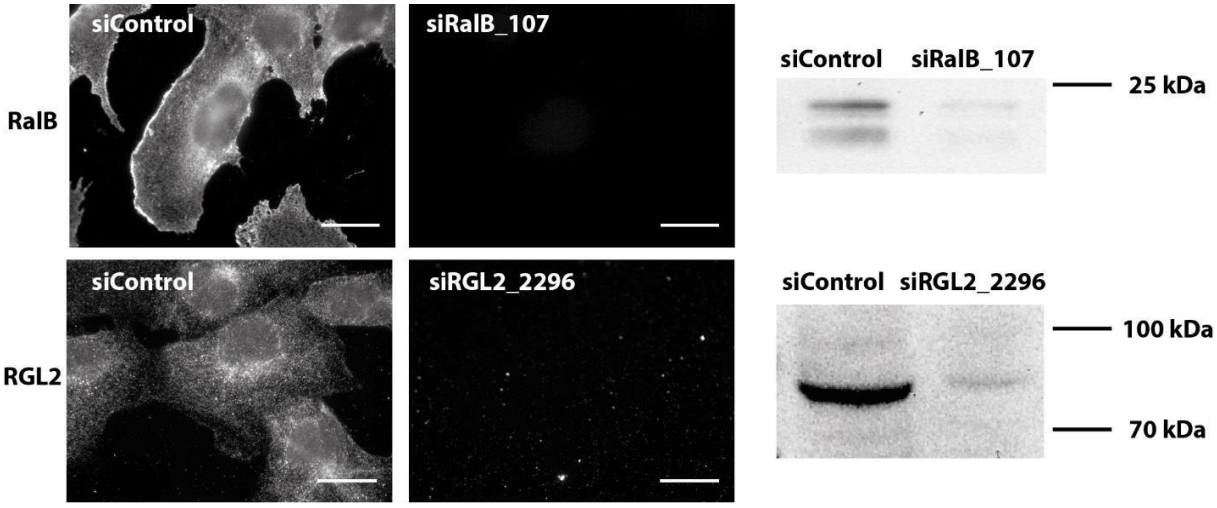

Figure S2. Validation of RGL2 and RalB antibodies for immune-fluorescence (IF) applications. Cell were transfected using non-targeting siControl, siRNA against RalB or siRNA against RGL2. Western blots show efficient protein depletions. Upon depletion of RalB or RGL2, there is a dramatic decrease of RalB or RGL2 IF signal, respectively, demonstrating the specificity of these antibodies and the reliability of the IF quantifications presented in this work. Scale bars are 20 µm.

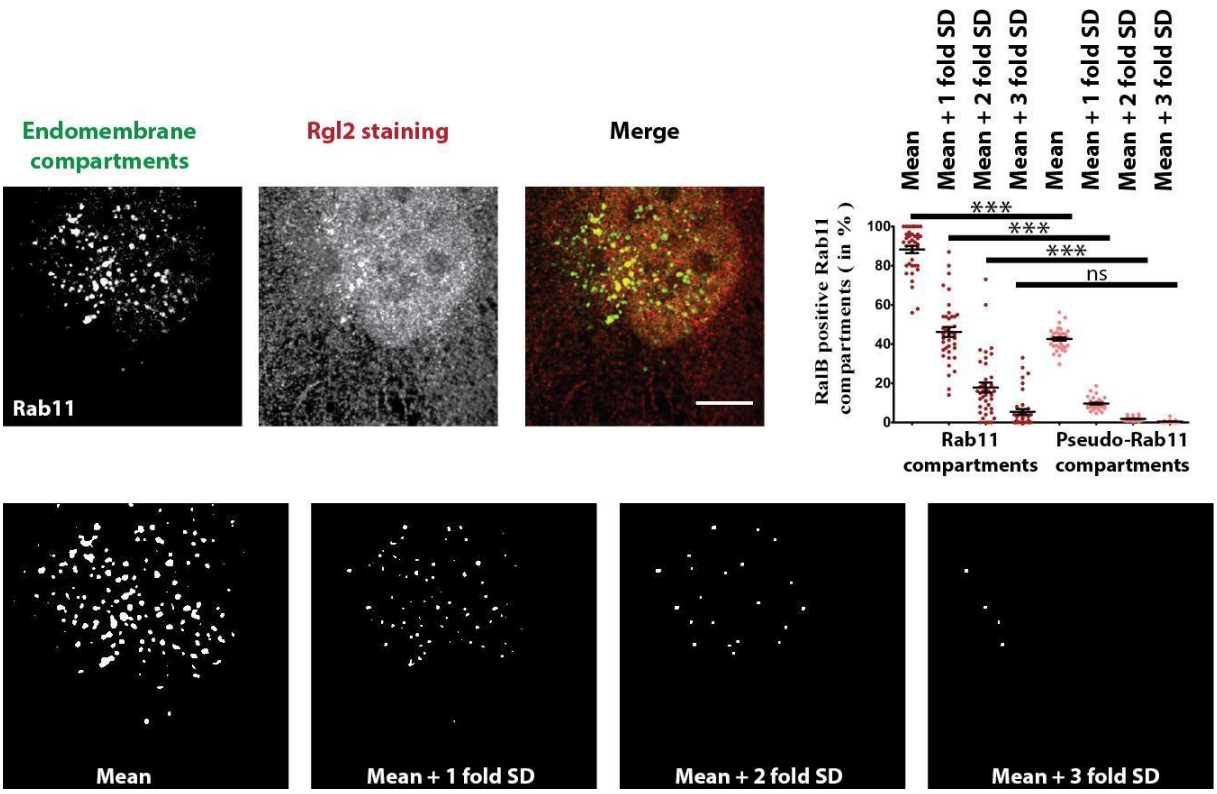

Figure S3. Comparison of thresholds to define positive compartment.
HEK-HT-H-RasV12 cells were transfected with GFP-Rab11 (marker of recycling endosomes), fixed and immunostained for RGL2. Representative confocal cross sections are shown (top left). The percentage (%) of Rab11 compartments positive for RGL2 as compared to the control pseudo-Rab11 compartments, is calculate using different thresholds: Mean (= mean RGL2 fluorescence intensity in segmented compartments), Mean + 1 fold Standard Deviation (SD), Mean + 2 folds SD, and Mean + 3 folds SD (top right). Bottom row depicts the loss of detection of recycling compartments with increase in threshold. Graph represents mean ± SEM of n = 39 cells from 4 independent experiments. For statistics Mann Whitney test was used. ** p value <0.01, *** p value <0.001. Scale bars are 10 µm.

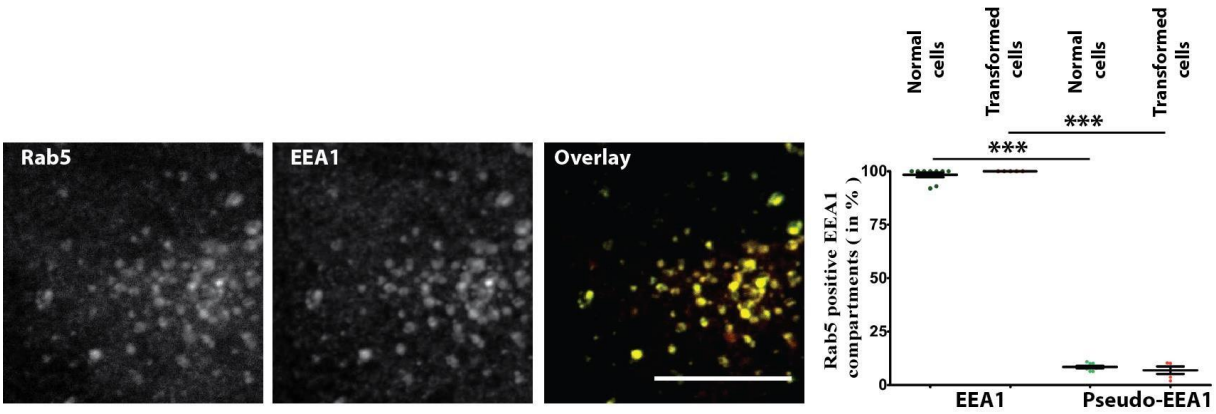

Figure S4. Validation of Pro@EMC analysis method using two different markers for the same compartment (early endosomes). HEK-HT (Normal cells) and HEK-HT-H-RasV12 (Transformed cells) were transfected with Rab5 (marker of early endosomes) and then stained with antibody against early endosomes (EEA1). Each dot corresponds to one cell. Quantification graph shows that virtually 100% of EEA1 compartments are positive for Rab5. Pseudo-EEA1 compartments are used as negative controls. Graph represents mean ± standard deviation of n = 5 to 10 cells. For statistics Mann Whitney test was used. ** p value < 0.01, *** p value < 0.001. Scale bars are 10 µm.

RASSF1A role in pro-invasive bronchial cells properties and proper cytokinesis via NDR2 control

Maureen Keller[1,2,#], Fatéméh Dubois[3,4,#], Sylvain Teulier[3], **Alexandre PJ Martin**[5], Jérôme Levallet[2], Elodie Maille[1,2], Solenn Brosseau[1,2,6], Nicolas Elie[7], Alexander Hergovich[8], Emmanuel Bergot[3,9], Jacques Camonis[5], Gérard Zalcman[5,6,*], Guénaëlle Levallet[3,4,*]

Manuscript under revision

[1] Normandie Université, UNICAEN, UMR 1086 INSERM, F-14032 Caen, France.
[2] Normandie Université, UNICAEN, UPRES-EA-2608, F-14032 Caen, France.
[3] Normandie Univ, UNICAEN, CEA, CNRS, ISTCT/CERVOxy group, F-14000 Caen, France, GIP CYCERON
[4] Service d'Anatomie et Cytologie Pathologique, CHU de Caen, F-14033 Caen. France
[5] U830 INSERM, "Génétique et Biologie des cancers" Centre de Recherche, Institut Curie, Paris, France
[6] Service d'oncologie thoracique, CIC 1425, Hôpital Bichat-Claude Bernard, AP-HP, Université Paris-Diderot
[7] Normandie Université, UNICAEN, SFR ICORE, Plateau CMABio3, F-14032 Caen. France
[8] University College London Cancer Institute, WC1E 6BT, London, United Kingdom.
[9] Service de Pneumologie & Oncologie thoracique, CHU de Caen, F-14033 Caen. France
[#] and [*] designed authors contributing respectively equally to this work.

Background of the project

RASSF1 is a tumor suppressor gene frequently inactivated in lung cancer leading to a YAP-dependent epithelial-mesenchymal transition (Dubois et al., 2016). A lot of efforts have been made in the past decades in order to understand the molecular events occurring around RASSF1. The team found that RASSF1 loss led to GEF-H1 inactivation (by phosphorylation on S885, partly), leading to RhoB inactivation that finally leads to YAP1 nuclear translocation with subsequent transcription of target genes associated with epithelial-mesenchymal transition and cell invasion/migration (see figure 35).

This work aims to identify the kinase leading to GEF-H1 inactivation in the context of RASSF1 depleted cells. The Hippo pathway kinases STK38 (aka NDR1) and STK38L (aka NDR2) attracted attention since they were previously reported to phosphorylate rabin8, a GEF for Rab GTPases, and also because GEF-H1 harbor a STK38/STK38L phosphorylation motif.

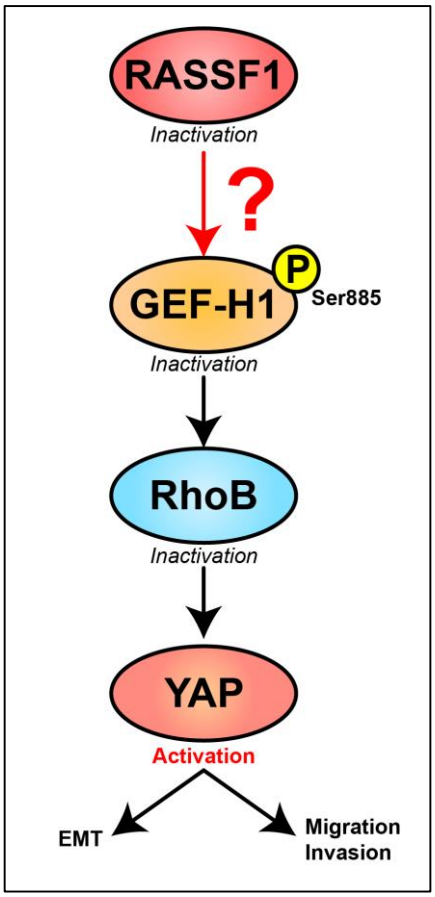

Figure 35 – Working hypothesis of the activation cascade implicated in YAP activation upon RASSF1 loss.

Summary of the results

STK38/STK38L kinases support the pro-tumoral properties induced by RASSF1 loss

In full agreement with previous work, we found that RASSF1 silencing resulted in increased cell migration and invasion (figure 1), increase that have been found severely impaired when silencing either STK38 or STK38L. Regarding the metastasis side of this story, we found that depletion of STK38 kinases (STK38 and STK38L) severely impaired tumor growth on xenografts. In addition, we found that STK38L, but not STK38, support the pro metastatic properties induced by RASSF1 (figure 1).

We then tested the contribution of STK38 kinases to the EMT undergone upon loss of RASSF1 and discovered that depletion of either STK38 or STK38L abolished mesenchymal markers expression (figure 2), supporting that inactivation of these kinases could prevent the EMT following loss of RASSF1.

Because the cell migration/invasion engendered by loss of RASSF1 was shown to be YAP-dependent (Dubois et al., 2016), we tested the contribution of STK38 and STK38L to YAP activation in this context. We found that both kinases supported the nuclear accumulation of YAP as well as the expression of its target genes (figure 3).

STK38L, the mediator resulting in GEF-H1 inactivation by phosphorylation

The above-described results prompted us to analyze whether STK38/STK38L kinases could be the intermediate effector responsible for GEF-H1 inactivation (by phosphorylation) upon RASSF1 loss, resulting in RhoB inactivation. To do so, we analyzed the activation status of GEF-H1, by following its S885 phosphorylation and found that silencing of STK38L, but not STK38, drastically reduced the phosphorylation of GEF-H1_S885 phosphorylation upon RASSF1 loss (figure 4). Because GEF-H1 is responsible of RhoB activation, by promoting GDP to GTP exchange, we analyzed if our kinases have also an impact on RhoB activation. We found that both STK38 and STK38L support RhoB activation upon RASSF1 loss (figure 4). Taken together, these results demonstrate that upon loss of RASSF1, STK38L could be the inactivator of GEFH1 (by phosphorylation), leading to RhoB inactivation.

In order to understand and characterize the molecular events occurring in this context, we then tested the direct contribution of STK38L to GEF-H1 inactivation. Using recombinant GST pull down assay, we found that GEF-H1 interacts with STK38L, but not with STK38 (figure 4). To go further, we found that GEF-H1 harbours a STK38/STK38L HxRxxS/T phosphorylation motif with the targeted amino acid being the serine 265. We discovered, using GEF-H1 mutants transfected into cells, that mutation of S265 into alanine, a non-phosphorylable mutant, abolished GEF-H1 phosphorylation of S885 (figure 4), suggesting that S265 phosphorylation is required for S885 phosphorylation, and thus GEF-H1 inactivation (see figure 36).

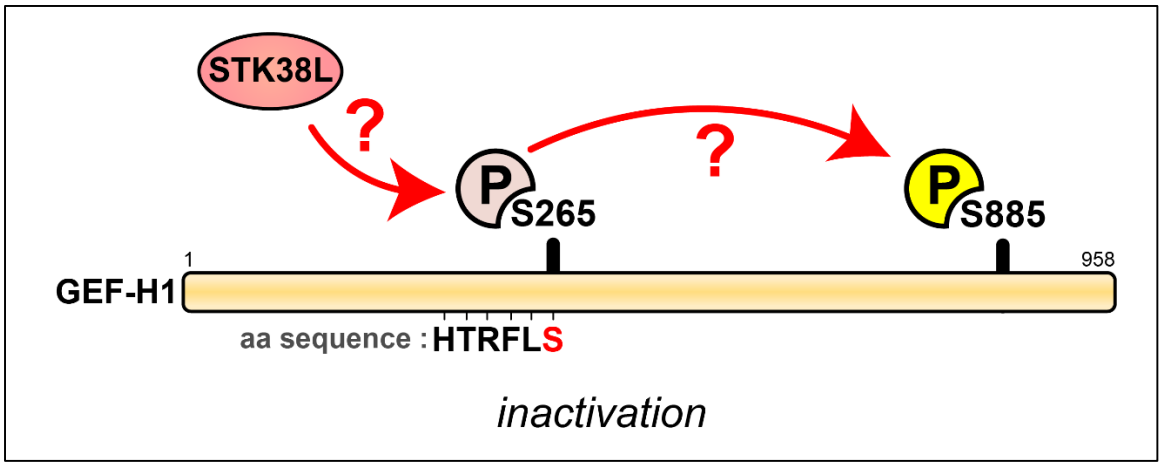

Figure 36 – Working hypothesis of GEF-H1 inactivation by specific phosphorylations.
In this hypothesis, the Hippo kinase STK38L phosphorylates S265 of GEF-H1, required for the subsequent phosphorylation of S885, leading to GEF-H1 inactivation.

We then sought for GEF-H1 S265 phosphorylation. Because there was no commercially available antibody against this specific phosphorylated amino acid, we choose to take advantage of mass spectrometry detection. Unfortunately, we failed to detect GEF-H1 phosphorylation on serine 265. This point will be detailed in the last section of this summary, regarding my specific contribution to this work.

RASSF1, GEF-H1, STK38L, and YAP are implicated in cytokinesis

RASSF1, STK38L, GEF-H1, and YAP have been reported to control cell division, but whether these proteins act together has never been investigated. In order to establish a direct link between these actors into this cellular mechanism, we started by studying the implication of the upper actor, RASSF1, in cell division. We found that RASSF1 loss leads to cytokinesis defect, in a YAP-dependent way (figure 5). We then analysed the contribution of STK38L and GEF-H1 to this process. We found that proper cytokinesis could be restored by overexpressing GEF-H1 in RASSF1 loss cells as well as silencing STK38L (figure 7). These results highlighted the RASSF1, STK38L, GEF-H1, YAP activation/deactivation cascade in this cellular process.

Discussion

In this work, we demonstrated that the metastatic effects attributed to RASSF1 loss in lung cancer cells act through a specific activation cascade. The tumor suppressor functions of RASSF1 would therefore pass via the inactivation the Hippo pathway kinase STK38L, that can be seen in this context as a pro tumoral effector, that leads to operational GEF-H1 and RhoB, resulting in the YAP terminal effector cytosolic sequestration.

As a general model, we propose that upon loss of RASSF1, STK38L gets activated and phosphorylates GEF-H1 on serine 265 with subsequent phosphorylation of serine 885, leading to GEF-H1 inactivation. This inactivation drives to RhoB inactivation resulting in YAP activation and phenotypes described in RASSF1 loss cells such as metastatic properties and cytokinesis defects. However, the hypothetic direct phosphorylation of GEF-H1 S265 by STK38L need to be further analyzed, either by kinase assay or by engineering a novel antibody raised against this specific phosphorylated amino acid.

My specific contribution to this project

When I took part of this project, it was in an advanced stage, and I already had an exquisite practice of large proteomics through intensive contacts with the INEM proteomic mass spectrometry platform, directed by Drs. Edelman and Guerrera, for my main project aiming to detect XPO1 phosphorylation by STK38 (see the results section). The PI of this project appealed to me for sample careful preparation in order to analyse GEF-H1 phosphorylation by STK38L using mass spectrometry.

To do so, I used H1299 lung cancer cell line exhibiting a RASSF1 complete silencing by hyper-methylation of its promoter. I transfected these cells with exogenous wild type GEF-H1 fused with GFP where STK38L (NDR2) was silenced, or not, with siRNA. I lysed the cells and performed a pull-down against GFP in order to enrich the exogenous GEF-H1. After ensuring an efficient STK38L (NDR2)

silencing as well as a good enrichment of GFP-GEF-H1 (see figure 37), I sent 4 mg of protein samples for mass spectrometry detection.

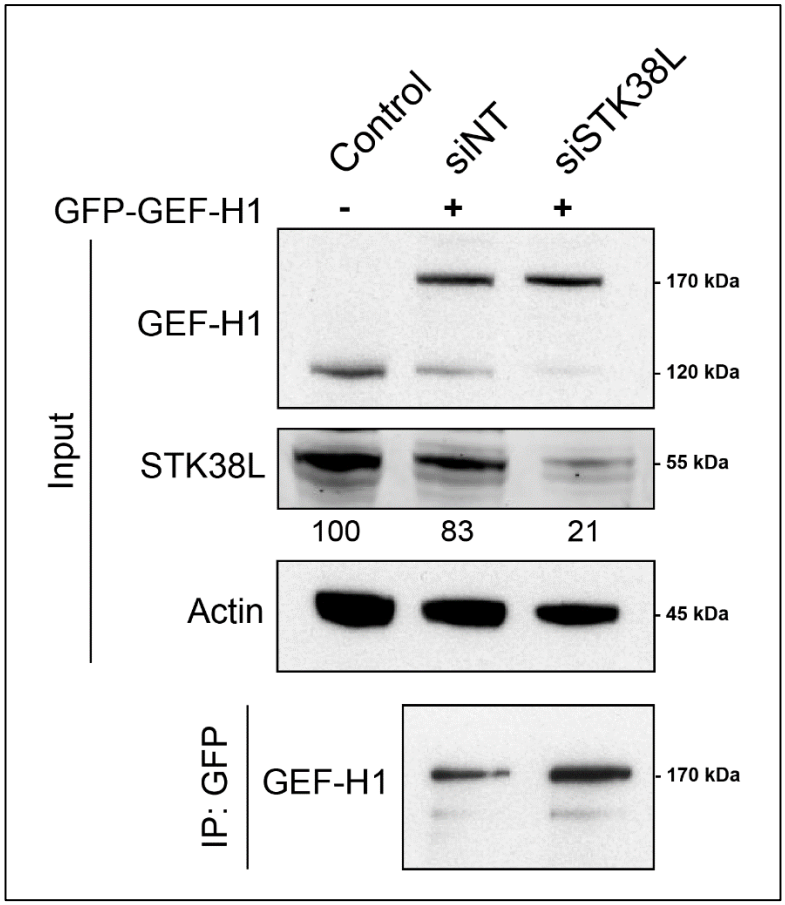

Figure 37 - Sample preparation for proteomic analysis.
H1299 cells were transfected with a specific siRNA targeting STK38L, with a control siRNA (siNT), or without siRNA. 24h later, cells were transfected with a plasmid expressing GFP-GEF-H1(wt). 48h later, cells were lysed and subjected to GFP-GEF-H1 purification using magnetic beads targeting GFP. Upper panel shows input of whole cell lysates and lower panel displays the result of GFP-GEF-H1 purification. The Western blot, using specific antibodies, indicates an efficient STK38L silencing (21% of remaining protein) as well as a good purification of GFP-GEF-H1.

Unfortunately, we failed to detect GEF-H1 S265 phosphorylation by mass spectrometry in all conditions despite the detection of the peptide including the serine 265 and being overly cautious in sample preparation (always at 4°C in presence of phosphatase inhibitors). This result is quite surprising given that serine 265 have been retrieved phosphorylated in a previous study (Rigbolt et al., 2011). One possible explanation can be attributed in the choice of the cell lines used. The 2011 study reporting serine 265 phosphorylation have been carried in human embryonic stem cells while our experiment has been done in H1299 cells. Another explanation could come from the detection method used: the mass spectrometry. As said above, I performed this experiment while I was seeking for XPO1 phosphorylation for my main project. As for GEF-H1, we failed to detect phosphorylation of XPO1_S1055, while it has been previously detected, also using mass spectrometry (Beausoleil et al.,

2004). On a side note, this failure in phosphorylation detection by mass spectrometry prompted us to engineer the specific anti phospho_S1055 against XPO1 in order to appreciate its phosphorylation status.

Despite the absence of GEF-H1 phospho-S265 detection, I was able to detect some post-translational modification of GEF-H1 other amino acids such as oxidation, carbamidomethylation, and phosphorylation. I found that STK38L silencing induced some changes in the phosphorylation status of some amino acids embedded in different regions of GEF-H1. Interestingly, I found an increase of phosphorylated serine 668 upon STK38L silencing, corresponding to an Erk phosphorylation motif (Sheridan et al., 2008). Unfortunately, because of a restricted time-scale, we did not pursue our analysis on STK38L impact on GEF-H1 phosphorylation and deactivation as well as the possible role of Erk.

RASSF1A role in pro-invasive bronchial cells properties and proper cytokinesis via NDR2 control

Maureen Keller[1,2,#], Fatéméh Dubois[3,4,#], Sylvain Teulier[3], Alexandre PJ Martin[5], Jérôme Levallet[2], Elodie Maille[1,2], Solenn Brosseau[1,2,6], Nicolas Elie[7], Alexander Hergovich[8], Emmanuel Bergot[3,9], Jacques Camonis[5], Gérard Zalcman[5,6,*], Guénaëlle Levallet[3,4,*]

1- Normandie Université, UNICAEN, UMR 1086 INSERM, F-14032 Caen, France.
2- Normandie Université, UNICAEN, UPRES-EA-2608, F-14032 Caen, France.
3- Normandie Univ, UNICAEN, CEA, CNRS, ISTCT/CERVOxy group, F-14000 Caen, France, GIP CYCERON
4- Service d'Anatomie et Cytologie Pathologique, CHU de Caen, F-14033 Caen. France
5- U830 INSERM, "Génétique et Biologie des cancers" Centre de Recherche, Institut Curie, Paris, France
6- Service d'oncologie thoracique, CIC 1425, Hôpital Bichat-Claude Bernard, AP-HP, Université Paris-Diderot
7- Normandie Université, UNICAEN, SFR ICORE, Plateau CMABio3, F-14032 Caen. France
8- University College London Cancer Institute, WC1E 6BT, London, United Kingdom.
9- Service de Pneumologie & Oncologie thoracique, CHU de Caen, F-14033 Caen. France

[#] and [*] designed authors contributing respectively equally to this work.

Correspondence:

Dr. Guénaëlle Levallet

Service D'Anatomie et Cytologie Pathologique

Normandie Univ, UNICAEN, CEA, CNRS, ISTCT/CERVOxy group CHU de Caen – Avenue de la côte de Nacre- 14032 Caen
Phone: + 33 2 31 06 31 34

Fax: +33 2 31 06 50 63

Email: guenaelle.levallet@unicaen.fr

ABSTRACT

RASSF1A, a tumor suppressor gene, is frequently inactivated in lung cancer leading to a YAP-dependent epithelial-mesenchymal transition (EMT). Such effects are partly due to the inactivation of the anti-migratory Rho GTPase, RhoB by as a consequence of the phosphorylation and inactivation of its GDP/GTP exchange factor (GEF), GEF- H1. The kinase responsible for GEF-H1 inactivation in RASSF1A-depleted cells is unknown. We demonstrate here that YAP-kinases NDR1/2 depletion reverts migration and metastatic properties of RASSF1A-depleted human bronchial epithelial cells (HBEC), by abolishing both EMT and YAP activation. We show that NDR2 interacts with GEF-H1 (which contains the NDR phosphorylation consensus motif HXRXXS/T), leading to its phosphorylation. We further report that the RASSF1A/NDR2/GEF-H1/RhoB/YAP axis is involved in proper cytokinesis in HBEC, since chromosome lagging and alteration of late cytokinesis steps are NDR- dependent in RASSF1A- or GEF-H1-depleted HBEC. To summarize, upon RASSF1A silencing, NDR2 gets activated, phosphorylates and inactivates GEF-H1. Then, the inability of RhoB to get activated leads to most of the phenotypes induced by RASSF1A loss in bronchial cells, including metastasis properties, YAP activation and cytokinesis defects.

INTRODUCTION

RASSF1A [Ras association (RalGDS/AF-6) domain family member 1] is a tumor and metastatic suppressor gene frequently inactivated in lung cancer (Dubois *et al*., 2016, Jiménez *et al*., 2017). RASSF1A inactivation also consists of an independent predictor of poor prognosis in resected early-stage non–small cell lung cancer (NSCLC), with a 5-year overall survival divided by 3 when RASSF1A silencing by promoter methylation is detected in the resected lung cancer specimens (de Fraipont *et al*., 2012). This worse prognosis value could be sustained by the disturbance of both Rho GTPases (Dubois *et al*., 2016, Lee *et al*., 2016), and Hippo signaling pathways (Guo *et al*., 2007, Dubois *et al*., 2016, Pefani *et al*., 2016). RASSF1A loss in non-transformed, immortalized human bronchial epithelial cells (HBEC), indeed leads to inactivation of RhoB (Dubois *et al*., 2016), a Rho GTPase with anti-cell migratory properties (Bousquet *et al*., 2009). It also leads to YAP transcription co- factor nuclear translocation, with subsequent epithelial-mesenchymal transition (EMT), again favoring cell migration and invasion (Dubois *et al.*, 2016). We showed that YAP nucleus translocation induced by RASSF1A knock-down was potentiated by the GTPase RhoB down-regulation observed concurrently (Dubois *et al.*, 2016). We also found that RhoB inactivation upon RASSF1A loss was the consequence of Rho guanine nucleotide exchange factor GEF-H1 inactivation, by its Ser885 phosphorylation (Dubois *et al.*, 2016). Our mechanistic investigations revealed that RASSF1A loss could block the PP2A-mediated GEF-H1 de-phosphorylation, leading to this RhoB inhibition (Dubois *et al.*, 2016, Bousquet *et al.*, 2009). However, additional questions remained unanswered, among them the identity of the kinase leading to GEF-H1 inactivation in RASSF1A-depleted HBEC. YAP is the terminal target of the Hippo signaling cascade of kinases, including MST1/2 (hippo) and NDR/LATS serine/threonine kinases, which directly regulate YAP activity (Zhang *et al.*, 2015). Among kinases from this Hippo pathway, the nuclear Dbf2-related (NDR) kinases, NDR1 (STK38) and NDR2 (STK38L) (Hergovich, 2013), captured our attention, since they were previously shown to phosphorylate and thus regulate rabin8, a GEF for Rab GTAPses, (Chiba *et al.*, 2013). We report here that knockdown of NDR kinases reverted the EMT, migration, metastatic properties and YAP activation induced by RASSF1A loss in HBEC. We further provide evidence for a direct NDR2/GEF-H1 interaction, leading to GEF-H1 Ser885 phosphorylation and inactivation, with subsequent RhoB down-regulation. Given the previously described involvement of GEF-H1 and NDR kinases in the regulation of cell cycle progression (Birkenfeld *et al.*, 2007, Cornils *et al.* 2011, Hergovich 2016), we investigated RASSF1A-depleted HBEC present cell cycle alterations. We report that RASSF1A knockdown actually induced abscission defects, which we achieved to revert by overexpressing GEF-H1 or depleting NDR-kinases. To summarize, based on these findings we propose a model in which, upon RASSF1A silencing, NDR2 gets activated, phosphorylates GEF-H1, leading to its inactivation. Then, the lack of RhoB activation leads to the phenotypes we described in RASSF1A-depleted HBEC: EMT, increase of migration, invasion, metastasis properties, YAP activation and cytokinesis defects.

RESULTS

NDR-kinases depletion reverts the migration and the metastatic properties induced by RASSF1A loss in HBEC.

RASSF1A and/or NDR1/2 knockdown in HBEC lines were achieved using two independent siRNAs for each target (TableS1)). At 48h post-transfection, wound healing (Fig.1A) and invasion (Fig.1B) assays were performed in the presence of mitomycin C, as previously described (Dubois *et al.*, 2016), to inhibit the contribution of cell division in wound repair, and thus restrict the effects of RASSF1A loss to the cell motility. In full agreement with our previous work (Dubois *et al.*, 2016), RASSF1A depletion in HBEC-3 cells resulted in increased cell migration and invasion (Figs. 1A and 1B). Here, we further observe that NDR kinases depletion significantly decreased the migration velocity of RASSF1A-depleted HBEC-3 cells (Fig.1A) and their ability to invade Matrigel® (Fig.1B). In addition, in none of the transfected conditions tested, cytochrome c was released (Fig.1C) or cell viability altered (Fig.1D). Thus, NDR knockdown reverted the bronchial cell migration increase induced by RASSF1A loss, independently of any impact on cell death. It is to note that NDR kinase silencing also decreased cells migration and invasion of the H1299 (Fig.S1A), A549 (Fig.S1A) and H1650 lung cancer cells (Movies S1 & S2 for siNeg and siNDR2 respectively) which exhibit a RASSF1A promoter hyper-methylation (with RASSF1A complete silencing). Indeed, the NDR2 silencing significantly decreased cells migration velocity of all these cells on collagen IV (Fig.S1A), while NDR1 or NDR2 depletion decreased H1299 (Fig.S1B), A549 (Fig.S1B) or H1650 (Fig.S1B) cells line ability to invade Matrigel®. That NDR knockdown decreased RASSF1A-depleted HBEC motility could not be explained by a difference in cell proliferation according to NDR content, or by a cell death increase, since only the PTEN-deleted H1650 cell line showed increased cell death upon NDR depletion (Fig.S1C).

To examine the effect of NDR1 or NDR2 depletion on metastasis properties of RASSF1A-depleted HBEC *in vivo*, we infected RASSF1A null lung cancer A549 or H1299 with lentivirus expressing shRNAs targeting specifically NDR1 or NDR2. Quantitative RT-PCR confirmed that NDR1 or NDR2 expression was decreased up to 80% by each shRNA constructs (Fig.1E for A549, Fig.SD for H1299). Injected in SCID−/− Beige mice, shNDR1- or shNDR2 A549 cells showed first signs of tumors at subcutaneous injection sites 25 days after injection, whereas tumors formed by control A549 cells emerged as soon as 21 days after injection (Fig.1E). Tumor growth was significantly decreased upon NDR1 or NDR2 knockdown compared to controls (Fig.1E), and while the xenografts from shcontrol A549 cells had all reached the critical size of 1000 mm3 as early as 35 days after implantation, significantly the xenografts from shNDR1 or shNDR2 A549 cells reached this size only at the 39th and 43rd day, respectively, after xenografts implantation (Fig.1E). H1299 cells, with p53 R175H mutation (Vaughan *et al.,* 2012), silenced for NDR1 developed xenograft with the same kinetic as H1299 control (Fig.S1D), while NDR2-depleted H1299 cells initially formed a xenograft as H1299 control cells but at the end of the experiment, are slightly smaller in size (Fig.S1D). Using immunohistochemistry, we confirmed that shNDR1 or NDR2 infected primary tumors still exhibited a decrease of NDR1 or NDR2 expression (Fig.1E for A549, Fig.SD for H1299). Finally, NDR2-depleted cells formed significantly less lung and liver metastatic tumor foci than shcontrol or shNDR1 cells (Fig.1F for A549, Fig.S1E for H1299), suggesting that metastatic properties induced by RASSF1A loss (Dubois *et al.,* 2016) could be reverted by NDR2 silencing. The effect of NDR silencing in RASSF1A-depleted cells suggested

that NDR kinases (and NDR2 more than NDR1) could contribute to metastatic effects of RASSF1A depletion.

NDR-kinases depletion reverts the EMT induced by RASSF1A loss in bronchial cells lines.

Since we previously reported that RASSF1A depletion increased HBEC motility in part by inducing EMT (Dubois *et al.*, 2016), we tested whether NDR kinases silencing could revert the EMT undergone by HBEC upon loss of RASSF1A. We quantified two epithelial markers (E-Cadherin, ZO-1) and two mesenchymal markers (N-Cadherin, Vimentin) expression by Western blotting in HBEC-3 cells knockdown for RASSF1A and/or NDR kinase (Fig.2A). We show that NDR1 or NDR2 depletion actually abolished mesenchymal markers expression in RASSF1A depleted HBEC-3 cells (Fig.2A, bottom histogram), while NDR2 silencing restored E-Cadherin expression impaired by RASSF1A knockdown but failed to completely restore ZO-1 expression (Fig.2A, upper histogram). We also find that the expression of epithelial and mesenchymal markers could also be altered by NDR1/2 manipulations of H1299 (Fig.2B) and A549 (Fig.2C) lung cancer cells.

On xenografts from A549 or H1299 cells depleted or not for NDR1 or NDR2, we also measured an increase in the expression of cadherin E in shNDR1 and shNDR2 A549 (Fig 2G) or H1299 (Fig 2H) cells. In A549, only sh-NDR2 A549 cells express cadherin at the cell membrane (Fig 2G). Conversely, we find a decrease of vimentin expression by shNDR1 as NDR2 A549 (Fig 2G) or H1299 (Fig 2H) cells when compared to shcontrol cells. Taken together, these data support that NDR kinases inactivation does prevent EMT following RASSF1A silencing in HBEC.

NDR-kinases depletion abolishes YAP activation in RASSF1A-depleted HBEC.

We previously reported that increase of RASSF1A-depleted HBEC-3 cell migration was YAP-dependent, YAP being involved in the EMT phenotypes upon RASSF1A reduction (Dubois *et al*., 2016). We wondered whether NDR depletion could revert the up-regulated YAP activity. We confirmed the increase of nuclear YAP by immunofluorescence following RASSF1A depletion in HBEC-3 cells (Fig.3A, (Dubois *et al*., 2016)) and found that NDR1 and/or NDR2 depletion significantly prevents YAP nuclear localization in RASSF1A-depleted HBEC-3 cells (Fig.3A) or in the RASSF1A- null H1650 or A549 cells (Fig.3B). We then show that depletion of either NDR1 or NDR2 diminishes two well-known transcriptional targets of YAP (Zhou *et al*., 2015): CTGF (Fig.3C, Fig.3E) or ANKDR1 mRNA species (Fig.3D, Fig.3F) in RASSF1A- depleted HBEC-3 cells (Fig.3C, Fig.3D), and RASSF1A-null H1650 and A549 cancer cells (Fig.3E, Fig.3F) respectively, supporting that in NDR- and RASSF1A-depleted HBEC, YAP was unable to regulate gene transcription.

On xenograft from A549 (Fig 3G) or H1299 (Fig 3H) cells depleted or not for NDR1 or NDR2, we measured that YAP intensity decreases when compared to shcontrol cells and is null in cells nuclei, again when compared to shcontrol cells which exhibit strong nuclear signal for YAP, except for shNDR1 H1299, for whom half of the nuclei still exhibit YAP staining (Fig 3H).

Taken together, these data support that NDR kinases inactivation, following RASSF1A silencing, prevents the YAP activation, as defined by nuclear localization and YAP-regulated transcription, in 'normal' immortalized bronchial as in lung cancer cells. Such data suggest the involvement of the NDR/YAP axis in the increased motility induced by RASSF1 depletion.

NDR2 interacts with GEF-H1 resulting in S885-GEF-H1 hyper-phosphorylation and subsequent GEF-H1 inactivation

The kinase leading to GEF-H1 hyper-phosphorylation/inactivation in RASSF1A- depleted HBEC is yet to be defined (Dubois *et al*., 2016). Our results presented in Figures 1,2 and 3 prompted us to test whether NDR kinases could be involved in GEF-H1 inactivation. To do so, we quantified phosphorylated Serine 885 GEF-H1 in HBEC-3 cells upon RASSF1A or NDRs depletion, by Western blotting and immunofluorescence (Fig.4A). Interestingly, we observed that NDR2 but not NDR1 silencing significantly decreased GEF-H1 phosphorylation in HBEC with RASSF1A depletion (Fig.4A). We previously reported that GEF-H1 inactivation led to RhoB inactivation in RASSF1A-depleted HBEC (Dubois *et al*., 2016). Thus, we also tested RhoB activation (-GTP, activated or -GDP, inactivated) first in RASSF1A null H1299 cells (Fig.4B), then in RASSF1A wild-type HBEC-3 cells (Fig.4C). By forcing re- expression of RASSF1A in H1299 cells, we observed an increase in activated (GTP- bound) form of RhoB (Fig.4B) confirming the link we previously reported between RASSF1A and RhoB activation (Dubois *et al*., 2016). We mimicked this effect of RASSF1A re-expression in H1299 cells by silencing NDR1 or NDR2, since NDR extinction increased active RhoB GTP-bound form, while rescuing NDR1 and NDR2 expression conversely decreased GTP-bound RhoB (Fig.4B). Thus, we provide the first demonstration that NDR depletion could restore RhoB activation in RASSF1A null HBEC. We confirmed such feature in RASSF1A wild-type HBEC-3 cells. Indeed, RASSF1A-RNAi decreased GTP-bound active form of RhoB in HBEC-3 cells (Fig.4C). Again, RhoB reactivation can be achieved in RASSF1A-depleted HBEC-3 cells by concurrent NDR2 silencing (Fig.4C). The siRNA-NDR2 impact on Rho-GTP accumulation was specific since expression of a siRNA-resistant NDR2 actually reversed Rho-GTP accumulation to normal levels (Fig.4C). Surprisingly, NDR1 silencing failed to reactivate RhoB upon RASSF1A depletion (Fig.4C). Taken together, these findings suggest that NDR (and NDR2 more repeatedly than NDR1) participate in the regulation GEF-H1 activity and the subsequent regulation of RhoB.

We uncovered a putative NDR phosphorylation motif HXRXXS/T (Hergovitch, 2012) at position 265 amino acid sequence from GEF-H1 (Fig.4D). Ser265-GEF-H1 has not been described to be required for GEF-H1 activity, although Ser265, located in the DBL-homology domain from GEF-H1, has been documented to be phosphorylated in phosphoproteomic analyses (Rigbolt *et al*., 2011), and hence might be involved in the regulation of GEF-H1. We looked for GEF-H1 and NDR2 co-staining in HBEC-3 cells by immunofluorescence and observed a stronger GEF-H1/NDR2 co-staining in RASSF1A-depleted HBEC-3 cells than in control HBEC-3 (siNeg), and a major co- staining in RASSF1A-depleted HBEC-3 cells expressing an exogenous wild-type GEF-H1 (Fig.4E). Such data support our hypothesis that upon RASSF1A silencing, NDR2 gets activated and phosphorylates GEF-H1. Using mass spectrometry, we failed to detect fluctuation of GEF-H1 phosphorylation on serine 265 upon NDR2 depletion, possibly because such variations could be of low magnitude or more probably labile (data not shown). Consequently, we focused on the demonstration of a physical interaction between NDR2 and GEF-H1. We failed to report NDR2/GEFH1 interaction by co-immunoprecipitation using commercially available antibodies against NDR2 or GEF-H1, and we hypothesize that such interaction could be favored by an intermediate in bronchial cells. Indeed, heparan-sulfate proteoglycan (HSPG) syndecan-1 (SDC1) could be this intermediate since SCD1 was previously reported to interact with GEF-H1 (Ridgway et al., 2012), to

influence Rho activation (Ibrahim *et al.,* 2012), and to decrease upon RASSF1A depletion (Dubois *et al.,* 2016). Using a SDC1 antibody, we detected both NDR2 and GEFH1 proteins in the immunoprecipitate from HBEC3 cell extracts, either in basal condition (with a control interferent RNA) or upon RASSF1A depletion (Fig.S2), demonstrating an *in vivo* interaction between NDR2 or GEF-H1 with SDC1. Using recombinant GST-NDR2, we successfully pulled-down endogenous GEF-H1 from HBEC-3 cell extracts depleted or not for RASSF1A (Fig.4F, GST-assay) showing a direct biochemical interaction between NDR2 and GEF-H1 proteins. As an important control, we also silenced GEF-H1 expression in HBEC-3 cells with a near-total efficacy (Fig.4F, right panel, input, second lane from the top), and then decreased the GEF-H1 protein amount retained by GST-NDR2 beads. In the same conditions, we failed to pull-down endogenous GEF-H1 with GST-NDR1, again suggesting that NDR2 is more likely to participate directly in GEF-H1 regulation, as supported by our findings on GEF-H1 phosphorylation and RhoB re-activation described in Figs. 4A, 4B and 4C. We co- transfected HBEC-3 cells with a GEF-H1 RNAi to eliminate endogenous GEF-H1, concurrently with a plasmid encoding for wild-type GEF-H1 (pls WT-GEF-H1) or for a mutant GEF-H1 protein, either containing a serine to alanine substitution at position 265 (pls GEF-H1 S265A) or a serine to alanine at position 885 (pls GEF-H1 S885A) (Fig.S3), both mutant proteins being unable to be phosphorylated on these alanine residues. We detected a strong phosphorylation at Ser885-GEF-H1 in total protein cell extract from WT-GEF-H1-transfected HBEC-3 cells, but not in extracts from GEF- H1-S885A or fS265A-transfected HBEC-3 cells (Fig.4F, input, top lane). Such finding did support the hypothesis that Phospho-Ser265 favors Phospho-Ser885 in GEF-H1. We finally evidenced that exogenous GST-NDR2 kinase induced strong GEF-H1 Ser885 phosphorylation on exogenously expressed wild-type GEFH-1 retained on beads, while NDR2 beads only retained a low amount of phosphoSer885 GEF-H1, reflecting the remaining endogenous pool after GEF-H1 RNAi transfection and exogenously expressed serine to alanine mutants, either S885A and more interestingly S265A (Fig.4F, GST assay). All these data strongly suggest a link between phosphorylation of Ser265-GEF-H1 and phosphorylation of Serine 885.

RASSF1A depletion delays abscission and alters cytokinesis in bronchial cells lines.

RASSF1A (Song *et al*., 2004, Guo *et al*., 2007, Whitehurst *et al*., 2008, Song *et al*., 2009), NDR kinase (Chiba *et al*., 2009, Gupta *et al*., 2014), GEF-H1 (Birkenfeld *et al*., 2007, Chircop, 2014) as YAP (Bui *et al.,* 2016) each were previously reported to control cell division, but whether these proteins act together has never been investigated.

By observing RASSF1A-depleted HBEC occurring mitosis, we detected no alteration in the definition of equatorial plan or the equatorial structure processing in RASSF1A- depleted HBEC-3 cells, with no detected abnormality of the main protagonists involved in such steps, as evidenced by normal MKLP1 (Fig.S4A), PRC1 (Fig.S4B) RhoA (Fig.S4C), Rac1 (Fig.S4D), or Ect2 (Fig.S4E) staining, in terms of protein amount or subcellular protein localization. Conversely, we noticed that RASSF1A inactivation increased chromosomes misalignment in HBEC-3 (Fig.S5A) supporting alterations in metaphase continuity and increased chromosome lagging in HBEC-3 cells (Fig.S5B) as in HBEC-3-RasV12 cells (Fig.S5C), suggesting a defect in sister chromatids separation at anaphase. We then reported that RASSF1A inactivation induced midbody persistence, as ***i)*** evidenced

by α-tubulin and Aurora B co-staining in HBEC-3 cells (Fig.5A) or HBEC-3-RasV12 cells (Fig.S5D) (Hu *et al.,* 2012), ***ii)*** the modification of expression of keys proteins for midbody establishment such as the increase of Anillin (Fig.S5F) and Aurora B (Fig.S5G) at midbodies, or the concurrent decrease of Citron kinase staining (Fig.S5H) in RASSF1A-depleted cells. Such data suggesting an abscission defect at telophase, and we noticed by time-lapse video- microscopy a significant lengthening of HBEC-3 cell division. In control HBEC-3 cells (siNeg), the transition from the onset of furrowing to completion of abscission lasted 23±2 min *vs.* 40±3 min in RASSF1A-depleted cells (Fig.5B, Movies S4 & S5). We also observed significantly more cells with failing mitosis (about 60% versus 2% for siNeg-transfected cells, $p<0.001$) (Fig.5C). There were increased numbers of ***i)*** round cells never entering into mitosis (Fig.5C, MovieS6), ***ii)*** cells initiating mitosis but never initiating cytokinesis (Fig.5C, MovieS7), or ***iii)*** cells never terminating abscission and exhibiting broad cytoplasmic bridges interconnecting daughter cells, each pointing a cytokinesis defect at different steps (Fig.5C, MovieS8) ($p<0.01$) and ***iv)*** increased numbers of bi- or multi-nucleated HEBC-3 cells (Fig.S5I) or HBEC-3-RasV12 cells (Fig.S5I), with independent initiation of mitosis for nuclei from a same HBEC-3 cell (shown by confocal acquisition of siRASSF1A transfected cells, MovieS8). Finally, we also observed significant cytoplasmic accumulation of Spastin and Fidgetin, two enzymes involved in midbody cut (Fig.5D), supporting the midbody abscission defect we suspected. We also observed significant alterations in the cell content of two crucial proteins for intracellular traffic, Rab11 small GTPase (increased) and Syntaxin16 (decreased) (Fig.5E), both of them being required for proper mitosis proceedings (Hehnly and Doxsey, 2014, Neto *et al.,* 2013).

All these data confirm that RASSF1A knockdown leads to profound mitosis process alterations in the HBEC-3 cell lines. Indeed, cytokinesis defect following RASSF1A depletion was evidenced by others, but only focusing on a single cytokinesis step:the midbody formation (Song *et al*. 2009). Evidence for RASSF1A involvement in others steps of cytokinesis was thus still lacking in the literature.

Cytokinesis disorders induced by RASSF1A depletion in bronchial cells lines are YAP dependent.

Since the migration and invasion phenotypes we previously described following the inactivation of RASSF1A were partly YAP-dependent (Dubois *et al*., 2016), we analyzed the YAP silencing effects on cytokinesis of HBEC-3 cells expressing or not RASSF1A. YAP depletion in RASSF1A wild-type HBEC-3 did not modify the number of multinucleated cells or of cells having persistent midbody, when compared to control HBEC-3 cells (Fig.5F). However, YAP depletion significantly decreased the number of multinucleated cells in RASSF1A-depleted HBEC-3 (Fig.5F, cf. immunofluorescence photographs) and the rate of cells with persistent midbody (Fig.5F, histogram).

Thus, we provide evidence that cytokinesis disorders induced by RASSF1A depletion in bronchial cells lines depend on YAP.

GEF-H1 and NDR2 co-staining is divergent in HBEC-3 and RASSF1A-depleted HBEC-3 cells during mitosis

Wondering whether NDR2-induced GEF-H1 inactivation in RASSF1A-depleted cells are responsible for the cytokinesis defect of these cells, we investigated how GEF- H1/NDR2 co-stain during mitosis in HBEC-3. We observed that co-staining of GEF- H1/NDR2 is not constant during the whole cell division and is modified

following RASSF1A silencing (Fig.6). In HBEC-3 cells, GEF-H1 and NDR2 co-staining was mainly observed at the early prophase (with a sub-cortical signal), during the establishment of the equatorial plane, at the end of telophase and during abscission (at the cleavage point) (Fig.6, left panel and histogram), suggesting an active involvement of NDR2 kinase in GEF-H1 activity regulation during such mitosis steps. Conversely, in RASSF1A-depleted HBEC-3 cells, NDR2/GEF-H1 co-staining features were considerably different at four stages of mitosis (Fig.6, right panel and histogram): ***i)*** the early prophase where the sub-cortical co-staining signal observed in control cells were here sparse and lower) ***ii)*** the equatorial plane step (where co-staining was fainter than in control cells), ***iii)*** the assembly of contractile ring (where, conversely co-staining was stronger in RASSF1A-depleted cells) and ***iv)*** the abscission step (with a lower signal at midbody). These findings suggest that mitosis alteration in RASSF1A depleted-cells could actually be induced by NDR2 activation and subsequent GEF-H1 inactivation in these cells.

GEF-H1 depletion mimics cytokinesis defects induced by RASSF1A silencing in HBEC-3 cells

We next tested whether GEF-H1 inactivation by NDR2 could explain cytokinesis disorders of RASSF1A depleted cells. We deleted GEF-H1 expression by siRNA in HBEC-3 cells (Fig.S6A) and observed that GEF-H1 silencing increased the proportion of binucleated cells (Fig. S6B) but not of cells with a persistent midbody (Fig. S6C). The co-depletion of both RASSF1A and GEF-H1 in HBEC-3 cells did not increase the number of multinucleated cells as compared with the single RASSF1A depletion (Fig. S6A), while conversely such co-depletion synergistically increased the proportion of attached daughter cells (Fig. S6B). This result reinforces our hypothesis that GEF-H1 inactivation by NDR2 leads to cytokinesis disorders in RASSF1A depleted cells, since GEF-H1 silencing mimics RASSF1A depletion effect.

GEF-H1 overexpression as NDR2 depletion restores a normal cytokinesis in RASSF1A-depleted cells

Next, we either re-introduced wild-type GEF-H1 expression or alternatively silenced NDR in RASSF1A-depleted HBEC-3 cells, before reevaluating multinucleated cells and cells with persistent midbody. We achieved to restore a normal cytokinesis in RASSF1A-depleted HBEC-3 cells with forced GEF-H1 overexpression (Fig.7A), since cells exhibited a 'normal' basal rate of bi-nucleated cells (Fig.7B) or of cells with persistent midbody (Fig.7C) upon such conditions, as compared with control HBEC-3 cells (transfected with an inactive RNAi).
Similarly, co-depletion of RASSF1A with NDR1 or NDR2 also rescued mitosis-phenotypes associated with RASSF1A loss of function. We actually observed that both NDR1 as NDR2 depletion decreased the rate of multinucleated RASSF1A-depleted HBEC-3 cells (Fig.7D). However, only NDR2 silencing also suppressed abscission failure, as monitored by the decrease of persistent midbodies, while co-depletion of RASSF1A and NDR1 had no obvious effect (Fig.7D). This last observation suggests that by controlling NDR2, RASSF1A participates to the proper progress of cytokinesis. In full support of these findings, in the RASSF1A-null H1299 lung cancer cells, NDR2, but not NDR1, depletion decreased significantly both multinucleated and the rate of cells linked with persistent midbody (Fig.7E).

RASSF1A, NDR2 kinase and RhoB-GEF-H1 signaling module could impact overall survival of lung cancer patients:

To further strengthen the functional link between RASSF1A/NDR2/GEF-H1 and RhoB proteins, we analyzed in publicly available databases whether mRNA expression of these protagonists could influence prognosis of resected early lung cancer patients from the CTGA cohort, as it was reported for RASSF1A in our IFCT-0002 series (De Fraipont *et al.,* 2012). We actually found that low amounts of RASSF1A (HR=0.69, 95%CI [0.53-0.90], p=0.0059 (Fig.S7A)), RhoB (HR=0.71 95%CI[0.56-0.90], p=0.0047 (Fig.S7B)), GEF-H1 (HR=0.71, 95%CI[0.57-0.87], p=0.00094 (Fig.S7C)) tumor mRNA species did predict worse overall survival in 681 patients with NSCLC, while, as predicted by our model, conversely, NDR2 mRNA high expression significantly predicted poorer survival. (HR=1.25, 95%CI[1-1.55], p=0.046 (Fig.S7C)).

Discussion

We recently presented data supporting that RASSF1A acts both as a tumor and metastasis gene suppressor in patients with early stage non-small cell lung cancer (NSCLC) (De Fraipont *et al.,* 2012, Dubois *et al.,* 2016). Actually, RASSF1A prevents epithelial-mesenchymal transition, migration and invasiveness since controlling activation of YAP, the terminal target of the Hippo pathway, RhoB a small anti- migratory GTPase protein *via* GEF-H1, its GDP/GTP exchange factor (Dubois *et al.,* 2016). Here, we identity the kinase Hippo NDR2 as the kinase leading to GEF-H1 inactivation in RASSF1A-depleted human bronchial cells (HBEC), and demonstrate that RASSF1A loss, by inducing GEF-H1 inactivation, also plays a critical role in cytokinesis control.

We had previously demonstrated that the nuclear localization of YAP is dependent on the inactivation of RhoB in RASSF1A depleted human bronchial cells (Dubois *et al.,* 2016). Here, we also investigated the place of Hippo kinases in cellular disorders due to RASSF1A inactivation, because ***i)*** the RhoB inactivation induced by RASSF1A depletion is leaded by the inactivation of its GTP exchange factor, GEF-H1 (Dubois et al., 2016), ***ii)*** previous work had shown that NDR kinases could inactivate some GEFs, such as rabin8 (Chiba *et al.,* 2013), and ***iii)*** we identified a NDR phosphorylation motif HXRXX**S/T** in the GEF-H1 sequence, on a Serine residue at 265 position (Fig.4D), within the DH domain, essential for the GDP/GTP exchange function of GEF-H1. We validate the hypothesis of a link between NDR2 kinase and the inactivation of GEF-H1 in depleted human bronchial cells of RASSF1A by assessing the Ser885-GEF-H1 phosphorylation status, or GTP-bound RhoB in HBEC-3 cells expressing or not RASSF1A and/or NDR1/2 and we actually reported that NDR2 depletion decreased Ser885-GEF-H1 phosphorylation (then the GEF-H1 inactivated form) (Fig.4A), while simultaneously increased GTP-bound activated RhoB (Fig.4B, C) in HBEC. Such actions were reverted when a RNAi-resistant NDR2-expressing plasmid was co-transfected along with the NDR2 siRNA (Fig.4B, C). We confirmed an increased co-staining of NDR2 and phosphorylated Ser885- GEF-H1 in RASSF1A depleted-HBEC (Fig.4E), sustaining a possible interaction between NDR2 and GEF-H1 in RASSF1A-depleted HBEC. We then report, by an exogenous protein-protein interaction test, that NDR2 can physically directly interact with GEF-H1, excepted when GEF-H1 was mutated on S265 or S885 (Fig.4F). Lastly, we were able to show an *in vivo* interaction of GEF-H1 and NDR2 using co- immunoprecipation of a third partner, SDC1. We report thus data suggesting that NDR2 could inhibit GEF-H1 activity, as shown by the increase S885-GEF-H1 reported following NDR2 transfection on HBEC (Fig.4A), following physical interaction and subsequent phosphorylation on S265. How phosphorylation of the Serine 265 on GEF-H1 could lead to increased phosphorylation of Serine 885, leading to the loss of GEF-H1 activity, should need additional structural studies, to confirm our hypothesis that this first phosphorylation, by inducing a conformational change, would favor subsequent serine 885 phosphorylation by other kinases. To support currently such hypothesis, we know that this serine was previously reported as being phosphorylated *in vitro* (Rigbolt *et al.,* 2011) and that GEFs are frequently inactivated by successive phosphorylations (Patel and Karginov, 2014). In addition, the NDR2 control on GEF-H1 activity is in line with the NDR regulation of rabin8, another GEF, previously described (Chiba *et al.,* 2013).

The NDR2 kinase is therefore probably the kinase responsible for the inactivation of GEF-H1 and the subsequent RhoB inactivation in RASSF1A depleted human bronchial cells. To reinforce this result, we show here that the inhibition

of NDR kinases (and thus the lack of GEF-H1/RhoB inhibition) on the one hand reverts the migratory phenotype and the metastatic properties of the depleted bronchial cells of RASSF1A (Fig.1 and Fig.S1), and on the other hand also prevents cytokinesis defects caused by the absence of RASSF1A in bronchial cells (Fig.5-7 and S3-S5).

That the extinction of NDR kinases inhibits the capacity of human bronchial cells depleted for RASSF1A is in line with the inhibition of both EMT (Fig.2) and YAP (Fig.3) induced by extinction of NDR kinases in RASSF1A-depleted HBEC (Dubois *et al.,* 2016). Another argument supporting this conclusion is the partial extinction of YAP expression in the nucleus of H1299 shNDR1 cells: these cells retain indeed the same capacities to form xenografts when implanted in SCID mice than shcontrol cells. This description of a role of NDR kinases in the control of cell motility is quite original. Nevertheless, that NDR1/2 kinases are involved in the control of these movements is not so surprising, since such control has already been assigned to their counterparts, the LATS1/2 kinases (Furth *et al.,* 2015): LATS1, in particular, controls the LIMK/Cofilin signaling pathway and thus the polymerization of actin filaments (Yang *et al.,* 2004). This work is also the first to report that NDR kinases can participate in the EMT/MET process: inhibition of NDR1/2 in HBEC depleted for RASSF1A allows a return to a basal level of expression of epithelial markers and decreased mesenchymal marker expression (Fig.2). The control exercised by NDR on the mesenchymal phenotype appears related to the control that NDR kinases exert on YAP. Indeed, we had reported that the EMT induced by RASSF1A silencing in HBEC was consistent with the abnormal activation of YAP in these cells (Dubois *et al.,* 2016). Here, we show that in the absence of NDR, the EMT of RASSF1A-depleted HBEC is canceled, which is correlated with YAP inactivation in HBEC with neither RASSF1A nor NDR kinases. That the extinction of NDR kinases lowers the presence of YAP in the nucleus and therefore its transcriptional activity in cells lacking RASSF1A is surprising. Indeed, YAP was shown to be a substrate for NDR kinases, such as LATS kinases (Zhang *et al.,* 2015, Hergovich, 2016), and phosphorylation of YAP by NDR/LATS kinases usually leads to its nuclear output and proteasome orientation (Hergovich, 2016). However, in RASSF1A-depleted HBEC, it is possible that the nuclear localization of YAP is not a consequence of the canonical Hippo pathway deregulation, but rather could be linked to the inactivation of RhoB (Dubois *et al.,* 2016). Thus, our data are not contradictory with the available literature since we show that NDR kinases are indeed at the origin of the inactivation of RhoB, by phosphorylating and leading to the inhibition of its GEF, GEF-H1. In the absence of NDR2, GEF-H1 is active, even in the absence of RASSF1A, leading to the activation of RhoB and thus allowing proper control of YAP.

NDR kinases may therefore up- or down-regulate YAP activity, depending on the cellular context, which could explain these kinases may behave as oncogenes (what our results in RASSF1A-depleted HBEC could support, by inactivating RhoB) or tumor suppressor genes as previously reported by other authors (Zhang *et al.,* 2015, Hergovich, 2016). Actually, YAP is able to induce the expression of genes involved in the reprogramming of cells from breast cancer lines to mammary stem cells (Kim *et al.,* 2015), and then exert pro-oncogenic action, but on the other hand, YAP could also exert anti-oncogenic functions by since RNAi extinction of YAP increased migration and invasion of mammary carcinoma cell lines, inhibited cell responses to paclitaxel, suppressed anoikis and promoted *in vivo* the occurrence of tumors in mice (Yuan *et al.,* 2008).

The link we established between the RhoB/GEF-H1/NDR2/YAP and RASSF1A led us to explore another process deregulated in RASSF1A depleted HBEC, the cytokinesis, since both GEFH1 and NDR were previously reported to play a role in such cell division step. Here, we provide evidence that the deregulation of one member of this interactome is sufficient to disrupt cytokinesis and in particular the middle or the late stage, in RASSF1A-knockdown cells, a feature which is consistent with ***i)*** the co-localization of RASSF1A with the microtubules, at contractile ring and midbody during cytokinesis (Dallol *et al.,* 2007; Liu *et al.,* 2008), ***ii)*** the localization of YAP to the midbody and spindle (Bui *et al.,* 2016), ***iii)*** the localization of GEF-H1 at the tips of cortical microtubules and the midbody (Birkenfield *et al.,* 2007), ***iv)*** in our immunofluorescence studies the lower co-staining of GEF-H1 and NDR2 at early prophase, at equatorial plane positioning and during midbody formation (Fig.5). Indeed, RASSF1A role in cytokinesis may be dependent of its ability to stabilize the cytoskeleton (Song *et al.,* 2005; Liu *et al.,* 2005, Dubois *et al.,* 2016), and/or to control the mechanical force exerted on the microtubules during cytokinesis (Arnette *et al.,* 2014). Alternatively, RASSF1A role could be independent of the cytoskeleton, and simply requires its ability to serve as a scaffold protein, which could be necessary for recruiting key proteins and/or vesicles. Consistent with this idea, for instance, we showed here that RASSF1A depletion abolished Ect2 accumulation at the cleavage furrow (see Figure S4, panel E). Ect2 downregulation was previously reported to contribute in a genetic instability (Carter *et al.,* 2006), inducing a broader activation of Rho in regions outside of the central spindle, then leading to cytokinesis failure (Normand and King, 2010). Thus, it is a reasonable assumption that RASSF1A depletion could also disrupt ECT2/Rho efficient activities for induction of the cleavage furrow at the correct location. We also observed a central spindle localization of Rac1 in RASSF1A depleted cells (see Figure S4, panel D), that may lead to inefficient contractile ring constriction by inducing adhesion at this site (Davies and Canman, 2012).

In addition, we confirmed that GEF-H1 depletion by siRNA, as GEF-H1 inactivation induced by RASSF1A depletion leads to cytokinesis disorders, while GEF-H1 overexpression in RASSF1A depleted lung cells restore appropriate cytokinesis.

Finally, that the consequences of the NDR1 kinase extinction are not systematically stackable to those of the NDR2 extinction was not unexpected: it is more and more documented that if the NDR/LATS kinases have many common roles due to their strong sequence homology, each kinase is also able to ensure its own functions (Hergovich, 2016). In line with such concept, we present here that NDR2 depletion entirely compensates for the effects of the absence of RASSF1A on cell processes, while the extinction of NDR1 only partially compensates for it.

Taking all the data presented in this work, we thus propose that upon silencing of RASSF1A, NDR2 gets activated, phosphorylates GEF-H1 on serine 265 with subsequent inhibitory phosphorylation of serine 885 and lack of RhoB activation, which in turn leads to all the phenotype we described in RASSF1A-depleted bronchial cells: EMT, migration, invasion, active YAP and cytokinesis defects (Fig.8).

Material and methods

Isogenic non-tumorigenic HBEC-3 and HBEC-3-KRasV12 bronchial cells (Dr.White, UT Southwestern Medical Center, Dallas, TX; (Levallet *et al*., 2012)), tumorigenic cancer-derived cell lines A549, H1650 and H1299 from ATCC, were grown and transfected at 30% confluence as previously described (Dubois *et al*., 2016). HBEC-3 and HBEC-3-KRasG12V were authenticated using standard karyotyping techniques as previously described (Dubois *et al*., 2016). A549, H1299 and H1650 were passaged for fewer than 6 months after receipt from ATCC. Cells, grown in their respective media, were transfected at 30% confluence, using Lipofectamine RNAiMAX® (Invitrogen™) with siRNA, plasmid DNA or control mimics (Dharmacon™) (Tables.S1). Non phosphorylatable GEF-H1 mutants (S265A, S885A) were generated by site-directed mutagenesis and confirmed by sequencing (Mutagenex, Inc, Suwanee, USA (FigureS2).

ShNDR1 or NDR2 and SCID mice xenograft

The experiments were performed according to the European Convention for the Protection of Vertebrates Used for Scientific Purposes (Project Authorization using Animals for Scientific Purposes reference: 2018030814474695 (# 13256)).
Groups of ten, strain 250, 6 weeks-old, female Fox Chase SCID−/− Beige mice from Charles River™ were anaesthetized according to the manufacturer's recommendations for xenografting. ShControl (MISSION® pLKO.1-puro Non-Target shRNA Control, Sigma-Aldrich) ShNDR1- (5'-CCGGGTATTAGCCATAGACTCTATTCTCGAGAATAGAGTCTATGGCTAATACTTTTTG-3', NM_007271.2-875s21c1, Sigma-Aldrich) or shNDR2- (5' CCGGGGCTTGCTTGGCGTAGATAACCTCGAGGTTATCTACGCCAAGCAAGCCTT TTTG-3', NM_015000.3-1353s21c1 Sigma-Aldrich) infected A549 (RASSF1A depleted), H1299 (RASSF1A depleted) or BEAS-2B (wild type RASSF1A) cells suspension (1×10^7 cells/0.1 ml) in a mixture of 1xDMEM and Matrigel® (BD Biosciences, CA) were injected sub-cutaneously in the left flank of each animal. Mice were monitored for tumor growth thrice a week. Tumors were allowed to grow to 1000 mm3 before euthanasia of the mice. The post-mortem examination included macroscopic description of lungs and liver. Tumor xenografts, lungs and liver were rapidly removed and fixed in PFA 4% for histological analysis.

Reverse Transcription-Quantitative real-time-PCR (RT-PCR)

After extraction, RT-PCR was done with each primer sets (Table S1) as described previously (Dubois *et al*., 2016). RT-PCR data were normalized to the human S16. Relative quantification was calculated using the $\Delta\Delta$**C**t method.

Immunoblotting

Whole cell protein extracts were prepared as previously described (Dubois *et al*., 2016), and proteins detected by immunoblotting with primary antibody (Table S2) diluted at 1:1000 in Tween (0.1%)-TBS buffer and HRP-conjugated secondary antibody and revealed by enhanced chemiluminescence with ECL kit (Promega™).

Immunofluorescence and image analysis

Transfected cells were fixed and permealized as described previously (Dubois *et al*., 2016). Primary antibodies (Table S2) were diluted at 1:100. The AlexaFluo633, AlexaFluo555 and 488-labelled (Invitrogen™) secondary antibodies were added for 1h. Coverslips were mounted with DAPI (Santa Cruz™), and image captured with

high-throughput confocal microscopy (FluoView FV1000, Olympus™).

Immunohistochemistry
Paraffin-embedded blocks were cut into 3-µm slices. Slides were de-paraffinized in xylene and rehydrated using standard techniques. After pretreatment with EDTA buffer (pH 9.0, 20 min, 100°C), slides were incubated at room temperature in 3% H2O2 for 5 min then in 0.5% tween (T)-PBS enriched by 5% Bovine Serum Albumin (BSA) for 60 min to block non-specific site. Slides were incubated overnight at 4°C with primary antibodies (Table S2) used at 1:200 dilution then revealed using respectively the Novolink (Leica) kits. Positive internal controls were systematically evaluated (normal epithelial cell). Negative controls omitted the primary antibody.

Wound healing assay
Transfected cells grown onto 24-well Collagen IV coated plates (BD Biocoat™) were pretreated with mitomycin C (1µg/ml) 12h before an artificial “wound” created at 0h. Photographs were taken (X10) at 0h and 6h. The distances subtracted across the wound at 0h and 6h were expressed as µm/h.

Invasion
A total of 20×10^3 cells were added in serum-free medium to the top invasion chambers of 24-well transwell plates containing cell culture insert with 8 µm pore size (BD BioCoat Matrigel® Invasion Chamber, BD Biosciences™). Complete media were added to the bottom chambers. At 48h, non-migrating (top) cells were removed, migrating (bottom) cells were stained with crystal violet.

Bromodeoxyuridine (BrdU) Incorporation Analysis
Cells were transfected with the indicated constructs. The next day, cells were labeled with BrdU (1:500 dilution, cell proliferation assay, Millipore) for 24 and 48h. Labeled cells were fixed for 30 min. After fixation, incorporated BrdU was detected immunochemically using anti-BrdU mouse monoclonal antibody followed by peroxidase-conjugated goat anti-mouse IgG antibody. The colored reaction product is quantified using a microplate reader at 450 nm.

DNA fragmentation assays
DNA fragmentation was assayed following manufacturer’s procedure (Cell Death Detection ELISA plus kit; Roche). Briefly, HBEC-3 cells (1×10^5 in 100 µL medium) 48h after transfection were washed, resuspended in 200 µL of lysis buffer supplied by the manufacturer, and incubated for 30 minutes at room temperature. After pelleting nuclei (200g, 10 minutes), 20 µL of the supernatant (cytoplasmic fraction) was use for the enzyme-linked immunosorbent assay (ELISA) following the manufacturer's standard protocol. Finally, absorbance at 405 nm (reference wavelength), upon incubating with a peroxidase substrate for 5 minutes, was determined with a microplate reader. Signals in the wells containing the substrate only were subtracted as background.

Viability
Cell viability was assessed by staining cells with Trypan blue solution (0%) and numbering non-viable (blue) cells under microscope (x20) in four 1 x 1 mm squares of one chamber and determining the average number of cells per square.

Co-immunoprecipitation and GTP-Rho, NDR2/GEF-H1 pull-down assays

Cells were lysed in chilled immunoprecipitation buffer and the cleared lysate (500 μg) incubated with 3 μg of the indicated antibody and 30 μL of protein-A agarose beads (Repligen) in 1 mL of IP buffer (13). Beads were resuspended in 30 μL of 2X Laemmli buffer and subjected to Western blotting. For GTP-Rho pulldown assays, cell lysates were incubated with beads glutathione-S-transferase (GST)-Rhotekin Rho binding domain (RBD) 45 minutes at 4°C and precipitates analyzed by Western blotting using RhoB or RhoA antibodies.

For NDR2 pulldown assays, cell lysates were incubated with glutathione-S-transferase (GST)-NDR1 or NDR2 (from Carna Biosciences, Japan) or GST-Rhotekin binding domain used as a negative control, 60 minutes at 4°C, and precipitates analyzed by Western blotting using GEF-H1 and phospho-GEF-H1 antibodies.

Live cell imaging and analysis

For time-lapse videomicroscopy, HBEC-3 cells were grown and transfected on 35-mm coverglass bottom dishes (MatTek) with siNeg or siRASSF1A (3×10^4 cells per dish) before imaging. The microscope was equipped with an open chamber (Pecon) equilibrated in 5% CO_2 and maintained at 37°C. Images were taken at 2-min intervals with a ×20 or ×60 objective using a RTKE camera (Spot) controlled by the Micromanager software. Video analysis was performed by ImageJ software.

Statistical analysis

Data are presented as means ± SEM of experiments realized at least three time independently. Statistical differences were determined either by the Student paired t- test for single comparison or by one-way analysis of variance (ANOVA) followed by Dunnett's Multiple Comparison Test to compare each conditions of an experiment with a single control (siNeg) (GraphPad Software, Inc. USA). Statistical significance was set at $p \leq 0.05$. Chi2 test was also used to test correlation between events and presence/absence of RASSF1A expression.

We used *kpm.plot.com* online software (Gyorffy *et al*. 2013), computing the RASSF1A, RhoB, SK38L/NDR2, GEF-H1 mRNA prognostic analyses in 681 Stage I-to-III patients, with gene-expression data and OS information downloaded from the GEO (Affymetrix microarrays only), EGA, and TCGA databases (2017 database release). OS analyses were dichotomized according to the median value.

Acknowledgments

F. Dubois and M. Keller were recipients of PhD. grants from the Association des Insuffisants Respiratoire de Basse-Normandie (AIR) and from Fondation pour la Recherche Médicale (FRM). E Maille was recipient of PhD. grants from both AIR and Région Basse-Normandie, S. Brosseau received a master grant from the FRM.This work was supported by research grants from Cancéropole Nord-Ouest (projets émergents) (to GZ), from Ligue contre le Cancer de Normandie (Comité du Calvados, Comité de l'Orne, Comité de l'Eure, Comité de la Manche) (to GZ and GL), from the Comité National des Maladies respiratoires (CMNR) (to GL).

Author contributions:

GL & GZ conceived and designed the experiments. GL, MK, FD, ST, AM, JL, EM and SB performed the experiments. GL, FD, MK, ST, JL and NE contributed to cellular and molecular biology experiments. AH, JC and EB provided technical and scientific support. GL and GZ wrote the manuscript with the help of all the authors. All authors approved the final manuscript.

Competing Interests statement: The authors declare that they have no competing interest.

References

Arnette C., Efimova N., Zhu X., Clark GJ., Kaverina I. Microtubule segment stabilization by RASSF1A is required for proper microtubule dynamics and Golgi integrity. Mol Biol Cell. 2014, 25(6):800-10.

Birkenfeld J, Nalbant P, Bohl BP, Pertz O, Hahn KM, Bokoch GM. GEF-H1 modulates localized RhoA activation during cytokinesis under the control of mitotic kinases. Dev Cell 2007;12(5):699-712.

Bousquet E, Mazieres J, Privat M, Rizzati V, Casanova A, Ledoux A, *et al*. Loss of RhoB expression promotes migration and invasion of human bronchial cells via activation of AKT1. Cancer research 2009;69(15):6092-9.

Bui DA, Lee W, White AE, Harper JW, Schackmann RC, Overholtzer M, Selfors LM, Brugge JS. Cytokinesis involves a nontranscriptional function of the Hippo pathway effector YAP. Sci Signal. 2016 Mar 1;9(417):ra23.

Carter SL., Eklund AC., Kohane IS., Harris LN., Szallasi Z. A signature of chromosomal instability inferred from gene expression profiles predicts clinical outcome in multiple human cancers. Nat Genet. 2006, 38: 1043–8.

Chiba S, Ikeda M, Katsunuma K, Ohashi K, Mizuno K:MST2- and Furry-mediated activation of NDR1 kinase is critical for precise alignment of mitotic chromosomes.Curr Biol 2009,19(8):675–681.

Chiba S, Amagai Y, Homma Y, Fukuda M, Mizuno K:NDR2-mediated Rabin8 phosphorylation is crucial for ciliogenesis by switching binding specificity from phosphatidylserine to Sec15.EMBO J 2013,32(6):874–885.

Chircop M. Rho GTPases as regulators of mitosis and cytokinesis in mammalian cells. Small GTPases. 2014;5. pii: e29770.

Cornils H, Kohler RS, Hergovich A, Hemmings BA. Human NDR kinases control G(1)/S cell cycle transition by directly regulating p21 stability. Mol Cell Biol. 2011 Apr;31(7):1382-95.

de Fraipont F, Levallet G, Creveuil C, Bergot E, Beau-Faller M, Mounawar M, *et al*. An apoptosis methylation prognostic signature for early lung cancer in the IFCT-0002 trial. Clinical cancer research : an official journal of the American Association for Cancer Research 2012;18(10):2976-86.

Dallol A., Cooper WN., Al-Mulla F., Agathanggelou A., Maher ER., Latif F. Depletion of the Ras association domain family 1, isoform A-associated novel microtubule-associated protein, C19ORF5/MAP1S, causes mitotic abnormalities.Cancer Res. 2007, 15;67(2):492-500.

Davies T., Canman JC. Stuck in the middle: Rac, adhesion, and cytokinesis. J Cell Biol. 2012, 3;198(5):769-71.

Dubois F, Keller M, Calvayrac O, Soncin F, Hoa L, Hergovich A, *et al*. RASSF1A Suppresses the Invasion and Metastatic Potential of Human Non-Small Cell Lung Cancer Cells by Inhibiting YAP Activation through the GEF-H1/RhoB Pathway. Cancer Res 2016;76(6):1627-40.

Furth N, Bossel Ben-Moshe N, Pozniak Y, Porat Z, Geiger T, Domany E, Aylon Y, Oren M. Down-regulation of LATS kinases alters p53 to promote cell migration. Genes Dev. 2015 Nov 15;29(22):2325-30.

Guo C, Tommasi S, Liu L, Yee JK, Dammann R, Pfeifer GP. RASSF1A is part of a complex similar to the Drosophila Hippo/Salvador/Lats tumor-suppressor network. Curr Biol 2007;17(8):700-5.

Gupta S, Govindaraghavan M, McCollum D. Cross talk between NDR kinase pathways coordinates cytokinesis with cell separation in Schizosaccharomyces pombe. Eukaryot Cell. 2014 Aug;13(8):1104-12.

Gyorffy B, Surowiak P, Budczies J, Lanczky A. Online survival analysis software to assess the prognostic value of biomarkers using transcriptomic data in non- small-cell lung cancer. PLoS One. 2013;8:e82241.

Hehnly H and Doxsey S. Rab11 endosomes contribute to mitotic spindle organization and orientation. Dev Cell. 2014 Mar 10;28(5):497-507.

Hergovich A. Mammalian Hippo signalling: a kinase network regulated by protein- protein interactions. Biochem Soc Trans. 2012 Feb;40(1):124-8.

Hergovich A. Regulation and functions of mammalian LATS/NDR kinases: looking beyond canonical Hippo signalling. Cell Biosc 2013;3:32-56.

Hergovich A. The Roles of NDR Protein Kinases in Hippo Signalling. Genes (Basel).
2016 May 18;7(5). pii: E21.

Hu CK, Coughlin M, Mitchison TJ. Midbody assembly and its regulation during cytokinesis. Mol Biol Cell. 2012 Mar;23(6):1024-34.

Ibrahim SA, Yip GW, Stock C, Pan JW, Neubauer C, Poeter M, Pupjalis D, Koo CY, Kelsch R, Schüle R, Rescher U, Kiesel L, Götte M. Targeting of syndecan-1 by microRNA miR-10b promotes breast cancer cell motility and invasiveness via a Rho-GTPase- and E-cadherin-dependent mechanism.

Int J Cancer. 2012 Sep 15;131(6):E884-96.
Jiménez AP, Traum A, Boettger T, Hackstein H, Richter AM, Dammann RH. The tumor suppressor RASSF1A induces the YAP1 target gene ANKRD1 that is epigenetically inactivated in human cancers and inhibits tumor growth. Oncotarget. 2017 May 23.
Kim, T., Yang, S.-J., Hwang, D., Song, J., Kim, M., Kyum Kim, S., Kang, K., Ahn, J., Lee, D., Kim, M., et al.. A basal-like breast cancer-specific role for SRF–IL6 in YAP-induced cancer stemness. 2015, Nat. Commun. 6.
Lee M-G, Jeong S-I, Ko K-P, Park S-K, Ryu B-K, Kim I-Y, *et al*. RASSF1A Directly Antagonizes RhoA Activity through the Assembly of a Smurf1-Mediated Destruction Complex to SuppressTumorigenesis. Cancer Res 2016;76(7):1847-59
Levallet G, Bergot E, Antoine M, Creveuil C, Santos AO, Beau-Faller M, *et al*. High TUBB3 expression, an independent prognostic marker in patients with early non-small cell lung cancer treated by preoperative chemotherapy, is regulated by K-Ras signaling pathway. Mol Cancer Ther 2012;11(5):1203-13.
Liu L., Broaddus RR., Yao JC., Xie S., White JA., Wu TT., Hamilton SR., Rashid A. Epigenetic alterations in neuroendocrine tumors: methylation of RAS- association domain family 1, isoform A and p16 genes are associ- ated with metastasis. Mod Pathol 2005, 18, 1632–1640.
Liu L., Guo C., Dammann R., Tommasi S., Pfeifer GP. RASSF1A interacts with and activates the mitotic kinase Aurora-A. Oncogene. 2008,16;27(47):6175-86.
Neto H., Kaupisch A., Collins LL., Gould GW. Syntaxin 16 is a master recruitment factor for cytokinesis. Mol Biol Cell. 2013, 24(23):3663-74.
Normand G, King RW. Understanding cytokinesis failure. Adv Exp Med Biol 2010;676:27-55.
Patel M, Karginov AV. Phosphorylation-mediated regulation of GEFs for RhoA. Cell Adh Migr. 2014;8(1):11-8.
Pefani DE, Pankova D, Abraham AG, Grawenda AM, Vlahov N, Scrace S, O' Neill E. TGF-β Targets the Hippo Pathway Scaffold RASSF1A to Facilitate YAP/SMAD2 Nuclear Translocation. Mol Cell. 2016 Jul 7;63(1):156-66.
Rigbolt KT, Prokhorova TA, Akimov V, Henningsen J, Johansen PT, Kratchmarova I, Kassem M, Mann M, Olsen JV, Blagoev B. System-wide temporal characterization of the proteome and phosphoproteome of human embryonic stem cell differentiation. Sci Signal. 2011 Mar 15;4(164):rs3.
Song MS, Song SJ, Ayad NG, Chang JS, Lee JH, Hong HK, *et al*. The tumour suppressor RASSF1A regulates mitosis by inhibiting the APC-Cdc20 complex. Nat Cell Biol 2004;6(2):129-37.
Song MS., Chang JS., Song SJ., Yang TH., Lee H., Lim DS. The centrosomal protein RAS association domain family protein 1A (RASSF1A)-binding protein 1 regulates mitotic progression by recruiting RASSF1A to spindle poles. J Biol Chem. 2005, 4;280(5):3920-7.
Song SJ, Kim SJ, Song MS, Lim DS. Aurora B-mediated phosphorylation of RASSF1A maintains proper cytokinesis by recruiting Syntaxin16 to the midzone and midbody. Cancer Res. 2009 Nov 15;69(22):8540-4.
Vaughan CA, Singh S, Windle B, Sankala HM, Graves PR, Andrew Yeudall W, Deb SP, Deb S. p53 mutants induce transcription of NF-κB2 in H1299 cells through CBP and STAT binding on the NF-κB2 promoter and gain of function activity. Arch Biochem Biophys. 2012 Feb 1;518(1):79-88.
Whitehurst AW, Ram R, Shivakumar L, Gao B, Minna JD, White MA. The RASSF1A tumor suppressor restrains anaphase-promoting complex/cyclosome activity during the G1/S phase transition to promote cell cycle progression in human epithelial cells. Mol Cell Biol 2008;28(10):3190-7.
Yang X, Yu K, Hao Y, Li DM, Stewart R, Insogna KL, Xu T. LATS1 tumour suppressor affects cytokinesis by inhibiting LIMK1. Nat Cell Biol. 2004 Jul;6(7):609-17.
Yuan, M., Tomlinson, V., Lara, R., Holliday, D., Chelala, C., Harada, T., Gangeswaran, R., Manson-Bishop, C., Smith, P., Danovi, S.A., et al. (2008). Yes-associated protein (YAP) functions as a tumor suppressor in breast. Cell Death Differ. 15, 1752.
Zhang L, Tang F, Terracciano L, Hynx D, Kohler R, Bichet S, Hess D, Cron P, Hemmings BA, Hergovich A, Schmitz-Rohmer D. NDR functions as a physiological YAP1 kinase in the intestinal epithelium. Curr Biol. 2015 Feb 2;25(3):296-305.
Zhou Z, Hu T, Xu Z, Lin Z, Zhang Z, Feng T, Zhu L, Rong Y, Shen H, Luk JM, Zhang X, Qin N. Targeting Hippo pathway by specific interruption of YAP-TEAD interaction using cyclic YAP-like peptides. FASEB J. 2015 Feb;29(2):724-32.

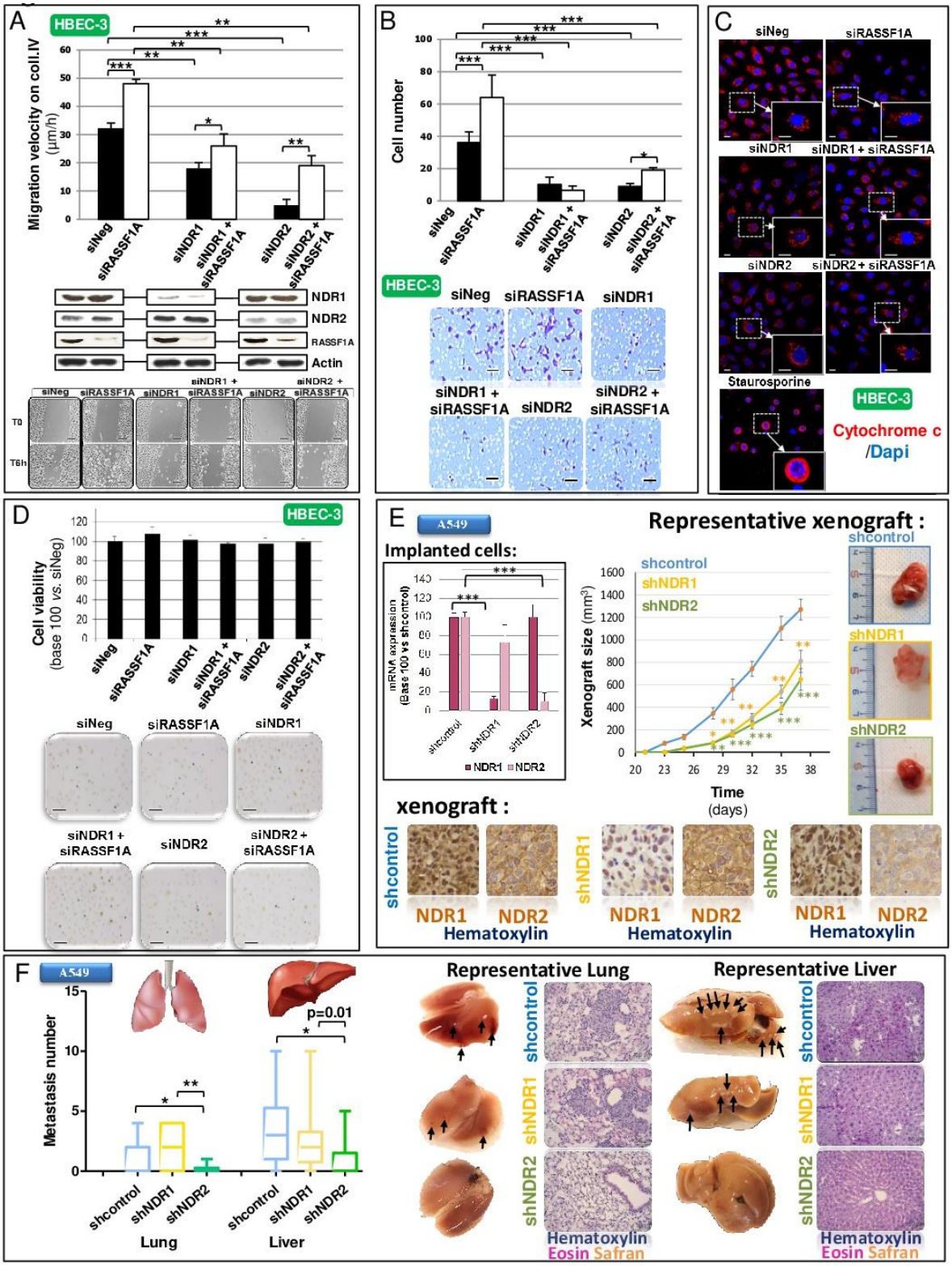

Figure 1: NDR depletion abolishes mobility and metastasis properties in HBEC with RASSF1A depletion without lead to HBEC death.

HBEC-3 were transfected with non-silencing siRNA (siNeg), siRASSF1A and/or with siNDR1 or siNDR2. Experiences were performed 48 hours after transfection. A549 cells were transfected with short hairpin RNA control (shcontrol), shNDR1 or shNDR2.

A) Wound healing assay of transfected HBEC-3 cells on collagen IV coating. Migration velocity is expressed in µm/h. Scale bar represents 100 µm.

B) Invasion capacity of transfected HBEC-3 cells on BioCoat Matrigel Invasion Chamber. Relative invasion normalized to that of the cells transfected with siNeg. Scale bar represents 80 µm.
C-D) HBEC-3 cells death was measured by evaluating cytochromeC releasing (**C**) and quantifying cell viability with Trypan blue coloration (**D**). **C-D**) Representative pictures are presented.
E-F) ShNDR1 or shNDR2-infected A549 cells suspension ($1x10^7$ cells in 0.1ml of Matrigel®) were injected subcutaneously in male Fox Chase $SCID^{-/-}$ Beige mice (Ten mice per group). **E**) Xenograft tumor size [length (L)/width (l)/thickness (e)] monitored thrice a week. Expression levels for NDR1 and NDR2 of the injected cells are presented on the left of the xenografts growth curves. Representative xenograft obtained after subcutaneous injection of shNDR1 or NDR2 cells are presented on the right of the xenografts growth curves. Representative expression of NDR1 or NDR2 assayed by immunohistochemistry on the shNDR1 or NDR2 cells are presented below the xenografts growth curves. **F**) Quantification of lung (on the left) and liver (on the right) microscopic nodules metastases for A549 cells expressing suNDR1, shNDR2 or shcontrol. Excised mice lung and liver as histologic photographs of the lung and liver metastases after subcutaneous injection with shNDR1, shNDR2 or shcontrol are presented below the quantification.
For all histograms, error bars indicate the standard error of the mean (SEM) of at least three independent experiments. *P<0.05, **P<0.01 and ***P<0.001, using an ANOVA test followed by Dunnett test.

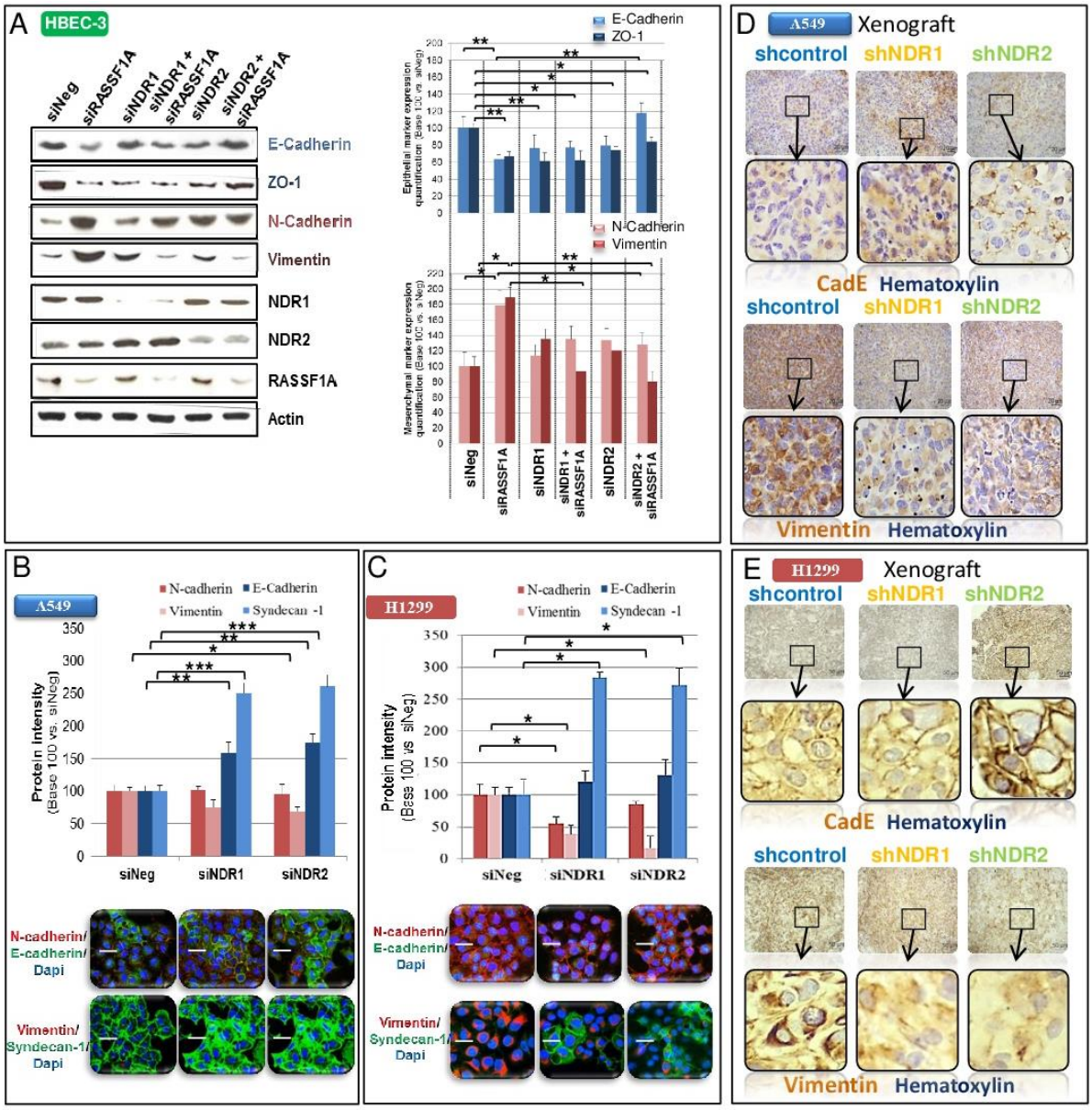

Figure 2: NDR depletion abolishes EMT induced by RASSF1A silencing in HBEC cells.
HBEC-3 (**A**), A549 (**B**) or H1299 (**C**) cells were transiently transfected with non-silencing siRNA (siNeg), siRASSF1A and/or with siNDR1 or siNDR2. **A-C**) Experiences were performed 48 hours after transfection.
D-E) Xenograft obtained after subcutaneous injection of shcontrol, shNDR1 or NDR2 A549 cells (**D**) or H1299 cells (**E**).
Epithelial phenotype was characterized by quantification of epithelial markers (E-Cadherin, syndecan-1 and/or ZO-1) and two mesenchymal markers (vimentin and/or N-cadherin) by western blot (**A**), Immunofluorescence (**B-C**) or immunohistochemistry (**D-E**).
For all histograms, error bars indicate the standard error of the mean (SEM) of at least three independent experiments. *P<0.05, **P<0.01 and ***P<0.001, using an ANOVA test followed by Dunnett's test.

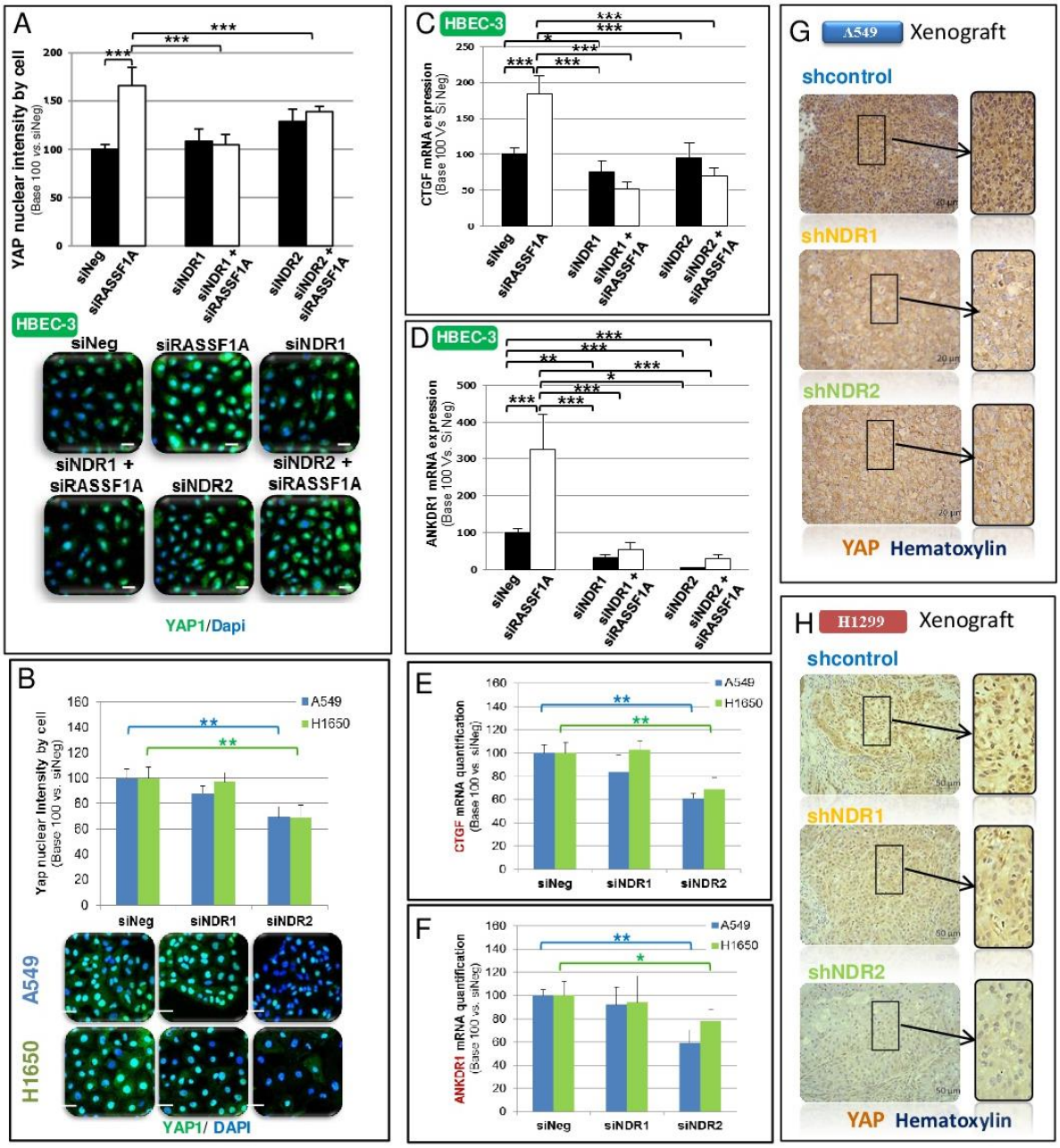

Figure 3: NDR depletion abolishes YAP activation induced by RASSF1A silencing in HBEC cells.

A-F) HBEC-3, H1650 or A549 cells were transiently transfected with non-silencing siRNA (siNeg), siRASSF1A and/or with siNDR1 or siNDR2. Experiences were performed 48 hours after transfection. **G-H**) Xenograft obtained after subcutaneous injection of shcontrol, shNDR1 or NDR2 A549 cells (**G**) or H1299 cells (**H**).

Quantification of YAP nuclear localization was assayed by immunofluorescence with DAPI for nucleus (**A-B**) or by immunohistochemistry (**G-H**)

C-F) Quantification of CTGF (**C, E**) & ANKDR1 (**D, F**) mRNA using actin as an internal control in HBEC-3 cells (**C-D**), H1650 and A549 cells (**E-F**).

For all histograms, error bars indicate the standard error of the mean (SEM) of at least three independent experiments. *P<0.05, **P<0.01 and ***P<0.001, using an ANOVA test followed by Dunnett's test.

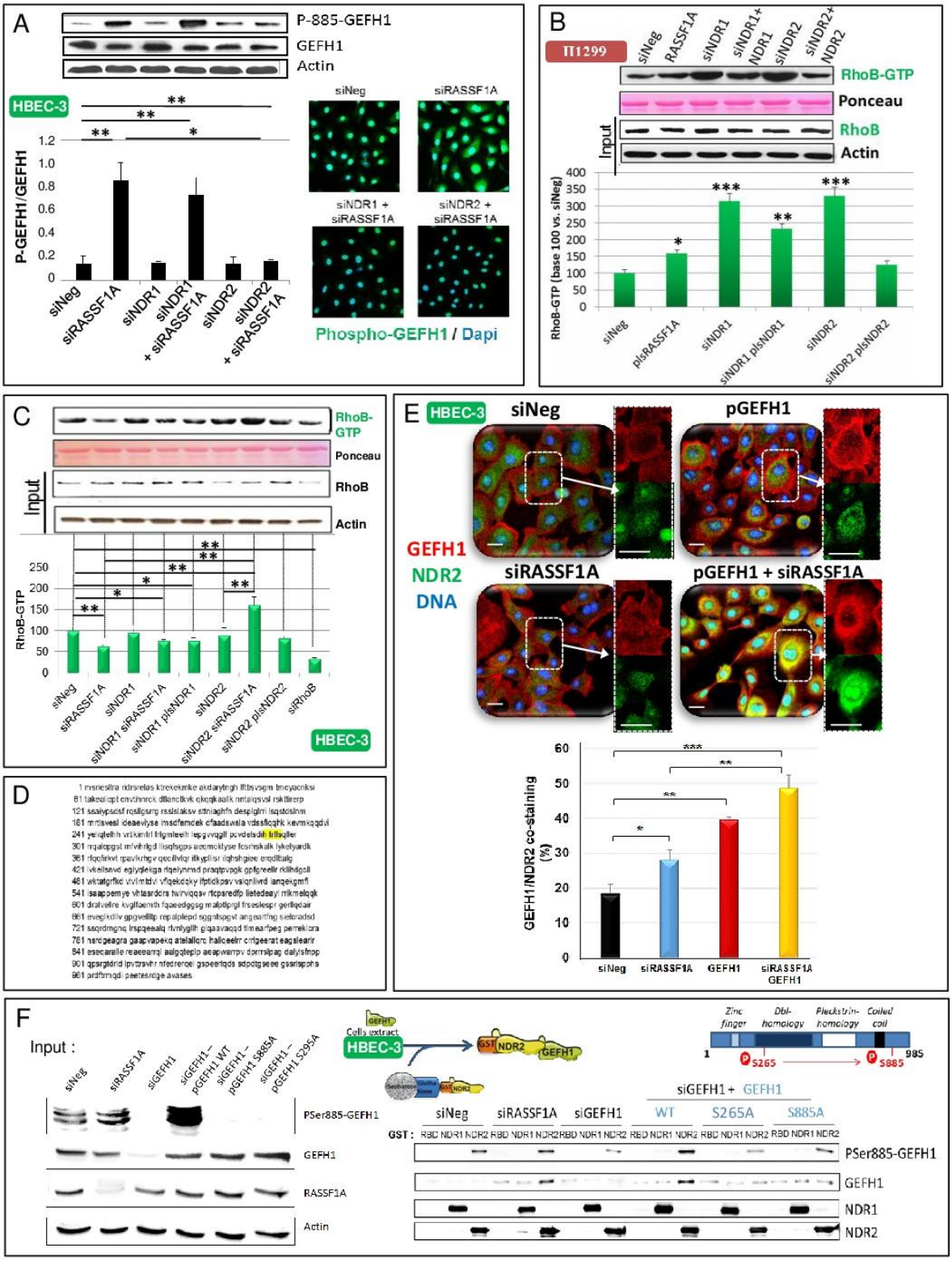

Figure 4: NDR2 interacts and phosphorylates GEF-H1 in HBEC.
HBEC-3 or H1299 cells were transiently transfected with non-silencing siRNA (siNeg) and/or siRASSF1A, siNDR1, siNDR2, siGEF-H1, pcDNA3-NDR1, pcDNA3-NDR2 or pcB6-GEF-H1. Experiences were performed 48 hours after transfection.
A) GEF-H1 phosphorylation status according NDR1/2 presence. Phosphorylation of the ser885 from GEF-H1 was assayed by western blot and normalized with total GEF-H1 expression.

B-C) GST-RBD pull-down assay in H1299 cells (**B**) and HBEC-3 cells (**C**) using siRhoB as control (**C**).
D) GEF-H1 sequence exhibits the HXRXXS/T pattern that recognized NDR kinases.
E) GEF-H1 and NDR2 co-staining assayed by immunofluorescence in HBEC-3 cells during interphase.
F) GST-NDR2 pull-down assay using siRNA & GEF-H1 plasmid as controls.
E) NDR2 phosphorylation on Ser265-GEFGH1 link with phosphorylation on Ser-885-GEF-H1A was assayed. NDR2 activity on HBEC-3 cells extracts previously transfected with pcB6-GEF-H1 wild type, mutated on Ser265 (S265A), or on Ser885 (S885A) was assayed by quantifying ser885-GEF-H1 phosphorylation status by western blot following normalization by total GEF-H1 expression.
For all histograms, error bars indicate the standard error of the mean (SEM) of at least three independent experiments. *P<0.05, **P<0.01 and ***P<0.001, using an ANOVA test followed by Dunnett's test

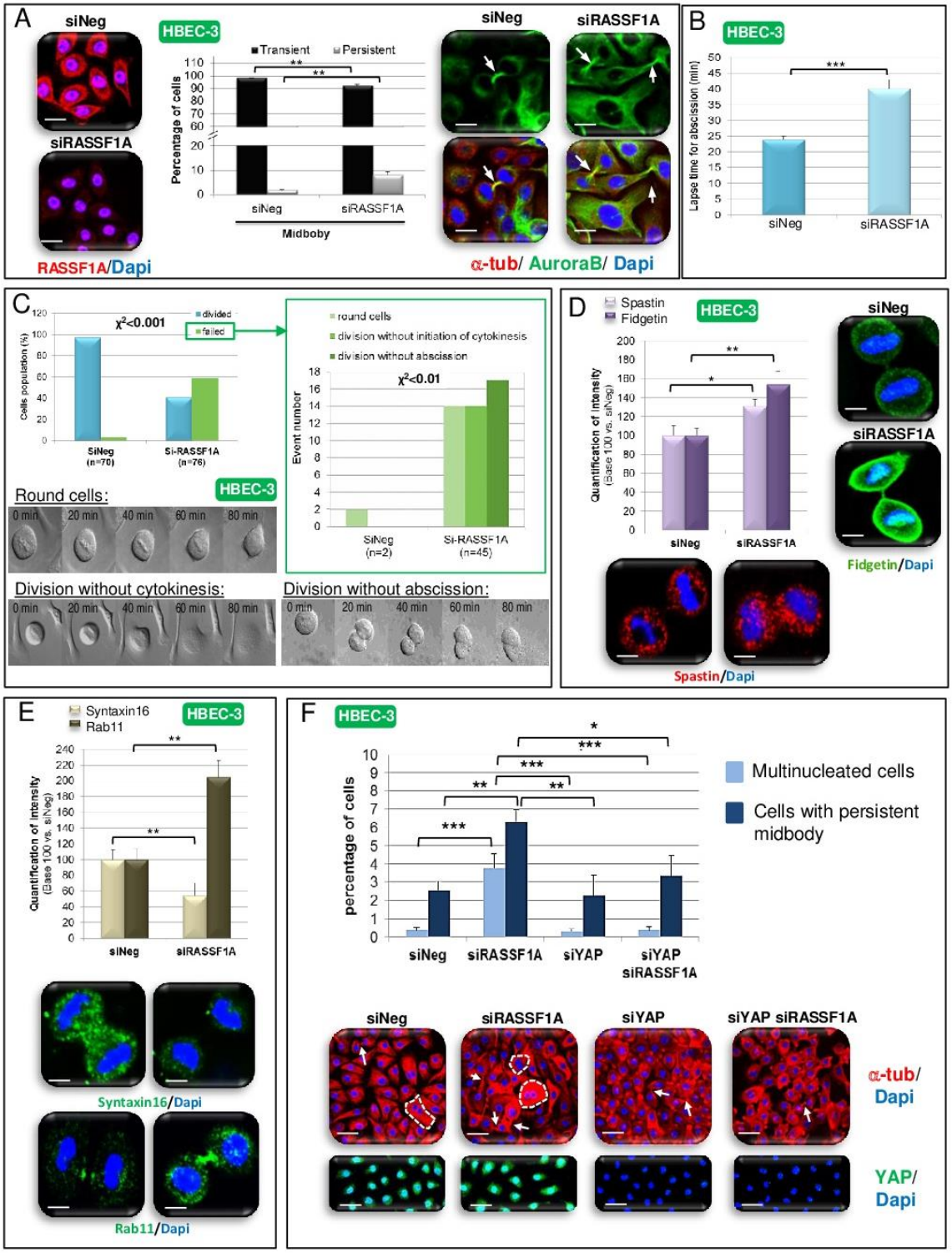

Figure 5. RASSF1A depletion induces YAP-dependent cytokinesis defect.
HBEC-3 cells were incubated with si-RASSF1A, siYAP and/or si-Neg (control). The photographs were obtained 48 hours after transfection.
At 48 h post-transfection, cells were fixed and stained with anti-RASSF1A (red), Anti-tubulin (red) and/or anti-AuroraB (green) antibodies and DAPI (blue). The number of cells with persistent midbody was quantified (**A**) as the lapse time for abscission (**B**) and the number of cells failing to divide following cytokinesis defect by scoring > 100 cells, imaged at 2 min intervals when rounded up (**C,** See also Supplementary Movies S1, S2, S3, S4, S5 and S6.). We further characterized the defect of enzyme responsible for microtubule cleavage at the last

step of abscission (Spastin (red) and Fidgetin (green)) (**D**), and major regulators of vesicle traffic (Rab11 and Syntaxin 16, in green) (**E**) by immunostaining with Dapi for the nucleus.
F) Percentage of HBEC-3 cells multinucleated and/or with persistent midbody was re-evaluate following RASSF1A and YAP silencing (as show by YAP staining (green)) and an immunostaining of the alpha-tubulin, with Dapi for the nucleus.
A, D-F) Scale bar represents 50 µm.
For all histograms, error bars indicate the standard error of the mean (SEM) of at least three independent experiments. *P<0.05, **P<0.01 and ***P<0.001, using an ANOVA test followed by Dunnett's test.
C) Correlation between RASSF1A presence and events was test using a Chi2 test.

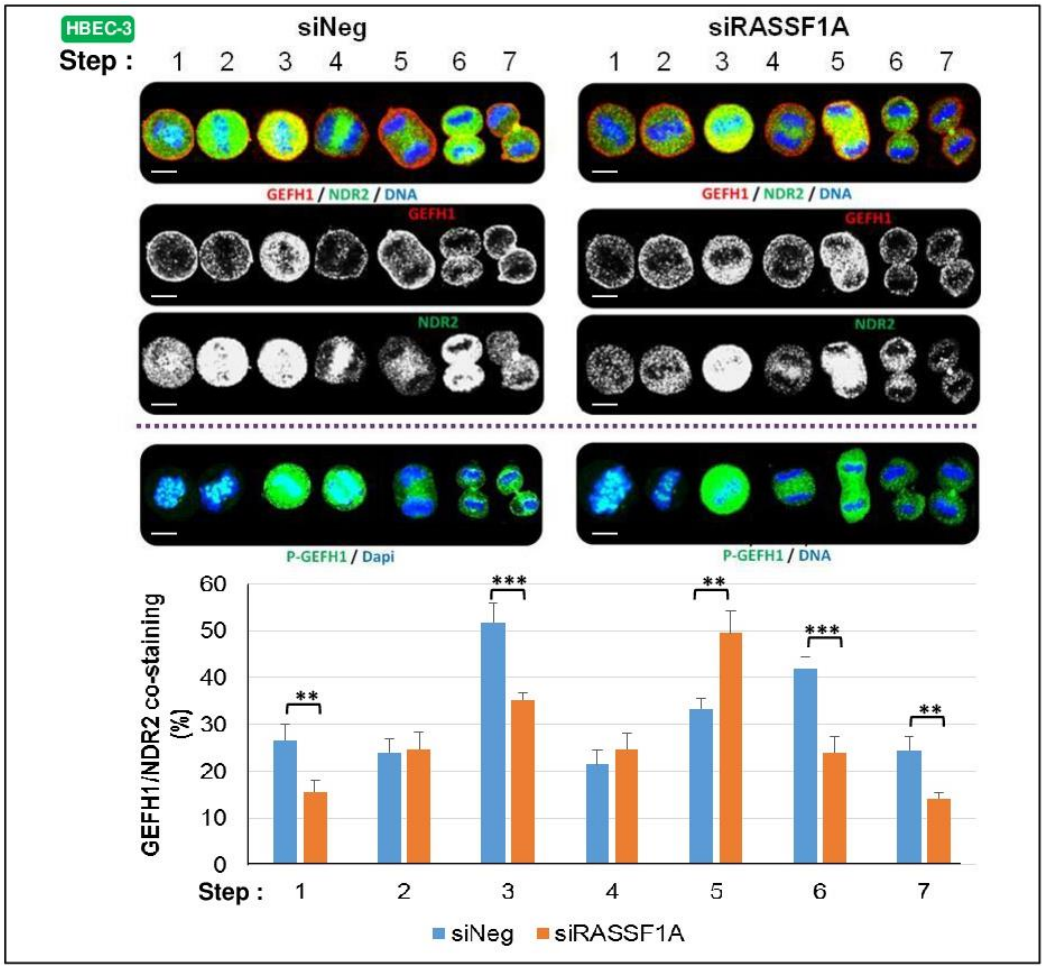

Figure 6: NDR2 and GEF-H1 are co-stained in HBEC-3 cells during cell division.
HBEC-3 cells were transiently transfected with non-silencing siRNA (siNeg), or siRASSF1A. The experiences were performed 48 hours after transfection.
Representative images are shown for NDR2 (green) and GEF-H1 (Red) during interphase. Localization was identified by immunofluorescence and confocal microscopy. Costaining was evaluated by ImageJ software. HBEC-3 cells were also stained with DAPI for DNA (Blue) and PSer885GEF-H1 (green) during mitosis.
For all histograms, error bars indicate the standard error of the mean (SEM) of at least three independent experiments. *P<0.05, **P<0.01 and ***P<0.001, using an ANOVA test followed by Dunnett's test.

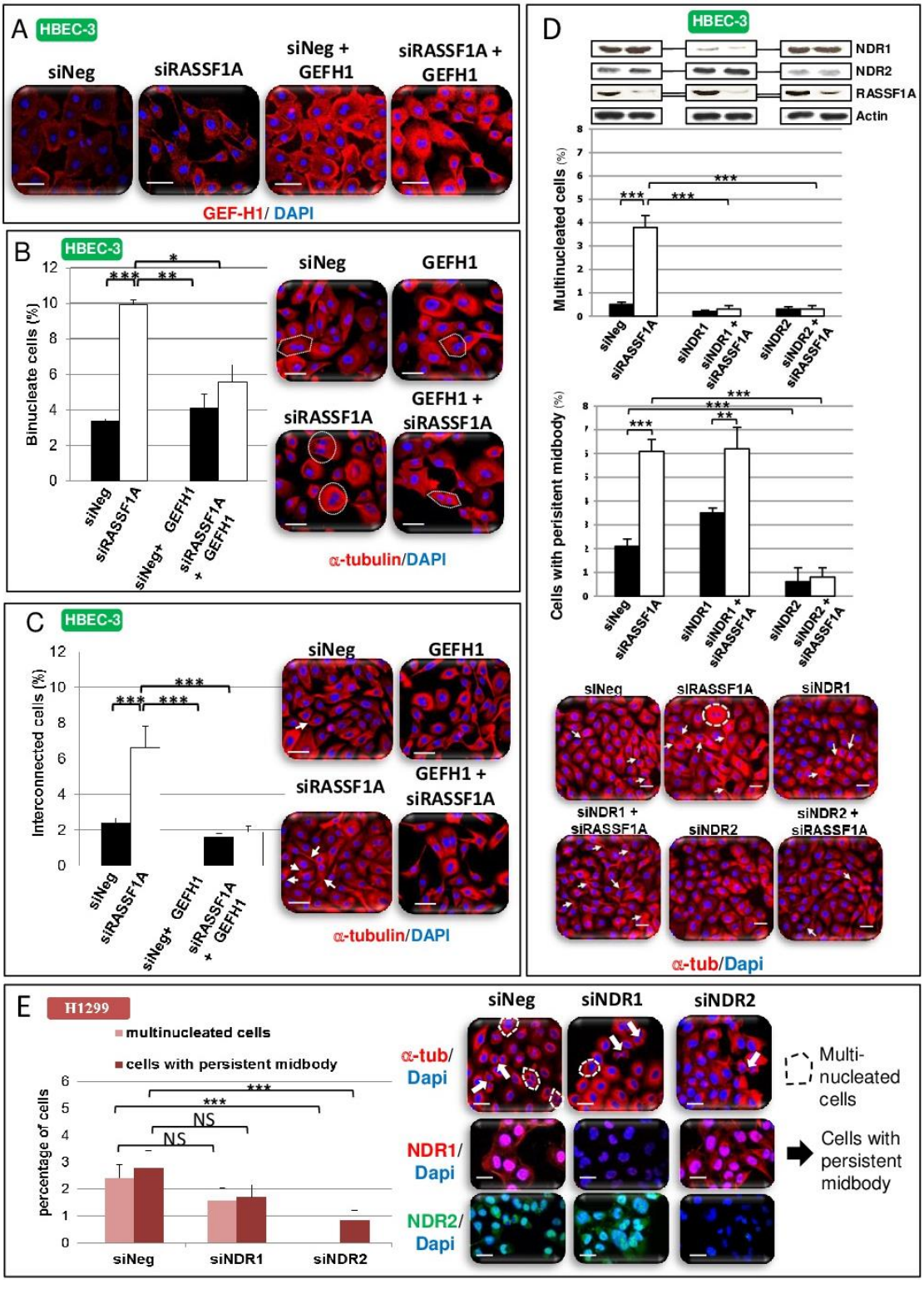

Figure 7: GEF-H1 overexpression as NDR depletion restores cytokinesis of RASSF1A depleted human bronchial cells.

HBEC-3 (**A-D**) or H1299 (**C**) cells were transiently transfected with non-silencing siRNA (siNeg), siRASSF1A and/or with siNDR1, siNDR2 or pcB6-GEF-H1 (**A**). Experiences were performed 48 hours after transfection.

The number of binucleate (**B, D, E**) and interconnected cells (**C, D, E**) were counted 48 hours after transfection after alpha-tubulin (red) and DNA (blue, DAPI) staining from cells over-expressing or not GEF-H1 (**A**) or silenced for NDR kinases (**D, E**) in HBEC63 (**C, D**) or H1299

(**E**) cells. These numbers are expressed as a percentage in control and siRNA-transfected cells.
For all histograms, error bars indicate the standard error of the mean (SEM) of at least three independent experiments. *P<0.05, **P<0.01 and ***P<0.001, using an ANOVA test followed by Dunnett's test.

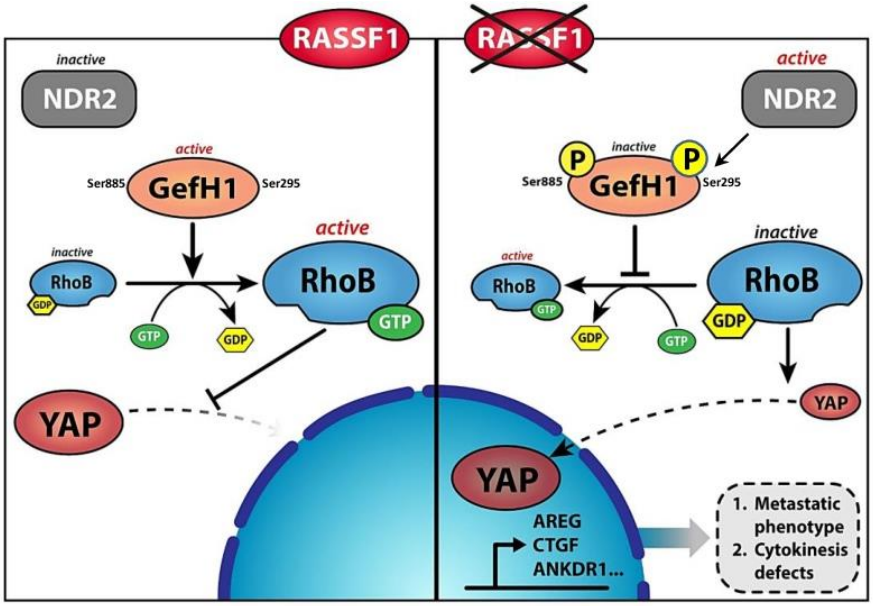

Figure 8. A proposal model for RASSF1A regulation of the NDR2/GEFH-1/RhoB/YAP axis.

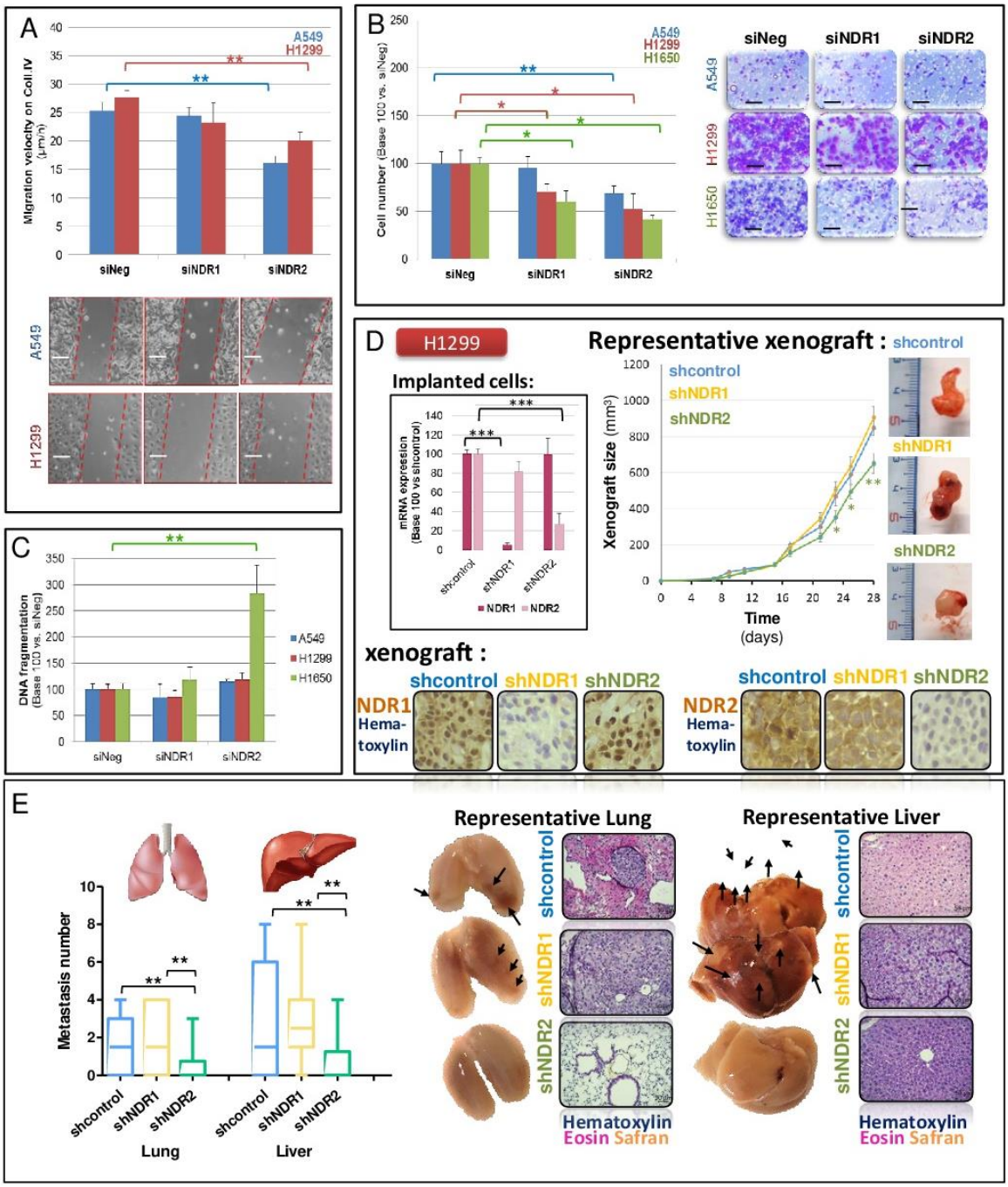

Figure S1: NDR depletion abolishes mobility and metastasis properties in HBEC with RASSF1A depletion without lead to cells death.

(**A-C**) H1299, A549 and H1650 were transfected with non-silencing siRNA (siNeg), siRASSF1A and/or with siNDR1 or siNDR2. Experiences were performed 48 hours after transfection.(**A**) Wound healing assay of transfected A549 or H1299 cells on collagen IV coating. Migration velocity is expressed in µm/h. Scale bar represents 100 µm.(**B**) Invasion capacity of transfected A549, H1299 or H1650 cells on BioCoat Matrigel Invasion Chamber. Relative invasion normalized to that of the cells transfected with siNeg. Scale bar represents 80 µm.(**C**) DNA fragmentation of transfected A549, H1299 or H1650 cells.(**D-E**) H1299 were transfected with short hairpin RNA control (shcontrol), shNDR1 or shNDR2. ShNDR1 or shNDR2-infected H1299 cells suspension ($1x10^7$ cells in 0.1ml of Matrigel®) were injected subcutaneously in male Fox Chase $SCID^{-/-}$ Beige mice (Ten mice per group). **D**) Xenograft tumor size [length (L)/width (l)/thickness (e)] monitored thrice a week. Expression levels for NDR1 and NDR2 of the injected cells are presented on the left of the xenografts growth curves. Representative xenograft and representative expression of NDR1 or NDR2 assayed by

immunohistochemistry on the shNDR1 or NDR2 xenograft are presented respectively on the right of and under the xenografts growth curves. **E**) Quantification of lung (on the left) and liver (on the right) microscopic nodules metastases for H1299 cells expressing suNDR1, shNDR2 or shcontrol. Excised mice lung and liver as histologic photographs of the lung and liver metastases after subcutaneous injection with shNDR1, shNDR2 or shcontrol are presented below the quantification. For all histograms, error bars indicate the standard error of the mean (SEM) of at least three independent experiments. *P<0.05, **P<0.01 and ***P<0.001, using an ANOVA test followed by Dunnett test.

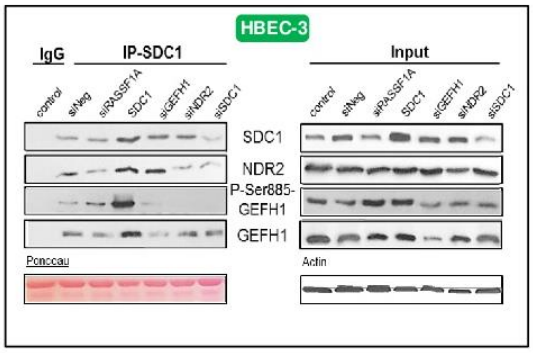

Figure S2. GEF-H1 as NDR2 co-immunoprecipitates with Syndecan-1 in HBEC.
HBEC-3 cells were incubated with si-RASSF1A, si-GEF-H1, si-NDR2, si-Syndecan-1 (SDC1), pcDNA3-SDC1 or si-Neg (control). At 48h post-transfection, proteins were extracted and Immunoprecipitation performed with antibody against SDC1. Proteins on the Immunoprecipitate were revealed by following western blot, using anti-GEFH1 (P885 or not), anti-SDC1, anti-NDR2 antibodies. Actin was used as internal control for Input and Ponceau staining for Immunoprecipitation.

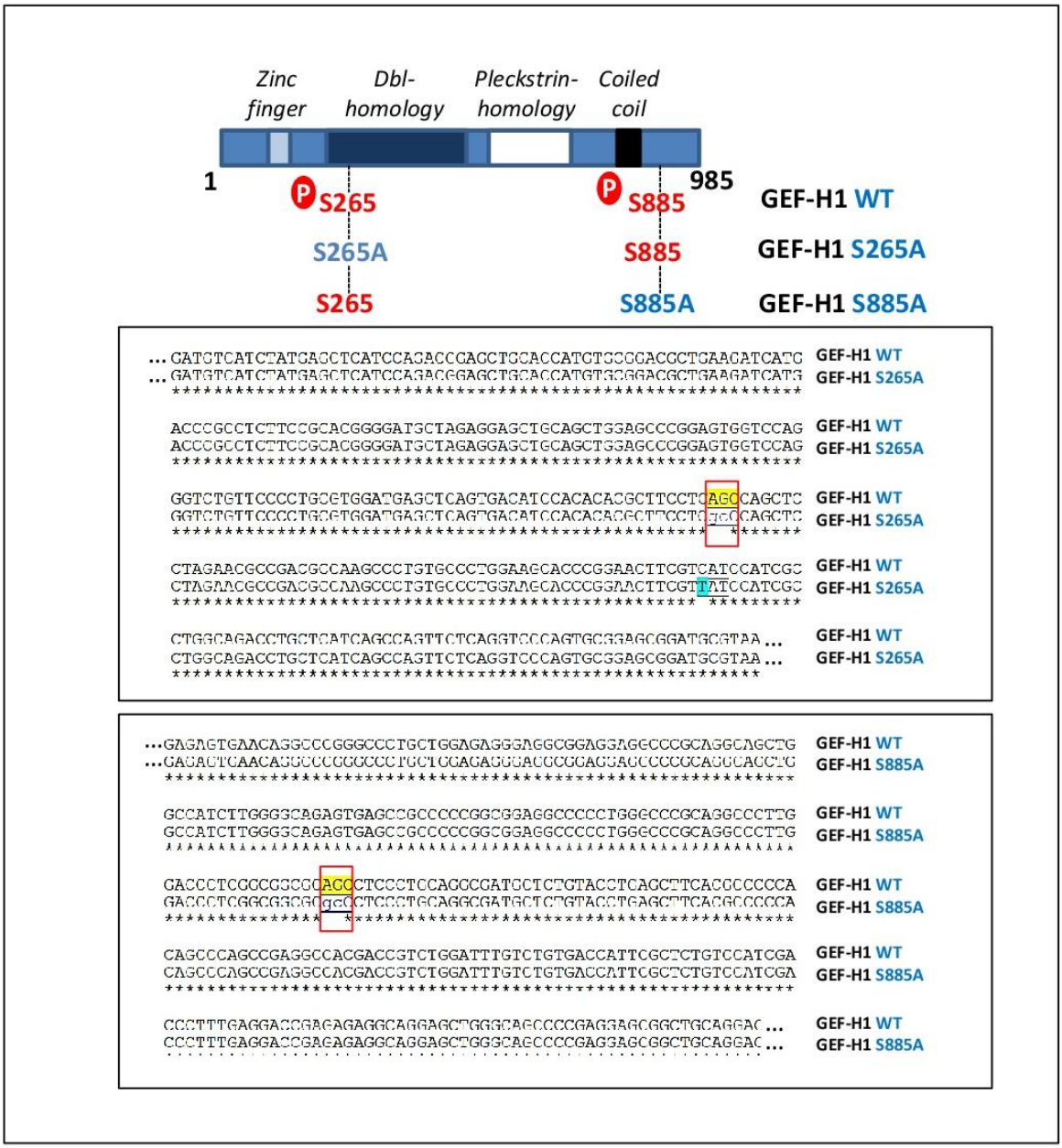

Figure S3: Sanger analysis of GEF-H1 S265A or S885A mutants.
Plasmids with the mutated sequence for GEF-H1 on Ser265 or 885 was confirmed by Sanger analysis.

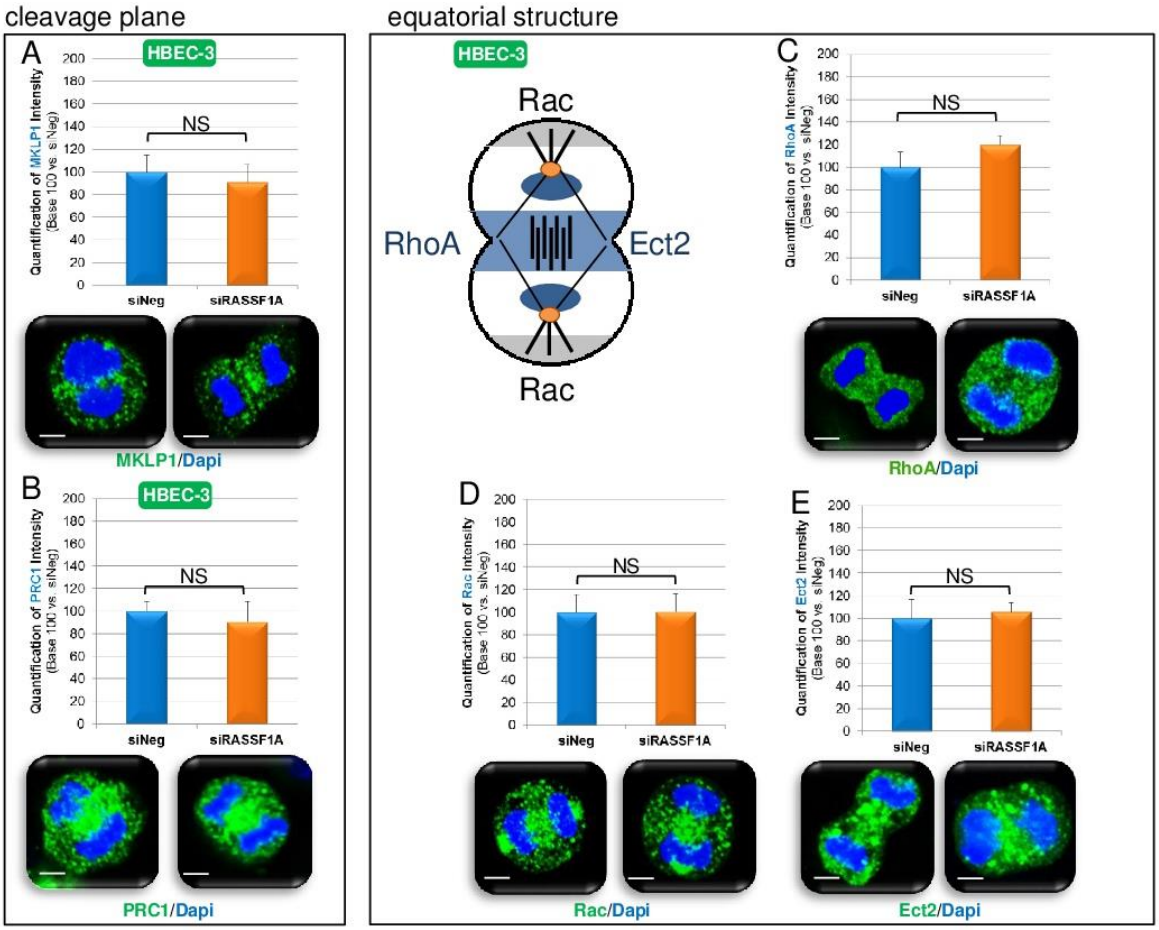

Figure S4. RASSF1A is not required for cleavage plan or equatorial structure of HBEC.
HBEC-3 or HBEC-3-RasV12 cells were incubated with si-RASSF1A or si-Neg (control). The photographs were obtained 48 hours after transfection. At 48 h post-transfection, cells were fixed and stained with Anti-MLKP1 (green, **A**) or Anti-PRC1 (green, **B**) for monitoring cleavage plane, with Anti-RhoA (green, **C**), Anti-Rac (green, **D**), or Anti-Ect2 (green, **E**) for monitoring equatorial structure.
A-E) Nuclei were paint with Dapi. Scale bar represents 50 µm.
For all histograms, error bars indicate the standard error of the mean (SEM) of at least three independent experiments. *P<0.05, **P<0.01 and ***P<0.001, using an ANOVA test followed by Dunnett test.

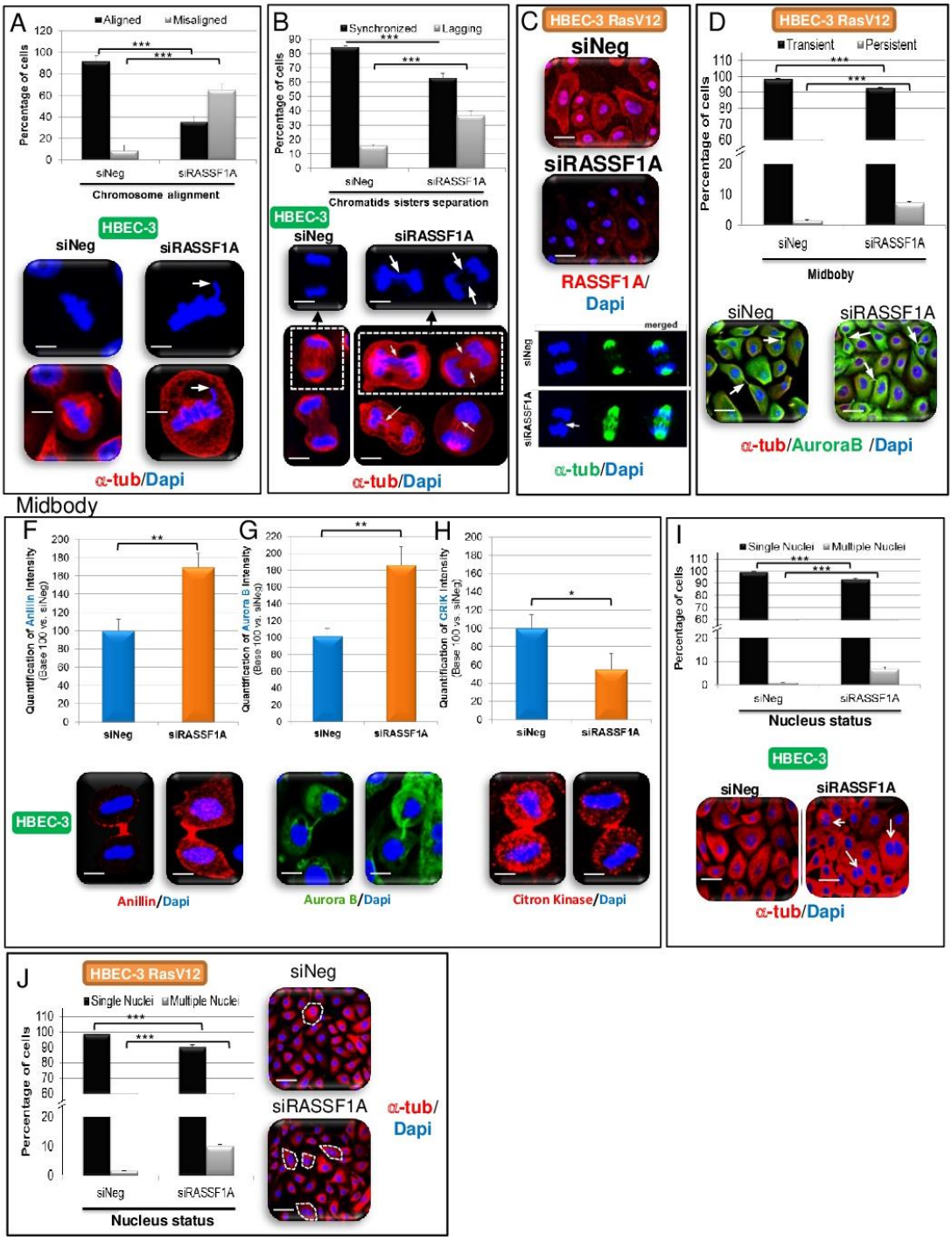

Figure S5. RASSF1A depletion induces defects on metaphase and anaphase and is required for midbody formation in HBEC cells.

HBEC-3 or HBEC-3-RasV12 cells were incubated with si-RASSF1A or si-Neg (control). The photographs were obtained 48 hours after transfection. At 48 h post-transfection, cells were fixed and stained with Anti-RASSF1A (red), Anti-tubulin (red or green in **D**) and DAPI (blue). The number of cells with misaligned chromosome during metaphase (**A:** HEBC-3), chromosome lagging during anaphase (**C:** HEBC-3, **D** HBEC-3-RasV12), the persistent midbody in HBEC-3 RasV12 cells following Anti-tubulin (red) and Anti-Aurora-B (green) co-staining (**D**), the expression of Anillin (red, **F**), Aurora-A green, **G**) or Citron Kinase (red, **H**) for monitoring midbody formation and cells with multiple nuclei (**I:** HEBC-3, **J:** HBEC-3-RasV12) were scoring. (**A-E**) Scale bar represents 50 µm. For all histograms, error bars indicate the standard error of the mean (SEM) of at least three independent experiments. *P<0.05, **P<0.01 and ***P<0.001, using an ANOVA test followed by Dunnett test.

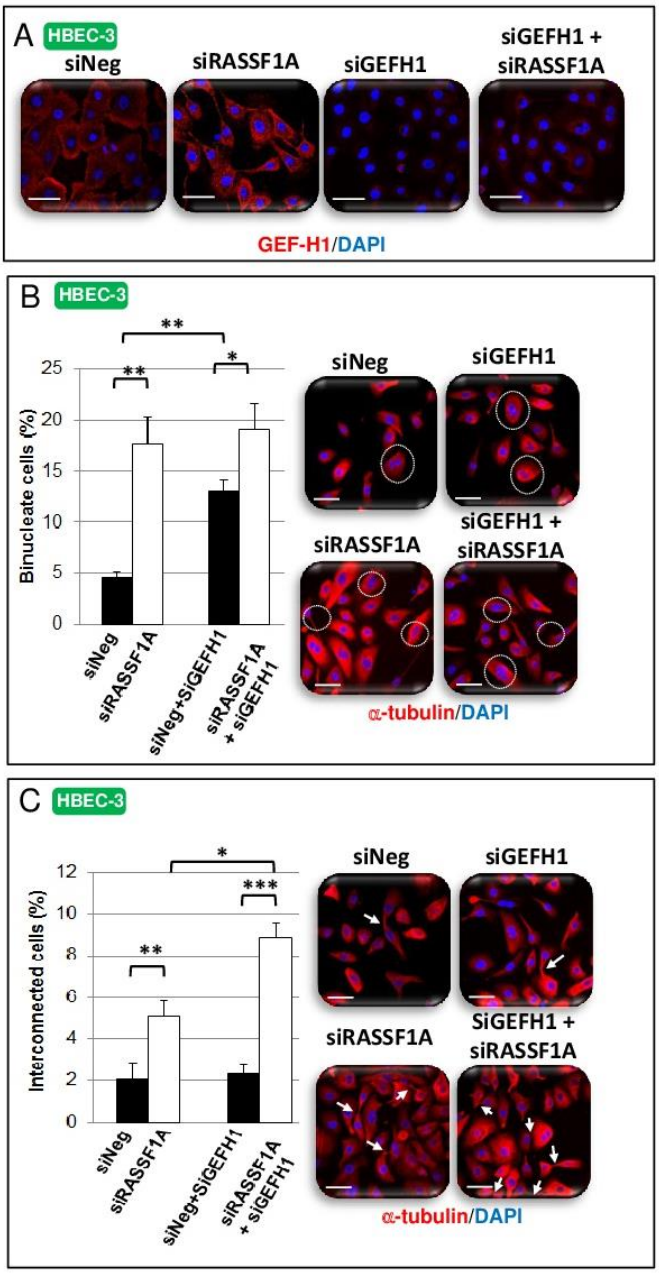

Figure S6: GEF-H1 silencing mimics cytokinesis failure induced by RASSF1A loss in HBEC-3 cells.

HBEC-3 cells were transiently transfected with non-silencing siRNA (siNeg), siRASSF1A and/or siGEF-H1 (A). The number of binucleate (**B**) and interconnected cells (**C**) were counted 48 hours after transfection after alpha-tubulin (red) and DNA (blue, DAPI) staining from cells expressing or not GEF-H1. These numbers are expressed as a percentage in control and siRNA-transfected cells. For all histograms, error bars indicate the standard error of the mean (SEM) of at least three independent experiments. *P<0.05, **P<0.01 and ***P<0.001, using an ANOVA test followed by Dunnett's test.

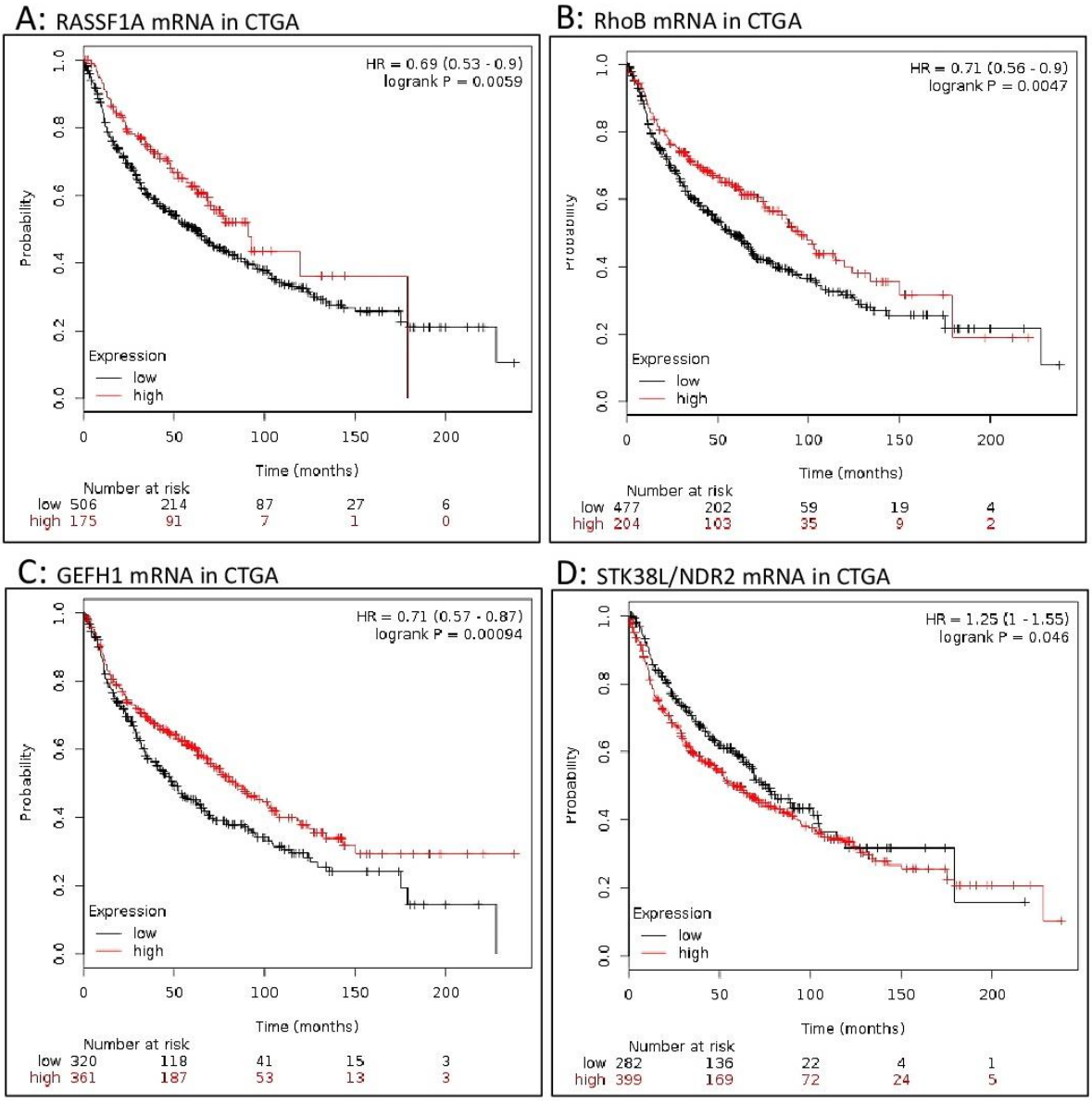

Figure S7: RASSF1A/RhoB/GEF-H1/NDR2 mRNA impacts on survival from of 681 patients with NSCLC, CTGA cohort.

Tables.

TableS1. Primers and siRNA sequences used in this work.

Target	siRNA sequence (5'>3')	Quantity per 10cm²	Primers for qRT-PCR Forward (F, 5'>3') Reverse (R, 5'>3')
RASSF1A	**siRNA1 :** GACCUCUGUGGCGACUUCATT	10 nmol	**F** : GGC GTC GTG CGC AAA GGC C **R** : GGG TGG CTT CTT GCT GGA GGG
	siRNA2 : CAAGGACGGUUCUUACACA	10 nmol	
GEF-H1	**siRNA1 :** GAAGGUAGCAGCCGUCUGU	20 nmol	**F** : ACA CGC TTC CTC AGC CAG CTAT TA **R** : AAT TGC TGG AAG CGT TTG TCT CGG
	siRNA2 : GAAUUAAGAUGGAGUUGCAUU	20 nmol	
Yap	**siRNA1 :** UGAGAACAAUGACGACCAA	10 nmol	**F** : GCC GGA GCC CAA ATC C **R** : GCA GAG AAG CTG GAG AGG AAT G
	siRNA2 : CCACCAAGCUAGAUAAAGA	10 nmol	
NDR1	**siRNA1 :** AAGTAATAGGCAGAGGAGCAT	25 nmol	**F** : GTG AGG TGC GGC TTG TTC A **R** : GTC ACG CTC CGC ACG AAT
	siRNA2 : AAGAGCAGGTTGGCCACATTC	25 nmol	
NDR2	**siRNA1 :** AAGTTACGTCGATCACAACAC	25 nmol	**F** : CTT GGC TTG GAT GAC TTT GAG **R** : GCT CTT TTT CAA GCA TAT CAG C
	siRNA2 : AAGACACCTTGACAGAAGAGG	25 nmol	
SDC1	**siRNA1 :** CAGGUGCAGGUGCUUUGCAAGAUA U	25 nmol	**F** : GGA GCA GGA CTT CAC CTT TG **R** : CTC CCA GCA CCT CTT TCC T
	siRNA2 : GCCCACCAAACAGGAGGAAUUCUAU	25 nmol	

TableS2. Antibodies used in this work.

Antibodies	SOURCE	IDENTIFIER
Rabbit polyclonal anti-Ect2 (clone C-20)	Santa Cruz Biotechnology	Cat# sc-1005, RRID:AB_2246263
Rabbit polyclonal anti-Fidgetin (clone H-146)	Santa Cruz Biotechnology	Cat# sc-68343, RRID:AB_2104670
Mouse monoclonal anti-Spastin (clone A-2)	Santa Cruz Biotechnology	Cat# sc-271247, RRID:AB_10613446
Mouse monoclonal anti-Katanin p80 B1 (clone C-4)	Santa Cruz Biotechnology	Cat# sc-377226
Mouse monoclonal anti-Citron Kinase (CRIK, clone 6)	Santa Cruz Biotechnology	Cat# sc-136283, RRID:AB_10610237
Mouse monoclonal anti-Anillin (clone B-10)	Santa Cruz Biotechnology	Cat# sc-271814, RRID:AB_10709437
Rabbit polyclonal anti-MKLP-1 (clone N-19)	Santa Cruz Biotechnology	Cat# sc-867, RRID:AB_631959
Mouse monoclonal anti-p53 (clone DO-7)	Santa Cruz Biotechnology	Cat# sc-47698, RRID:AB_628083
Rabbit polyclonal anti-Sox9 (clone H-90)	Santa Cruz Biotechnology	Cat# sc-20095, RRID:AB_661282
Mouse monoclonal anti-E-Cadherin (clone 32A8)	Cell Signaling Technology	Cat# 5296S, RRID:AB_10706939
Rabbit monoclonal anti-Cyclin D1 (clone 92G2)	Cell Signaling Technology	Cat# 2978S, RRID:AB_10692801
Rabbit monoclonal anti-Cyclin D2 (clone D52F9)	Cell Signaling Technology	Cat# 3741S, RRID:AB_2070685
Mouse monoclonal anti-Cyclin D3 (clone DCS22)	Cell Signaling Technology	Cat# 2936S, RRID:AB_10698739
Rabbit monoclonal anti-p21 Waf1/Cip1 (clone 12D1)	Cell Signaling Technology	Cat# 2947, RRID:AB_823586
Rabbit monoclonal anti-p27 Kip1 (clone SX53G8.5)	Cell Signaling Technology	Cat# 3686, RRID:AB_2077850
Rabbit monoclonal anti-Phospho-Rb (Ser795)	Cell Signaling Technology	Cat# 9301S, RRID:AB_330013
Mouse monoclonal anti-Rb (clone 4H1)	Cell Signaling Technology	Cat# 9309S, RRID:AB_10696874
Rabbit monoclonal anti-RhoA (clone 67B9)	Cell Signaling Technology	Cat# 2117, RRID:AB_10693922
Rabbit monoclonal anti-RhoB	Cell Signaling Technology	Cat# 2098S, RRID:AB_2179103
Rabbit monoclonal anti-Rab11a/b (clone D4F5)	Cell Signaling Technology	Cat# 5589S, RRID:AB_10693925
Rabbit monoclonal anti-Rac1/2/3	Cell Signaling Technology	Cat# 2465S, RRID:AB_10695732
Rabbit monoclonal anti-Phospho-Cofilin (Ser3) (clone 77G2)	Cell Signaling Technology	Cat# 3313S, RRID:AB_2244926
Rabbit monoclonal anti-Cofilin (clone D3F9)	Cell Signaling Technology	Cat# 5175, RRID:AB_10622000
Rabbit monoclonal anti-PRC1	Cell Signaling Technology	Cat# 3639S, RRID:AB_11178940
Rabbit monoclonal anti-phospho-LATS1/2 (clone Ser909)	Cell Signaling Technology	Cat# 9157, RRID:AB_2133515
Rabbit monoclonal anti-LATS1	Cell Signaling Technology	Cat# 9153S, RRID:AB_2296754
Rabbit monoclonal anti-LATS2	Cell Signaling Technology	Cat# 5888, RRID:AB_10835233
Rabbit monoclonal anti-	Cell Signaling Technology	Cat# 3841S,

phospho-LIMK (Thr508)/LIMK2 (Thr505)		RRID:AB_2136946
Rabbit monoclonal anti-LIMK1	Cell Signaling Technology	Cat# 3842S, RRID:AB_10698882
Rabbit monoclonal anti-phospho-MST1 (Thr183)/MST2 (Thr180)	Cell Signaling Technology	Cat# 3681S, RRID:AB_330269
Rabbit monoclonal anti-MST1	Cell Signaling Technology	Cat# 3682S, RRID:AB_10694384
Rabbit monoclonal anti-MST2	Cell Signaling Technology	Cat# 3952S, RRID:AB_10694853
Rabbit monoclonal anti-Sox2 (clone D6D9)	Cell Signaling Technology	Cat# 3579, RRID:AB_2195767
Rabbit monoclonal anti-phospho-YAP (Ser127)	Cell Signaling Technology	Cat# 4911S, RRID:AB_2218913
Rabbit monoclonal anti-YAP	Cell Signaling Technology	Cat# 14074S
Rabbit polyclonal anti-ZO-1	Cell Signaling Technology	Cat# 5406S, RRID:AB_1904187
Rabbit monoclonal anti-GEF-H1 (clone 55B6)	Cell Signaling Technology	Cat# 4076S, RRID:AB_10699018
Rabbit monoclonal anti-phospho-GEF-H1 (S885)	Cell Signaling Technology	Cat# 14143S
Anti-rabbit IgG, HRP-linked Antibody	Cell Signaling Technology	Cat# 7074, RRID:AB_2099233
Anti-mouse IgG, HRP-linked Antibody	Cell Signaling Technology	Cat# 7072S, RRID:AB_10708988
Mouse monoclonal anti-Tubulin	Sigma-aldrich	Cat# T9028, RRID:AB_261811
Rabbit polyclonal anti-Aurora B	Sigma-aldrich	Cat# A5102, RRID:AB_476740
Mouse monoclonal anti-NDR1	abcam	Cat# ab194428
Mouse monoclonal anti-NDR2	abcam	Cat# ab139292
Mouse monoclonal anti-Syntaxin-16	abcam	Cat# ab134945
Mouse monoclonal anti-RASSF1A	eBioscience	Cat# 14-688-82
Mouse monoclonal anti-N-Cadherin	eBioscience	Cat# 14-3259-82
Mouse monoclonal anti-Cytochrome c	BD Pharma	Cat# 556432, RRID:AB_396416
Goat polyclonal anti-Syndecan-1 (SDC1)	R&D	Cat# AF2780, RRID:AB_442186
Donkey anti-Mouse IgG (H+L) Secondary Antibody, Alexa Fluor 555	Invitrogen	Fisher Scientific Cat# 10398212
Donkey anti-Rabbit IgG (H+L) Secondary Antibody, Alexa Fluor 488	Invitrogen	Fisher Scientific Cat# 10424752
Donkey anti-Rabbit IgG (H+L) Secondary Antibody, Alexa Fluor 647	Invitrogen	Fisher Scientific Cat# 10543623
Donkey anti-Goat IgG (H+L) Secondary Antibody, Alexa Fluor 488	Invitrogen	Fisher Scientific Cat# 10246392

RÉSUMÉ

STK38 est une kinase appartenant à la voie de signalisation Hippo et possédant de multiples fonctions dans des cellules tant normales que cancéreuses. De précédents travaux, réalisés par notre équipe et par des collaborateurs, ont permis d'identifier le rôle central de STK38 dans la progression du cycle cellulaire, la duplication centrosomale, l'apoptose, ainsi que l'activité transcriptionnelle. De plus, STK38 est nécessaire à l'autophagie et la résistance à l'anoïkis, deux processus supportant respectivement la résistance et la dissémination des cellules cancéreuses.

Dans ce travail, nous avons découvert que STK38 interagit avec différents partenaires protéiques, pour un total de plus 250 protéines identifiées, en fonction du contexte cellulaire. Dans le détail, nous avons trouvé que STK38 augmente son association avec des protéines cytoplasmiques lors de l'autophagie induite par carence nutritive, alors que STK38 augmente son association avec des partenaires nucléaires, au détriment de partenaires cytoplasmiques, lors du détachement à la matrice extracellulaire. Nous avons découvert que STK38 navigue entre le noyau et le cytoplasme, en fonction du contexte cellulaire, sous la dépendance de XPO1. Nous avons caractérisé STK38 comme le tout premier activateur de XPO1 via la phosphorylation du domaine auto-inhibiteur de XPO1, phosphorylation nécessaire à la présentation de sa région de liaison du cargo. En plus de décider de sa propre disponibilité subcellulaire, STK38 régule également l'export nucléaire d'effecteurs protéiques, tels que Beclin1, YAP1 et Centrin, effecteurs ayant été caractérisés comme impliqués dans certaines fonctions liées à STK38.

Ces résultats révèlent que de multiples fonctions cellulaires, semblant régulées par une unique protéine, une kinase dans notre cas, STK38, peuvent en fait être expliquées par un mécanisme moléculaire unique : réguler la distribution subcellulaire d'effecteurs clés en modulant l'activité exportrice de XPO1 via la phosphorylation de sa région auto-inhibitrice.

MOTS CLÉS

Cancer, STK38, XPO1, Autophagie, YAP, Hippo

ABSTRACT

The Hippo pathway STK38 kinase is implicated in multifarious biological processes in both normal and cancer cells. Previous work performed by our team and collaborators have identified the central role of STK38 in cell cycle progression, centrosome duplication, apoptosis, and transcriptional activity. Moreover, STK38 is required for autophagy and anoïkis resistance in Ras-driven cells, two processes supporting cancer cell resistance and dissemination respectively.

In this work, we discovered that STK38 associates with more than 250 identified interactors, depending on the cellular context. In details, we found that STK38 increases its association with cytoplasmic proteins upon nutrient starvation-induced autophagy, while STK38 increases its interaction with nuclear proteins to the detriment of cytoplasmic ones upon ECM detachment. Furthermore, we discovered that STK38 shuttles between the nucleus and the cytoplasm depending on the context in a XPO1-dependent manner. We characterized STK38 as the first activator of XPO1 by phosphorylating XPO1's auto-inhibitory domain: this phosphorylation being required for the presentation of XPO1's cargo docking site. In addition of being its own gatekeeper, STK38 regulates the subcellular distribution of several effectors, such as Beclin1, YAP1, and Centrin, effectors that play a crucial role in STK38-related well characterized functions.

Taken together, these results presented in this work reveal that multifarious functions harboured by a single protein, a kinase in our case, STK38, can be explained by a unique molecular mechanism: regulating the subcellular distribution of key effectors by modulating XPO1 export activity through phosphorylation of its auto-inhibitory domain. STK38 is in charge of controlling the supply chain of components of these machineries assembled in the cytoplasm.

KEYWORDS

Cancer, STK38, XPO1, Autophagy, YAP, Huppo